Studies on tear evaporation and ocular surface temperature

by

Mana Monfared

A thesis
presented to the University of Waterloo
in fulfillment of the
thesis requirement for the degree of
Doctor of Philosophy
in
Vision Science

Waterloo, Ontario, Canada, 2025

© Mana Monfared 2025

Examining Committee Membership

The following served on the Examining Committee for this thesis. The decision of the Examining Committee is by majority vote.

External Examiner	Dr Shehzad A Naroo, PhD Professor at Aston University
Supervisor	Dr Paul J. Murphy, PhD Professor at University of Waterloo
Internal Members	Dr Lyndon W Jones, DSc, FCOptom Professor at University of Waterloo
	Dr William Ngo, OD, PhD Assistant Professor at University of Waterloo
	Dr Shamroze Khan, OD Associate Clinical Professor at University of Waterloo
Internal-External Member	Dr Dale Martin, PhD Assistant Professor at University of Waterloo

Author's Declaration

I hereby declare that I am the sole author of this thesis. This is a true copy of the thesis, including any required final revisions, as accepted by my examiners.

I understand that my thesis may be made electronically available to the public.

Abstract

Introduction

Evaporative Dry Eye (EDE), the most prevalent subtype of Dry Eye Disease (DED), is primarily driven by excessive tear loss from the ocular surface due to deficiencies in the tear film's lipid layer. Accurate and repeatable measurement of Tear Evaporation Rate (TER) and related ocular surface parameters, such as Ocular Surface Temperature (OST), Lipid Layer Thickness (LLT), and Non-Invasive Tear Break-Up Time (NITBUT) is essential for understanding tear film instability and guiding clinical decision-making. However, measurement variability, lack of standardized protocols, and limitations in existing instrumentation have hindered the adoption of TER and OST assessment in routine practice. This thesis addresses these challenges through a series of *in vitro* and *in vivo* experiments aimed at quantifying tear film dynamics and optimizing measurement methodologies.

Overall Aims

The primary aim of this research was to characterize tear evaporation and ocular surface thermal behavior under a range of physiological and controlled conditions. This thesis specifically sought to:

1. Quantify the evaporation rates of distilled water versus an aqueous artificial tear solution (TheraTears®) *in vitro*.
2. Assess how changes in exposed ocular surface area and LLT affect TER using model eyes.
3. Investigate the effect of lipid-based artificial tears on LLT, TER, and NITBUT *in vivo* (PHASE I).
4. Optimize OST measurement parameters using ResearchIR software to improve accuracy and reproducibility.

5. Examine regional variation in OST and blink-related cooling profiles *in vivo* (PHASE II).
6. Integrate *in vitro* and *in vivo* findings to build a comprehensive model of tear film dynamics with implications for EDE diagnosis.

Methods and Materials

The experiments were conducted using custom-built and commercially available devices. *In vitro* studies used aluminum model eyes with varied surface areas and lipid layer simulations (via CALMO® Eye Spray) to evaluate their effect on TER, measured using the Waterloo Evaporimeter. *In vivo* studies were performed on healthy participants using the LipiView® II interferometer, OCULUS Keratograph® 5M, and FLIR A655sc thermal camera integrated with ResearchIR software. Data collection included real-time measurements of TER, LLT, NITBUT, and OST, with particular focus on blink-related cooling and temperature gradient analysis. Each experiment followed standardized protocols for blink control, Region of Interest (ROI) selection, and repeatability validation. Statistical analysis was performed using SPSS, with significance set at $p < 0.05$.

Results

In vitro results demonstrated no significant difference in TER between distilled water and TheraTears®, suggesting that aqueous-based artificial tears do not provide meaningful evaporative protection. These findings also confirm that both distilled water and TheraTears® may be used interchangeably in laboratory-based evaporation studies where lipid content is not a critical variable. In contrast, increasing LLT using CALMO® spray led to a marked reduction in TER, and model eyes with larger surface areas consistently exhibited higher evaporation rates. *In vivo*, lipid eye drop instillation produced a significant increase in LLT, a prolongation of NITBUT, and a decrease in TER. OST monitoring revealed distinct blink-related cooling patterns, particularly in

eyes with thinner lipid layers. Optimized OST protocols using ResearchIR improved temporal resolution and reproducibility across participants. Phase II confirmed consistent regional temperature variability and strong correlations between LLT, TER, and post-blink cooling.

Conclusions

This research confirms that LLT and ocular surface area are critical determinants of TER. Non-lipid formulations, such as TheraTears®, are ineffective in limiting TER, while lipid-based interventions significantly improve tear film stability both thermally and structurally. OST can be used as a reliable, non-invasive surrogate for assessing tear film dynamics when measured with optimized protocols. The Waterloo Evaporimeter and ResearchIR-enabled thermography provide robust, reproducible platforms for studying tear evaporation and cooling responses. These findings support a multimodal diagnostic approach integrating TER, LLT, NITBUT, and OST for the evaluation and management of EDE.

Acknowledgements

First and foremost, I would like to express my deepest gratitude to my supervisor, **Dr. Paul Murphy**. He was far more than an academic advisor; he became a father figure to me in Canada. His profound wisdom, quiet strength, and unwavering support helped guide me through every challenge of this PhD journey. But more than that, *he taught me how to be a real human,* how to lead with integrity, to care deeply about others, and to face hardship with humility and strength. I will carry those lessons with me always. I am also immensely grateful to his wonderful wife, **Kathinka,** whose warmth and kindness have made me feel at home in a foreign land.

I am sincerely thankful to my committee members for their insight and encouragement**. Dr. Lyndon Jones** has been a pillar of knowledge and professionalism; I have learned so much from his critical eye, scientific precision, and generous mentorship. I also wish to extend my appreciation to **Dr. William Ngo** and **Dr. Shamroze Khan** for their valuable feedback and ongoing support throughout the development of this thesis.

Although not officially part of my committee, **Dr. Debbie Jones** has played a meaningful role in my journey. Her thoughtful guidance and genuine kindness made a lasting impression on me. She has been a role model and a comforting presence throughout my time here.

I would also like to acknowledge **Dr. Kristine Dalton**, who served as a graduate officer, but was much more than that to me. She supported me through countless challenges, not just with academic processes but with personal care and compassion.

To my lab mates and colleagues: thank you for making the research environment so collaborative and uplifting. **Dr. Ehsan Zarei Bidaki**, your advice and friendship were greatly appreciated. **Navid Shahsavari**, you were like a brother to me. Your constant help, positive energy, and support made even the hardest days lighter.

I am also grateful to the graduate students and members of **GIVS** for their camaraderie, and to **Angela Hare**, our coordinator, who went above and beyond to help without ever expecting anything in return. Her quiet dedication made many things easier behind the scenes.

Thank you to all the **patients and volunteers** who took part in my research- your participation was essential, and I am deeply thankful.

Finally, I want to express my profound gratitude to **my family**, who stood by me through every step of this journey. To my late mother, whose memory inspires me every day; to my dear father, whose love and encouragement from afar have kept me going. To my stepmother, Forough, thank you for being by his side and for your generosity of spirit. And to my wonderful brothers, Vahid and Hamid, I love you dearly, your belief in me has meant the world.

This thesis is not only the result of years of study and research, but also the product of the incredible people who supported me, intellectually, emotionally, and spiritually, along the way. I am forever grateful.

Dedication

To my mother

Your love is still my compass, even though you are no longer here. I carried your memory with me through every late night, every challenge, and every small victory. This work is a piece of you.

And to my father

Even from a distance, your quiet strength and belief in me gave me the courage to keep going. Thank you for standing by me in every way you could.

This journey has been for both of you.

Table of Contents

List of Figures……...xiv

List of Tables……...……xxvi

List of Abbreviations……xxx

Chapter 1 Introduction 1

Chapter 2 Literature Review 5

2.1 Tear Film 5

2.1.1 Structure 5

2.1.2 Function 8

2.2 Tear Film Evaporation 9

2.2.1 Factors Affecting the Rate of Tear Evaporation 12

2.2.2 Measurement of Tear Film Evaporation 15

2.2.3 Challenges in Measuring Tear Film Evaporation: Variability in Existing Methods .. 25

2.3 Ocular Surface Temperature 28

2.3.1 Significance of Ocular Surface Temperature Measurement 28

2.3.2 Measurement of Ocular Surface Temperature 29

2.3.3 Challenges in Measuring Ocular Surface Temperature: Variability in IR Thermography Methods 34

2.4 Rationale and Objectives 49

Chapter 3 Methodology 50

3.1 Waterloo Evaporimeter 50

3.1.1 Purpose and Background 50

3.1.2 Equipment and Experimental Setup 50

3.1.3 Experimental Procedure and Measurement Protocol 53

3.1.4 Data Analysis 57

3.2 ThermOcular Camera 58

3.2.1 Purpose and Background 58

3.2.2 Equipment and Experimental Setup 59

3.2.3 Experimental Procedure and Measurement Protocol 63
3.2.4 Data Analysis 65
3.3 ResearchIR® Software 66
3.3.1 Purpose and Background 66
3.3.2 Equipment and Experimental Setup 67
3.3.3 Data Analysis 71
3.4 LipiViewII® Ocular Surface Interferometer 72
3.4.1 Purpose and Background 72
3.4.2 Equipment and Experimental Setup 73
3.4.3 Data Analysis 76
3.5 OCULUS Keratograph 5M® 77
3.5.1 Purpose and Background 77
3.5.2 Equipment and Experimental Setup 78
3.5.3 Data Analysis 80
Chapter 4 Experiments 81
4.1 *In vitro* examination of distilled water versus TheraTears® 81
4.1.1 Overview 81
4.1.2 Materials and Methods 82
4.1.3 Results 88
4.1.4 Discussion 90
4.1.5 Limitations and Future Directions 92
4.1.6 Conclusion 93
4.2 *In vitro* evaporimetry of different of model eye sizes and lipid layer thicknesses 95
4.2.1 Overview 95
4.2.2 Materials and Methods 96
4.2.3 Results 102
4.2.4 Discussion 104
4.2.5 Limitations and Future Directions 105
4.2.6 Conclusion 106

4.3 Investigating Tear Film Dynamics Following Lipid Eye Drop Instillation (PHASE I).. 107
4.3.1 Overview 107
4.3.2 Materials and Methods 108
4.3.3 Results 117
4.3.4 Discussion 137
4.3.5 Limitations and Future Directions 138
4.3.6 Conclusion 140
4.4 Optimizing Measurement Parameters for OST Assessment Using ResearchIR Software 141
4.4.1 Overview 141
4.4.2 Materials and Methods 143
4.4.3 Results 149
4.4.4 Discussion 165
4.4.5 Limitations and Future Directions 169
4.4.6 Conclusion 171
4.5 Investigating Tear Film Dynamics Following Lipid Eye Drop Instillation (PHASE II) 172
4.5.1 Overview 172
4.5.2 Materials and Methods 173
4.5.3 Results 180
4.5.4 Spatial Variation in OST and Impact of ROI Size 196
4.5.5 Discussion 216
4.5.6 Limitations and Future Directions 218
4.5.7 Conclusion 220
Chapter 5 Discussion 221
5.1 Overview and Integration of Findings 221
5.2 Tear Film Lipid Layer. Functional Role in Evaporation Dynamics 222
5.3 Utility and Validation of Measurement Technologies 223
5.4 Artificial Tear Formulations and Evaporation Control 225
5.5 Inter-relationships between LLT, NITBUT, TER, and OST 227

5.6 Limitations 228
5.7 Conclusion 230
5.8 Novelty of the Thesis 231
References 233
Appendices 253

List of Figures

Figure 2-1: The tear film structure showing the mucins and galectin of the glycocalyx, soluble mucins and proteins in the muco-aqueous layer and the surface lipid layer[44] (Image from: Craig JP, Willcox MDP, Argüeso P, et al. The TFOS International Workshop on Contact Lens Discomfort: report of the contact lens interactions with the tear film subcommittee. Invest Ophthalmol Vis Sci. 2013;54(11): TFOS123-156. doi:10.1167/iovs.13-13235). 7

Figure 2-2: Schematic illustrating the physical factors involved in tear thinning leading to tear film break-up (touchdown of the lipid layer onto the glycocalyx). (Image created by the author). 10

Figure 2-3: Classification of evaporimeters based on chamber design (closed, open, semi-open) and ventilation type (ventilated, unventilated) (Image created by the author). 17

Figure 2-4: Transepidermal water loss measurement and a schematic overview of the open-chamber device measuring probe[148] (Image from: Fluhr JW, Darlenski R. Trans-Epidermal Water Loss (TEWL). In: Berardesca E, Maibach HI, Wilhelm KP, eds. Non-Invasive Diagnostic Techniques in Clinical Dermatology. Springer; 2014:353-356. doi:10.1007/978-3-642-32109-2_32). 19

Figure 2-5: A schematic design of DEvice© ocular hygrometer. The figure shows a side and rear view of the schematic representation of a mono sensor diagnostic prototype with: an eyepiece cup (10); the sensor (20) placed inside it; a processing board (30) equipped with processor (31), memory (34) and wireless connection device (32); the optional connection cable (33); a digital screen (40) with buttons (41); and a rechargeable power supply battery (50) placed in the handle.[149] (Image from: Gaudenzi D, Mori T, Crugliano S, et al. AS-OCT and Ocular Hygrometer as Innovative Tools in Dry Eye Disease Diagnosis. Applied Sciences. 2022;12(3):1647. doi:10.3390/app12031647). 21

Figure 2-6: The closed-chamber ventilated tear evaporimeter invented by Miguel F. Refojo and Maurizio Rolando[8] (Image from: Rolando M, Refojo MF. Tear evaporimeter for measuring water evaporation rate from the tear film under controlled conditions in humans. Experimental Eye Research. 1983;36(1):25-33. doi:10.1016/0014-4835(83)90086-6)..... 23

Figure 2-7: Modified ServoMed EP-3 (open-chamber, unventilated) evaporimeter measuring tear film evaporation using temperature and RH sensors [150](Image from: Trees GR, Tomlinson A. Effect of artificial tear solutions and saline on tear film evaporation. Optom Vis Sci. 1990;67(12):886-890. doi:10.1097/00006324-199012000-00002.)..... 25

Figure 2-8: Classification of infrared thermography (IRT) systems based on configuration and level of automation (Image created by the author). 35

Figure 2-9: Ocular surface marking and OST acquisition using the novel “diamond” method[185] (Image from: Tan LL, Sanjay S, Morgan PB. Static and Dynamic Measurement of Ocular Surface Temperature in Dry Eyes. J Ophthalmol. 2016;2016(1). doi:10.1155/2016/7285132). 36

Figure 2-102-10: Dual camera system introduced by Kamao et al. Internal camera architecture and mirror installation[186] (Image from: Kamao T, Yamaguchi M, Kawasaki S, Mizoue S, Shiraishi A, Ohashi Y. Screening for dry eye with newly developed ocular surface thermographer. Am J Ophthalmol. 2011;151(5):782-791). 47

Figure 3-1: Front view of the Waterloo Evaporimeter showing the cables that transmit real-time relative humidity (RH) and temperature data from the sensors inside the goggles to the Arduino Uno R3 microcontroller within the enclosed control box(Image created by the author). 51

Figure 3-2: Rear view of the Waterloo Evaporimeter. Three small holes have been drilled into the goggle. Two holes (yellow arrows) are for screws to attach sensors. The third hole allows air within the goggle to interact with the sensor (Image created by the author). 51

Figure 3-3: Data acquisition interface of the *Goggle* software for the Waterloo Evaporimeter, displaying real-time monitoring of RH and temperature changes for each goggle (right and left eyes). The software graphs RH trends over time while providing numerical data for precise analysis of tear evaporation dynamics (Image created by the author). 53

Figure 3-4: Experimental set-up for the Waterloo Evaporimeter, showing the fixation cross for gaze stabilization, digital temperature and RH monitor, evaporimeter goggles, data acquisition laptop running the *Goggle* software, and fan used for baseline RH restoration within the goggle between measurements (Image created by the author). 55

Figure 3-5: A study participant positioning the Waterloo Evaporimeter goggles for tear evaporation rate measurement (Image created by the author). 56

Figure 3-6: (A) Teledyne FLIR IR A655sc IR camera equipped with a germanium close-up lens for enhanced ocular imaging; (B) Standalone germanium close-up lens with protective casing, designed for high-precision IRT. Image source: Teledyne FLIR (www.flir.com). 60

Figure 3-7: (A) Teledyne FLIR BFS 51S5C-C machine vision camera, designed for high-speed, high-resolution imaging with a Sony IMX250 CMOS sensor; (B) Fujinon HF12.5SA-1 close-up lens, optimized for macro imaging and precise focus control, enhancing image clarity and field of view. Image source: Teledyne FLIR (www.flir.com). 61

Figure 3-8*:* Custom-modified slit-lamp biomicroscope equipped with the ThermOcular dual-camera system, integrating a Teledyne FLIR BFS 51S5C-C visible camera and a Teledyne FLIR A655sc IR camera for synchronized imaging. The set-up ensures precise alignment, stable fixation, and high-resolution OST measurement[214].(Image from: Bidaki EZ, Wong A, Murphy PJ. A novel system for ocular surface temperature measurement and tracking. *IEEE Access*. 2023;11:140893-140899. doi:10.1109/ACCESS.2023.3341354) 62

Figure 3-9: Synchronized imaging output from the ThermOcular system, displaying visible-light (left) and IR (right) eye images. The visible camera captures high-resolution anatomical details, while the IR camera recorded OST distribution, highlighting temperature variations across the eyelid and corneal region[214] (Image from: Bidaki EZ, Wong A, Murphy PJ. A novel system for ocular surface temperature measurement and tracking. *IEEE Access*. 2023;11:140893-140899. doi:10.1109/ACCESS.2023.3341354) 65

Figure 3-10: IR imaging analysis using ResearchIR software (Teledyne FLIR LLC, Wilsonville, OR, USA), displaying OST mapping of the same patient. The upper image uses a grayscale palette, while the lower image applies a colour palette to enhance temperature contrast (Image created by the author). 68

Figure 3-11: ResearchIR software (Teledyne FLIR LLC, Wilsonville, OR, USA) interface during ocular surface temperature recording. The "Record" button (top toolbar, red circle) is used to initiate thermal video capture. The real-time video stream is displayed in the main window, with tools for region-of-interest (ROI) selection, temperature monitoring, and data export options visible on the right panel (Image created by the author). 70

Figure 3-12: ROI selection in ResearchIR software (Teledyne FLIR LLC, Wilsonville, OR, USA), demonstrating three different methods for extracting temperature data: Cursor 1 (single pixel location), Cursor 2 (3×3 pixel average), and Ellipse 1 (custom region averaging multiple pixels). The software generates temporal temperature plots for each ROI, illustrating how temperature changes over time at each location (Image created by the author). 72

Figure 3-13: The LipiViewII Ocular Surface Interferometer (Johnson & Johnson Vision Care, Inc., Jacksonville, Florida, USA) showing the system initialization screen, and participants chin-rest/head-rest (Image created by the author). 74

Figure 3-14: A side view of the LipiViewII Ocular Surface Interferometer (Johnson & Johnson Vision Care, Inc., Jacksonville, Florida, USA), showing the camera system, chin-rest, and head-rest support (Image created by the author). 75

Figure 3-15: The LipiViewII Ocular Surface Interferometer (Johnson & Johnson Vision Care, Inc., Jacksonville, Florida, USA) displaying LLT measurement results. The screen shows a real-time interferometric image of the ocular surface, LLT values in nanometers, and a graphical representation of blink patterns and tear film stability analysis (Image created by the author). .. 77

Figure 3-16: OCULUS Keratograph 5M (Oculus GmbH, Wetzlar, Germany) system set up for non-invasive tear film analysis, including Placido ring topography, meibography, and NITBUT assessment. The system is integrated with a computer for real-time imaging and data analysis (Image created by the author). 79

Figure 4-1: The selected aluminum model eye with an exposed surface area of 1.75 cm^2, designed to simulate the human ocular surface for evaporation measurements. The elliptical aperture represents the exposed tear film (Image created by the author). 83

Figure 4-2: Laboratory oven (Fisher Scientific) used to precondition the model eye and test solutions (distilled water and TheraTears®) to 34°C, simulating physiological OST before evaporation measurements (Image created by the author). 85

Figure 4-3: Controlled environment chamber (Model 5503-11 Package E, Electro-Tech Systems Inc.) used to maintain stable temperature (34°C) and RH (40%) during evaporation measurements. The chamber is equipped with the Waterloo Evaporimeter, a heating plate, and a digital monitoring system to ensure precise experimental conditions (Image created by the author)..... 85

Figure 4-4: Mean ERs for distilled water and TheraTears®, presented as mean ± SD (n = 8 per group). No statistically significant difference was observed between the two conditions (p = 0.292, Paired t-test). 89

Figure 4-5: Real-time RH trend (in seconds) inside the Waterloo Evaporimeter goggle for distilled water and TheraTears®. 90

Figure 4-6: The two selected model eye sizes: 1.25 cm² (left) and 2.5 cm² (right) used for the experiment (Image created by the author). 97

Figure 4-7: CALMO® Eye Spray Packaging[234] (Image from: CandorVision. Calmo Eye Spray Packaging [Internet]. Montreal: CandorVision; [cited 2025 Mar 13]. Available from: https://www.candorvision.com/calmo-eye-spray) 98

Figure 4-8: Top view of the modified swimming goggles, with arrows indicating the small holes drilled into each eyepiece chamber. These openings facilitated the addition of saline, enabling precise measurement of the chamber volume (Image created by the author).....113

Figure 4-9: Representative ImageJ analysis of PAS measurement. The exposed ocular surface area was delineated manually using the Polygon Selections Tool in the ImageJ software (v1.52k, NIH, USA), with vertices placed along the upper and lower eyelid margins. A calibration ruler was included in the field of view to enable precise scaling and quantification of the enclosed area in square centimeters (cm²) (Image created by the author).....115

Figure 4-10: Boxplot representation of LLT before and after lipid drop instillation (n=23). A statistically significant increase in LLT was observed following instillation (Wilcoxon Signed-Rank test, $p < 0.001$). LLT values are presented as median and interquartile range due to non-normal distribution. The median line for the After Instillation condition overlaps with the top edge

of the box due to a ceiling effect at 100 nm, the maximum measurable limit of the LipiView II device. 121
Figure 4-11: Bar graph illustrating the change in mean ± SD NITBUT First Measurement before and after lipid drop instillation (n=23). A statistically significant decrease in NITBUT First was observed after drop instillation (paired t-test, p = 0.008). 122
Figure 4-12: Bar graph illustrating the change in mean ± SD TER before and after lipid drop instillation (n=23). A statistically significant increase in TER was observed post-instillation (paired t-test, p = 0.019). 123
Figure 4-13: Pairwise scatter plots with regression lines showing relationships among changes in LLT, first and average NITBUT, and TER following lipid eye drop instillation (n = 23). Pearson correlation coefficients revealed no statistically significant relationships among LLT, NITBUT, and TER changes. Only the relationship between NITBUT first and average changes was significant (r = 0.94, p < 0.001). Shaded areas represent 95% confidence intervals. 125
Figure 4-14: Scatter plots with regression lines illustrating the relationship between TER change and PAS and VIG (n = 23). Pearson correlation analysis showed a weak positive correlation between PAS and TER change (r = 0.150), and no meaningful correlation between VIG and TER change (r = -0.021). Shaded regions represent 95% confidence intervals; neither relationship was statistically significant. (TER change = post-instillation TER – pre-instillation TER). 127
Figure 4-15: Correlation heatmaps for Low LLT (left, n = 11) and High LLT (right, n = 14) groups, illustrating relationships among changes (post–pre) in LLT, NITBUT First, NITBUT Average, and TER following lipid eye drop instillation. Strong correlations (r > 0.92) were observed only between NITBUT First and NITBUT Average in both groups. Correlations involving LLT and TER were weak and not statistically significant. 132

Figure 4-16: Correlation heatmaps for Low RH (left, n = 12) and High RH (right, n = 13) groups, illustrating relationships among LLT change, NITBUT (first and average) change, and TER change following lipid drop instillation. LLT correlations (Spearman's rank) with other parameters were weak and non-significant in both groups. Strong positive Pearson correlations were observed only between NITBUT First and Average changes ($r \geq 0.93$, $p < 0.001$) in both RH groups. 136

Figure 4-17: Simulated OST cooling profiles following a blink during short (5 sec) and long (15 sec) IBIs. 142

Figure 4-18: OST measurement locations: Superior Cornea (1), Temporal Cornea (2), Inferior Cornea (3), Nasal Cornea (4), and Central Cornea (5); Circular Central Region (average OST over a defined area of a circle with a 2 cm diameter) (6); Temporal Sclera (7), and Nasal Sclera (8) (Image created by the author). 147

Figure 4-19: Standardized ROI selection using a clear overlay template to ensure consistent placement across participants. The corneal ROIs (red markers) were aligned at a uniform location by referencing the canthus of the eye, while the scleral ROIs (yellow markers) were positioned at fixed distances from the corneal center (Image created by the author). 148

Figure 4-20: RTC across interblink intervals (n = 7), shown as mean ± SD for Location 5 (Central Cornea). Significant differences were found across intervals ($p < 0.001$, repeated-measures ANOVA), with 2 sec showing the steepest decline. Error shading represents SD; 2 sec differed significantly from all longer intervals. 153

Figure 4-21: Scatter plot of RTC vs. IBI (n = 7) for Location 5 (Central Cornea). A significant negative correlation was observed ($r = –0.64$, $p < 0.001$), indicating that longer IBIs are associated with slower cooling. Shaded area shows 95% CI. 154

Figure 4-22: Examples of OST temperature traces at the center of the cornea for different IBIs. 155

Figure 4-23: RTC distribution for corneal vs. scleral regions across all IBIs (n = 7). RTC was significantly greater in corneal locations compared to scleral (Wilcoxon signed-rank test W = 0.000, p = 0.016). Boxes show median and IQR. 158

Figure 4-24: Mean RTC correlation among corneal locations across IBIs (n = 7). The highest correlation at 6 sec IBI suggested synchronized temperature changes, while decreasing correlation at longer IBIs indicates increasing thermal variability. 159

Figure 4-25: Heatmaps of RTC correlation across cursor locations at different IBIs (n = 7). Strong correlations (red) indicate synchronized temperature changes, while weaker correlations (blue) reflect increasing thermal variability. 161

Figure 4-26: ICC values for RTC across individual cursors (orange) and cursor combinations (blue). All combinations exceeded the high-reliability threshold (ICC ≥ 0.9), while single cursors ranged from moderate to high reliability. Cursor 5 was the most reliable individual location... 163

Figure 4-27: ICC values for RTC based on the number of sequences averaged. Averaging 3 sequences yielded the highest reliability (ICC = 0.91), surpassing the high-reliability threshold (dashed line). 165

Figure 4-28: LLT before, 5 min after, and 20 min after drop (n = 27), shown as median and IQR. LLT increased significantly from baseline to 5 min ($p < 0.001$) and remained significantly elevated at 20 min ($p = 0.002$). No significant difference was found between 5 and 20 min ($p = 0.513$). 186

Figure 4-29: NITBUT (first) before, 5 min after, and 20 min after drop (n = 27), shown as mean ± SD. A statistically significant reduction was observed from baseline to 20 min ($p = 0.005$). Changes

between baseline and 5 min (p = 0.214) and between 5 and 20 min (p = 0.127) were not significant. 188

Figure 4-30: NITBUT (average) before, 5 min after, and 20 min after drop (n = 27), shown as mean ± SD. A statistically significant reduction occurred from baseline to 20 min (p = 0.007). No significant difference was found between baseline and 5 min (p = 0.290) or between 5 and 20 min (p = 0.166)..... 189

Figure 4-31: TER before, 5 min after, and 20 min after drop (n = 27), shown as mean ± SD. TER increased significantly from baseline to 5 min (p < 0.001) and from baseline to 20 min (p = 0.007). No significant difference was found between 5 and 20 min (p = 0.939). 191

Figure 4-32: Pairwise scatter plots with regression lines showing relationships among changes in LLT, NITBUT (first and average), and TER at 5 min after drop instillation (n = 27). Shaded areas represent 95% confidence intervals. A strong correlation was found between NITBUT first and average change (r = 0.94, p < 0.001). NITBUT first changes was significantly and negatively correlated with TER change (r = –0.50, p = 0.0082). 194

Figure 4-33: Pairwise scatter plots with regression lines and 95% confidence intervals showing relationships among changes in LLT, NITBUT (first and average), and TER at 20 min after drop instillation (n = 27). A strong correlation was observed between NITBUT first and average change (r = 0.86, p < 0.001). Other relationships, including those between LLT and NITBUT or TER, and between NITBUT and TER, were not statistically significant. 195

Figure 4-34: Concentric ROIs used for measuring RTC. Each ring represents a different ROI size, ranging from 1 pixel to 516 pixels. 197

Figure 4-35: Boxplot illustrating RTC across six concentric ROI sizes (1, 9, 52, 104, 208, and 516 pixels), derived from OST measurements (n = 27). Median RTC values and interquartile ranges remained consistent across ROI sizes. 199
Figure 4-36: Schematic of vertically aligned 5×5-pixel ROIs used to measure RTC. 201
Figure 4-37: Boxplot illustrating RTC distribution across vertical corneal locations (S2, S1, Center, I1, and I2), derived from OST measurements (n = 27). Median RTC values and interquartile ranges remained consistent across vertical corneal locations, with slightly greater variability observed in superior regions. 203
Figure 4-38: Correlation heatmap of RTC across five vertically aligned ocular surface ROIs (n = 27). Stronger correlations (shown in red) indicate more synchronized temperature changes between regions, while weaker correlations (blue) reflect greater regional thermal variability. 205
Figure 4-39: Linear regression analysis of mean RTC values across five vertically aligned corneal locations (from superior to inferior: S2, S1, Center, I1, I2). The regression revealed no statistically significant linear gradient (slope = 0.001, r = 0.36, p = 0.556), indicating minimal spatial variation in RTC under the current measurement conditions. Shaded areas represent the 95% confidence interval of the regression line. 206
Figure 4-40: Interaction effect of time and location on RTC. Line plot of mean RTC across 6 seconds at each vertical ROI (n = 27). Error bars shown with shadings represent standard deviation. 208
Figure 4-41: RTC across five corneal regions measured at six 0.5-second intervals. Values represent mean RTC (n = 27) from 0 to 3 seconds. Error bars shown with shadings represent standard deviation. 212

Figure 4-42: Mean RTC across five vertical corneal regions over a 6-second IBI, combining 0.5-sec and 1-sec interval data (n = 27). Shaded regions represent initial slope deceleration (blue) and evaporative cooling phase (pink). 216

List of Tables

Table 2-1: Reported thickness ranges of the tear film and its individual layers, based on various imaging and analytical techniques from the literature. Values vary depending on measurement method, blink timing, and anatomical location. 7

Table 2-2: Comparative overview of IRT-based OST measurement protocols, showing differences in ROI selection, measurement durations, and imaging modalities across key investigations. 38

Table 4-1: Specifications of TheraTears® lubricant eye drops 86

Table 4-2: Comparison of evaporation rates between distilled water and TheraTears®. 88

Table 4-3: Specifications of CALMO Eye Spray 99

Table 4-4: Distribution of water and CALMO® Eye Spray volumes for each LLT condition in the 1.25 cm^2 and 2.5 cm^2 model eyes. The total volume of each model eye was maintained constant, with increasing sprays representing progressively thicker lipid layers, and the corresponding water volume adjusted accordingly. 101

Table 4-5: Mean ER ± SD across different LLT conditions for the 1.25 cm^2 and 2.5 cm^2 model eyes. 103

Table 4-6: Two-way ANOVA results assessing the main effects of LLT, model eye size, and their interaction on ER. 103

Table 4-7: Specifications of Systane Complete® lipid eye drop. 110

Table 4-8: Specifications of Sensitive Eyes® Saline Plus Solution 114

Table 4-9: Summary of the experimental procedure of the study. 116

Table 4-10: Participant demographics and environmental conditions. 118

Table 4-11: Tear film characteristics before and after lipid drop instillation 119

Table 4-12: Normality analysis of tear film characteristics (Shapiro-Wilk test). 119

Table 4-13: Summary table of inferential statistical analysis 120

Table 4-14: Correlation analysis of changes in LLT, NITBUT, and TER..... 124

Table 4-15: Correlation analysis between PAS, VIG, and TER change. (TER change = post-instillation TER – pre-instillation TER)..... 126

Table 4-16: LLT Group distribution based on baseline LLT measurements. 129

Table 4-17: Descriptive statistics of tear film parameter changes in low LLT and high LLT groups. 130

Table 4-18: Wilcoxon signed-rank (LLT) and paired t-test (NITBUT, TER) comparisons of tear film parameters before and after lipid drop instillation in Low LLT and High LLT groups. 131

Table 4-19: RH group distribution based on baseline ambient relative humidity measurements. 134

Table 4-20: Descriptive statistics of tear film parameter changes in low RH and high RH groups. 134

Table 4-21: Wilcoxon signed-rank (LLT) and paired t-test (NITBUT, TER) comparisons of tear film parameters before and after lipid drop instillation in Low RH and High RH groups. 135

Table 4-22: Blinking protocol with predefined IBIs and rest periods for OST measurement. ... 145

Table 4-23: Mean RTC and ΔT (± SD) at the center of the cornea for different IBIs. 150

Table 4-24: Normality test results (Shapiro-Wilk test) for RTC and ΔT. 150

Table 4-25: Repeated measures ANOVA results for RTC and ΔT..... 151

Table 4-26: Tukey's HSD results for RTC 152

Table 4-27: Mean ± SD of RTC across different IBIs at various corneal and scleral locations . 156

Table 4-28: Shapiro-Wilk normality test results for RTC values at each corneal location 157

Table 4-29: ICC values for averaged and single cursor measurements 162

Table 4-30: ICC for RTC measurements..... 164

Table 4-31: Summary of the experimental procedure of the study. 178
Table 4-32: Participant demographics and environmental conditions 180
Table 4-33: Tear film characteristics before and after lipid drop instillation 181
Table 4-34: Normality analysis of tear film characteristics (Shapiro-Wilk test) 182
Table 4-35: Summary table of inferential statistical analysis 184
Table 4-36: Results of the post-hoc analysis comparing LLT measurements across three different time points 185
Table 4-37: Results of the post-hoc analysis comparing NITBUT measurements across three different time points 187
Table 4-38: Results of the post-hoc analysis comparing TER measurements across three different time points. 190
Table 4-39: Correlation analysis of changes (5 minutes post-instillation) 192
Table 4-40: Correlation analysis of changes (20 minutes post-instillation) 192
Table 4-41: RTC descriptive statistics across ROI sizes. 198
Table 4-42: Descriptive statistics for the RTC across five vertically aligned ocular surface ROIs. 202
Table 4-43: Pairwise Wilcoxon signed-rank tests comparing RTC across five vertically aligned ROIs. 205
Table 4-44: Friedman test results comparing RTC across 6-time intervals for each vertical ROI (25-pixel) 209
Table 4-45: Statistically significant pairwise Wilcoxon signed-rank test with Bonferroni correction comparisons of RTC across six one-second intervals at the S1 corneal region. Only comparisons with p-values less than 0.05 are shown. 210

Table 4-46: Friedman test results comparing RTC across 0.5-second intervals at each ROI. 213

Table 4-47: Statistically significant Wilcoxon signed-rank test comparisons across 0.5-second intervals at I1 and I2 ROI. 214

List of Abbreviations

°C	Degrees Celsius
%	Percent
ANOVA	Analysis of Variance
cm / cm^2 / cm^3	Centimeter / Square Centimeter / Cubic Centimeter
DED	Dry Eye Disease
EDE	Evaporative Dry Eye
ER	Evaporation Rate
$g/cm^2/s$	Grams per Square Centimeter per Second
$g/m^2/h$	Grams per Square Meter per Hour
HSD	Honestly Significant Difference
IBI	Inter Blink Interval
ICC	Intraclass Correlation Coefficient
IQR	Interquartile Range
IR / IRT	Infrared / Infrared Thermography
I1/I2	Inferior 1/ Inferior 2
LLT	Lipid Layer Thickness
LMM	Linear Mixed-Effects Model
LogMAR	Logarithm of the Minimum Angle of Resolution
MATLAB	MATrix LABoratory
MGD	Meibomian Gland Dysfunction
mN/m	Millinewtons per Meter
NITBUT	Non-Invasive Tear Break-Up Time
PAS	Palpebral Aperture Size
OCRNet	Object-Contextual Representations for Semantic Segmentation

OST	Ocular Surface Temperature
RH	Relative Humidity
ROI	Region of Interest
RTC	Rate of Temperature Change
SD	Standard Deviation
SPSS	Statistical Package for the Social Sciences
S1/ S2	Superior 1/ Superior 2
TBUT	Tear Break-Up Time
TER	Tear Evaporation Rate
TFLL	Tear Film Lipid Layer
TFOS	Tear Film & Ocular Surface Society
ΔT	Absolute Temperature Change
µl / µm	Microliter / Micrometer
VA	Visual Acuity
VIG	Volume Inside Goggle
vs.	Versus

Chapter 1 Introduction

Dry eye disease (DED) is a common ocular surface disorder affecting an estimated 5-50% of the global population, with prevalence rising to 10–20% in adults over the age of 40.[1–3] The high prevalence of DED places a considerable burden on public health systems and society at large. The economic burden of DED is substantial. Yu et al. reported that DED costs the U.S. economy approximately US $11,302 per patient each year, mainly due to reduced work productivity and additional healthcare needs.[4] A more recent Canadian study estimated that DED costs each patient about C $24,331 per year, with higher costs seen in more severe cases. Most of this burden came from time missed at work and reduced efficiency while working due to eye discomfort.[5]

The Tear Film and Ocular Surface Society Dry Eye Workshop II (TFOS DEWS II) classifies DED into three primary categories: aqueous deficient, evaporative, and mixed. Among these, the evaporative sub-type (EDE) is the most prevalent, accounting for over 86% of cases, and is predominantly linked to meibomian gland dysfunction (MGD).[6] Tear film instability and excessive tear evaporation are hallmark features of this condition, contributing to symptoms of eye dryness and irritation, blurred vision, and ocular surface damage.

In response to these clinical challenges, the TFOS DEWS II report highlighted the need for reliable, objective methods to measure tear evaporation, recognizing evaporation as a core feature of disease pathophysiology.[7] A key tool in this effort is evaporimetry, a non-invasive technique that quantifies the rate of aqueous tear loss from the ocular surface by monitoring changes in relative humidity (RH) in the air immediately in front of the eye.[4–7] Evaporimetry not only provides insight into tear film behavior, but also assists in diagnosing DED and evaluating therapeutic interventions, especially for EDE.[12–22]

Within the broader framework of tear film diagnostics, ocular surface temperature (OST) has emerged as a valuable parameter for assessing tear film dynamics.[23–26]

However, beyond a general physiological relevance, OST is directly linked to rate of evaporation from the tear film.[27] As water molecules evaporate from the tear film, they absorb latent heat, which enables them to leave the liquid, leading to surface cooling. This cooling effect is more pronounced when the superficial lipid layer is deficient or unstable, making OST an indirect yet sensitive marker of tear film evaporation.[27,28] Studies have demonstrated that a thinner lipid layer correlates with steeper post-blink temperature declines, while thicker, more stable layers preserve thermal integrity. [27–29] Thus, OST could be used alongside evaporimetry and non-invasive tear break-up time (NITBUT) to build a multi-dimensional profile of tear film stability.

The measurement of OST has benefited greatly from technological advances in infrared thermography (IRT). Earlier systems relied on static image capture and manual region of interest (ROI) selection, which were subject to observer bias and limited reproducibility.[30] The development of computer-assisted software platforms, such as ResearchIR (FLIR Systems, Wilsonville, OR, USA), has transformed OST analysis.[31] These platforms offer automated ROI selection, real-time frame-by-frame tracking, and advanced statistical outputs, enabling researchers to capture dynamic blink-related cooling effects and regional temperature variations with high accuracy.[31,32] The integration of ResearchIR with high-resolution IR cameras (e.g., FLIR A655sc) allows for high-speed ocular IRT, providing the granularity required to detect subtle differences in tear film behavior.[27,30] IRT has proven particularly valuable in DED diagnostics, where blink-induced cooling rates and OST gradients provide clinically relevant markers of evaporative loss and tear film disruption.

Complementing these thermal and evaporative metrics, NITBUT serves as a crucial measure of tear film resilience and optical integrity.[33] Devices such as the OCULUS Keratograph 5M® utilize near-infrared radiation Placido ring projection to measure NITBUT, offering a dye-free, repeatable alternative to traditional tear break-up time (TBUT) methods. This approach provides spatially and temporally resolved information on tear film disruption, helping to characterize evaporative loss and ocular surface instability with greater sensitivity. Numerous studies have established a strong correlation between shortened NITBUT and increased evaporation, reinforcing its diagnostic value in EDE.[27]

At the heart of tear film stability is the lipid layer, which acts as the primary evaporation barrier. Secreted by the meibomian glands, this layer is composed of non-polar and polar lipids that spread over the aqueous-mucus layer during blinking, reducing moisture loss and stabilizing the film.[6,34] In cases of MGD or lipid layer deficiency, evaporation can increase by 4 to 17 times, accelerating tear break-up and worsening symptoms.[35–37]

Consequently, the accurate assessment of lipid layer thickness (LLT) is critical for diagnosing and managing EDE. Traditional methods lacked objectivity and reproducibility, but recent advances, particularly in interferometric imaging, have enabled nanometer-level quantification of LLT. The LipiView® II Ocular Surface Interferometer (Johnson & Johnson Vision Care, Inc., Jacksonville, FL, USA) is one such device. It uses white-light interferometry to evaluate LLT, and near-infrared radiation to assess meibomian gland structure and function, facilitating a comprehensive analysis of tear film health.

Together, these measurement technologies of evaporimetry, OST analysis, NITBUT, and LLT imaging offer a robust, objective framework for studying the dynamics of the tear film and the

pathophysiology of DED. This thesis builds on these tools to explore the relationship between evaporation, lipid supplementation, and tear film stability, both *in vitro* and *in vivo*.

Chapter 2 Literature Review

This chapter reviews existing literature on the tear film's structure and functions, highlighting the crucial role of the tear film in maintaining ocular health and preventing evaporation-related tear loss. It examines the mechanisms and influential factors of tear film evaporation, relevant to DED. The review assesses various evaporimeters, categorized by their chamber design and ventilation methods, discussing their applications, advantages, and methodological inconsistencies. Additionally, it covers OST measurement, particularly IRT, noting advancements and remaining challenges. Lastly, it identifies gaps in current methodologies, establishing a foundation for the research objectives.

2.1 Tear Film

2.1.1 Structure

The tear film was originally thought to consist of three layers: lipid, aqueous, and mucus.[38] The outermost lipid layer, produced by meibomian glands in the eyelids, plays a key role in protecting the eye. These glands, located just behind the eyelashes, release meibum during blinking, which helps distribute the lipids evenly over the eye's surface.[20] This layer is made up of lipids such as sterol esters, wax esters, cholesterol, fatty acids, and fatty alcohols.[39–41] It has a two-part structure, with a thick, non-polar outer phase over a polar base layer.[42] Beneath the lipid layer lies the aqueous layer, a watery component secreted by the lacrimal glands. The innermost layer, made of mucus, is formed by goblet cells in the conjunctiva.[43]

Modern research has replaced the three-layer model with a more integrated view. The tear film is now described as being composed of a thin lipid layer covering an aqueous-mucin gel phase that connects to transmembrane mucins in a corneal epithelial bound glycocalyx.[44] Figure 2-1

illustrates this contemporary understanding of tear film architecture, highlighting the surface lipid layer, the muco-aqueous phase, and the underlying glycocalyx.

The aqueous-mucin layer forms the bulk of the tear film and contains proteins, electrolytes, glucose, oxygen, and gel-forming mucins.[45,46] Mucins are concentrated close to the corneal surface,[47] where the glycocalyx is securely bound to microvilli on corneal and conjunctival epithelial cells.[45,46]

Reports on the thickness of the total tear film vary widely, ranging from 2.7 to 46 μm.[44,45,48–54] The lipid layer is the thinnest, measuring between 13 nm and 170 nm,[44,45,55–58] with values falling between 32 nm and 46 nm[59] or 61.8 nm and 75.5 nm.[57] Aqueous layer thickness ranges from 2.2 to 7 μm,[46,60] while the aqueous-mucin layer is thought to be between 3.8 to 4.2 μm thick.[58] The glycocalyx mucin layer, which is around 1 μm thick over the conjunctiva,[29] may contribute significantly to the overall tear film thickness according to some studies.[49] A summary of the reported thickness ranges for each tear film layer, along with associated references, is presented in Table 2-1 to facilitate clearer comparison and interpretation.

Reported differences in tear film thickness can arise due to variations in testing methods, how invasive the method used for measuring thickness is, and the time since the last blink. A detailed overview of techniques used to measure tear film thickness can be found in Bai and Nichols' review.[61]

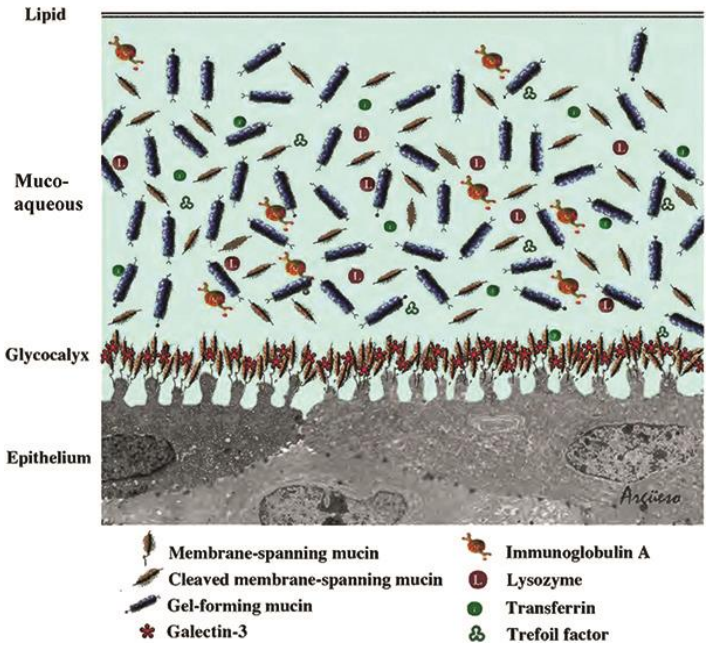


Figure 2-1: The tear film structure showing the mucins and galectin of the glycocalyx, soluble mucins and proteins in the muco-aqueous layer and the surface lipid layer[44] (Image from: Craig JP, Willcox MDP, Argüeso P, et al. The TFOS International Workshop on Contact Lens Discomfort: report of the contact lens interactions with the tear film subcommittee. Invest Ophthalmol Vis Sci. 2013;54(11): TFOS123-156. doi:10.1167/iovs.13-13235).

Table 2-1: Reported thickness ranges of the tear film and its individual layers, based on various imaging and analytical techniques from the literature. Values vary depending on measurement method, blink timing, and anatomical location.

Layer	**Reported Thickness**
Lipid layer	13 - 170 nm [45,55–58,62]
Aqueous layer	2.2 - 7 µm [46,60]
Aqueous-mucin layer	3.8 - 4.2 µm [58]
Mucin/glycocalyx layer	~1 µm [29,49]
Total tear film	2.7 - 46 µm [44,45,48–54]

2.1.2 Function

The tear film plays a crucial role in maintaining ocular health and function by performing several essential tasks. It creates a smooth optical interface between the cornea and the external environment, facilitating clear vision.[63–65] Additionally, it provides lubrication to ensure that the eyelids move effortlessly over the ocular surface during each blink.[46,66] By mechanically removing dust and debris with every blink, the tear film helps maintain the hygiene of the eye.[67,68] It also defends the eye against pathogens by utilizing proteins, antibodies, and phagocytic cells as part of its protective mechanisms.[66,69] Furthermore, the tear film nourishes the corneal epithelium with vital components such as oxygen, glucose, and vitamins, while removing metabolic byproducts, including carbon dioxide and lactate, from the cornea.[70]

Each layer of the tear film contributes uniquely to its overall functionality. The lipid layer primarily prevents evaporation of the inner layers, with studies showing that evaporation occurs 4 [35,36] to 17 times faster[37] when this layer is absent. The lipid layer non-polar phase serves as a reservoir for wax and cholesterol esters and regulates the exchange of water vapor, oxygen, carbon dioxide, and ions.[42] The polar phase stabilizes the lipid layer by orienting the hydrophilic molecular heads toward the aqueous layer, which is vital for maintaining lipid layer structure and integrity.[71] The lipid layer also acts as a barrier against dust particles, protecting the ocular surface.[46] The aqueous layer ensures hydration of the ocular surface, clears debris, nourishes epithelial cells, and provides defense against infections through antibacterial proteins like lysozyme.[38,46] Mucins play a significant role in stabilizing the tear film, reducing friction during blinking, smoothing the optical surface, aiding in the spread of the lipid and aqueous layers, and helping to clear debris and pathogens.[44,45,72] Supporting the entire tear film structure, the glycocalyx layer provides additional stability and integrity.[46]

For a more in-depth exploration of the tear film's structure and functions, detailed discussions can be found in the TFOS DEWS II Pathophysiology report[56] and the CLEAR report on the anatomy and physiology of the anterior eye.[45]

2.2 Tear Film Evaporation

Tear evaporation refers to the continuous loss of water from the tear film into the surrounding air. It is a normal physiological process that helps drive tear dynamics. Low to moderate levels of tear evaporation are thought to stimulate regular blinking and tear secretion to keep the eye surface moist.[73] During the interblink interval (IBI), some tear fluid evaporates, which gradually increases the tear film's salt concentration (osmolarity); if a blink is delayed for too long, the tear film can thin sufficiently that dry spots (tear film break-up) develop on the cornea.[74] Blinking restores the balance by spreading fresh tears over the exposed eye surface and re-forming the tear film layers, which refreshes the moisture and resets the evaporation cycle.[74] Thus, under normal conditions, evaporation and tear replenishment work together to maintain a stable ocular surface.

Tear film evaporation is largely controlled by the quality and structure of the outer lipid layer. As reported, the lipid layer acts as an evaporation barrier to significantly slows moisture loss from the eye. To understand the changes in the lipid layer during this process, it is helpful to consider the effect of blinking on the tear film. During eye closure, the lipid layer is swept downward with the movement of the eyelid and is compressed into a small space (Kessing's space) that is formed on eyelid closure behind the upper eyelid and the globe.[75] From this reservoir, the lipid is drawn back over the tear film aqueous/mucin gel during eyelid opening. This action spreads the lipid over the eye and reforms the tear film.[76] Ideally, the lipids are evenly spread over the aqueous/mucin gel, since this will enhance overall tear film stability. Once the tear film has stabilized after the reforming process of blinking, evaporation from the tear film begins to have an effect. This causes

a reduction in the aqueous layer volume and a thinning of the tear film. As evaporation continues, the lipid layer is drawn ever closer to the underlying mucous until the lipid layer lies on top of the foundational glycocalyx and tear film break-up occurs at that location.[77] Figure 2-2 illustrates the physical processes involved in tear film thinning and eventual break-up, emphasizing the role of lipid layer collapse and its interaction with the glycocalyx.

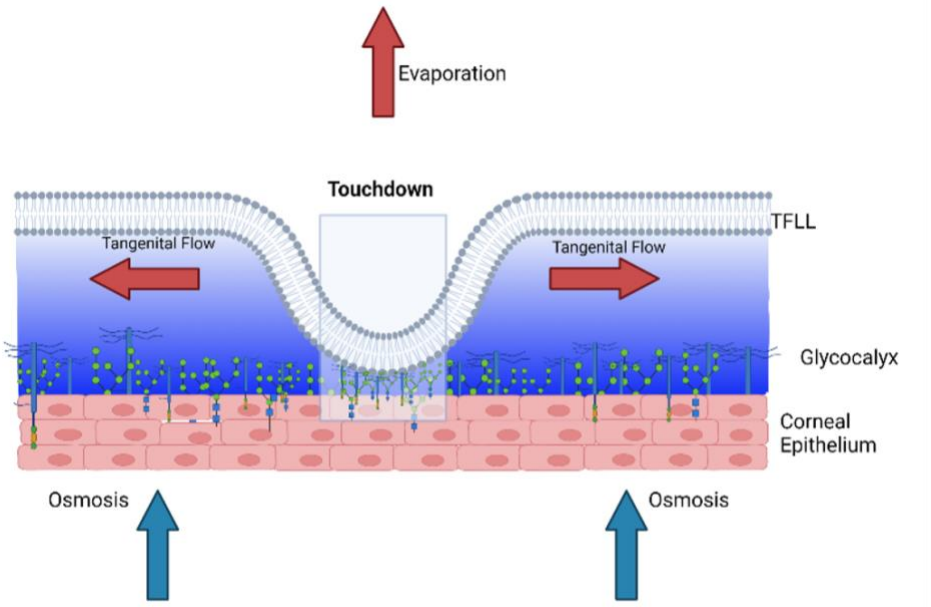


Figure 2-2: Schematic illustrating the physical factors involved in tear thinning leading to tear film break-up (touchdown of the lipid layer onto the glycocalyx). (Image created by the author).

However, variations in the lipid composition and chemistry produce variation in the thickness of the lipid layer, and in this variation lies the seed of increased tear film instability. A key feature of the lipid layer is its surface tension, but as tear evaporation occurs, the surface tension accentuates any variations in lipid composition to produce areas of thinner lipid layer.[78–80]At this point, the effect of evaporation from the tear film becomes more pronounced in those areas with a thinner lipid layer, and the tear film thins more rapidly leading to earlier ‘touchdown’ of the lipid layer in

that area. ‘Touchdown’ occurs when the inner polar molecules of the lipid layer touch the glycocalyx of the corneal epithelium.[77,81] Tear thinning is also affected by other physical forces within the tear film, such as osmotic flow, Marangoni forces, and diffusion, which further influence the rate of tear thinning. A fuller explanation of the processes involved can be found in the article by King-Smith et al.[77]

The time duration over which the tear film is undergoing evaporative tear loss, but before a touchdown of the lipid layer has occurred, is described as the tear break-up time (TBUT). TBUT describes the time period between a tear film reforming blink to the first appearance of a breakdown in the tear film stability. Imaging of the breakdown can be achieved using a variety of methods including fluorescein dye instillation, lipid layer interference pattern, and mire reflection distortion.[82–84] A normal TBUT depends on the method of measurement, but can range from 3 to 132 seconds, with an average of 27 seconds.[85] The structural integrity of the tear film is maintained by involuntary blinks. Studies have shown that the average spontaneous blink rate in normal individuals ranges from 6 to 20 blinks per minute, corresponding to an interblink interval of approximately 3 to 10 seconds, depending on factors such as task demand, lighting, and ocular surface condition[86–89] A problem can develop, however, if the break-up time is shorter than the IBI. When this occurs, the ocular surface will experience short periods of drying that stresses the ocular surface epithelia and can produce symptoms of discomfort.[90,91] Keeping the eyes open for a prolonged period of time, even for someone with good tear stability, will also distort the stability of the tear film, and produce randomly distributed breaks in the tear film.[92,93]

Empirical findings align with this perspective, revealing that the addition of a lipid layer can reduce evaporation by approximately 20–30%.[61] Notably, human tears evaporate at substantially lower rates than pure water under the same conditions (e.g. 34 °C at 30% RH)[96], indicating that the tear

film's composition (lipid layer) helps resist evaporation. By contrast, introducing tear proteins or mucins has virtually no effect on evaporation rates.[94] Consequently, a deficient or absent lipid layer leads to much faster tear evaporation, causing the tear film to break up far more quickly (i.e. greatly reduced TBUT) and resulting in an unstable tear film.[35,97]

Environmental conditions significantly influence how quickly the tear film evaporates. Key factors include ambient RH, temperature, and air flow, all of which must be carefully controlled when assessing tear evaporation.[98] The factors influencing the rate of tear evaporation are comprehensively examined in the following section.

2.2.1 Factors Affecting the Rate of Tear Evaporation

2.2.1.1 Ocular factors

The tear evaporation rate (TER) is heavily influenced by the tear film's quality and stability, which is greatly determined by the thickness and quality of the lipid layer.[99] This is because the aqueous layer is protected by the lipid layer from evaporation. If the lipid layer is removed or thinned, water molecules are more able to escape from the underlying aqueous layer.

Generally, when a larger ocular surface area is exposed to the atmosphere, there is a greater opportunity for more water molecules to escape to the air and, therefore, a higher TER will occur.[100] Besides inherent eye size and palpebral aperture variations in the population, eye gaze position also has an effect. In eye up-gaze, as well as in a straight-ahead position, a proportionally larger portion of the eye are exposed to air, resulting in a much higher TER, x3.4 and x2.5, respectively, than an eye down-gaze position.[101]

OST can influence the TER since a warmer eye will provide additional heat energy to the water molecules in the tear film, permitting more of them to escape and produce a higher TER. Overall, it has been suggested by some researchers that an increase in OST due to an increase in body

temperature could consequently increase tear evaporation.[102,103] On the other hand, it is believed by some other researchers that higher eye surface temperatures leads to a greater mobility of lipids over the aqueous layer leading to a more stable tear film, and subsequently less tear evaporation.[23] Blinking is essential for maintaining a stable tear film.[91] Blinking is part of a reflexive corneal response to ocular surface cooling due to tear evaporation, and thus blink rate can affect TER.[104,105] The movement of the lids evenly spreads the tear film over the eye surface, restabilizing the tear film and decreasing TER.[106] Blinking is a major stimulus for meibum secretion and enhancing LLT, and any reduction in blink rate consequently can cause a higher TER.[107] However, a higher blink-rate than normal can increase TER, although this effect is greater at higher TERs.[108,109] Incomplete blinking can also increase TER as a result of an uneven tear film distribution across the eye surface. This kind of blinking is prevalent in patients with psychological fatigue or patients with prolonged work on visual display units.[110]

2.2.1.2 Environmental factors

RH refers to the amount of water vapor present in the air at any specific air temperature. RH is expressed as the percentage of the maximum amount of water vapor that a known volume of air can contain at a particular temperature. Since evaporation is affected by the capacity of the air to absorb water, air with a high RH already has a higher concentration of water molecules and has a limited capacity to absorb more. Air with low RH has a lower concentration of water molecules and thus has a higher capacity to absorb more. Consequently, evaporation will occur more easily in a low RH atmosphere producing a higher evaporation rate, and the converse is true for a high RH atmosphere. As a result, it has been shown that changes in RH will impact TER significantly.[74,111]

Ambient temperature plays a significant role in tear evaporation. A higher liquid temperature will result in a higher TER, since a molecule's kinetic energy is proportional to its temperature. The higher ambient temperature could assist water molecules with the energy needed for their escape to the air and evaporation. Alternatively, heat can also energize lipids. In the presence of a large migration of lipids to the mucin layer and interaction with them, the stability of the tear film may be decreased and consequently, TER may increase. Chronic exposure to both very high and very low ambient temperatures may result in increased tear evaporation and dry eye symptoms.[111,112] Dry (low RH) air currents can accelerate TER, as may occur in deserts or arid regions[112], and a warm airflow can provide the kinetic energy that water molecules require to escape from the ocular surface. Accordingly, when there is a warm and dry wind that moves horizontally or downward along the head region, the stability of the tear film decreases significantly, which increases the TER.[113]

2.2.1.3 Systemic factors

The measurement timepoint during the day may be a factor in TER measurement. LLT is greater in the morning than the afternoon due to overnight accumulation of oil on the lid margin and to increased meibum release from the eyelid glands just after wakening in the morning. This suggests that there is reduced evaporation from the tear film in the morning, or potentially more variability.[114]

With increasing age, both structural and functional changes in eye anatomy and physiology occur in both men and women. The blink rate decreases, as well as tear stability and LLT. An age-related decrease in blink rate can occur in older subjects, which may lead to an increase in TER, particularly if tear stability is also reduced.[115] On the other hand, some studies describe an increase in LLT with aging, as well as a greater amount of lipid in women than men until the age of 60

years, suggesting an effect of hormonal changes on lipid secretion[116] that produces less evaporation in elderly subjects.[117] Older subjects may have a lower OST, which may also have an inhibitory effect on tear evaporation.[118] However, Craig and Tomlinson found no relationship between TER and age or gender, and suggested that any potential increase in TER in older subjects is a result of pathological complications.[119]

The effect of the subject's sex on TER is still controversial. Guillon and Maissa reported a greater TER in women than men.[109,120–122] However, another study showed that OST was 0.16°C higher in male participants, which could be a trigger of higher TER in this sex.[123]

Some important sex hormones are known to affect meibomian gland function, which may alter lipid layer structure. These changes are linked to an increase in EDE and likely produce an increase in the TER, although this has not been demonstrated.[124] Androgens can stimulate meibomian gland lipid secretion, and any deficiency in meibum production due to aging or some other disorders (e.g., Parkinson's disease) will adversely affect TER.[41,125–129] Estrogen and progesterone, on the other hand, are stimulators for the secretion of inflammatory cytokines and enhance secretion in the meibomian glands[130–133] and lacrimal glands.[134,135] However, some studies argue that an alteration in the level of estrogen and progesterone will not change subjective symptoms and objective measurements, such as tear turnover rate, osmolarity, stability, and TER.[136,137]

2.2.2 Measurement of Tear Film Evaporation

Evaporimetry is a technique used to measure the rate of water loss from a surface through evaporation. This method is commonly applied in dermatology to evaluate trans-epidermal water loss as an indicator of skin barrier function.[138]

Measuring TER is a critical diagnostic tool for distinguishing EDE from other forms of DED.[139] Excessive tear evaporation plays a crucial role in EDE, where tears evaporate too quickly to

maintain a stable tear film.[34] The most common cause of EDE is MGD, where insufficient lipid secretion leads to a deficient lipid layer, allowing the aqueous tears to evaporate rapidly.[34] This results in tear film instability, hyperosmolarity, and ocular surface inflammation, key features of dry eye pathophysiology.[74]

Evaporimeters quantify the evaporation rate by assessing how quickly the tear film loses moisture under controlled conditions, helping clinicians evaluate tear stability and lipid layer function. Increased TER is a hallmark of EDE, often correlating with shortened TBUT and elevated tear osmolarity, both of which are key markers for DED diagnosis.

2.2.2.1 Types of Evaporimeters

Evaporimeters are instruments designed to measure trans-epidermal water loss by detecting changes in humidity and temperature. These devices typically include temperature and RH sensors to assess the evaporation rate of water from the skin or other surfaces. They are widely used in dermatology, biomedical research, and material science to evaluate barrier function and moisture loss.[138,140]

The classification of evaporimeters can be based on their chamber design and ventilation characteristics, as illustrated below (Figure 2-3).

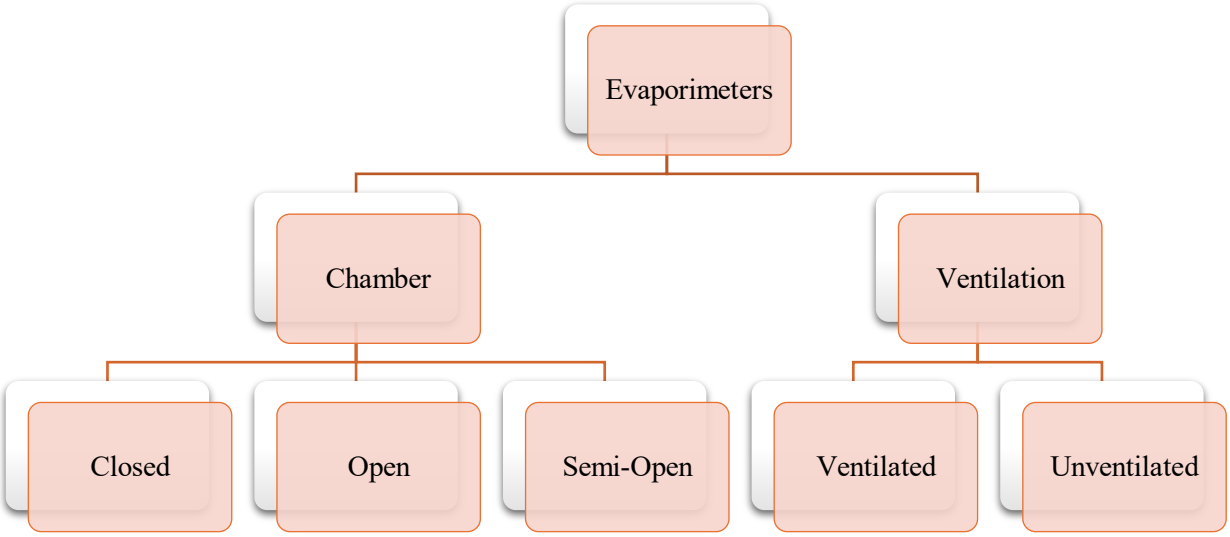


Figure 2-3: Classification of evaporimeters based on chamber design (closed, open, semi-open) and ventilation type (ventilated, unventilated) (Image created by the author).

2.2.2.1.1 Evaporimeter Classification According to Measurement Chamber Design

Open-Chamber Evaporimeters

Open-chamber evaporimeters are instruments designed to measure the TER by assessing the rate at which water vapor is lost from the tear film into the surrounding environment. These systems continuously expose RH and temperature sensors to ambient air, allowing for real-time trans-epidermal water loss measurement.[138] They require an acclimation period for sensor stabilization and are highly sensitive to environmental changes, such as air currents and temperature fluctuations.[138,141] Despite their sensitivity, open-chamber devices provide continuous data acquisition, making them advantageous for long-term studies.[142,143]

These instruments often employ sensors to detect water vapor flux near the eye. The TER is calculated by:

$$TER = \frac{Jopen - Jclosed}{A}$$

Where:

- J_{open} is the evaporation rate with the eye open.
- J_{closed} is the evaporation rate with the eye closed (serving as a baseline to account for non-ocular water loss).
- A is the exposed ocular surface area.

In these instruments, TER is expressed in grams per square meter per hour ($g/m^2/h$) or grams per square centimeter per second ($g/cm^2/s$), depending on the measurement system and study design. One example of an open-chamber evaporimeter is the Tewameter® TM Hex (Courage + Khazaka Electronic GmbH, Cologne, Germany) (Figure 2-4). The Tewameter® TM Hex is an advanced open-chamber evaporimeter designed to measure trans-epidermal water loss, providing insights into the skin's barrier function. The TM Hex has 30 sensor pairs arranged in six columns to enhance measurement accuracy and reliability.[144–146] In the current literature, there is a paucity of studies evaluating the application of the Tewameter® TM Hex in measuring TER, but a study employing the Tewameter® TM 300, the predecessor of the TM Hex, utilized modified goggles to measure trans-epidermal water loss from the ocular area. The findings indicated significantly higher trans-epidermal water loss in patients with DED compared to control subjects, suggesting increased tear evaporation in DED patients.[147]

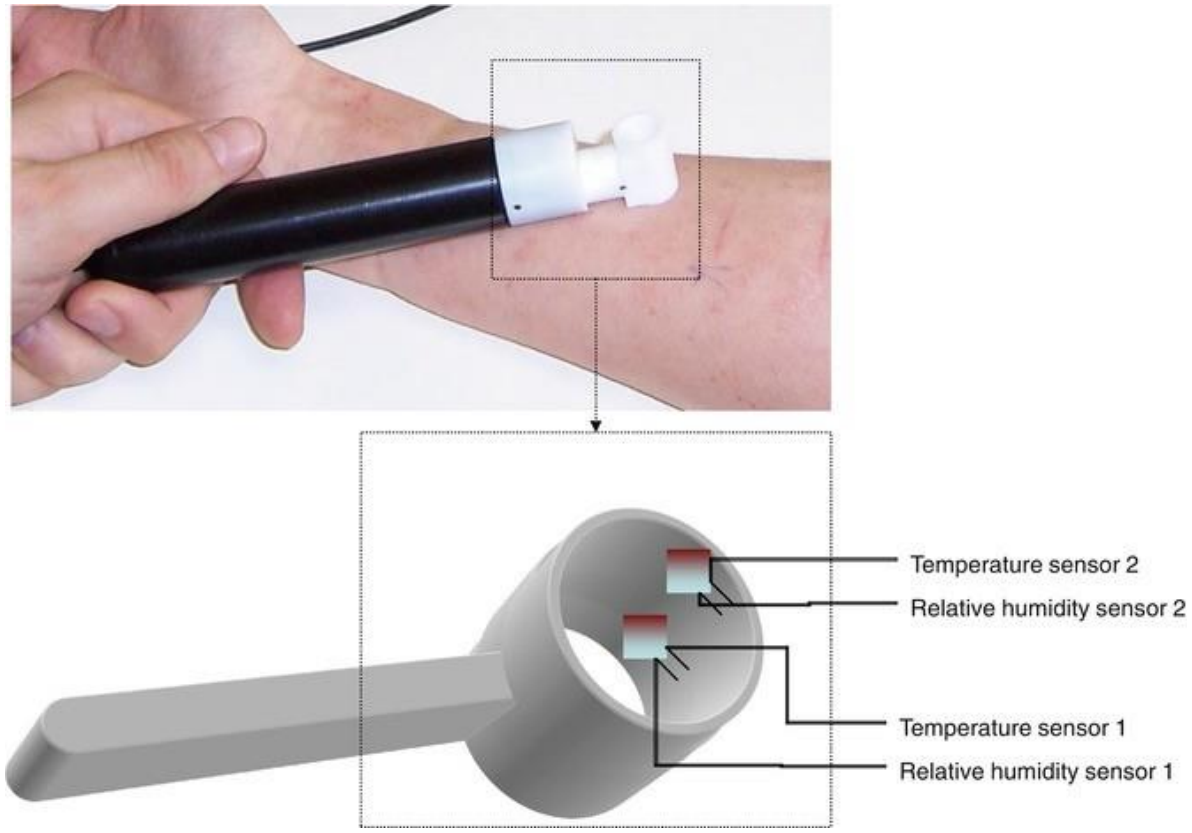


Figure 2-4: Transepidermal water loss measurement and a schematic overview of the open-chamber device measuring probe[148] (Image from: Fluhr JW, Darlenski R. Trans-Epidermal Water Loss (TEWL). In: Berardesca E, Maibach HI, Wilhelm KP, eds. Non-Invasive Diagnostic Techniques in Clinical Dermatology. Springer; 2014:353-356. doi:10.1007/978-3-642-32109-2_32).

Closed-Chamber Evaporimeters

Closed-chamber systems isolate the measuring environment by enclosing the sensor within a chamber placed on the skin, effectively isolating it from external environmental factors.[138] This design allows for improved control over internal conditions, such as RH and temperature, thereby enhancing the accuracy of TER measurements. However, water vapor can accumulate within the chamber, leading to an increase in RH, which requires a break between measurements to allow the chamber to return to baseline conditions.[138,140]

The measurement process involves monitoring changes in RH and temperature within the chamber over time. The TER is calculated using the following formula:

$$TER = \frac{\Delta RH}{\Delta t} \times K$$

Where:

- ΔRH is the change in RH within the chamber over the measurement period Δt.
- K is a device-specific calibration constant that accounts for the chamber's volume, sensor sensitivity, and other factors.

This formula quantifies the mass of water evaporated per unit area of the ocular surface over a specified time period, typically expressed in grams per square meter per hour ($g/m^2/h$).

A notable example is the DEvice Hygrometer© (AI, Rome, Italy), which measures tear film evaporation by detecting RH fluctuations in a controlled pre-ocular micro-environment (Figure 2-5).[149] This non-contact method facilitates objective TER assessment, though its clinical applicability remains under investigation.

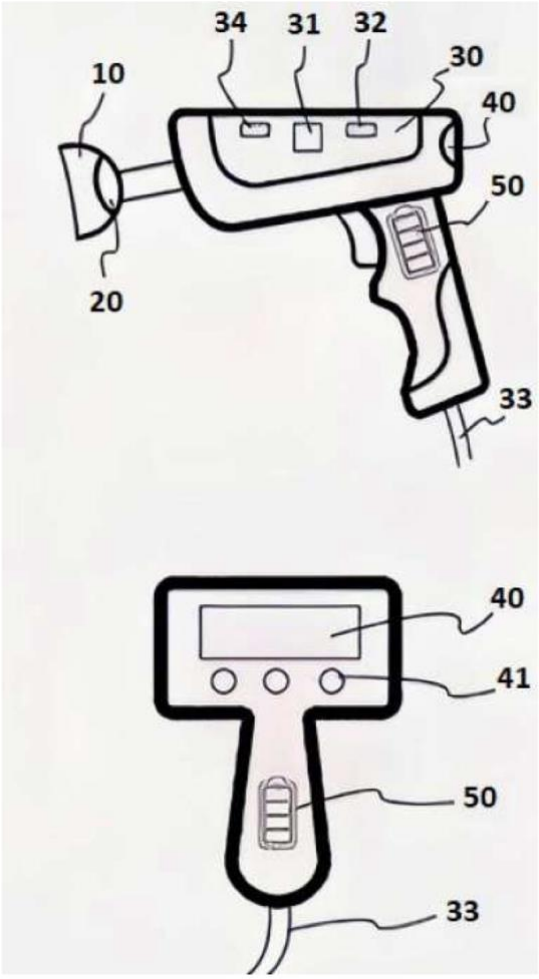


Figure 2-5: A schematic design of DEvice© ocular hygrometer. The figure shows a side and rear view of the schematic representation of a mono sensor diagnostic prototype with: an eyepiece cup (10); the sensor (20) placed inside it; a processing board (30) equipped with processor (31), memory (34) and wireless connection device (32); the optional connection cable (33); a digital screen (40) with buttons (41); and a rechargeable power supply battery (50) placed in the handle.[149] (Image from: Gaudenzi D, Mori T, Crugliano S, et al. AS-OCT and Ocular Hygrometer as Innovative Tools in Dry Eye Disease Diagnosis. Applied Sciences. 2022;12(3):1647. doi:10.3390/app12031647).

Semi-Open Chamber Evaporimeters

Semi-open chamber evaporimeters incorporate an open grid that allows for continuous water vapor escape while shielding the sensor from air currents.[138] This design aims to balance the controlled environment of closed chambers with the natural exposure of open chambers. However, it is

important to note that semi-open chambers may have larger standard errors in measurement compared to closed chambers, likely due to increased susceptibility to environmental variations.[138] The fundamental formula for measuring the TER in semi-open chamber evaporimeters is similar to that used in closed-chamber devices.

2.2.2.1.2 Evaporimeter Classification According to Ventilation Control Design

Evaporimeters are also categorized based on the presence or absence of ventilation:

Ventilated Evaporimeters

Ventilated evaporimeters introduce a controlled flow of dry gas into the pre-ocular chamber at a predefined humidity level (low RH) , and measure RH at both the entry and exit points.[138,140] These instruments provide highly controlled conditions and improved measurement precision, but require specialized set-ups and are more expensive.

The TER in ventilated-chamber systems is calculated using the following formula:

$$TER = \frac{Q \times (\Delta RH)}{A}$$

Where:

- Q is the volumetric airflow rate through the chamber.
- ΔRH represents the difference in RH between the inlet and outlet air streams.
- A denotes the exposed ocular surface area.

This formula quantifies the mass of water evaporated per unit area of the ocular surface over a specified time period, typically expressed in grams per square meter per hour ($g/m^2/h$).

An example of a closed-chamber ventilated evaporimeter is that developed by Miguel F. Refojo and Maurizio Rolando (Figure 2-6). The device features a sealed goggle design that isolated the

eye from external conditions. It included air inlets and outlets for controlled airflow, preventing RH buildup. RH and temperature sensors inside the chamber measured water vapor changes to calculate the TER.[8]

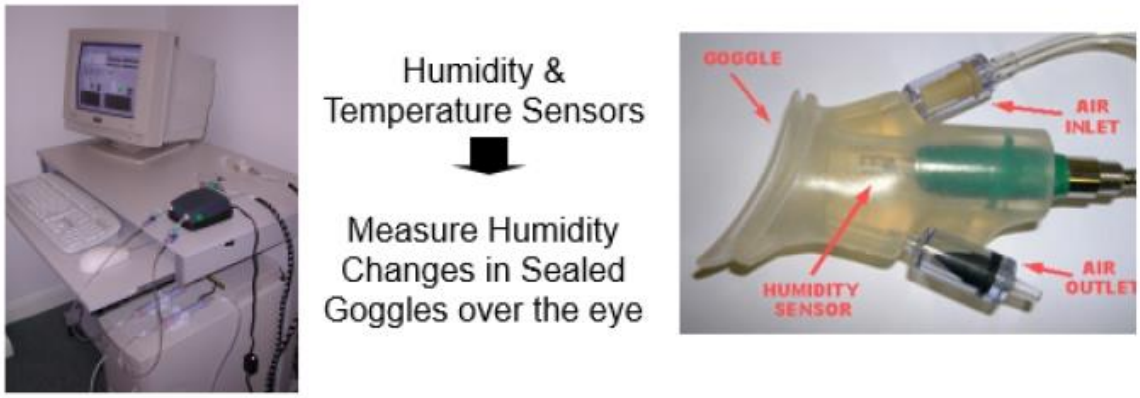


Figure 2-6: The closed-chamber ventilated tear evaporimeter invented by Miguel F. Refojo and Maurizio Rolando[8] (Image from: Rolando M, Refojo MF. Tear evaporimeter for measuring water evaporation rate from the tear film under controlled conditions in humans. Experimental Eye Research. 1983;36(1):25-33. doi:10.1016/0014-4835(83)90086-6).

Unventilated Evaporimeters

Unventilated evaporimeters are devices used to measure evaporation rates without the aid of externally introduced airflow or ventilation. Unlike ventilated evaporimeters, which actively circulate air around the surface being tested, unventilated evaporimeters rely solely on the passive diffusion of water vapor. They measure changes in RH or mass within a defined chamber or area adjacent to the evaporation surface.[138] Unventilated evaporimeters are available in both closed and open chamber designs.

The TER is calculated using the following formula:

$$TER = \frac{\Delta RH}{\Delta t} \times K$$

Where:

- ΔRH is the change in RH within the chamber over the measurement period Δt.
- K is a device-specific calibration constant that accounts for the chamber's volume, sensor sensitivity, and other factors.

This formula quantifies the mass of water evaporated per unit area of the ocular surface over a specified time period, typically expressed in grams per square meter per hour ($g/m^2/h$).

An example of an unventilated evaporimeter is the Modified ServoMed EP-3 evaporimeter, an open-chamber design featuring a semi-enclosed measurement space positioned close to the ocular surface (Figure 2-7). It employs temperature and RH sensors to monitor natural, passive tear film evaporation without the influence of artificial airflow, providing accurate TER assessment.[150]

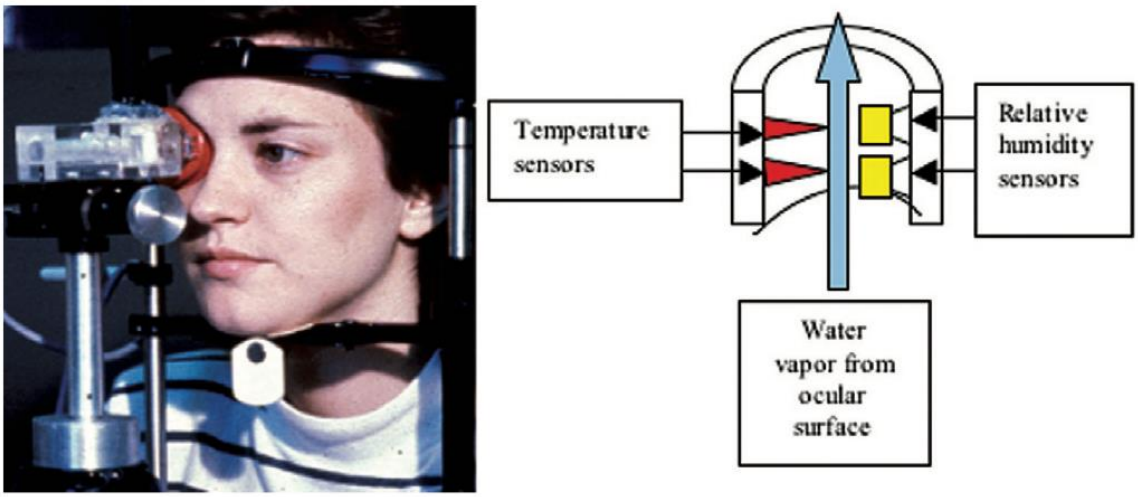


Figure 2-7: Modified ServoMed EP-3 (open-chamber, unventilated) evaporimeter measuring tear film evaporation using temperature and RH sensors [150](Image from: Trees GR, Tomlinson A. Effect of artificial tear solutions and saline on tear film evaporation. Optom Vis Sci. 1990;67(12):886-890. doi:10.1097/00006324-199012000-00002.).

2.2.3 Challenges in Measuring Tear Film Evaporation: Variability in Existing Methods

Over the years, the development and refinement of evaporimeters have led to significant variations in instrumentation components and experimental protocols. Differences in sensor technology, sampling intervals, testing duration, participant instructions, and the physical properties of measurement chambers contribute to discrepancies in data across studies. Below is a breakdown of key methodological differences.

Sampling Frequency: Advancements in sensor technology have enabled more frequent data collection, leading to improved temporal resolution in evaporimetry research. The sampling intervals across studies range from every 0.2 seconds,[151] 0.25 seconds,[152] 1 second,[147] 2 seconds,[15] to as long as every 10 seconds.[9] These variations impact the ability to detect transient changes in evaporation and may influence the precision of derived TER.

Measurement Duration: Excluding the time required for ventilation, the duration of evaporation assessments varies significantly. Studies have reported measurement times as brief as less than 10 seconds,[153] while others extend to 1 minute,[8] 100 seconds,[152] 110 seconds,[9] 2 minutes,[10,154] and up to 5 minutes.[155] McCulley et al.,[17] using a Mathers-based evaporimeter, documented the time required for RH changes within the chamber - 14.5 seconds to shift from 25% to 35% RH and 22.5 seconds from 35% to 45% RH. The chosen duration influences the stability of evaporation readings and the extent of ocular adaptation during measurement.

Blink Control Strategies: Blinking plays a crucial role in maintaining tear film stability, and different studies have adopted distinct approaches to managing participant blink rates. Many studies allow natural blinking,[9,10,147,152,155,156] which better represents real-world conditions. However, some researchers standardize IBIs, instructing participants to blink every three seconds[18,157] or every five seconds,[152] while others restrict blinking for up to one minute.[8,153,158,159] Even when using the commercially available Eye-VapoMeter (closed-chamber, unventilated evaporimeter) methodologies are inconsistent. Some studies require participants to hold their eyes open for the duration of the test,[153,158,160,161] particularly for brief assessments lasting less than 10 seconds,[153] while others permit spontaneous blinking.[159,162] These inconsistencies highlight the necessity for standardized protocols to enhance cross-study comparisons.

Open vs. Closed Eye Measurements**:** A significant portion of the evaporimeter chamber's internal area (77%) is covered by periorbital skin,[10] which contributes 5% to 18% of the total measured evaporation rate when using the Eye-VapoMeter system.[10,163] This highlights the importance of distinguishing between ocular surface evaporation and periorbital skin evaporation to ensure accurate assessment of TERs. The mean ± SD evaporation rates for periorbital skin have been reported as $3.73 \pm 2.4 \times 10^{-7}$ g/cm²/s in mixed dry-eye and non-dry-eye participants,[10] 11.9 ± 1.8

$\times 10^{-7}$ g/cm²/s in non-dry-eye subjects, and $16.1 \pm 5.9 \times 10^{-7}$ g/cm²/s in individuals with floppy eyelid syndrome.[164] To isolate evaporation attributable to the ocular surface, most researchers calculate the difference in evaporation rates between open-eye and closed-eye conditions.[9,10,13,17,150,152–155,159–162,165–167] However, alternative protocols exist, such as using closed-eye measurements solely for instrument calibration[168] or as a baseline before ventilation.[8] Some researchers, like Bilkhu et al.,[158] opted against closed-eye assessments, instead using repeated measurements in the same participant as a control.

Use of Occlusive Agents to Reduce Skin Evaporation: To minimize moisture loss from the periorbital skin during evaporimetry, some researchers have applied petroleum jelly as an occlusive barrier, resulting in a significant reduction in skin evaporation by 70% to 87.6%.[10,153,160,169] When this method is combined with closed-eye measurements, which suppress tear evaporation, it enables the calculation of a baseline skin-related evaporation rate. This baseline can then be subtracted from open-eye values, allowing for a more accurate estimation of tear-specific evaporation. Together, this approach has been shown to reduce the overall measured evaporation rate by approximately 64.1%.[153] Petroleum jelly has also been used around the edges of measurement goggles to prevent air leakage and maintain a controlled testing environment .[163] The effectiveness of petroleum jelly highlights the importance of accounting for skin-related evaporation when measuring ocular surface water loss.

Variation in Evaporimeter Chamber Volume: The physical dimensions of evaporimeter measurement chambers influence the internal micro-environment and evaporation dynamics. Previously studied chamber or goggle volumes varied considerably, with reported values including 16 cm³ for swimming goggles, 20 cm³,[152] 25 cm³,[10] and larger setups such as a 44 cm³ goggle-and-cylinder system[9] or an 80 cm³ total volume when incorporating external ventilation tubing.[8] The

larger the chamber, the more it can buffer RH fluctuations, potentially impacting measurement sensitivity and response time.

2.3 Ocular Surface Temperature

The concept of heat has been of interest to scientists and clinicians for over 2,000 years as it is one of the physiological properties of the human body. Hippocrates, in 400 BC, wrote "*And in whatever part of the body heat or cold is seated, there is disease" (Aphorisms IV.39).* All metabolic events in the body produce heat, and that heat must be dissipated, which is one of the fundamental parameters of tissue metabolism. Conduction and convection transfer heat to the body surface, principally through the vascular system, which then radiates that heat into the surrounding environment. Therefore, it is reasonable to measure temperature to gain a deeper understanding of physiology, a feature that has been recognized by numerous researchers in this field.[24,25,170]

2.3.1 Significance of Ocular Surface Temperature Measurement

OST measurement is particularly helpful for understanding and monitoring diseases that affect the temperature of the eye (e.g., glaucoma), where changes in OST can be a precursor to vision loss.[26] By measuring OST, researchers can identify changes in tissue metabolism and monitor the progression of the disease, potentially allowing for more effective treatments and improved outcomes. Various conditions, such as DED, can also cause inflammation of the ocular surface, which in turn affects OST.[171] Measuring OST can help to identify these changes and provide an accurate assessment of the degree of inflammation, allowing for a more precise diagnosis and treatment of DED. In addition, it can be used to evaluate the effectiveness of existing treatments and determine if additional interventions are necessary.

Tear film parameters are known to affect OST. Studies have consistently found that shorter tear break-up times lead to more significant decreases in OST during the IBI.[27,172] A larger tear volume, an unstable tear film, and increased blink frequency were all associated with significant changes in OST cooling rate.[172–176] Since these parameters define DED, OST measurement has the potential to be used as a screening tool.

2.3.2 Measurement of Ocular Surface Temperature

2.3.2.1 Early Techniques

Advancements in OST measurement have mirrored the broader progress in body thermometry techniques. In ancient civilizations, temperature was assessed only in relative terms. The Greeks and Egyptians relied on touch to evaluate body temperature, a practice that persisted until the 16th and 17th centuries. By the middle of the 17th Century, Galileo had invented a thermoscope. The principle behind Galileo's invention was to observe the expansion and contraction of air or liquid to determine temperature changes. As a result of this concept, mercury-in-glass thermometers were invented, which allowed for more accurate measurements of temperature. The mercury thermometer has traditionally been the standard tool for temperature measurement across the globe. However, due to growing concerns over mercury toxicity and hygiene, it is increasingly being supplanted by alternatives, such as thermocouples, thermistors, and radiometers for measuring middle ear temperature. Today's disposable sterile thermocouples operate on the same principle, but they are more accurate and easier to handle due to advancements in technology and materials. Furthermore, liquid crystal thermography provides another method for assessing surface temperature. Technological advancements in the 1970s enabled practical applications of Lehmann’s 19th-century discovery that certain cholesteric esters change color in response to temperature fluctuations. These liquid crystals can be embedded within plastic or rubber sheets

and placed on the skin, thereby generating a thermographic image with color-coded temperature variations. However, due to their low resolution, their usage today is largely confined to simple diagnostic tools, such as Feverscan strips (Robinson Healthcare, Workshop, UK), commonly applied to children's foreheads for fever detection.[177] All these methods require direct contact between the device and the patient, measuring temperature through conducted heat. However, the most significant advancements in body temperature measurement over the past 40 years have focused on techniques that detect radiated heat from the body's surface.

OST measurement technology has evolved over the same time period. OST measurement was initially based on direct contact with the eye surface, such as with thermistors and mercury bulbs. The results were, however, inaccurate due to the conductive heat exchange between the probe and the ocular surface and reflex tearing, leading to poor resolution.[178,179]

2.3.2.2 Infrared Thermography

Remote sensing enables the detection of radiated heat from efficient emitters, such as the human body's surface. This non-contact technique is particularly beneficial in OST measurement, offering several advantages over direct contact methods. By being non-invasive, the technique enhances patient comfort, and reduces the risk of measurement interference, making it a preferable choice in both clinical and research settings.[33,178,180,181]

Unlike contact-based approaches, which can alter local temperature due to mechanical pressure or heat transfer, infrared thermography (IRT) provides a passive, real-time assessment of temperature distribution across the ocular surface. This capability allows for the evaluation of temperature variations over a broader area rather than a single point, thereby minimizing the risk of misinterpretation caused by localized vascular activity. For instance, blood vessels near a contact

sensor may create an artificial impression of widespread temperature elevation, whereas IRT accurately captures regional variations without direct interference.

Two other key advantages of IRT are its speed and efficiency, enabling rapid temperature assessments without disrupting natural physiological conditions. Furthermore, IRT allows for flexible measurement approaches by capturing either the entire ocular surface or focusing on a specific ROI, such as the central cornea or limbus. This level of precision is particularly valuable in studying ocular thermodynamics, tear film behavior, and pathological changes that may not be detectable through conventional techniques.

By offering a comprehensive, accurate, and non-invasive method, IRT has emerged as the standard method for obtaining OST. The first attempt to measure OST using IRT was made by Mapstone in 1968. He employed an optical bolometer to quantify the radiation emitted from the eye's surface, demonstrating that this technique provided a more accurate temperature measurement than traditional contact thermometry.[176] Mapstone investigated factors determining OST,[182] investigated interocular differences in OST,[183] and developed thermographic profiles of various eyes .[180] Many studies of the ocular surface have been influenced by his work. IRT technologies have recently advanced to increase the accuracy of OST measurement, and they are increasingly being applied to individuals with and without ocular surface diseases.

Research on IR measurement of the eye indicates that the primary source of radiated heat detected by IR imaging originates from the tear film, which functions as both an absorber and emitter of infrared radiation: absorbing IR from deeper ocular structures, such as the cornea, and re-emitting the absorbed energy, which is then captured by a detector, such as a thermal camera. The thickness of the tear film is a critical factor in determining the extent of radiation absorption from underlying

layers. In cases where the tear film is significantly reduced or absent, the temperature recorded reflects that of the cornea itself.

Empirical findings indicate that a tear film thickness ranging between 4–10 μm results in the absorption of approximately 55–80% of IR radiation from deeper ocular layers, respectively. When the tear film exceeds 20 μm in thickness, it completely absorbs IR radiation from underlying structures, ensuring that the detected emission originates exclusively from the tear film.[49,184] The high sensitivity of IRT to tear film variations underscores its potential as a valuable tool for assessing tear film stability.

2.3.2.2.1 Single-Point vs Dynamic Measurement Approaches in IR Thermography

IRT allows for two distinct types of measurements:

Single time point measurement: This approach evaluates OST at a specific moment, such as immediately following a blink. Several studies have explored variations in single-point OST measurements between individuals with DED and healthy controls. Some researchers have found that DED subjects exhibit significantly lower OST compared to controls across multiple time points, including immediately after a blink and at subsequent intervals of 5 and 10 seconds.[185] In contrast, other investigations have reported a slightly higher mean OST in the DED group, with one study documenting a mean OST of 32.38 ± 0.69°C in DED patients compared to 31.94 ± 0.54°C in controls ($p<0.001$).[171] Furthermore, some studies have highlighted differences in temperature gradients across the ocular surface, with findings indicating that the temperature differential between the central cornea and limbus is significantly greater in DED individuals than in healthy subjects.[171] The higher limbal temperature is hypothesized to result from limbal hyperemia, which could contribute to the regional OST variations observed in DED patients. However, not all studies have reported significant differences in single-point OST measures

between DED and control groups, with some investigations failing to detect meaningful distinctions immediately following a blink.[186]

Dynamic measurement: This method assesses the OST cooling rate over a defined period, such as during the 10 seconds following a blink. Compared to single-point OST assessments, dynamic OST measurements have demonstrated a stronger correlation with DED, as the cooling rate reflects tear film instability and evaporation. Several studies have reported that DED subjects exhibit a more pronounced temperature decline over the 10-second post-blink period compared to controls, reinforcing the idea that increased tear evaporation contributes to DED pathophysiology.[187] In addition, another study that specifically examined a shorter IBI (3 seconds) found that the rate of change in OST at the corneal center declined from 1.00 to ~0.93 in the DED group, whereas the temperature drop was less pronounced in the control group (1.00 to ~0.96).[31] These findings have led to growing interest in OST cooling rate as a potential screening tool for DED, particularly for identifying patients with EDE.

While dynamic OST measurements show a clearer relationship with DED, single-point OST measurements remain an area of debate due to inconsistencies in findings. Several factors may contribute to these discrepancies, including differences in the studied population, measurement methodologies, and timing of temperature assessments, such as whether the measurement occurs immediately after a blink or a few seconds later. Although single-point OST measures may not consistently distinguish DED from healthy controls, some researchers propose that they may be effective in differentiating EDE from Aqueous Deficient Dry Eye. One study reported that patients with EDE exhibit a higher initial OST than those with Aqueous Deficient Dry Eye, a finding attributed to a greater volume of tears distributed uniformly across the ocular surface, which helps maintain a higher baseline OST.[187] However, due to the increased rate of tear film evaporation in

EDE, these patients also exhibit a greater OST cooling rate compared to those with Aqueous Deficient Dry Eye. Based on these observations, IRT has been proposed as a potentially valuable tool for determining the underlying etiology of DED.[187]

2.3.3 Challenges in Measuring Ocular Surface Temperature: Variability in IR Thermography Methods

While these measurement approaches focus on different temporal aspects of OST assessment, the effectiveness of IRT also depends on the hardware configuration of the imaging system and the analytical methods used to process the captured thermal data.

IRT systems used for OST measurement can be classified into single-camera and dual-camera configurations, each with its own advantages and limitations (Figure 2-8). A considerable body of research has explored the application of IRT in OST measurement, employing various methods for analyzing the captured IR images. These analytical approaches are designed to extract relevant temperature data and can differ based on image processing techniques, ROI selection, and measurement protocols.

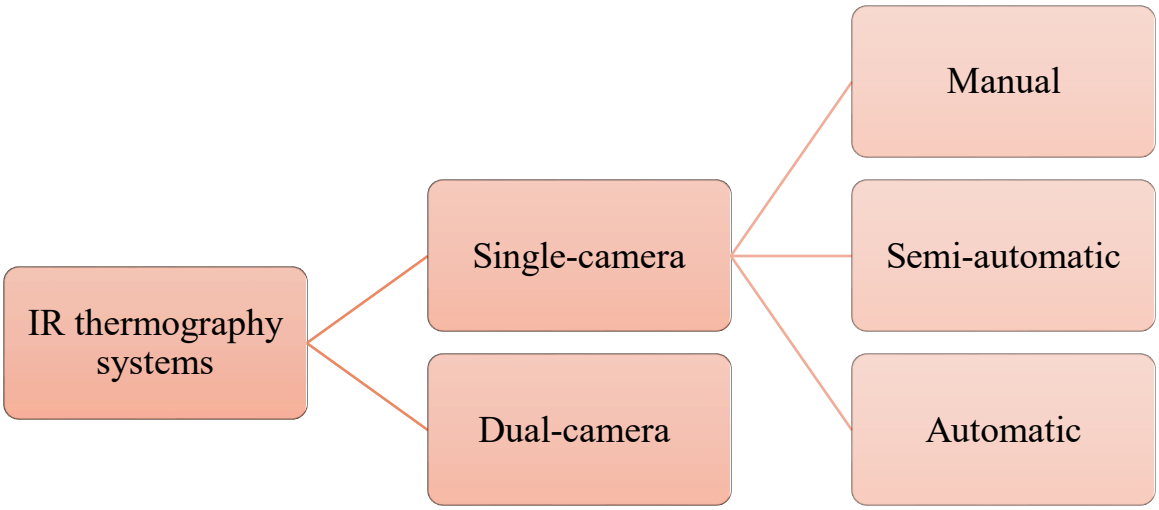


Figure 2-8: Classification of infrared thermography (IRT) systems based on configuration and level of automation (Image created by the author).

Single-camera systems rely solely on an IR camera to capture temperature data from the ocular surface. However, due to the lack of visible-light imaging, accurately defining the ROI, particularly the corneal boundary, presents a significant challenge. These systems can be categorized into manual, semi-automatic, and fully automated methods, each varying in the degree of user involvement and the level of precision achieved.

Manual methods require the user to select measurement points on the cornea, making them highly dependent on subjective input. Early studies, such as those conducted by Efron et al., measured OST at eleven points along a horizontal meridian across the cornea, spaced 0.5 mm apart.[188] Morgan et al. used a different approach by defining five 10×10 pixel boxes of approximately 1 mm^2 each along the same meridian.[189] Other studies, including those by Galassi et al. and Sodi et al., positioned five measurement points at specific corneal locations to investigate temperature

variations in conditions such as primary open-angle glaucoma (POAG) and central retinal vein occlusion (CRVO).[190,191] Chiang et al. and Ng et al. introduced a circular ROI, typically 4.4 mm diameter, to evaluate OST changes over time.[192,193] Building on these manual approaches, Tan et al. introduced a diamond-shaped ROI selection method for OST measurement, incorporating specific anatomical landmarks across the ocular surface (Figure 2-9). Their approach placed measurement points at the temporal and nasal limbus, extreme temporal and nasal conjunctiva, mid-temporal and mid-nasal conjunctiva, and the geometric center of the cornea. This configuration provided a structured framework for capturing temperature variations across different ocular regions, offering a broader spatial assessment of OST.[185]

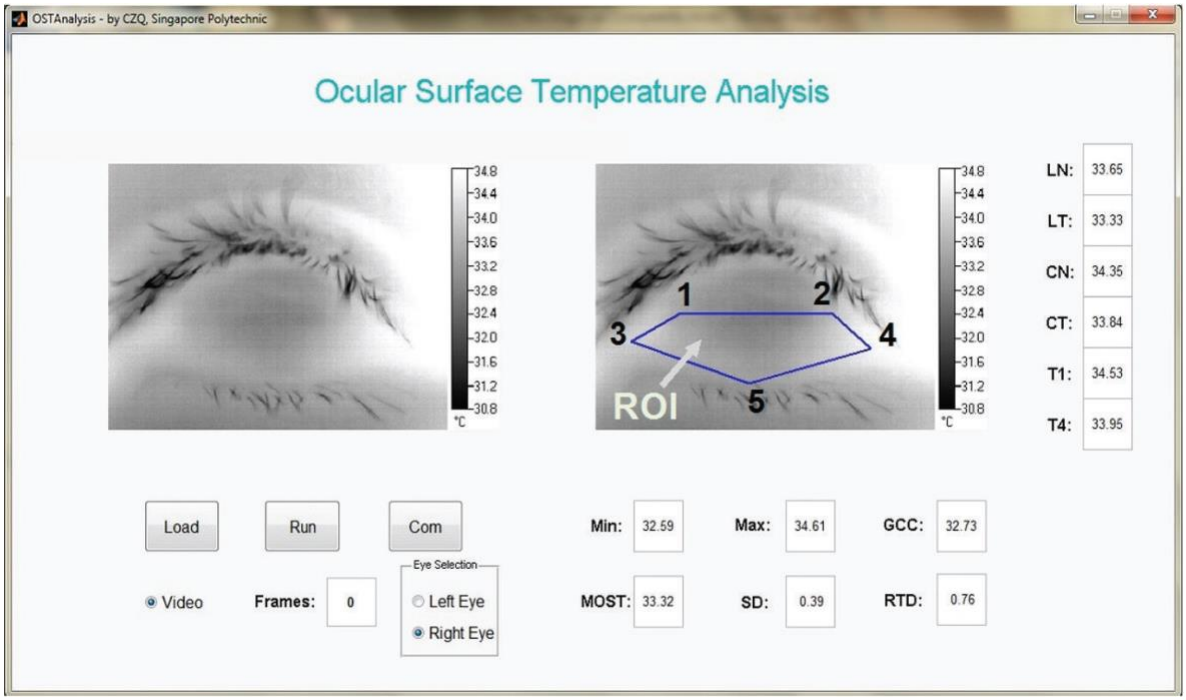


Figure 2-9: Ocular surface marking and OST acquisition using the novel "diamond" method[185] (Image from: Tan LL, Sanjay S, Morgan PB. Static and Dynamic Measurement of Ocular Surface Temperature in Dry Eyes. J Ophthalmol. 2016;2016(1). doi:10.1155/2016/7285132).

While these studies have provided valuable insights, the reliance on manual selection methods has introduced significant limitations, including inter-operator variability, increased workload, and subjective bias. One key challenge in manually drawing the ROI is the difficulty in consistently identifying anatomical boundaries, especially in thermal images where contrast may be low and corneal borders are not sharply defined. Variations in lighting, eye position, and blink-induced motion blur can further complicate accurate ROI placement. Even minor discrepancies in ROI size, shape, or placement can significantly alter temperature readings, especially in small and highly sensitive thermal zones. These challenges have motivated researchers to explore alternative methodologies, including semi-automatic and fully automated techniques, which aim to improve reproducibility and efficiency in OST measurement. Table 2-2 presents a comparative overview of published studies using IRT for OST assessment, highlighting variations in ROI selection strategies, measurement durations, and imaging modalities across different research protocols.

Table 2-2: Comparative overview of IRT-based OST measurement protocols, showing differences in ROI selection, measurement durations, and imaging modalities across key investigations.

Year	Investigator	Measurement Area	Duration	Blinking Condition	Temperature Measurement Device
1993	Morgan et al.[194]	Five anatomical points across a line running horizontally through the centre of the cornea	4- 5 seconds	No blinking	NEC6T62 (NEC San-ei Instruments, Tokyo, Japan)
1995	Morgan et al.[189]	Five anatomical locations along the horizontal meridian running through the centre of the cornea, 10 x 10 pixels in size	5 seconds after a 3 second period of eye closure	No blinking	NEC6T62 (NEC San-ei Instruments, Tokyo, Japan)
1996	Fujishima et al.[104]	Central cornea	10 seconds	No blinking	THI-500 (Tasko Japan, Osaka, Japan)
1997	Mori et al.[105]	Central cornea, a box measuring 20 X 20 pixels, or 3.3 mm^2	10 seconds	No blinking	Thermal Vision Laird 3 (Nikon Corp, Tokyo, Japan)

Year	Investigator	Measurement Area	Duration	Blinking Condition	Temperature Measurement Device
2000	Craig et al.[170]	Mean of central cornea pixels	4– 5 seconds after a 3 second period of eye closure	No blinking	NEC6T62 (NEC San-ei Instruments, Tokyo, Japan)
2005	Zelichowska et al.[195]	Central cornea	0, 5, 10 and 15 seconds after opening the eye	No blinking	ThermaCam SC-1000 (FLIR Systems, Oregon, USA)
2005	Singh and Bhinder[196]	Full ocular surface	Closed and open eye temperature for 5 seconds	No blinking	IR and remote heat sensor (MT2 -Raytak, USA)
2006	Chiang et al.	Central cornea (region of 4.4 mm diameter and 22 pixels) and periphery	Minimum of 4.5 seconds	No blinking	Infrared Thermal Imager (BOEING U3000A, DRS Sensors & Targeting Systems, USA)

Year	Investigator	Measurement Area	Duration	Blinking Condition	Temperature Measurement Device
2007	Sodi et al.[191]	Central cornea, nasal and temporal canthi (five anatomic points equally spaced out, across a line running horizontally through the center of the cornea and connecting medial and lateral canthi)	15 seconds	No blinking	AGEMA Thermovision 800 LWB (AGEMA Infrared Systems 1991 AB, Donderyd, Sweden)
2007	Purslow & Wolffsohn[172]	An area of 4 mm in diameter at Geometric Corneal Center (GCC)	8 seconds	No blinking	ThermoTracer 7102MX (NEC San-ei Instruments, Tokyo, Japan)
2007	Galassi et al.[190]	Five anatomical points across a line running horizontally through the centre of the cornea	20 seconds	No blinking	AGEMA Thermovision 800 LWB (AGEMA Infrared Systems 1991 AB, Donderyd, Sweden)
2009	Tan et al.[179]	Geometric Corneal Center	4 - 5 seconds	No blinking / Upper lid lifted by a cotton bud	ThermoTracer TH9100MV (NEC San-ei Instruments, Tokyo, Japan)

Year	Investigator	Measurement Area	Duration	Blinking Condition	Temperature Measurement Device
2011	Kamao et al.[186]	Three circular ROI: central cornea with 4mm in diameters, nasal and temporal conjunctiva with 2 mm diameters	10 seconds	No blinking	Tomey TG 1000 (TOMEY Corporation, Nagoya, Japan)
2011	Su et al.[198]	ROI determined by four curves connected between four manually set apexes (top and bottom of the eye, left and right corners of the eye)	6 seconds	No blinking	Custom non-contact system containing an uncooled microbolometer sensor (BOEING U3000A, DRS Sensors & Targeting Systems, USA)
2012	Kottaiyan et al.[199]	Central cornea	5 seconds	No blinking	Thermovision A40 (FLIR Systems, Oregon, USA)
2012	Klamann et al.[200]	Full ocular surface	10 seconds	No blinking	Tomey TG 1000 (Tomey Corp, Nagoya, Japan)
2014	Su et al.[201]	Full ocular surface, area of tear break-up	6 seconds	No blinking	IT-85 (United Integrated Services Co., Taiwan)
2014	Gonnermann et al.[202]	Full ocular surface	More than 10 seconds	No blinking	Tomey TG 1000 (Tomey Corp, Nagoya, Japan)

Year	Investigator	Measurement Area	Duration	Blinking Condition	Temperature Measurement Device
2014	Azharuddin et al.[203]	Corneal surface	15 seconds	No blinking	FLIR SC305 (FLIR Systems, Oregon, USA)
2014	Acharya et al.[204]	Full ocular surface	20 seconds	No blinking	VarioTHERM head II (Dresden, Germany)
2015	Li et al.[27]	Corneal surface, tear film break-up regions	Until tear film break-up 15.5 ± 10.3 seconds	Holding eyes open as long as possible	FLIR A655sc (FLIR Systems, Oregon, USA)
2015	Zhang et al.[205]	Central cornea, 7~9 mm circular	25 seconds	Blinking every 5 seconds	FLIR SC325 (FLIR Systems, Oregon, USA)
2015	Versura et al.[206]	Central cornea, 4 mm circular	10 seconds	No blinking	Tomey TG 1000 (Tomey Corp, Nagoya, Japan)
2016	Matteoli et al.[207]	Central cornea, temporal and nasal canthi, and sclero-conjunctival limbi	7 seconds	No blinking	FLIR A320 (FLIR Systems, Oregon, USA)

Year	Investigator	Measurement Area	Duration	Blinking Condition	Temperature Measurement Device
2016	Tan et al.[185]	Geometric corneal center, extreme temporal and nasal conjunctiva, mid-temporal and nasal conjunctiva, temporal and nasal limbi	10 seconds	No blinking	NEC TH9420 (NEC San-ei Instruments, Tokyo, Japan)
2017	Sudarshan et al.[208]	Upper half and lower half regions of the ocular surface (cornea + conjunctiva)	20 seconds	No blinking	VarioTHERM head II device (Dresden, Germany)
2018	Matteoli et al.[209]	Central cornea and surrounding areas	7 seconds	No blinking	FLIR 320A (FLIR Systems, Oregon, USA)
2020	Matteoli et al.[210]	Five anatomical regions (central cornea, nasal/temporal conjunctiva, canthi)	7 seconds	No blinking	FLIR 320A (FLIR Systems, Oregon, USA)
2021	Ding et al.[30]	Full ocular surface	Until discomfort onset (MIBP) 14.5 ± 16.3 seconds	Holding eyes open as long as possible	FLIR A655sc (FLIR Systems, Oregon, USA)

Year	Investigator	Measurement Area	Duration	Blinking Condition	Temperature Measurement Device
2021	Su et al.[31]	Nasal, corneal, and temporal areas, each 3 mm in diameter	4 seconds	No blinking	IT-85 (United Integrated Services Co., Taiwan)
2024	Kim et al.[32]	Localized tear film break-up regions	Until discomfort onset	Holding eyes open as long as possible	FLIR A655sc (FLIR Systems, Oregon, USA)
2024	Coroneo et al.[28]	Full ocular surface	Until discomfort onset	Holding eyes open as long as possible	TearView (Beyond 700, Castle Hill, NSW, Australia)

A close examination of Table 2-2 reveals significant variations in the methodologies employed across studies. Earlier investigations primarily focused on central corneal measurements, often using small, fixed pixel regions to define the ROI. In contrast, later studies expanded their scope to include wider ROIs, incorporating regions such as the limbus, conjunctiva, and full ocular surface to provide a more comprehensive thermal profile. Measurement durations also varied widely, ranging from short (4–5 seconds) snapshots to prolonged 20–25 second intervals, reflecting differences in study objectives and technological advancements.

Additionally, blinking conditions were inconsistent across studies, with some protocols requiring sustained eye opening to capture continuous data, while others incorporated controlled blinking intervals to simulate real-world conditions. The diversity in IRT protocols underscores the lack of standardization in OST measurement, making direct comparisons across studies challenging. This methodological variability highlights the need for more consistent and automated approaches to ensure greater reproducibility and clinical applicability. While many earlier studies relied on manual ROI selection, recent advancements have led to the development of semi-automatic and fully-automatic approaches, incorporating image processing algorithms and AI-driven segmentation to reduce subjectivity and enhance measurement precision.

Acharya et al. introduced a method that segmented the cornea based on assumed circular geometry, reducing the need for full manual selection.[211] Matteoli et al. developed a technique using fixed eye shapes and geometric transformations, improving inter-subject comparison accuracy.[209] While these approaches improved efficiency, they still required some level of user intervention for fine-tuning and validation.

With advances in computer vision and machine learning, fully automatic OST measurement methods have been developed, eliminating the need for manual selection. Tan et al. proposed a

snake algorithm combined with a target-tracing function to automatically segment the cornea and extract temperature data.[179] Shuang et al. implemented an active contour-based segmentation algorithm that further improved accuracy compared to earlier techniques.[212] These automated methods significantly enhanced reproducibility and efficiency in OST measurement. However, their reliability depended on the robustness of the underlying algorithms and the quality of the input IR images.

In contrast to single-camera systems, dual-camera configurations integrate an IR camera with a visible-light camera to improve corneal segmentation accuracy by leveraging anatomical features visible in standard imaging. Several variations of dual-camera designs have been explored in previous research. Kamao et al. developed a system in which a moving mirror alternated between visible and IR imaging, requiring manual OST extraction from the acquired images (Figure 2-10).[186] Su et al. introduced a germanium beam-splitter that allowed simultaneous visible and IR imaging of the eye, but the method still depended on manual interpretation for tear film analysis.[201] Li et al. improved upon these techniques by synchronizing two separate cameras using external software, facilitating a comparative analysis of tear film dynamics.[27] Kricancic et al. further refined dual-camera imaging by incorporating a semi-reflecting germanium beam-splitter, improving the alignment between the IR and visible images.[213]

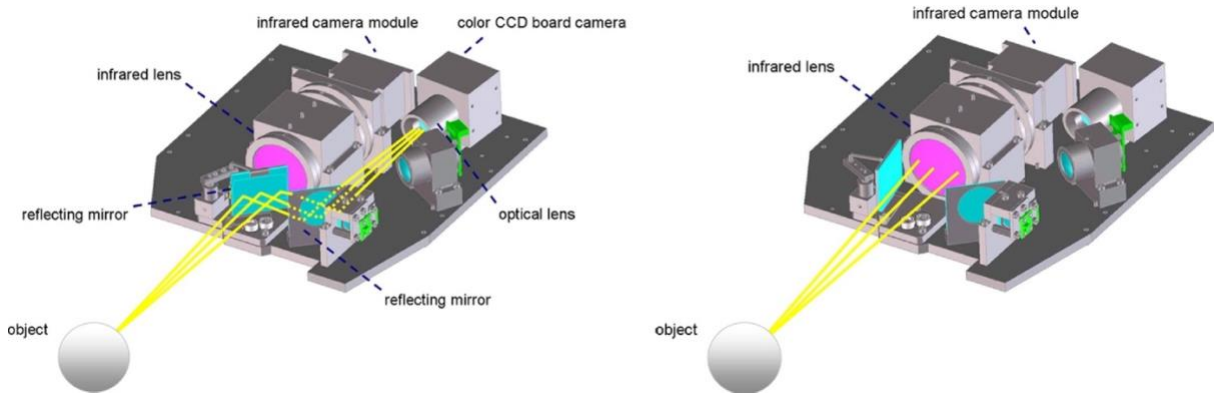


Figure 2-102-11: Dual camera system introduced by Kamao et al. Internal camera architecture and mirror installation[186] (Image from: Kamao T, Yamaguchi M, Kawasaki S, Mizoue S, Shiraishi A, Ohashi Y. Screening for dry eye with newly developed ocular surface thermographer. Am J Ophthalmol. 2011;151(5):782-791).

Despite the improved accuracy in corneal localization and segmentation offered by dual-camera systems, additional challenges related to camera alignment, synchronization, and post-processing were introduced. Proper calibration and image registration are essential to ensure that the IR and visible images correspond accurately. Hardware-based triggering mechanisms or software-controlled synchronization techniques were commonly employed to minimize discrepancies between the captured frames. On the other hand, while single-camera systems offer a simpler set-up, they require sophisticated segmentation techniques to compensate for the lack of visible-light guidance. In contrast, dual-camera systems provide enhanced localization and tracking capabilities but involve greater complexity in terms of system design and data processing. The selection of the imaging system depends on the specific requirements of the study, with a balance needed between accuracy, automation, and practicality in OST measurement.

All of the methods described have made a contribution to OST measurement, but there are some weaknesses with each method. For example, the manual methods need an experienced user input, and the semi-automatic and automatic methods (single IR camera) use images in which the corneal

boundary is indistinct and therefore only an approximation of the boundary can be provided. The dual camera systems provided better localization accuracy, but the method still requires user input. None of the described methods can localize the cornea with high accuracy and track it over time. Also, the methods cannot detect and remove blink artefacts from the image sequences.

Improvements can be made by overlaying high-resolution visible and IR images, captured using a dual camera system, to maintain tracking of OST during eye movement and blinking, and detection of the elliptical palpebral aperture. Such a system provides an opportunity to analyze the ocular surface with much improved accuracy. This innovation led to the development of the ThermOcular imaging system, a cutting-edge system designed to revolutionize OST analysis by enabling precise real-time tracking of temperature fluctuations. With its advanced imaging capabilities, ThermOcular offers a powerful tool for DED diagnosis and management, contact lens research, and investigating the thermal triggers of blinking, paving the way for a deeper understanding of ocular surface dynamics.[214] The ThermOcular system will be used for studies in this thesis and is reported in more detail in Chapter 3.

2.4 Rationale and Objectives

This thesis aims to advance the scientific understanding of tear film dynamics by critically examining the biophysical and physiological mechanisms governing tear evaporation and tear film stability. Given the high prevalence of evaporative dry eye and the recognized limitations in current diagnostic modalities, this work seeks to develop and validate integrative, non-invasive approaches capable of capturing the complex interactions between tear film structure, function, and environmental influences.

The specific objectives of this research are to:

- Elucidate the impact of lipid layer integrity and ocular surface exposure on TER, with an emphasis on isolating the contributions of structural and surface area variables under controlled and physiologically relevant conditions.
- Investigate the thermodynamic behavior of the tear film through the analysis of OST and establish the relevance of OST as an indirect marker of evaporative loss and tear film instability.
- Examine the relationship between structural parameters (e.g., lipid layer thickness) and functional indicators (e.g., NITBUT and evaporation rate), thereby contributing to a more cohesive understanding of tear film homeostasis.
- Refine and validate quantitative methods for assessing tear film dynamics by integrating humidity-based evaporimetry and IRT with advanced imaging techniques, enabling precise, real-time characterization of tear film stability and evaporative behavior.

Through these aims, the thesis seeks to contribute to the refinement of DED diagnostics and to inform future strategies for the assessment and management of tear film dysfunction.

Chapter 3 Methodology

3.1 Waterloo Evaporimeter

3.1.1 Purpose and Background

EDE is the most common type of DED,[215] and is caused by a poor-quality tear film. In order to effectively treat patients, it is important for eye care practitioners to be able to differentiate between the different causes of DED.[216] Evaporimetry is a non-invasive method of assessing the rate of evaporation of the tear film from the front surface of the eye. The Waterloo Evaporimeter (Murphy Laboratory of Experimental Optometry, Waterloo, Canada) is a prototype goggle-based system designed to simultaneously measure TER from both eyes. It overcomes limitations of existing evaporimeters, such as the Eye-Vapometer[153] (Delfin Technologies Ltd., Finland), by providing real-time, bilateral measurements..

3.1.2 Equipment and Experimental Setup

3.1.2.1 Evaporimetry System Components

The experimental setup consisted of the following components:

Modified swimming goggles (Arena Zoom X-Fit, Arena Distribution SA, Lugano, Switzerland): equipped with a Sensirion SHT31 relative humidity and temperature sensor (Sensirion AG, Stäfa, Switzerland) mounted inside each goggle to enable real-time data acquisition of RH and temperature within the goggle. Figure 3-1 provides a front view of the modified goggles, highlighting the external wiring used to transmit data to the control system. Figure 3-2 shows a rear view of the Waterloo Evaporimeter, illustrating the sensor mounting points and cable routing.



Figure 3-1: Front view of the Waterloo Evaporimeter showing the cables that transmit real-time relative humidity (RH) and temperature data from the sensors inside the goggles to the Arduino Uno R3 microcontroller within the enclosed control box(Image created by the author).



Figure 3-2: Rear view of the Waterloo Evaporimeter. Three small holes have been drilled into the goggle. Two holes (yellow arrows) are for screws to attach sensors. The third hole allows air within the goggle to interact with the sensor (Image created by the author).

Data Acquisition System: Both sensors are linked to an Arduino Uno R3 microcontroller (Arduino, Monza, Italy) which are housed within an enclosed plastic control box. A USB connection facilitated communication between the microcontroller and a Fujitsu Lifebook S Series laptop. A custom software (*Goggle*, Dr. Ehsan Zare Bidaki, University of Waterloo) was used for real-time recording and analysis of temperature and RH data collected by the sensors.

Additional experimental equipment: Included a fixation target to ensure consistent eye positioning, a 7-inch foldable fan (Mainstays, Walmart, Bentonville, Arkansas, USA) used to assist in resetting

RH inside the goggles between trials, a digital temperature and RH sensor for monitoring room conditions (RH411, Omega Engineering, Norwalk, Connecticut, USA), and an adjustable-height table to optimize participant comfort.

3.1.2.2 Software and Data Logging

The *Goggle* software was specifically developed for the Waterloo Evaporimeter, providing real-time monitoring and precise recording of temperature and RH changes within the goggles. Figure 3-3 illustrates the software's data acquisition interface, showcasing dual-eye tracking, numerical output, and real-time graphical trends that facilitate precise analysis of tear evaporation dynamics. It simultaneously captures sensor measurements from both eyes every 0.25 seconds, offering high temporal resolution for detailed analysis of tear evaporation dynamics.

The software interface featured graphical representations illustrating RH trends over time. Distinct red and black lines represent RH changes for the right and left eyes, respectively. Accompanying these graphs, numerical data provides precise temperature and RH measurements, enabling immediate detection of anomalies or patterns.

While measurement frequency was adjustable, a sampling frequency of 4 Hertz (every 0.25 seconds) was chosen for this study. This selection provided an optimal balance between data resolution and file manageability, effectively capturing rapid and subtle changes without excessive data generation.

Data were digitally stored in *.doc* files, and graphical outputs of RH and temperature trends are saved as *.png* images. This structured approach ensured data integrity, facilitates detailed retrospective analyses, and supports comparative studies and longitudinal monitoring of ocular surface evaporation.



Figure 3-3: Data acquisition interface of the *Goggle* software for the Waterloo Evaporimeter, displaying real-time monitoring of RH and temperature changes for each goggle (right and left eyes). The software graphs RH trends over time while providing numerical data for precise analysis of tear evaporation dynamics (Image created by the author).

3.1.3 Experimental Procedure and Measurement Protocol

Participants were instructed to arrive at the clinic having been awake for at least two hours and were required to acclimatize to the experimental room for 15 minutes before testing. This allowed the tear film to stabilize to the room environment from any outside environmental effects (e.g. exposure to wind, temperature variations, or RH fluctuations). It aided in preventing artificial variations in TER due to environmental changes. Participants were required to remove any eye make-up and to avoid wearing contact lenses for at least 12 hours before testing to prevent interference with measurements.

Petroleum jelly (Vaseline®, Unilever, Toronto, Ontario, Canada) was applied around the eye to create an effective barrier for evaporation from the skin and to maintain a sealed environment within the goggles. Petroleum jelly was transferred from its original container into a paper cup using a cotton-tipped applicator at each test visit. Participants received a new cotton-tipped applicator and a mirror to apply a thin, uniform layer of petroleum jelly around the eye, carefully avoiding the eyelid margins. Petroleum jelly was applied prior to the first set of baseline measurements. After completing the measurements, participants removed the petroleum jelly by closing their eyes and gently wiping the area with a tissue in a nasal-to-temporal direction, again taking care to avoid the lid margins to prevent contamination.

Environmental conditions were carefully controlled by conducting the tests in a room without windows or airflow to eliminate external fluctuations in RH. Additionally, ambient temperature and RH were recorded prior to each measurement.

3.1.3.1 Open-Eye Measurement

Metronome-Controlled Blinking: A metronome was used to standardize blink intervals, producing auditory cues every 3 seconds (20 times per minute). Participants were instructed to blink whenever they heard the metronome sound, ensuring a consistent and controlled blinking pattern throughout the measurement process. During the measurement, participants were required to maintain fixation on a designated cross target to minimize eye movement and maintain uniform gaze conditions. Figure 3-4 presents the complete experimental setup, including the fixation cross, Waterloo Evaporimeter goggles, environmental monitor, data acquisition system, and the fan used to restore baseline humidity between trials.

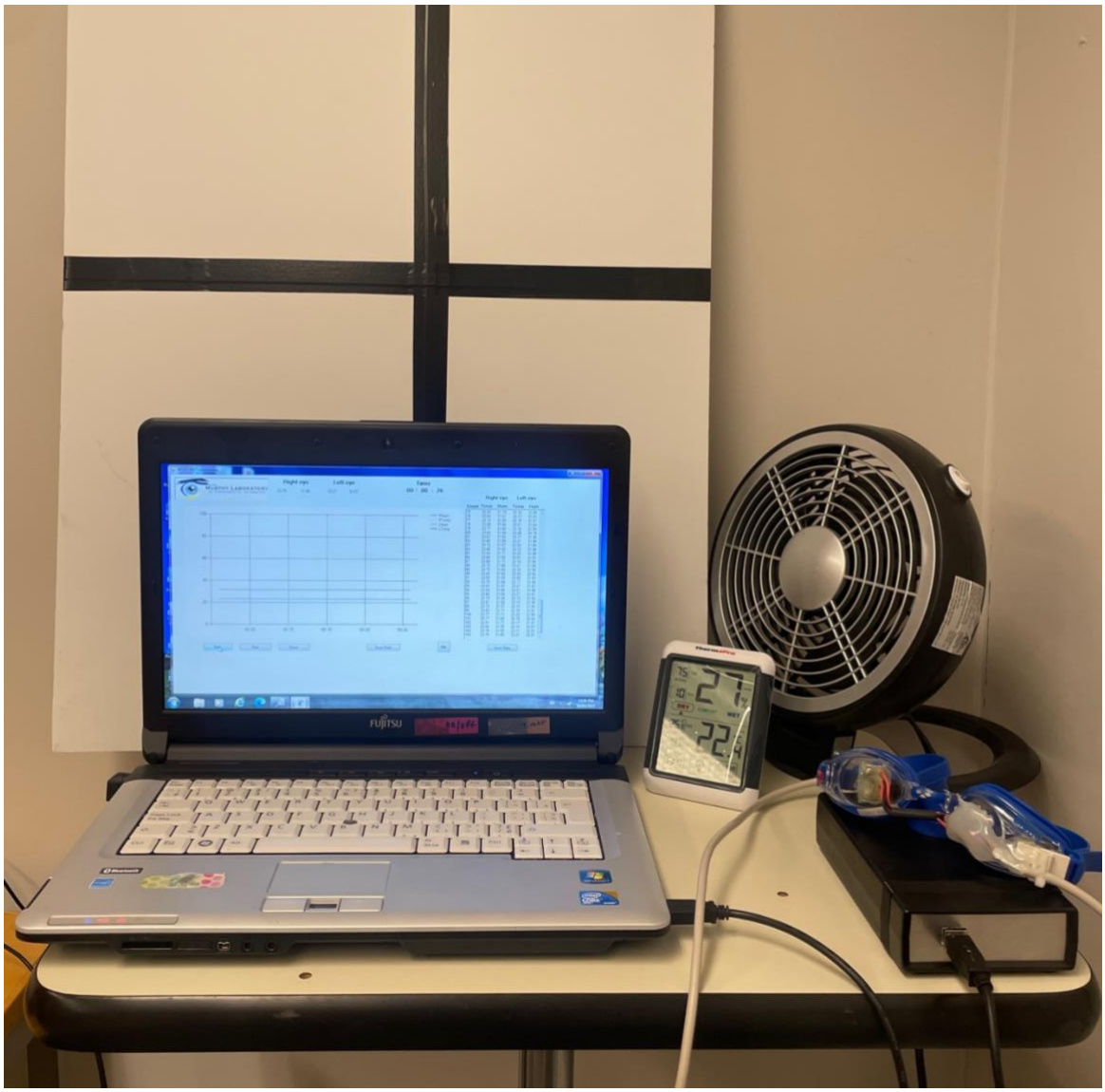


Figure 3-4: Experimental set-up for the Waterloo Evaporimeter, showing the fixation cross for gaze stabilization, digital temperature and RH monitor, evaporimeter goggles, data acquisition laptop running the *Goggle* software, and fan used for baseline RH restoration within the goggle between measurements (Image created by the author).

Starting the Measurement: Prior to initiating each measurement, the investigator recorded the ambient room temperature and RH using a digital thermo-hygrometer. Participants were then instructed to place the modified swimming goggles over their eyes, and to press them against the skin around the eyes to form a secure, tight seal against their face. They were asked to fixate

steadily on a designated cross-target to maintain a stable gaze. At this point, the investigator activated the *Goggle* software by clicking on the "On" icon, which changed the data collection mode from black to red, indicating the start of recording. Throughout the 20-second measurement interval, participants were specifically instructed to keep their eyes open, to remain as still as possible, and to blink in time with the auditory cues provided by the metronome set at 20 blinks per minute. Figure 3-5 illustrates a participant positioning the Waterloo Evaporimeter goggles during measurement, demonstrating the proper set-up used for assessing TER.

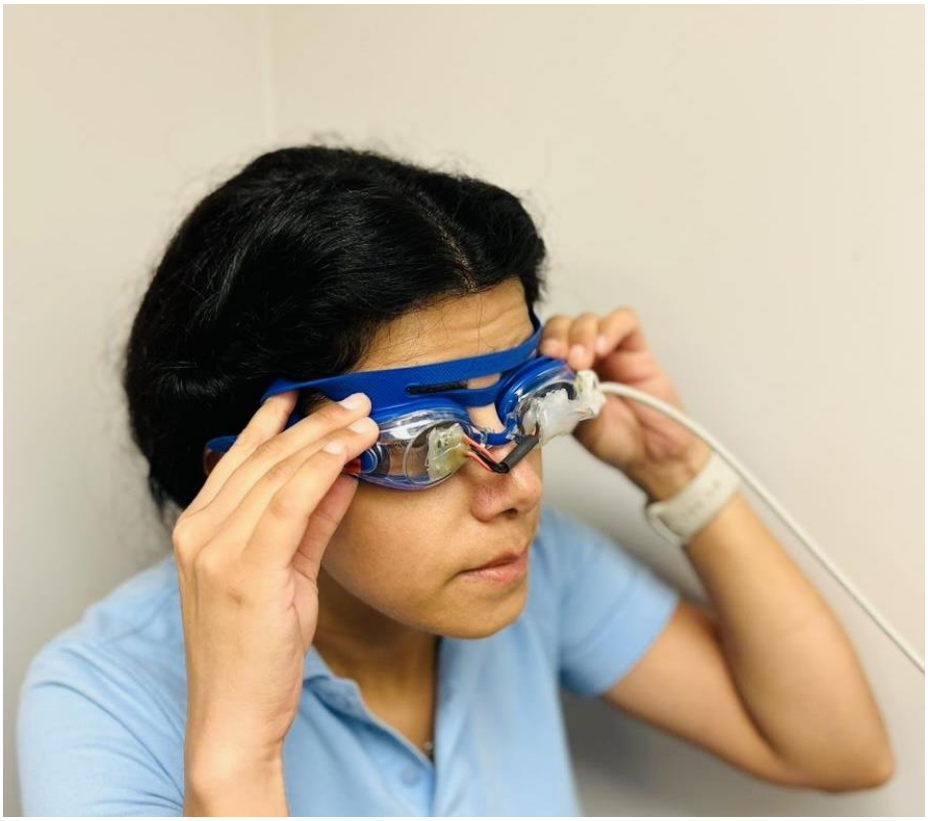


Figure 3-5: A study participant positioning the Waterloo Evaporimeter goggles for tear evaporation rate measurement (Image created by the author).

Ending the Measurement: At the end of the 20-second measurement period, participants were instructed to carefully remove the goggles. Immediately following this, the investigator clicked the "Off" icon on the software control screen, switching the data collection display from red to

black, clearly indicating the conclusion of the recording session. To prevent any residual moisture build-up within the goggles and to ensure accurate conditions for subsequent measurements, the evaporimeter was exposed to controlled airflow from a fan until sensor recorded RH levels returned to the pre-measurement baseline.

3.1.3.2 Closed-Eye Measurement

The closed-eye measurement followed the same procedure as the open-eye measurement, with participants instructed to gently, but firmly, close their eyes throughout the 20-second recording period. Participants maintained a comfortable and steady position while keeping the goggles securely sealed against their face. Immediately after data collection, the evaporimeter goggles were removed, and controlled airflow from a fan was used to reset the internal RH to baseline levels in preparation for subsequent recordings.

Following the final measurement for each participant, the investigator clicked on the "Save Data" icon on the software control screen to store the recorded session data as a *.doc* file. Additionally, "Save Chart" was clicked to save a graphical image (*.png*) of the temperature and RH trends captured during the measurement session. Finally, the investigator clicked on the "Reset" icon to clear the software interface, preparing the software for the next participant.

3.1.4 Data Analysis

The TER calculation was performed using statistical analysis software after exporting the recorded data from the *Goggle* operating software. Although the software captured real-time changes in RH and temperature inside the goggles, it did not directly calculate TER.

The TER calculation process involved exporting the numerical RH data, recorded every 0.25 seconds, into a statistical analysis program (such as SPSS or Excel). Within this program, the RH values were plotted against time to generate a RH-time graph for each measurement session. Only

the RH data within the 5 to 20 second interval were used, as this portion consistently represented the most stable and linear phase of RH increase.[217] Linear regression analysis was then applied to the data obtained, and the slope coefficient of the best-fit linear regression line was extracted. This slope coefficient directly represented the rate of change of RH, serving as the quantitative measure for TER.

Absolute slope values were used rather than percentage changes to accurately represent the actual rate of RH increase within the goggles, thus providing a clear, precise quantification of the evaporation rate.

3.2 ThermOcular Camera

3.2.1 Purpose and Background

OST is a vital biomarker for evaluating tear film stability, inflammation, and ocular health. IRT allows accurate, non-contact, real-time OST measurements, significantly improving diagnostic precision.

The ThermOcular imaging system is a dual-camera IRT device designed to measure OST non-invasively with high precision. It integrates an IR camera and a visible-light camera, both mounted on a slit-lamp biomicroscope.[214] This configuration enables synchronized real-time IR imaging, ensuring accurate localization and temperature mapping of the ocular surface.

The system employs automated segmentation algorithms to isolate the cornea, minimizing artifacts and improving measurement accuracy.[201] These algorithms first detect the corneal boundary using high-resolution visible-light images, which are then mapped onto the thermal frames to define the temperature measurement region. This process ensures that only corneal temperature is captured, avoiding interference from surrounding tissues. By providing detailed temperature profiles across

the ocular surface, ThermOcular allows for the assessment of tear film dynamics, blink-related cooling, and regional temperature variations. This is particularly useful for identifying localized tear film instability, as earlier studies have shown that areas of fluorescein tear film breakup correspond closely to regions of lower ocular surface temperature, indicating higher local evaporation rates.[194] In the current study, these cooler regions were specifically examined using infrared thermography to assess their spatial and temporal behavior following a blink. This approach is consistent with findings from other researchers who also demonstrated a strong spatial correlation between tear breakup areas and ocular surface cooling, confirming that localized evaporative loss can be mapped thermographically and is central to understanding EDE mechanisms.[27,30]

Compared to traditional methods, ThermOcular offers a non-contact, repeatable, and highly sensitive approach to OST measurement, making it an essential tool for both clinical diagnostics and research applications.[214]

3.2.2 Equipment and Experimental Setup

3.2.2.1 ThermOcular System Components

The experimental set-up included a Teledyne FLIR A655sc IR camera (Teledyne FLIR LLC, Wilsonville, OR, USA) featuring a 640×480 pixel resolution, a spectral range of 7.5–14 µm, and thermal sensitivity of less than 0.05°C. A full-frame size was utilized at a frame rate of 25 Hertz to achieve optimal temporal resolution. The camera was equipped with a polished germanium close-up lens, which has a high refractive index ($n \approx 4.0$ for wavelengths between 2-14 µm) and is transparent to IR, facilitating detailed and precise thermal imaging of the eye and surrounding tissues. Figure 3-6 displays the IR camera system with its mounted germanium lens (A) and the

standalone close-up lens with protective casing (B), both components critical for high-precision thermographic capture.



Figure 3-6: (A) Teledyne FLIR IR A655sc IR camera equipped with a germanium close-up lens for enhanced ocular imaging; (B) Standalone germanium close-up lens with protective casing, designed for high-precision IRT. Image source: Teledyne FLIR (www.flir.com).

The visible imaging component of the experimental setup included a FLIR BFS 51S5C-C camera (Teledyne FLIR LLC, Wilsonville, OR, USA) designed to capture synchronized visible light images for anatomical reference. This camera featured a CMOS Sony IMX250 sensor (SONY Group Corp, Tokyo, Japan) with a pixel size of 3.45 µm, resolution of 2464×2056 pixels (5 MP), and a frame rate of 75 frames per second. Additionally, the camera offered a dynamic range of 71 decibels, a saturation capacity of 10330 for excellent low-light performance, and full-range Red, Green, Blue color output. The camera was equipped with a Fujinon HF12.5SA-1 close-up lens (Fujifilm Corp, Tokyo, Japan) featuring a focal length of 12.5 mm, providing a field of view of 12×9 cm at a working distance of 17 cm. Manual focus control allowed precise adjustments for

sharp and clear macro imaging. Figure 3-7 presents the imaging system, showing the FLIR BFS 51S5C-C camera with its CMOS sensor (A) and the attached Fujinon lens (B), which enables high-resolution, close-range anatomical visualization.



Figure 3-7: (A) Teledyne FLIR BFS 51S5C-C machine vision camera, designed for high-speed, high-resolution imaging with a Sony IMX250 CMOS sensor; (B) Fujinon HF12.5SA-1 close-up lens, optimized for macro imaging and precise focus control, enhancing image clarity and field of view. Image source: Teledyne FLIR (www.flir.com).

The mounting system consisted of a slit-lamp biomicroscope integrated with an adjustable positioning arm, accompanied by a head-rest and chin-rest to ensure stable and precise positioning of the participant's head during measurements. The video output from both cameras was controlled using a PC computer running specialized software that managed data acquisition, image processing, and synchronization between the IR and visible cameras. Additionally, the software employed OCRNet segmentation algorithms to accurately isolate and analyze the corneal ROI for temperature measurements. Co-registration between the visible and thermal images was achieved

by capturing synchronized frames from both cameras and applying a spatial mapping algorithm that aligned the segmented corneal region from the visible image onto the corresponding thermal frame. This ensured that temperature extraction was performed precisely within the anatomically defined corneal area. Figure 3-8 illustrates the complete ThermOcular system mounted on the slit-lamp biomicroscope, showing the integration of the FLIR BFS 51S5C-C visible camera and the FLIR A655sc IR camera for synchronized, high-resolution OST measurements.



Figure 3-8: Custom-modified slit-lamp biomicroscope equipped with the ThermOcular dual-camera system, integrating a Teledyne FLIR BFS 51S5C-C visible camera and a Teledyne FLIR A655sc IR camera for synchronized imaging. The set-up ensures precise alignment, stable fixation, and high-resolution OST measurement[214].(Image from: Bidaki EZ, Wong A, Murphy PJ. A novel system for ocular surface temperature measurement and tracking. *IEEE Access*. 2023;11:140893-140899. doi:10.1109/ACCESS.2023.3341354)

3.2.2.2 Software and Data Logging

The ThermOcular software synchronized the IR and visible camera feeds, enabling precise simultaneous data collection. It processed real-time imagery, applying advanced machine learning-based segmentation to accurately isolate ocular structures, particularly the cornea. Data were continuously recorded over a predefined measurement interval and subsequently saved for detailed analysis.

3.2.3 Experimental Procedure and Measurement Protocol

Participants were instructed to arrive at the clinic having been awake for at least two hours and were required to acclimate to the experimental room for 15 minutes before testing. This acclimatization period allowed the tear film to stabilize, reducing potential artificial variations in OST due to sudden environmental changes. Environmental conditions were carefully controlled in a room without windows or airflow to eliminate external RH fluctuations. Prior to each measurement, ambient temperature and RH were recorded.

Participants were required to remove any eye make-up and refrain from wearing contact lenses for at least 12 hours prior to testing, to prevent interference with temperature measurements. Additionally, participants were instructed to blink naturally for 1-2 minutes before starting measurements, further ensuring tear film stabilization and reducing the risk of provoking tear film break-up.

Participants were seated comfortably with their heads stabilized using a chin-rest and head-rest. The investigator carefully aligned the IR and visible cameras to ensure proper framing of the participant's eye. Participants were instructed to fixate on a designated target positioned beyond the instrument to maintain stable gaze conditions.

Depending on the specific study protocol, blinking patterns were controlled differently. Participants were either allowed to blink normally or were instructed to refrain from blinking, holding their eyes open as long as possible during data collection. Once the participant was ready, the investigator initiated synchronized IR and visible imaging by clicking on the "Record" icon on the custom ThermOcular software (Dr. Ehsan Zare Bidaki, University of Waterloo). The video recordings lasted up to 15 seconds, based on individual study requirements.

At the end of the measurement period, the investigator clicked on the "Stop Recording" icon in the software to conclude the data collection. Immediately following this, the recorded IR and visible image data were automatically saved to the system database. After completing the final measurement, the investigator ensured that all data files were accurately labeled and securely backed up for subsequent detailed analysis. Figure 3-9 presents a representative output from the ThermOcular system, showing synchronized visible-light (left) and IR (right) images of an eye. The visible image provides high-resolution anatomical detail, while the IR image illustrates OST distribution, emphasizing regional variations across the eyelid and corneal surface.



Figure 3-9: Synchronized imaging output from the ThermOcular system, displaying visible-light (left) and IR (right) eye images. The visible camera captures high-resolution anatomical details, while the IR camera recorded OST distribution, highlighting temperature variations across the eyelid and corneal region[214] (Image from: Bidaki EZ, Wong A, Murphy PJ. A novel system for ocular surface temperature measurement and tracking. *IEEE Access*. 2023;11:140893-140899. doi:10.1109/ACCESS.2023.3341354)

3.2.4 Data Analysis

3.2.4.1 OST Calculation

OST values were extracted from the IR images using ResearchIR software (FLIR Systems, Wilsonville, OR, USA). Temperature data was processed to calculate mean OST, temperature gradients across the corneal surface, and post-blink temperature recovery rates. Temporal and spatial analyses were applied to assess dynamic changes in OST. The software applied frame selection criteria to exclude blurred or misaligned images and employed median filtering to smooth temperature fluctuations.

3.2.4.2 ROI Selection

The ROI selection varied by study, but the selection of the chosen ROI was standardized for each study using a clear overlay template. To ensure consistent and standardized ROI placement across

all participants, a clear overlay template was used to align the corneal center at a uniform location by referencing the canthus of the eye. Although anatomical landmarks were visible, the overlay ensured that the distances between the central and peripheral ROIs remained consistent across participants, improving spatial standardization (Figure 4-19). This method ensures that measurements across different individuals remain comparable by maintaining consistent distance measurements between the corneal center and peripheral ROIs, reducing variability and improving reproducibility in data collection. The ROI was manually adjusted using visible anatomical landmarks to ensure precision in temperature mapping. Automated segmentation algorithms, such as OCRNet, further refined the corneal boundaries to minimize artifacts and enhance measurement accuracy.

3.3 ResearchIR® Software

3.3.1 Purpose and Background

IRT has evolved substantially from early static image methods, which required manual analysis and were prone to observer bias. Modern software-driven approaches, such as ResearchIR (FLIR Systems), now enable automated, real-time temperature tracking, precise ROI selection, and sophisticated statistical analysis. These advancements significantly enhance the accuracy, reproducibility, and practical utility of OST measurements, making ResearchIR a valuable tool in clinical diagnostics and research, particularly for investigating tear film dynamics, blink-induced cooling, and ocular surface inflammation.

3.3.2 Equipment and Experimental Setup

3.3.2.1 ResearchIR Software Capabilities

ResearchIR software (FLIR Systems, Wilsonville, OR, USA) is an advanced IR imaging analysis platform designed for real-time temperature extraction and processing, specifically compatible with FLIR thermal cameras, such as the FLIR A655sc used in these studies. It supports real-time IR video streaming, frame-by-frame playback, and precise temperature data extraction.

The software allows flexible ROI selection, offering adjustable ROI sizes and resolutions for detailed temperature mapping, with options for both manual and automated adjustments. Statistical data extraction features include the ability to calculate, and report mean, maximum, and minimum temperature values within selected regions, with results exportable in *.csv* format for further statistical analysis.

ResearchIR supports high-speed frame rates for real-time IR video analysis and includes advanced image processing features, such as thermal contrast adjustment for enhanced visibility of temperature variations, noise filtering and smoothing algorithms to improve measurement accuracy, and histogram generation to facilitate detailed analysis of OST distributions.

Additionally, the software supports comprehensive data export and integration functionalities, including raw thermal data exports compatible with MATLAB, Python, and Excel. It also allows for the overlay of IR and visible images, significantly improving spatial alignment and facilitating more precise interpretation and analysis of IR imaging data. Figure 3-10 demonstrates OST mapping of the same patient using ResearchIR software, with the upper image presented in grayscale and the lower image utilizing a colour palette to enhance thermal contrast.

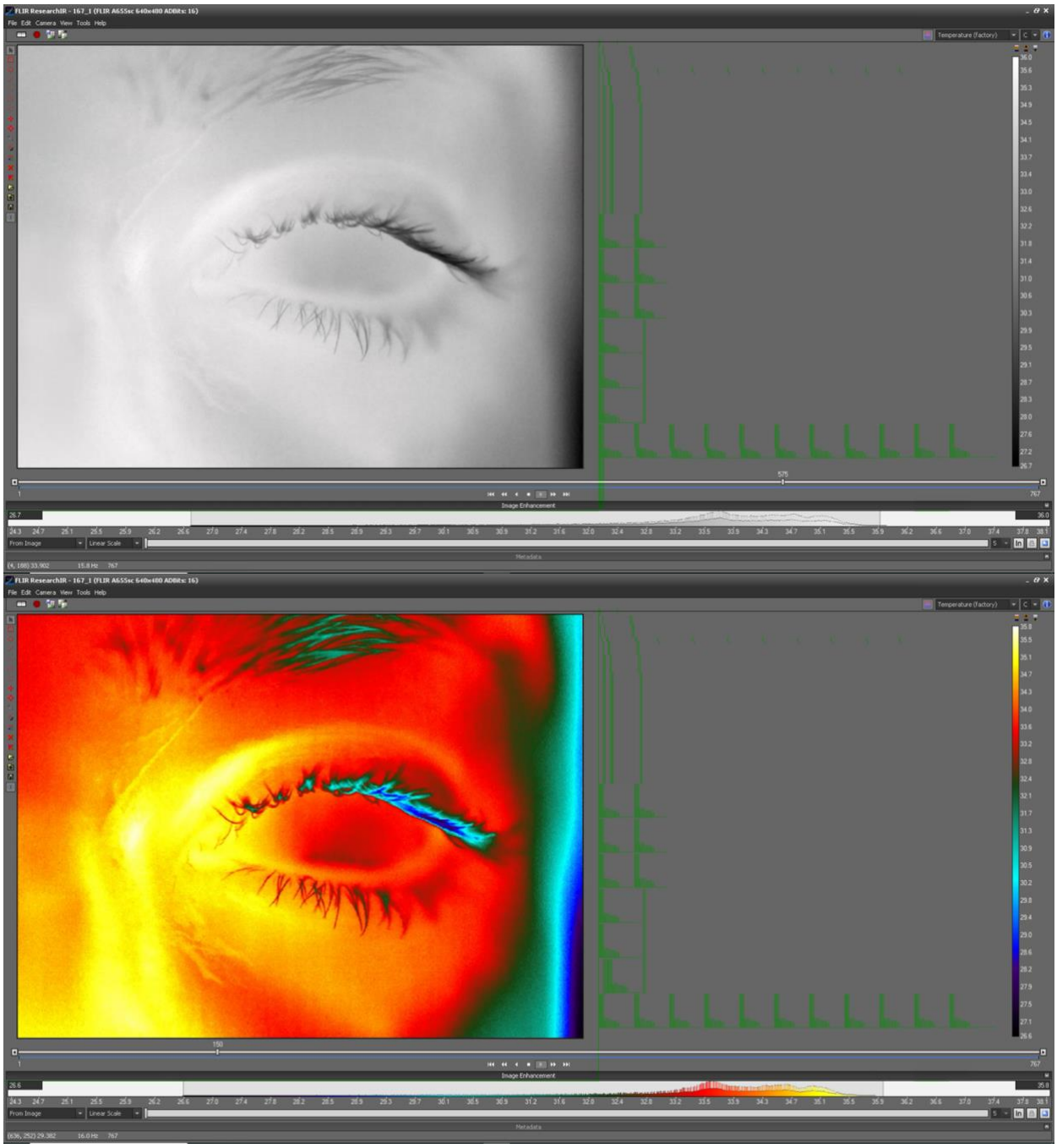


Figure 3-10: IR imaging analysis using ResearchIR software (Teledyne FLIR LLC, Wilsonville, OR, USA), displaying OST mapping of the same patient. The upper image uses a grayscale palette, while the lower image applies a colour palette to enhance temperature contrast (Image created by the author).

3.3.2.2 Experimental Procedure and Measurement Protocol

The FLIR A655sc IR camera was connected to the ResearchIR software using a high-speed data link. Prior to measurement, the camera was calibrated, with parameters including frame rate, focus, and thermal range adjusted to ensure optimal imaging performance.

Participants were comfortably positioned using a chin-rest and head-rest to maintain head stability during measurements. Participants were instructed to fixate on a pre-defined target to maintain consistent and stable eye positioning throughout the recording.

The investigator initiated IR data capture within the ResearchIR software interface by selecting the “Record” button located on the top toolbar (as shown in the software interface screenshot – Figure 3-11). A real-time IR video stream was recorded, typically for a duration of up to 15 seconds, depending on the specific study protocol.

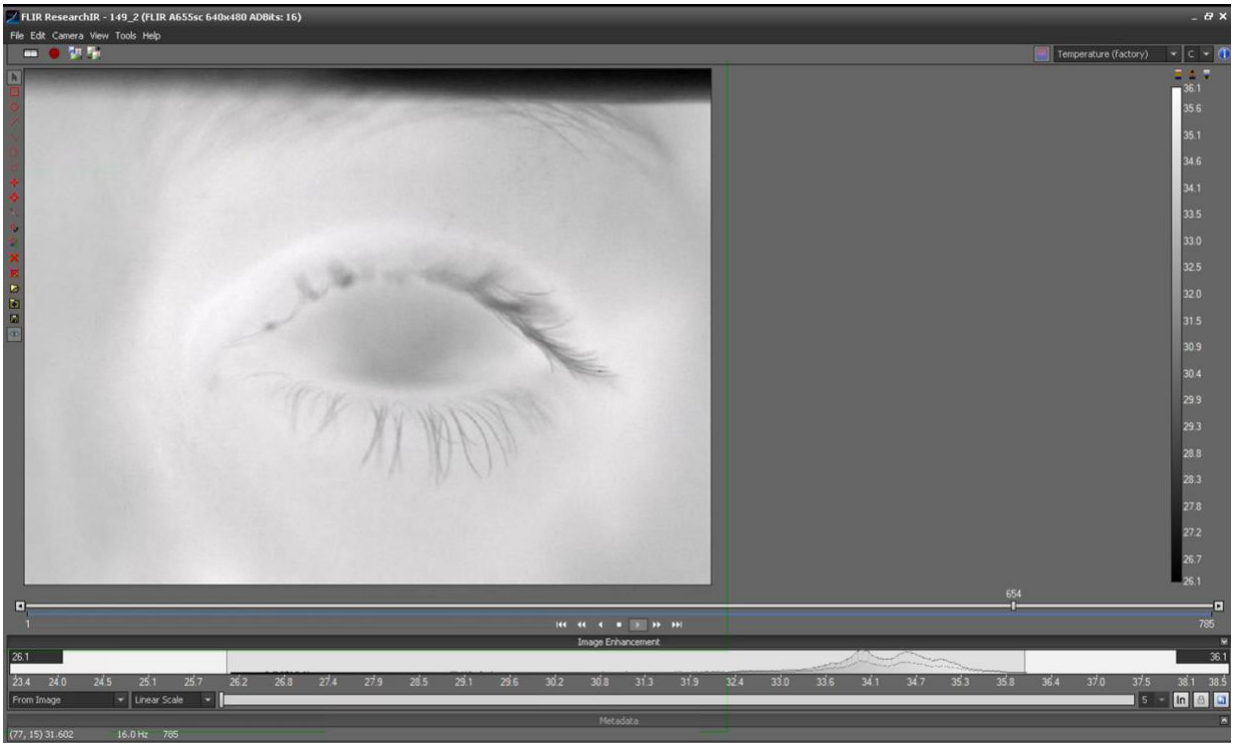


Figure 3-11: ResearchIR software (Teledyne FLIR LLC, Wilsonville, OR, USA) interface during ocular surface temperature recording. The "Record" button (top toolbar, red circle) is used to initiate thermal video capture. The real-time video stream is displayed in the main window, with tools for region-of-interest (ROI) selection, temperature monitoring, and data export options visible on the right panel (Image created by the author).

Upon completion of each recording session, the investigator clicked the "Stop" button to end data acquisition. The IR data was automatically saved in ResearchIR's proprietary format. For subsequent analysis, temperature profiles were exported as .csv files using the "Export CSV" function in the software's data output panel. All recorded data files were systematically stored and backed up for further analysis and reporting.

3.3.3 Data Analysis

3.3.3.1 OST Calculation

The ResearchIR software extracted temperature values from the selected ROI. OST was calculated as the mean temperature over time, and temperature gradients across the cornea are analyzed. Post-blink cooling rates and tear evaporation effects were evaluated using time-series analysis.

3.3.3.2 ROI Selection

The ocular regions were manually selected using ResearchIR's ROI tool**.** To ensure consistent and standardized ROI placement across all participants, a clear overlay template was used to align the corneal center at a uniform location by referencing the canthus of the eye. This method ensures that measurements across different individuals remain comparable by maintaining consistent distance measurements between the corneal center and peripheral ROIs, reducing variability and improving reproducibility in data collection. The software provided temperature values specific to the selected corneal area**.** The ROI size and resolution can be adjusted by selecting different pixel densities and regions to refine temperature mapping accuracy based on study requirements. Averaging of measurements across a larger ROI (e.g., elliptical region) reduces the impact of individual pixel noise, leading to more stable temperature readings, whereas single-pixel ROIs provide higher spatial specificity, but may be more affected by sensor noise. Figure 3-12 illustrates three ROI selection methods within the ResearchIR software: a single pixel (Cursor 1), a 3×3 pixel average (Cursor 2), and a custom elliptical region (Ellipse 1), each linked to a real-time temporal temperature plot for dynamic analysis.

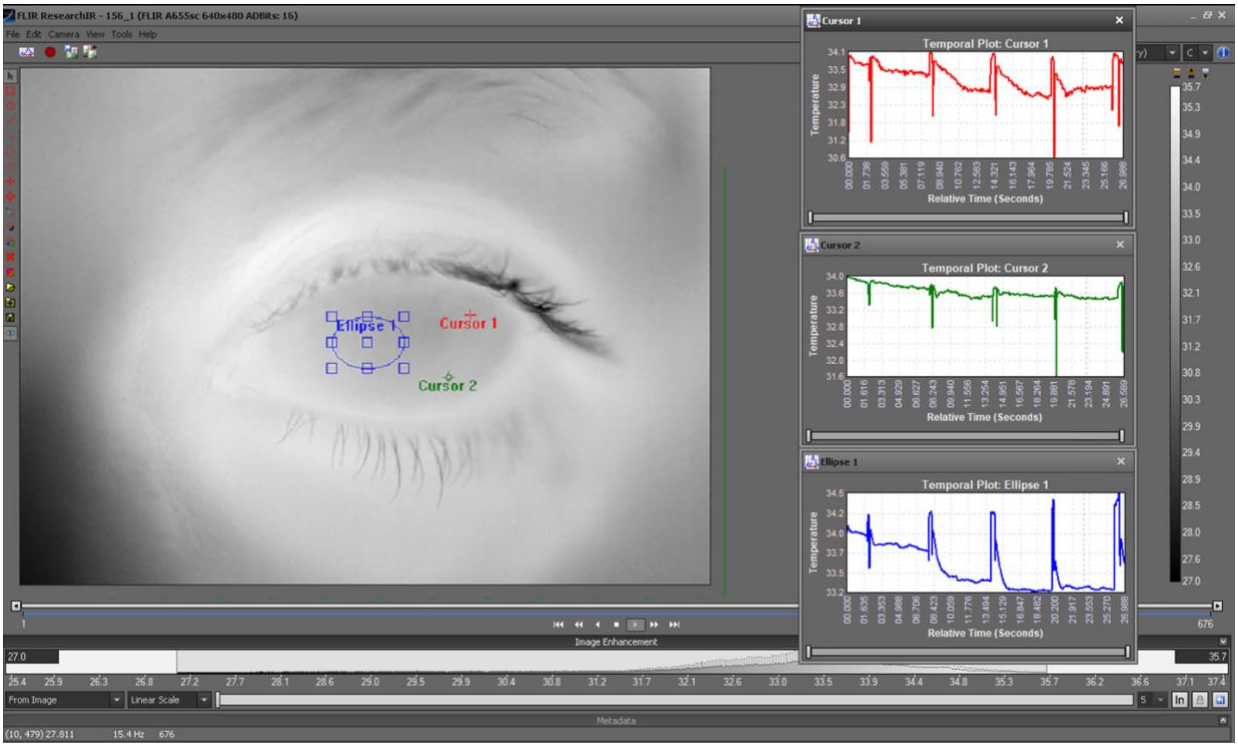


Figure 3-12: ROI selection in ResearchIR software (Teledyne FLIR LLC, Wilsonville, OR, USA), demonstrating three different methods for extracting temperature data: Cursor 1 (single pixel location), Cursor 2 (3×3 pixel average), and Ellipse 1 (custom region averaging multiple pixels). The software generates temporal temperature plots for each ROI, illustrating how temperature changes over time at each location (Image created by the author).

3.4 LipiViewII® Ocular Surface Interferometer

3.4.1 Purpose and Background

The lipid layer of the tear film, primarily produced by the meibomian glands, is essential for reducing tear evaporation, maintaining ocular surface stability, and supporting clear vision. Dysfunction or absence of this layer can significantly increase tear evaporation, leading to dry eye symptoms and discomfort. Accurate measurement of LLT is thus critical in diagnosing EDE associated with MGD.

The LipiViewII Ocular Surface Interferometer (Johnson & Johnson Vision Care, Inc., Jacksonville, Florida, USA) employs advanced interferometric imaging techniques to objectively quantify LLT with nanometer-level precision. Utilizing white-light interferometry, LipiViewII captures interference patterns from the tear film, providing accurate and reproducible LLT measurements. Additionally, the system incorporates near-infrared radiation imaging to visualize meibomian gland morphology, enabling comprehensive assessments of gland structure and lipid secretion quality.

By combining precise LLT measurement, meibomian gland imaging, and detailed blink analysis (including partial and complete blinks), LipiViewII facilitates thorough evaluation and differentiation of EDE conditions. Its high reproducibility and accuracy have been validated through comparative studies with other ocular surface analyzers, underscoring its effectiveness in both clinical practice and research settings.

3.4.2 Equipment and Experimental Setup

3.4.2.1 LipiViewII System Components

The LipiViewII Ocular Surface Interferometer system includes a visible light camera, which captures high-resolution white-light interferometry images from the eye surface which are then used to measure LLT with nanometer-level precision. Additionally, a near-infrared radiation camera provides detailed images of the meibomian glands, facilitating structural analysis for gland dropout and dysfunction. The system is equipped with an adjustable fore-head and chin-rest to ensure accurate positioning of the participant and to maintain consistent imaging conditions. An integrated illumination system, comprising a controlled white-light source for interferometric imaging and a near-infrared radiation source for meibomian gland visualization, supports optimal

image acquisition. A touchscreen display and control system provide a user-friendly, real-time interface for capturing images, analyzing data, and managing data storage.

Ambient lighting in the examination area was dimmed and carefully controlled to prevent interference with the white-light interferometry imaging process, and to support accurate lipid layer measurements and reliable imaging of the meibomian glands. Figure 3-13 displays the LipiViewII system and monitor at initialization, while Figure 3-14 presents a side view, highlighting the key components responsible for accurate alignment and stable image acquisition.



Figure 3-13: The LipiViewII Ocular Surface Interferometer (Johnson & Johnson Vision Care, Inc., Jacksonville, Florida, USA) showing the system initialization screen, and participants chin-rest/head-rest (Image created by the author).



Figure 3-14: A side view of the LipiViewII Ocular Surface Interferometer (Johnson & Johnson Vision Care, Inc., Jacksonville, Florida, USA), showing the camera system, chin-rest, and head-rest support (Image created by the author).

3.4.2.2 Experimental Procedure and Measurement Protocol

Participants were instructed to arrive at the clinic having been awake for at least two hours. Upon arrival, participants were required to acclimate briefly to the controlled testing environment, a room without windows or airflow, to eliminate external fluctuations in RH. Prior to each measurement, ambient temperature and RH were recorded.

Participants were advised to remove any eye make-up and refrain from using artificial tears, eye drops, or skincare products near the eyes for at least 12 hours before testing. This prevented potential artifacts in imaging and promoted accurate lipid layer thickness measurements.

During the measurement session, participants were comfortably positioned at the LipiViewII device, aligning their forehead and chin securely against the rests provided to maintain stability. Participants fixated on a designated target to ensure a stable gaze throughout the imaging process. Each session involved a standardized 30-second video recording, during which LLT, blink rate, and blink patterns were analyzed automatically by the LipiViewII software. The software computed average, minimum, and maximum LLT values and identified partial and complete blinks. All recorded data were securely stored for subsequent statistical analysis, ensuring consistency and reproducibility across all measurements.

3.4.3 Data Analysis

The LipiViewII software automatically processes recorded data, providing quantitative LLT values, blink dynamics, and meibomian gland imaging results. Blink rate analysis, including partial and complete blinks, which are automatically detected and quantified to evaluate tear film stability. Figure 3-15 displays the LipiViewII interface during an LLT assessment, featuring a real-time interferometric image, LLT values in nanometers, and graphical tracking of blink behavior and tear film stability metrics.

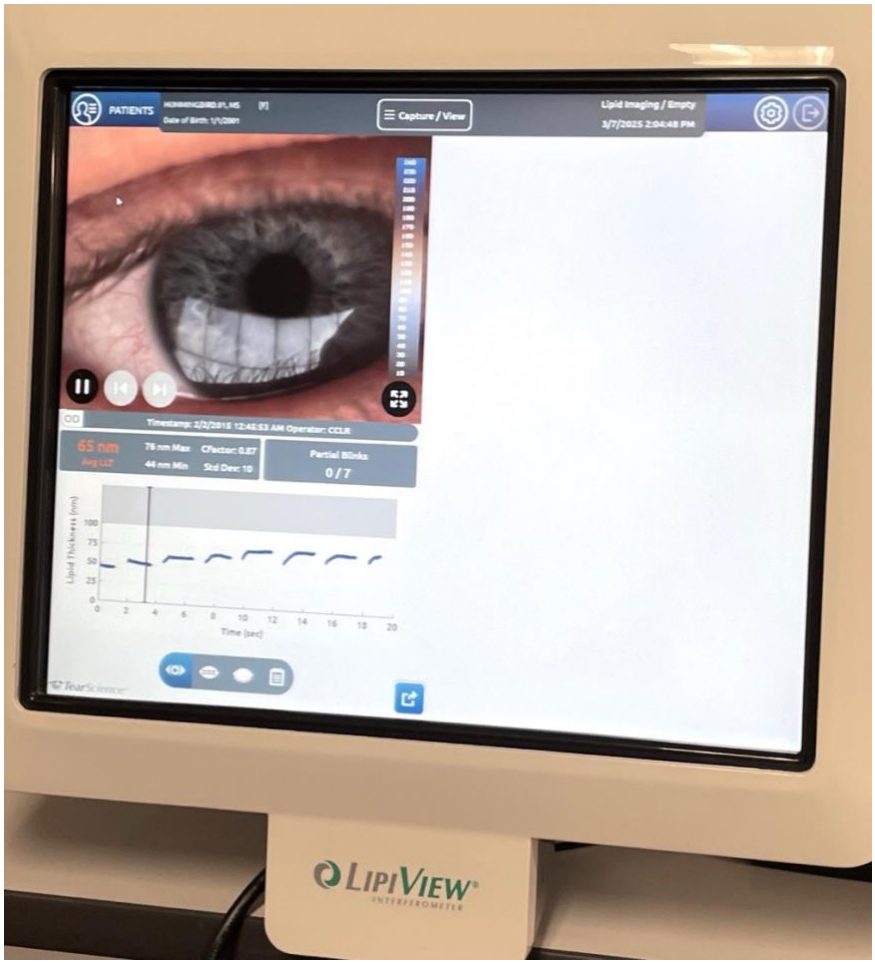


Figure 3-15: The LipiViewII Ocular Surface Interferometer (Johnson & Johnson Vision Care, Inc., Jacksonville, Florida, USA) displaying LLT measurement results. The screen shows a real-time interferometric image of the ocular surface, LLT values in nanometers, and a graphical representation of blink patterns and tear film stability analysis (Image created by the author).

3.5 OCULUS Keratograph 5M®

3.5.1 Purpose and Background

NITBUT is an objective measure of tear film stability, assessing the duration between a complete blink and the initial disruption of the tear film without using fluorescein dye. A stable tear film is essential for clear vision, ocular comfort, and preventing surface damage, particularly in conditions

like DED and MGD. The OCULUS Keratograph 5M (Oculus GmbH, Wetzlar, Germany) is a non-contact, high-resolution imaging system, that combines corneal topography with advanced tear film analysis. It employs Placido ring illumination and near-infrared radiation imaging to accurately assess tear film stability, lipid layer quality, and meibomian gland structure in a non-invasive, repeatable manner. Integrating NITBUT measurements from the Keratograph 5M with OST analyses and evaporimetry provides deeper insights into tear film dynamics, evaporation rates, and overall ocular surface health.

3.5.2 Equipment and Experimental Setup

3.5.2.1 OCULUS Keratograph5M System Components

The OCULUS Keratograph 5M system incorporates several advanced imaging modalities for comprehensive ocular surface assessment. NITBUT is measured using Placido ring projection, where the system detects distortions in the reflected rings as indicators of localized tear film destabilization. Infrared meibography employs near-infrared radiation to visualize meibomian gland dropout and atrophy, which are key indicators of MGD and evaporative DED. Additionally, the system offers ocular surface redness analysis, assessing conjunctival hyperaemia through detailed evaluation of vessel density and distribution. Tear meniscus height measurement capabilities deliver quantitative evaluations of aqueous tear production, further enhancing the assessment of tear film dynamics.

The experimental set-up followed specific lighting conditions recommended by the manufacturer to optimize image acquisition. The room lighting was dimly controlled to eliminate external reflections that could interfere with Placido ring imaging accuracy. Near-infrared radiation diodes within the device were used exclusively for NITBUT and meibography assessments, minimizing reflex tearing triggered by bright light exposure, thus ensuring accurate and consistent

measurement conditions. Figure 3-16 shows the OCULUS Keratograph 5M system configured for non-invasive tear film analysis, including its imaging modules and computer integration for real-time data capture and interpretation.



Figure 3-16: OCULUS Keratograph 5M (Oculus GmbH, Wetzlar, Germany) system set up for non-invasive tear film analysis, including Placido ring topography, meibography, and NITBUT assessment. The system is integrated with a computer for real-time imaging and data analysis (Image created by the author).

3.5.2.2 Experimental Procedure and Measurement Protocol

Participants were instructed to arrive at the clinic having been awake for at least two hours. They were advised to avoid using eye drops, make-up, or contact lenses for at least 12 hours prior to

testing, consistent with the preparation guidelines for the ThermOcular, LipiViewII, and Waterloo Evaporimeter assessments. Upon arrival, participants acclimatised briefly to a controlled testing environment without windows or airflow to prevent external fluctuations in RH. Ambient temperature and RH were recorded before each measurement.

Prior to measurements, participants were instructed to blink naturally several times to ensure a uniform distribution of the tear film across the ocular surface. Participants were then seated comfortably, with their heads stabilized by the integrated chin and forehead rests. The participant's eye was aligned centrally within the Keratograph 5M's optical path to facilitate precise Placido ring projection for tear film analysis.

The Keratograph 5M automatically recorded NITBUT by detecting distortions in the Placido ring reflections on the tear film. Two primary parameters were measured: NITBUT-first, indicating the time to the first observable tear break-up on the cornea, and NITBUT-average, representing the mean tear film stability across multiple corneal locations. Each eye underwent three consecutive NITBUT measurements to ensure repeatability and accuracy. The system software generated detailed topographical tear film maps to illustrating the locations and severity of tear break-up.

3.5.3 Data Analysis

NITBUT values (First and Average) were automatically extracted by the system. Statistical analyses were conducted to compare NITBUT measurements with tear evaporation rates and OST variations, providing a comprehensive evaluation of tear film stability.

Chapter 4 Experiments

4.1 *In vitro* examination of distilled water versus TheraTears®

4.1.1 Overview

Evaporation is a fundamental physical process in which molecules at the surface of a liquid possess, or gain, sufficient energy to transition into a gaseous state and move from the liquid into the atmosphere directly above the liquid surface. The evaporation rate (ER) of a liquid is influenced by various factors, including chemical composition, molecular weight, intermolecular forces, and environmental conditions, such as RH and temperature.[44,218]

Water, being a simple polar molecule with low molecular weight, exhibits a relatively high ER due to the water molecule having weak intermolecular forces compared to more complex, polymer-based solutions.[219]

By contrast, the natural tear film is a highly specialized, multilayered fluid that has evolved to resist evaporation. It consists of a superficial lipid layer that reduces aqueous loss, an aqueous-mucin layer that binds water to the ocular surface, and underlying glycocalyx structures that support stability. Together, these components act synergistically to limit tear film thinning and evaporation between blinks, thereby maintaining optical clarity and ocular surface health.[34,37,77]

Artificial tears, designed to mimic natural tears, such as artificial tear formulations often contain viscosity-enhancing agents, like carboxymethylcellulose, glycerin, hyaluronic acid or hydroxypropyl methylcellulose, which reduce the ER and prolong the ocular surface retention time for the artificial tears.[220,221]

A comparative assessment of the ER of an artificial tear against that of distilled water will not only provides insight into the evaporation-limiting capacity of the formulation but will also serve to

evaluate the sensitivity and performance of the Waterloo Evaporimeter in detecting subtle differences in evaporation under standardized conditions. As part of this experiment, the ER of distilled water and TheraTears® (Akorn Consumer Health, Ann Arbor, MI, USA) were measured using the Waterloo Evaporimeter. TheraTears® was chosen due the hypothesis that its higher viscosity, electrolyte balance, and mucoadhesive properties, will cause TheraTears® to evaporate at a significantly lower rate than distilled water, as it is formulated to mimic the function of natural tears and reduce tear film instability.[12,222]

The primary objective of this experiment was to quantify the differences in ERs between distilled water and a hypo-osmolar, electrolyte-enhanced artificial tear formulation- containing a viscous polymer (e.g., carboxymethylcellulose) and balanced electrolytes- to assess how such a solution might reduce tear evaporation, a key mechanism underlying EDE.[215,223] A secondary objective was to validate the performance and sensitivity of the Waterloo Evaporimeter in detecting subtle changes in evaporation dynamics under controlled experimental conditions.

4.1.2 Materials and Methods

4.1.2.1 Experimental Design and Model Eye Selection

An *in vitro* experiment was conducted to assess the ERs of distilled water and TheraTears®, using a custom-designed model eye (Manufactured by Mr. Daniel Knappert, London, UK) to simulate the exposed ocular surface. The model eye featured an elliptical aperture with an exposed surface area of 1.75 cm² (Figure 4-1). A calibrated volume of 1.2 mL of test solution was pipetted into the model eye chamber during each trial, corresponding to the total internal volume of the model eye.



Figure 4-1: The selected aluminum model eye with an exposed surface area of 1.75 cm², designed to simulate the human ocular surface for evaporation measurements. The elliptical aperture represents the exposed tear film (Image created by the author).

The central anterior cornea has a surface area of approximately 1.2–1.5 cm², as reported by Kwok using geometric modeling of the human cornea.[224] However, during open-eye conditions, particularly between blinks, the total exposed ocular surface includes additional regions beyond the central cornea, such as the adjacent bulbar conjunctiva. The 1.75 cm² model was therefore selected to better approximate this full exposed area, offering a closer match to physiological conditions during evaporative tear loss**.**

The model eye was fabricated from aluminum and featured an elliptical aperture with a capacity of 1.2 mL to hold the test liquid. Distilled water and TheraTears® were chosen as the two test solutions, representing pure aqueous evaporation versus an ophthalmic lubricant designed to mimic the tear film.

4.1.2.2 Experimental Setup

To replicate OST**,** the model eye, distilled water, and TheraTears® were pre-conditioned overnight in an oven (Fisher Scientific, Waltham, Massachusetts, USA) at 34°C, which is consistent with normal OST immediately after a blink[225] (Figure 4-2). As shown in Figure 4-3, the experiment was

conducted in a controlled environment chamber (Model 5503-11 Package E, Electro-Tech Systems Inc., Glenside, Pennsylvania, USA), set to 34°C and 40% RH.



Figure 4-2: Laboratory oven (Fisher Scientific) used to precondition the model eye and test solutions (distilled water and TheraTears®) to 34°C, simulating physiological OST before evaporation measurements (Image created by the author).

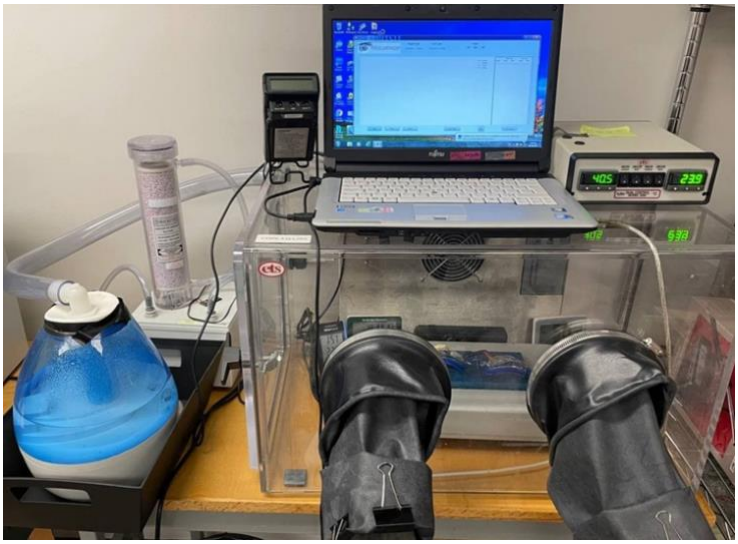


Figure 4-3: Controlled environment chamber (Model 5503-11 Package E, Electro-Tech Systems Inc.) used to maintain stable temperature (34°C) and RH (40%) during evaporation measurements. The chamber is equipped with the Waterloo Evaporimeter, a heating plate, and a digital monitoring system to ensure precise experimental conditions (Image created by the author).

Following the establishment of a physiologically controlled environment, appropriate selection of test solutions was undertaken to simulate relevant tear film conditions. To fulfill this objective, TheraTears® was chosen.

TheraTears® is a preservative-free, electrolyte-balanced artificial tear solution formulated to rehydrate the ocular surface, support pH balance, and reduce tear film osmolarity over time**.** The active ingredient, sodium carboxymethylcellulose 0.25% w/w, acts as a lubricant that enhances tear film stability and reduces evaporation.[226–228] Additionally, the solution's borate buffer system plays a role in enhancing retention of the solution on the ocular surface.[221,229] The full specifications of TheraTears® are presented in Table 4-1.

Table 4-1: Specifications of TheraTears® lubricant eye drops

Product Name	TheraTears®
Manufacturer	Akorn, USA
Type	Aqueous solution
Key Active Ingredient	Sodium Carboxymethylcellulose (0.25%) – Lubricant
Inactive Ingredients	Boric Acid, Calcium Chloride, Magnesium Chloride, Potassium Chloride, Sodium Bicarbonate, Sodium Chloride
Lipid Components	None (primarily aqueous based)
Preservative	Preservative-free
pH	7.4
Osmolarity	250-270 mOsm/kg
Intended Use	Aqueous Deficient Dry Eye
Mechanism of Action	Replenishes lost moisture, mimics natural tears
Clinical Efficacy	Studies show improvement in dry eye symptoms and tear stability

4.1.2.3 Experiment Procedure

Filling the Model Eye**:** While inside the oven, a large sample of distilled water and TheraTears® were transferred into small plastic cups to facilitate easier and faster sampling. From these cups, 1.2 mL of pre-warmed liquid was withdrawn using an Eppendorf Reference 100–1000 µL micropipette (Eppendorf, Hamburg, Germany) and transferred into the model eye chamber.

Evaporation Measurement**:** The model eye (Figure 4-4) was quickly transferred from the oven to the environmental chamber and placed on a 34°C heating plate (Digital Heatblock, VWR, Radnor, Pennsylvania, USA) to preserve thermal equilibrium and simulate physiological ocular surface conditions during the evaporation measurements**.** The right-eye goggle of the Waterloo Evaporimeter was gently placed over the model eye to form a tight seal and prevent external airflow interference. The Waterloo Evaporimeter software **(***Goggle***,** Dr. Ehsan Zare-Bidaki, Murphy Laboratory of Experimental Optometry, Waterloo, Canada**)** was initiated within 10 seconds of evaporimeter goggle sealing to begin data collection. RH and temperature were recorded four times per second for 30 seconds to capture evaporation dynamics.

Post-Measurement Handling**:** After each trial, the remaining liquid in the model eye was discarded and the model eye was dried with Kimwipe tissues (Kimtech Science, Roswell, GA, USA)**.** The model eye was then returned to the oven for re-equilibration to 34°C before the next measurement. This process was repeated for a total of 16 measurements (8 for distilled water, 8 for TheraTears®). To minimize experimental drift between trials, measurements were spaced at least three hours apart to allow for full drying, temperature stabilization, and recovery of consistent baseline conditions in the model eye.

4.1.2.4 Data Collection

The Waterloo Evaporimeter provided continuous RH and temperature data from within the sealed goggle**,** and these data were analyzed to determine the ERs of the two test liquids.

4.1.3 Results

The ERs of distilled water and TheraTears® were analyzed to determine whether there was a significant difference between the two test conditions. A Shapiro-Wilk test confirmed that both datasets were normally distributed. Based on these results, a paired t-test was performed, showing no statistically significant difference in ERs between distilled water and TheraTears® (Table 4-2).

Table 4-2: Comparison of evaporation rates between distilled water and TheraTears®.

Condition	**Mean ER ± SD (mL/min)**	**Shapiro-Wilk W value**	**Shapiro-Wilk p-value**	**Paired t-test**	**Paired t-test p-value**
Distilled Water	0.28 ± 0.02	0.97	0.92	t (7) = –1.14	0.29
TheraTears®	0.29 ± 0.03	0.90	0.45		

Figure 4-4 below presents a bar graph showing the mean ± standard deviation of ERs for the two test liquids. The mean ERs were similar between distilled water and TheraTears®, with overlapping standard deviation error bars, indicating no apparent trend toward reduced evaporation in the TheraTears® condition. These results confirm that, under the *in vitro* experimental conditions used in this study, TheraTears® did not demonstrate a statistically significant reduction in ER compared to distilled water.

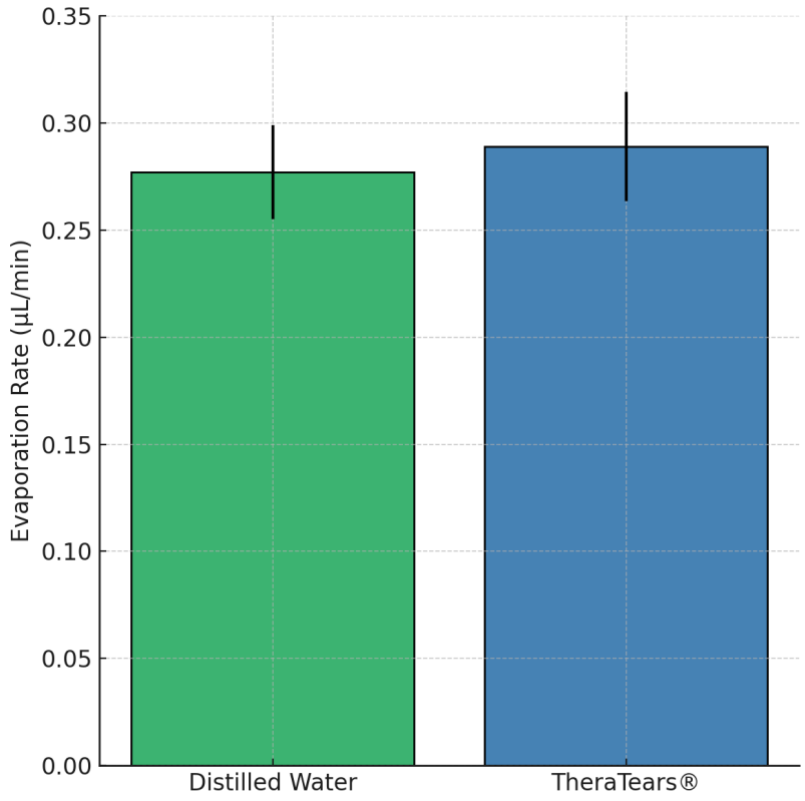


Figure 4-4: Mean ERs for distilled water and TheraTears®, presented as mean ± SD (n = 8 per group). No statistically significant difference was observed between the two conditions (p = 0.292, Paired t-test).

Figure 4-5 showed the real-time increase in RH inside the Waterloo Evaporimeter goggle during the evaporation experiment for distilled water and TheraTears®, demonstrating a nearly identical RH trend over time.

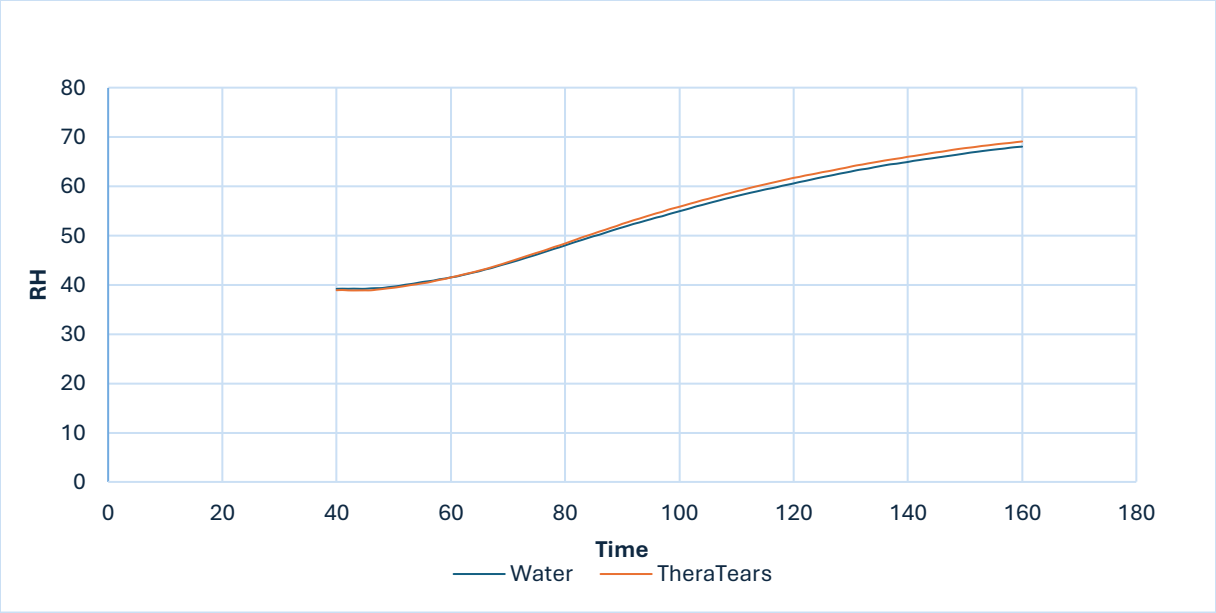


Figure 4-5: Real-time RH trend (in seconds) inside the Waterloo Evaporimeter goggle for distilled water and TheraTears®.

4.1.4 Discussion

This study evaluated the ERs of distilled water and TheraTears® under controlled *in vitro* conditions. The findings indicate that while TheraTears® exhibited a slightly higher mean ER compared to distilled water, the difference was not statistically significant**.**

Artificial tears are formulated to mimic the properties of the natural tear film, with the goal of maintaining ocular hydration and reducing evaporation. Although viscosity-enhancing agents, like carboxymethylcellulose, hyaluronic acid, and glycerin, are known to improve tear film stability, these results indicate that the presence of electrolyte blends (e.g., calcium, magnesium, potassium, sodium, phosphate, and bicarbonate) and osmolarity-balancing components[20,44] did not significantly reduce evaporation compared to distilled water. This is likely due to the absence of a lipid layer in the experimental set-up and in TheraTears® itself, which behaves similarly to water

in an evaporation-driven mode.[76,218] Lipid-based formulations, by contrast, have been shown to provide greater resistance to evaporation and warrant further investigation.[230,231] This suggested that further testing on lipid-containing artificial tears may provide greater insights into evaporation control**.**

It is important to note that the evaporation measurements in this study were limited to a 30-second observation window. This duration likely captured only the initial, rapid loss of unbound water from the tear substitute, rather than the slower, sustained phase in which viscosity-enhancing agents and bound water contribute to tear film stability. In effect, the results may represent the immediate behavior of the solution on the ocular surface, rather than its longer-term evaporative resistance. Under this model, the lack of measurable difference between distilled water and the electrolyte-rich formulation aligns with what might be expected for many artificial tears in the early post-instillation period. Extending the measurement duration in future studies would allow for a more complete assessment of the solution's capacity to retain moisture and support tear film stability over time.

Given the absence of a significant difference in evaporation rates and considering the small absolute amount of evaporated volume relative to the total, these findings suggest that distilled water and TheraTears® behave similarly under short-term, controlled *in vitro* conditions. This may be relevant for experimental setups focused on relative comparisons in evaporation, though it does not necessarily reflect the broader physical behavior of artificial tear formulations in clinical use. This may be applicable in certain *in vitro* ocular surface models focused on evaporation, though more research is needed before drawing broader conclusions about the suitability of different tear substitutes. However, it is important to recognize that in clinical applications those factors beyond

evaporation, such as osmolarity, lubrication, and ocular surface compatibility, should be considered when selecting an artificial tear solution.

In addition to evaluating the artificial tear formulation, this study also aimed to assess the performance of the Waterloo Evaporimeter. The results support its utility as a sensitive measurement tool capable of detecting subtle changes in RH within the goggle chamber. While no reference device was used in this experiment, the Waterloo Evaporimeter had previously been informally compared with the Delfin Eye VapoMeter in Dr. Wong's work, providing some early validation of its sensitivity.[217] In this context, "sensitive" refers to the device's ability to record RH changes at 0.25-second intervals, enabling fine-grained slope calculations for evaporation rate. The consistent RH trends observed across repeated trials further support its utility for detecting relative changes in controlled in vitro settings. These real-time RH recordings enabled accurate calculation of ER, demonstrating that the evaporimeter is well-suited for controlled experimental studies examining tear film dynamics and artificial tear performance.

4.1.5 Limitations and Future Directions

This study has several limitations that should be acknowledged. First, the *in vitro* model does not account for dynamic factors present in the human tear film, such as blinking, tear turnover, and lipid layer interactions**.** Since the Tear Film Lipid Layer (TFLL) plays a major role in reducing evaporation**,** the experimental set-up may not fully replicate real-world conditions.[76,218] Future studies should consider *ex vivo* or *in vivo* methodologies to assess the performance of TheraTears® in more clinically relevant conditions.

Additionally, the experiment was conducted at a fixed environmental RH and temperature**,** which may not reflect real-world variations. Changes in RH, airflow, and temperature fluctuations could

influence ERs, and future research should explore a broader range of environmental conditions to assess formulation performance across different climates.

Another limitation is the relatively short measurement period (30 seconds), which may not have been sufficient to capture the full evaporation profile of the test solutions. This time frame primarily reflects the loss of unbound or freely mobile water in the tear substitute rather than the more physiologically relevant bound fraction that interacts with the ocular surface or is retained by viscosity-enhancing agents. Artificial tears, including electrolyte-rich formulations containing viscosity modifiers such as carboxymethylcellulose, often show an initial rapid evaporation phase as the unbound water dissipates, followed by a slower phase governed by the bound water fraction. By restricting measurements to the early phase, the experiment may have underestimated the longer-term protective effects of the formulation. Consequently, the absence of a statistically significant difference between distilled water and the electrolyte-rich solution in this study is perhaps unsurprising and may reflect a general characteristic of many artificial tear formulations under short measurement conditions, rather than a true equivalence in their performance over extended periods.

Finally, comparing different artificial tear formulations, particularly those with higher viscosity agents, lipid-based components, or novel tear film stabilizers, could provide further insights into which formulations offer superior evaporation resistance**.** Given the findings of this study, future work should focus on evaluating lipid-containing artificial tears and their effectiveness in minimizing evaporation under physiological conditions.

4.1.6 Conclusion

This study found no significant difference in ERs between distilled water and TheraTears®. While this may suggest similar evaporation behavior under tightly controlled *in vitro* conditions, the

absolute volume of fluid lost was small relative to the total volume tested, and the findings should not be overinterpreted. These results do not imply that the two are interchangeable in clinical settings. The study highlights the importance of considering tear film dynamics, lipid layer presence, and the specific context of use when evaluating artificial tear performance. Future research should focus on *in vivo* assessments and lipid-based formulations to better understand strategies for optimizing tear film stability and reducing evaporation in DED management.

4.2 *In vitro* evaporimetry of different of model eye sizes and lipid layer thicknesses

4.2.1 Overview

A critical determinant of TER is the LLT of the tear film. The lipid layer, primarily composed of oils secreted by the meibomian glands, serves as a barrier to evaporation. A healthy, adequately thick lipid layer stabilizes the tear film and reduces evaporation. Conversely, dysfunction of the meibomian glands can lead to a compromised lipid layer, resulting in increased TER and contributing to DED conditions.[232] Empirical studies have demonstrated that a thinner lipid layer correlates with heightened TER, resulting in reduced tear film stability.[76,233] Furthermore, the extent of the ocular surface exposed to the environment significantly impacts TER. Larger exposed areas facilitate greater evaporation, as evidenced by studies showing that TER is higher in patients with obstructive MGD compared to normal subjects.[9] These insights underscore the intricate interplay between lipid layer integrity and ocular surface exposure in maintaining tear film stability and preventing excessive evaporation. In summary, TER is governed by a multifaceted interplay of factors, including the integrity of the lipid layer, the extent of ocular surface exposure, environmental conditions, and individual physiological characteristics. Understanding these elements is essential for developing effective strategies to manage and treat conditions like DED. Given these findings, both LLT and ocular surface size directly impact TER**.**

In this second *in vitro* evaporimetry experiment, the effect of different model eye sizes and varying LLTs was tested to observe their potential effects on water ER. These insights will contribute to understanding the biophysical mechanisms underlying tear evaporation**,** providing important implications DED research and treatment strategies.

This experiment aimed to confirm that thicker lipid layers decrease ER by enhancing tear film protection against moisture loss, while larger ocular surface areas increase ER by exposing a greater surface to ambient conditions.

4.2.2 Materials and Methods

4.2.2.1 Experimental Design and Model Eye Selection

An *in vitro* experiment was conducted to evaluate the effect of LLT and ocular surface size on ER. A custom-designed model eye system was used to simulate the exposed ocular surface. The model eyes were fabricated from aluminum and featured an elliptical aperture with a capacity to hold the test liquid. Unlike the previous study, which employed a single model eye size of 1.75 cm^2, this study utilized two different model eye sizes: 1.25 cm^2 (M1.25) and 2.5 cm^2 (M2.50) (Figure 4-6). The aperture volume of the M1.25 and M2.50 model eyes were 900 µL and 1750 µL, respectively. The selection of these sizes was based on their ability to represent a range of ocular surface exposures, with the smaller model eye mimicking lower exposure conditions (such as a partially closed eyelid or a smaller corneal exposure area) and the larger model eye representing higher exposure conditions, which occur in wide-open eye positions or individuals with larger palpebral fissures. These variations allowed for a more comprehensive assessment of how ocular surface area interacts with LLT in influencing ERs.



Figure 4-6: The two selected model eye sizes: 1.25 cm² (left) and 2.5 cm² (right) used for the experiment (Image created by the author).

Two primary test solutions were used in this experiment: distilled water (to simulate an aqueous tear film) and distilled water with added CALMO® Eye Spray as a lipid layer on top (to mimic different LLTs). (Table 4-3). The distribution of water and spray within each model was carefully determined to ensure consistency across conditions. The volume of lipid for each LLT condition was based on a single, full, spray puff size of 25 µL, as reported by the company, with increasing amounts representing progressively thicker lipid layers. The use of a spray, rather than an eye drop, was intentional and offered several methodological advantages. First, the spray produces a fine mist that spreads evenly across the water surface, resulting in a uniform and reproducible lipid layer- an outcome more difficult to achieve with a conventional drop, which tends to disperse unevenly and may form localised accumulations. Second, the formulation of CALMO® Eye Spray is specifically designed to create a stable lipid layer that integrates well with the aqueous phase,

closely mimicking the tear film's lipid component in vivo. This is particularly important in a model system where surface uniformity directly affects evaporation dynamics. Finally, the measured spray puff volume provided a consistent and easily quantifiable lipid dose, enabling precise control over LLT conditions and reducing variability between trials.



Figure 4-7: CALMO® Eye Spray Packaging[234] (Image from: CandorVision. Calmo Eye Spray Packaging [Internet]. Montreal: CandorVision; [cited 2025 Mar 13]. Available from: https://www.candorvision.com/calmo-eye-spray)

CALMO® Eye Spray (Figure 4-7) was chosen for its ability to stabilize the lipid layer of the tear film, addressing one of the root causes of dry eye by reducing excessive tear evaporation. The spray contains liposomes, which can form a stabilizing lipid-like film on the surface and thereby help reduce evaporation. It also includes dexpanthenol (pro-vitamin B5), which serves mainly as a moisturizer and supports epithelial protection, though it does not directly influence evaporation. The liposomes are composed of soy lecithin, a plant-derived phospholipid. While not a natural

constituent of the tear film, soy lecithin has amphiphilic properties that allow it to spread across aqueous surfaces, reduce surface tension, and improve lipid coverage. These characteristics make the spray suitable for creating controlled variations in lipid layer thickness (LLT) in the model eye system. The ingredients of CALMO® Eye Spray, as provided in the official package insert, are summarized in Table 4-3:

Table 4-3: Specifications of CALMO Eye Spray

Product Name	CALMO® Eye Spray
Manufacturer	Scope Eyecare, Germany
Type	Lipid-based spray
Key Active Ingredient	Soy Lecithin – Lipid Layer Stabilizer
Inactive Ingredients	Sodium Chloride, Ethanol, Vitamin A, Vitamin E, Purified Water
Lipid Components	Soy Lecithin
Preservative	Preservative-free
pH	6.8-7.4
Osmolarity	Not specified (spray application)
Intended Use	EDE & MGD
Mechanism of Action	Stabilizes the lipid layer, reduces evaporation, and improves meibomian gland function
Clinical Efficacy	Clinical data suggests improved lipid layer stability and reduced tear evaporation

4.2.2.2 Experimental Setup

To replicate physiological OST, the model eyes and test solutions were pre-conditioned overnight in an oven (Fisher Scientific, Waltham, Massachusetts, USA) at 34°C, the reported normal human OST. The experiment was conducted in a controlled environmental chamber (Model 5503-11 Package E, Electro-Tech Systems Inc., Glenside, Pennsylvania, USA), set to 34°C and 40% RH to maintain stable testing conditions.

4.2.2.3 Experiment Procedure

Filling the Model Eye: While still inside the oven, the model eyes were filled with pre-warmed distilled water using an Eppendorf Reference 100–1000 µL micropipette (Eppendorf, Hamburg, Germany), with the volume adjusted according to the experimental condition. The total liquid volume was determined by the model eye size: 0.9 mL for the 1.25 cm^2 model eye and 1.75 mL for the 2.5 cm^2 model eye. Depending on the assigned LLT condition (No Lipid, Thin, Medium, or Thick), a portion of the total volume was filled with distilled water, and the remainder was supplemented by dispensing the required number of CALMO® Eye Spray puffs (1, 2, 3, 4 or 6) directly onto the water surface. The spray nozzle was positioned perpendicular to the model eye and maintained at a fixed distance of approximately 2–3 cm above the liquid surface to ensure an even mist coverage without disturbing the aqueous layer. No stirring or agitation was performed after spray application, allowing the lipid layer to spread naturally. Details of the water and CALMO® volumes are summarized in Table 4-4.

Table 4-4: Distribution of water and CALMO® Eye Spray volumes for each LLT condition in the 1.25 cm² and 2.5 cm² model eyes. The total volume of each model eye was maintained constant, with increasing sprays representing progressively thicker lipid layers, and the corresponding water volume adjusted accordingly.

	1.25 cm² Model Eye (Volume: 0.9 mL)			**2.5 cm² Model Eye (Volume: 1.75 mL)**		
LLT Condition	Water Volume (mL)	CALMO® Volume (mL)	Number of Spray Puffs	Water Volume (mL)	CALMO® Volume (mL)	Number of Spray Puffs
No Lipid	0.90	0.00	0	1.75	0.00	0
Thin LLT	0.86	0.05	1	1.66	0.09	2
Medium LLT	0.81	0.09	2	1.57	0.18	4
Thick LLT	0.77	0.14	3	1.48	0.27	6

These variations were chosen to assess the influence of LLT on evaporation, with progressively increasing amounts of lipid spray representing thin, medium, and thick lipid layers.

Evaporation Measurement: The model eye was transferred from the oven to the environmental chamber and placed on a 34°C heating plate (Digital Heatblock, VWR, Radnor, Pennsylvania, USA). The right-eye goggle of the Waterloo Evaporimeter was carefully placed over the model eye to form a tight seal, minimizing external airflow interference. The Waterloo Evaporimeter software (*Goggle*, Dr. Ehsan Zare-Bidaki, Murphy Laboratory of Experimental Optometry, Waterloo, Canada) was initiated within 10 seconds of sealing to begin data collection. RH and temperature data were recorded four times per second for 30 seconds to capture evaporation dynamics.

Post-Measurement Handling: After each trial, the remaining liquid was discarded, and the model eye was dried with Kimwipe tissues (Kimtech Science, Roswell, GA, USA). The model eye was returned to the oven for re-equilibration to 34°C before the next measurement. This process was repeated four times for each condition, ensuring repeatability and statistical robustness. To minimize experimental drift, each measurement was conducted at least three hours apart, ensuring the model eye was fully dried and re-equilibrated before each trial.

4.2.2.4 Data Collection

The Waterloo Evaporimeter provided continuous RH and temperature data from within the goggle, which were analyzed to determine the ER under different LLT and ocular surface area conditions.

4.2.3 Results

The Mean ER ± SD for each LLT condition in the 1.25 cm^2 and 2.5 cm^2 model eyes is presented in Table 4-5. Each LLT condition was tested five times for both model eye sizes, resulting in a total of 40 measurements. After performing the Shapiro-Wilk test and confirming that the data were normally distributed, a two-way ANOVA was conducted to determine the statistical significance of the effects of LLT, model eye size, and their interaction on evaporation rate. The results are shown in Table 4-6.

Table 4-5: Mean ER ± SD across different LLT conditions for the 1.25 cm² and 2.5 cm² model eyes.

LLT Condition	Mean ER ± SD (µL/min)	
	Model Eye 1.25 cm²	**Model Eye 2.5 cm²**
No Lipid	0.300 ± 0.012	0.320 ± 0.024
Thin LLT	0.300 ± 0.043	0.316 ± 0.015
Medium LLT	0.300 ± 0.045	0.305 ± 0.026
Thick LLT	0.297 ± 0.040	0.306 ± 0.023

Table 4-6: Two-way ANOVA results assessing the main effects of LLT, model eye size, and their interaction on ER.

Parameter	F-Statistic	P-Value
LLT	5.420	**0.009**
Model Eye Size	6.780	**0.032**
LLT × Model Eye Size Interaction	2.145	0.104

The two-way ANOVA revealed a statistically significant main effect of LLT on evaporation rate ($F(3, 24) = 5.42$, $p = 0.009$), indicating that changes in lipid layer thickness significantly influenced ER. A significant main effect was also observed for model eye size ($F(1, 24) = 6.78$, $p = 0.032$), with the larger surface area associated with higher ER. However, the interaction between LLT and model eye size was not statistically significant ($F(3, 24) = 2.145$, $p = 0.104$), suggesting that the effect of LLT on ER was consistent across both model eye sizes. Although statistically

significant, the absolute changes in ER were very small (≈0.005–0.010 µL/min) and only become apparent when reported to three decimals.

Given the significant main effect of LLT on evaporation rate, a post hoc Tukey HSD test was conducted to examine pairwise differences between LLT conditions. The results revealed that the Medium LLT condition resulted in significantly lower ER compared to both the No Lipid ($p = 0.031$) and Thin LLT conditions ($p = 0.015$). No other pairwise comparisons reached statistical significance.

4.2.4 Discussion

This study investigated the impact of LLT and ocular surface size on ER under controlled conditions. The findings indicate that both factors significantly influence ER, with thicker lipid layers, simulated using CALMO® Eye Spray reducing ER, and larger surface areas producing higher ER across all conditions.

The TFLL plays a crucial role in maintaining ocular surface health by minimizing water loss. A study demonstrated that a model TFLL composed of 40% wax esters, 40% cholesteryl esters, and 20% polar lipids reduced water ER by 11% at a surface pressure of 47 mN/m. This underscores the importance of lipid composition and thickness in controlling tear evaporation. [235]

The efficacy of liposomal eye sprays in stabilizing the TFLL has been documented in previous studies. For instance, a study comparing high and low phospholipid concentration eye sprays found that higher concentrations significantly improved ocular comfort and tear film stability.[236] This aligns with the results from this study, suggesting that the liposomal components of CALMO® Eye Spray contribute to tear film stabilization and help reduce tear evaporation.

The results from this study align with these findings, showing a progressive reduction in ER with increasing LLT. Specifically, the No Lipid condition exhibited the highest ER, while the Thick

LLT condition showed the lowest. This suggested that thicker lipid layers provide enhanced stability to the tear film, effectively reducing moisture loss.

In addition to the influence of LLT, this study revealed that the larger ocular surface area (M2.50 model eye) consistently exhibited higher ER across all LLT conditions. This observation supports the hypothesis that increased exposed ocular surface area leads to greater evaporation. This finding aligns with previous research demonstrating that TER increase proportionally with ocular surface area.[108]

Understanding the relationship between ocular surface area and TER is crucial for comprehending tear dynamics and developing effective treatments for DED. These insights highlight the importance of considering both LLT and ocular surface area in managing tear evaporation and maintaining ocular surface health.

The findings from this study have important implications for both experimental and clinical settings. The observation that TER decreases with increasing LLT suggested that artificial tear formulations with lipid-based components may be more effective in reducing evaporation-related tear film instability. Moreover, the significant impact of ocular surface area on TER underscores the importance of considering palpebral fissure size and blink rate when assessing DED severity and designing treatment strategies.

In experimental settings, the results validate the need for including lipid-mimicking agents in *in vitro* tear film models to achieve physiologically relevant results. Additionally, the influence of ocular surface area suggested that model eye selection should closely mimic natural human corneal exposure for accurate tear film evaporation studies.

4.2.5 Limitations and Future Directions

While this study provides valuable insights, several limitations must be acknowledged:

The experimental set-up was conducted in a static environment, thereby excluding the dynamic spreading and redistribution of the lipid layer that would normally occur during blinking. Furthermore, although RH and temperature were carefully controlled, real-world fluctuations in environmental conditions, such as climate and airflow, may also influence TER. Additionally, although CALMO® Eye Spray was used to simulate the lipid layer, it does not fully replicate the complex structural and biochemical properties of the natural tear film. Moreover, the thickness of the lipid layer was not directly measured; instead, it was assumed based on the number of spray applications. While this approach allowed for relative comparisons, interferometry measurement techniques would provide a more accurate and objective assessment of lipid layer thickness.

Future research should explore incorporating a blinking mechanism in experimental set-ups to better understand lipid redistribution and tear film break-up, for example using the OcuBlink device (OcuBlink Inc., Toronto, Canada).[237] It should also involve testing additional lipid-based artificial tears to compare their effectiveness in reducing evaporation. Furthermore, expanding the range of environmental conditions, particularly RH and airflow, would provide valuable insight into how these variables influence TER.

4.2.6 Conclusion

This study demonstrated that LLT and ocular surface size are critical factors influencing TER. Thicker lipid layers significantly reduced TER, while larger exposed ocular surfaces led to higher ERs. These findings support the clinical relevance of lipid-based artificial tears in managing EDE and emphasize the need for precise *in vitro* models that replicate physiological conditions. Future research should focus on dynamic tear film interactions, environmental variability, and enhanced lipid-mimicking formulations to further advance our understanding of tear film stability and evaporation control.

4.3 Investigating Tear Film Dynamics Following Lipid Eye Drop Instillation (PHASE I)

4.3.1 Overview

The tear film, particularly the lipid layer produced by the meibomian glands, plays a critical role in regulating tear evaporation and maintaining tear film stability. By significantly reducing moisture loss from the ocular surface, the lipid layer ensures adequate lubrication and protects against DED symptoms.[35,238] TER serves as an essential diagnostic parameter for identifying EDE, a condition linked to MGD.[6,239] The second *in vitro* study used an eye model with CALMO® eye spray to demonstrate the efficacy of lipid supplementation in reducing tear film evaporation, emphasizing the clinical relevance of lipid-based therapies. However, while *in vitro* models provide controlled environments to examine fundamental tear film dynamics, they lack the complexity of physiological variables present *in vivo*, such as blink rate, OST, and natural tear turnover.

To bridge this gap, the current study aimed to evaluate these effects *in vivo*. Specifically, to investigate the interrelationships among LLT, NITBUT, and TER under physiological conditions. Studying these parameters concurrently provided a comprehensive understanding of their inter-dependency and offered clinically significant insights into tear film dynamics.[7]

Additionally, this study aimed to validate the performance and reliability of the Waterloo Evaporimeter to measure TER simultaneously from both eyes. This device offers enhanced precision, bilateral measurement capabilities, and improved temporal resolution compared to existing evaporimeters such as the Eye-Vapometer (Delfin Technologies, Finland).[200,240]

Therefore, the purposes of this experiment were two-fold:

(1) To validate the accuracy and reliability of the Waterloo Evaporimeter,

(2) To investigate the impact of lipid-based eye drop instillation on LLT, NITBUT, and TER, aiming to clarify their interrelated dynamics under physiological conditions.

4.3.2 Materials and Methods

4.3.2.1 Subjects and Ethical Approval

This study received ethics clearance through a University of Waterloo Research Ethics Board (REB #44425). The study adhered to the tenets of the Declaration of Helsinki.

Twenty-five healthy adult participants (mean age 35.3 ± 8.25 years; 17 males, 8 females) were enrolled in the study. Inclusion criteria required participants to be 18 years or older, have no known active ocular disease or infection, and be able to comply with the study protocol, including refraining from contact lens wear, eye make-up, and ocular lubricants on the day of the study visit. Participants also needed to be awake for at least two hours prior to the study visit. Exclusion criteria included the presence of any active ocular disease or infection, recent ocular surgery within the past six months, or the use of systemic or ocular medications that could potentially influence tear film properties. Individuals with a known sensitivity to Systane Complete® eye drops or petroleum jelly, as well as those with a history of refractive surgery or aphakia, were also excluded.

All subjects provided written informed consent before participating in the study.

4.3.2.2 Sample Size Determination

The required sample size for this study was determined using an *a priori* power analysis conducted in G*Power (Version 3.1.9.7; Heinrich Heine University Düsseldorf, Germany) for a repeated-measures ANOVA (within-subjects) design. Assuming a medium effect size ($f = 0.25$, equivalent to Cohen's $d \approx 0.5$), with $\alpha = 0.05$ and power $(1–\beta) = 0.80$, the analysis indicated a minimum of 54 participants would be required to detect an effect of that size with the specified level of

statistical power. The effect size assumption was based specifically on TER as the primary outcome, guided by pilot data reported in the doctoral thesis of Dr. Stephanie Wong, which evaluated short-term changes in TER following lipid-based eye drop instillation using a comparable evaporimetry setup.[217] Although this study also included NITBUT and LLT, TER was selected as the reference variable for sample size estimation due to the availability of comparable pilot data.

To ensure adequate statistical power and allow for possible attrition or data exclusion, a total of 60 participants was targeted for recruitment in this study.

4.3.2.3 Instrumentation

The following instruments were used for this study, with their detailed specifications previously described in the methodology chapter and thus not repeated here:

- Waterloo Evaporimeter: TER. (Section 1-1)
- Keratograph 5M® (Oculus, Germany): NITBUT. (Section 3-5)
- Tear Science LipiView II® (Johnson & Johnson Vision, USA): LLT. (Section 3-4)

Systane Complete® Eye Drop (Alcon, Canada) is a commercially available preservative-free, sterile, lipid-based white emulsion formulated to supplement the natural tear lipid layer. It contains nano-sized lipid droplets ingredients that collectively function to stabilize the lipid layer, improve tear film integrity, enhance tear film stability, and subsequently reduce tear evaporation. The choice of Systane Complete® was based on its proven clinical effectiveness, extensive usage, and well-established safety profile, providing an appropriate model to examine changes in tear film parameters. Table 4-7 summarizes the key specifications of Systane Complete®.

Table 4-7: Specifications of Systane Complete® lipid eye drop.

Product Name	Systane Complete®
Manufacturer	Alcon, USA
Type	Oil-in-water nano emulsion
Key Active Ingredient	Propylene Glycol (0.6%) – Lubricant
Inactive Ingredients	Boric Acid, Edetate Disodium, Hydroxypropyl Guar, Mineral Oil, Polyoxyl 40 Stearate, Sorbitol, Sorbitan Tristearate, Purified Water
Lipid Components	Dimyristoyl Phosphatidylglycerol (DMPG), Mineral Oil
Preservative	POLYQUAD(Polyquaternium-1) 0.001%
PH	7.4
Osmolarity	300 mOsm/kg
Intended Use	EDE & Mixed DED
Mechanism of Action	Restores the lipid layer, stabilizes the tear film, reduces evaporation
Clinical Efficacy	Demonstrated effectiveness in improving LLT and reducing symptoms of DED

4.3.2.4 Experimental Procedure

The experimental tasks were conducted in the following chronological order:

4.3.2.4.1 Baseline Measurements

Demographic, ocular, and medical history data were collected for each participant. This included information on age, sex, contact lens use, recent use of eye drops, history of ocular surgeries or infections, use of ocular or systemic medications or supplements, and any known sensitivities to eye drops or petroleum jelly, as well as a history of epilepsy.

Entrance visual acuity (VA) was assessed using a Bailey-Lovie LogMAR chart to confirm that participants had normal or corrected-to-normal vision prior to the experiment.

LLT was then measured using the LipiView II device, followed by three consecutive NITBUT measurements obtained with the Keratograph 5M.

To prepare for evaporimetry, petroleum jelly was carefully applied around the eyes to ensure an airtight seal with the evaporimeter goggles and to block evaporation from the skin surrounding the eyes. TER was measured with the participant's eyes open, while blinking every three seconds for a duration of 20 seconds, guided by a metronome. After ventilating the goggles to restore baseline RH levels, TER was measured again with the eyes closed for 20 seconds.

4.3.2.4.2 Lipid Drop Instillation

One drop of Systane Complete® was instilled into randomly chosen one eye followed by a wait period of five minutes to allow for absorption and stabilization.

4.3.2.5 Post-Drop Measurements

LLT was measured using the LipiView II® device. Following this, three consecutive NITBUT measurements were obtained using the Keratograph 5M®. Post-drop TER was then assessed, beginning with an open-eye measurement during which participants blinked every three seconds for 20 seconds, guided by a metronome. After ventilating the goggles to restore baseline RH, TER was measured again with the eyes closed for 20 seconds.

4.3.2.5.1 Additional Measurements

The Waterloo Evaporimeter is designed to measure TER within a controlled chamber. The second *in vitro* study demonstrated that the exposed ocular surface area significantly impacts ER. It is also likely that the volume of the goggle chamber will impact the measured TER.

A larger goggle volume provides more space for water vapor accumulation, potentially affecting the RH gradient inside the chamber by influencing the rate at which water molecules diffuse from the tear film. This internal volume can vary between individuals depending on facial structure and the degree of ocular protrusion (i.e., the relative position of the eye in the orbit). Therefore, quantifying the exact volume of the goggle chamber is necessary to ensure consistency across measurements and to control for inter-individual anatomical variations.

Similarly, the palpebral aperture size (PAS) determines the extent of the exposed ocular surface area. A larger exposed area allows for greater evaporative loss due to increased interaction between the tear film and the surrounding air. By measuring PAS, individual anatomical differences that could contribute to variability in TER can be considered.

These additional measurements enhanced the precision of the evaporimetry assessments by providing a more comprehensive understanding of the factors influencing tear film evaporation, allowing for more accurate interpretation of inter-subject differences in DED studies.

The following measurement techniques were used to quantify the goggle chamber volume and palpebral aperture size:

Waterloo Evaporimeter Goggle Volume: The participant was seated upright in a consulting chair with their head positioned against a headrest for stability. The participant then placed a pair of modified Arena Zoom X-Fit® swimming goggles (Arena Distribution SA, Lugano, Switzerland) over their eyes and adjusted the strap to ensure a secure fit. These modified goggles featured a small opening at the top of each eyepiece, designed to facilitate the introduction of liquid into the chamber (Figure 4-8). To measure the volume of the goggle chamber, Sensitive Eyes® Saline Plus Solution (Bausch + Lomb, USA) - a buffered, isotonic saline solution selected for its ocular biocompatibility - was drawn into a 30 mL BD (Becton, Dickinson and Company, Franklin Lakes,

New Jersey, USA) Plastic Syringe using a 200 µL pipette tip. The detailed specifications of Sensitive Eyes Saline Plus Solution are summarized in Table 4-8.

The initial volume of saline in the syringe was recorded in milliliters. With their eyes closed, the participant remained still as saline was gradually introduced into the eyepiece chamber until completely filled. The final volume remaining in the syringe was then recorded to the nearest milliliter. The difference between the starting and ending volume was used to determine the total volume within each goggle chamber for that participant.



Figure 4-8: Top view of the modified swimming goggles, with arrows indicating the small holes drilled into each eyepiece chamber. These openings facilitated the addition of saline, enabling precise measurement of the chamber volume (Image created by the author).

Table 4-8: Specifications of Sensitive Eyes® Saline Plus Solution

Product Name	Sensitive Eyes® Saline Plus Solution
Manufacturer	Bausch + Lomb, USA
Type	Buffered isotonic saline solution
Key Active Ingredient	Sodium Chloride (0.9%)
Inactive Ingredients	Boric Acid, Sodium Borate, Potassium Chloride, Calcium Chloride, Magnesium Chloride, Preservative (POLYQUAD® 0.001%)
Lipid Components	None
Preservative	POLYQUAD® (Polyquaternium-1) 0.001%
PH	Approximately 7.0
Osmolarity	~300 mOsm/kg
Intended Use	Rinsing and storing soft contact lenses; ocular surface irrigation
Mechanism of Action	Maintains isotonicity with the eye to prevent irritation; helps rinse away debris
Clinical Efficacy	Gentle on sensitive eyes; helps maintain ocular comfort; not a tear substitute

PAS: The anterior segment of the eye was photographed using a Canon EOS 60D digital camera (Canon, Tokyo, Japan) mounted on a Zeiss slit-lamp biomicroscope. Images of each eye were captured at 5× magnification, with additional external illumination provided by a Canon Macro Twin Lite flash to enhance visibility. To establish a calibration reference, participants held a ruler beneath each eye during image acquisition. The photographs were analyzed using ImageJ software (Version 1.52k, National Institutes of Health, USA). The Polygon tool was used to delineate the

boundaries of the upper and lower eyelids, allowing for precise measurement of the exposed ocular surface area. The enclosed region between the eyelids was quantified in square centimeters (cm^2) as a measure of the visible ocular surface area. An example of the ImageJ-based delineation process used for PAS measurement is shown in Figure 4-9.

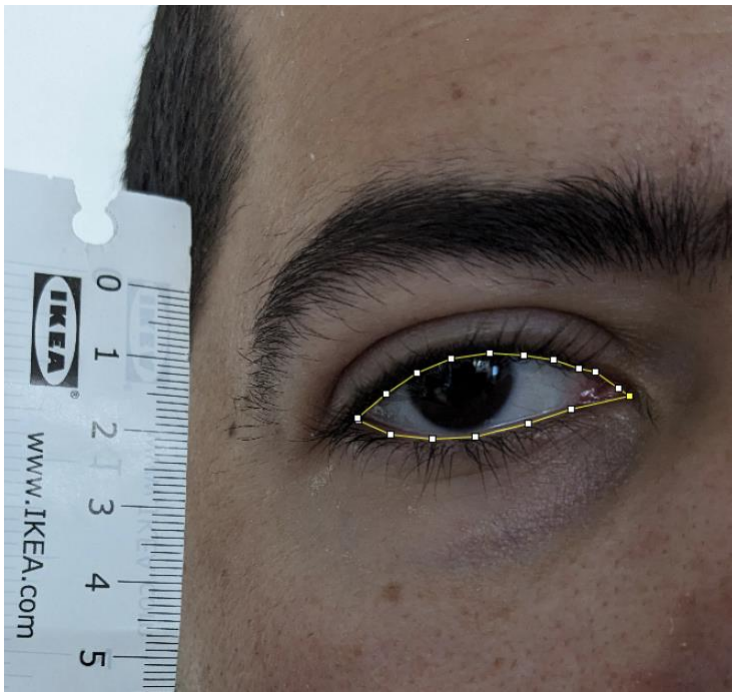


Figure 4-9: Representative ImageJ analysis of PAS measurement. The exposed ocular surface area was delineated manually using the Polygon Selections Tool in the ImageJ software (v1.52k, NIH, USA), with vertices placed along the upper and lower eyelid margins. A calibration ruler was included in the field of view to enable precise scaling and quantification of the enclosed area in square centimeters (cm^2) (Image created by the author).

4.3.2.5.2 Completion Procedures

Exit visual acuity was reassessed using the Bailey-Lovie LogMAR chart to confirm that no adverse effects had occurred during testing. Participants then completed a study completion form and received remuneration for their participation.

The following table (Table 4-9) summarises the structured sequence of experimental procedures conducted throughout the study.

Table 4-9: Summary of the experimental procedure of the study.

Baseline Measurements	Collection of demographic data, ocular, and medical history
	Entrance VA with Bailey-Lovie LogMAR chart
	LLT with LipiView II
	NITBUT with Keratograph 5M
	TER with Waterloo Evaporimeter
Lipid Drop Instillation	Instillation of one drop of Systane Complete® into one eye
	Wait period of 5 minutes
Post Drop Measurements (@ 5 minutes)	LLT with LipiView II
	NITBUT with Keratograph 5M
	TER with Waterloo Evaporimeter
Additional Measurements	Waterloo Evaporimeter Goggle Volume
	PAS with a Canon EOS 60D digital camera
	Exit VA with Bailey-Lovie LogMAR chart

4.3.2.6 Statistical Analysis

All statistical analyses were conducted using SPSS (IBM Corp., Armonk, NY, USA). To assess data normality, the distribution of LLT, NITBUT, and TER values before and after lipid drop instillation was evaluated using the Shapiro-Wilk test. Variables that deviated from normality were analyzed using non-parametric methods.

Comparative analyses were conducted to examine changes in tear film parameters pre- and post-instillation. Due to its non-normal distribution, LLT was analyzed using the Wilcoxon Signed-Rank test. In contrast, NITBUT and TER values, which followed a normal distribution, were analyzed using paired-sample t-tests.

To explore sub-group differences, participants were categorized into low and high LLT groups based on the median baseline LLT value, as well as low and high RH groups based on the median ambient humidity. Differences between these groups were evaluated using independent t-tests for normally distributed variables or Mann-Whitney U tests for non-normally distributed variables.

Pearson correlation analyses were conducted to investigate the relationships between changes in LLT, NITBUT, and TER following lipid drop instillation. Additional correlation analyses were performed to assess the influence of environmental factors (RH and temperature) and anatomical factors (PAS and VIG) on TER measurements.

Finally, the Intraclass Correlation Coefficient (ICC) was calculated to assess the repeatability and reliability of TER measurements obtained with the evaporimeter. An ICC value greater than 0.80 was considered indicative of excellent reliability.

4.3.3 Results

4.3.3.1 Participant Demographics and Environmental Conditions

An initial sample size calculation for Phase I indicated that 54 participants were needed to achieve adequate statistical power. Recruitment was planned for 60 to allow for exclusions. However, after enrolling 25 participants, interim analysis suggested that the 5-minute observation period was too short to fully capture post-instillation changes. At that point, recruitment was paused, and the protocol was revised to include a 20-minute follow-up period and the addition of OST measurements using the ThermOcular camera. As a result, the current dataset represents a partial

phase of the study, and the reduced sample size is acknowledged as a limitation. Table 4-10 presents the demographic characteristics of the participants along with the environmental conditions under which the measurements were taken.

Table 4-10: Participant demographics and environmental conditions.

Characteristics	**Mean ± SD or n**
Age (years)	35.3 ± 8.3
Sex	17 Male, 8 Female
Eye Measured (OD/OS)	14 OS, 11 OD (randomly chosen)
Room Temperature (°C)	22.5 ± 0.6
Ambient RH (%)	48.5 ± 12.2

4.3.3.2 Tear Film Characteristics Before and After Lipid Drop Instillation

The primary tear film characteristics evaluated in this study were LLT, NITBUT, and TER. These parameters were measured at baseline (before lipid eye drop instillation (Systane Complete)) and repeated following administration of an eye drop. Table 4-11 summarizes the descriptive statistics for LLT, NITBUT, and TER measurements, illustrating the tear film dynamics associated with lipid supplementation. NITBUT was recorded as both the First Measurement only and as the Average of three measurements.

Table 4-11: Tear film characteristics before and after lipid drop instillation

Parameter	Before Drop (Mean ± SD)	After Drop (Mean ± SD)
LLT (nm)	57.5 ± 15.5	85.9 ± 18.1
NITBUT (sec)		
First Measurement	16.6 ± 6.1	13.9 ± 6.4
Average Measurement	18.3 ± 5.2	17.2 ± 5.0
TER (g/m²/hr)	0.08 ± 0.06	0.11 ± 0.06

4.3.3.3 Normality Analysis of Tear Film Characteristics

The normality of distributions for LLT, NITBUT, and TER measurements, both before and after lipid eye drop instillation, was assessed using the Shapiro-Wilk test. The results are summarized in the Table 4-12.

Table 4-12: Normality analysis of tear film characteristics (Shapiro-Wilk test).

Parameter	Condition	Shapiro-Wilk W	p-value
LLT (nm)	Before Drop	0.84	**0.006**
	After Drop	0.76	**<0.001**
NITBUT (sec)			
First Measurement	Before Drop	0.96	0.229
	After Drop	0.93	0.116
Average Measurement	Before Drop	0.94	0.062
	After Drop	0.96	0.492
TER (g/m²/hr)	Before Drop	0.87	**0.002**
	After Drop	0.92	0.229

Following normality analysis, appropriate inferential statistical methods were selected to evaluate differences in tear film characteristics before and after the instillation of lipid-based eye drops. Due to the non-normal distribution of LLT, a non-parametric Wilcoxon Signed-Rank test was used. In contrast, NITBUT and TER were normally distributed, allowing for the application of paired-sample t-tests.

4.3.3.4 Comparative Analysis of Tear Film Characteristics Before and After Lipid Drop Instillation

A comparative analysis of LLT, NITBUT and TER was completed. The summary of these statistical analyses, including test statistics and p-values, is presented in Table 4-13.

Table 4-13: Summary table of inferential statistical analysis

Parameter	**Statistical Test**	**Before Drop**	**After Drop**	**Test Statistic**	**p-value**
LLT (nm)	Wilcoxon Signed-Rank	Median: 54 (IQR: 51–58)	Median: 99 (IQR: 92-100)	Z = 0.00	**<0.001**
NITBUT (sec)					
First Measurement	Paired-sample t-test	16.6 ± 6.1	13.9 ± 6.4	t (24) = 2.92	**0.008**
Average Measurement	Paired-sample t-test	18.3 ± 5.2	17.2 ± 5.0	t (24) = 2.02	0.055
TER ($g/m^2/hr$)	Paired-sample t-test	0.08 ± 0.06	0.11 ± 0.06	t (24) = -2.53	**0.019**

Note: LLT values are reported as median (IQR) due to non-normal distribution, whereas NITBUT and TER values are presented as mean ± SD. Statistical significance is defined as $p \leq 0.05$.

4.3.3.4.1 LLT

A Wilcoxon Signed-Rank test revealed a statistically significant increase in LLT after lipid drop instillation (median before drop = 54 nm, median after drop = 99 nm, $Z = 0.0$, $p < 0.001$), confirming the effectiveness of lipid supplementation in enhancing the lipid layer. This change is visually represented in Figure 4-10, which displays LLT values before and after lipid drop instillation.

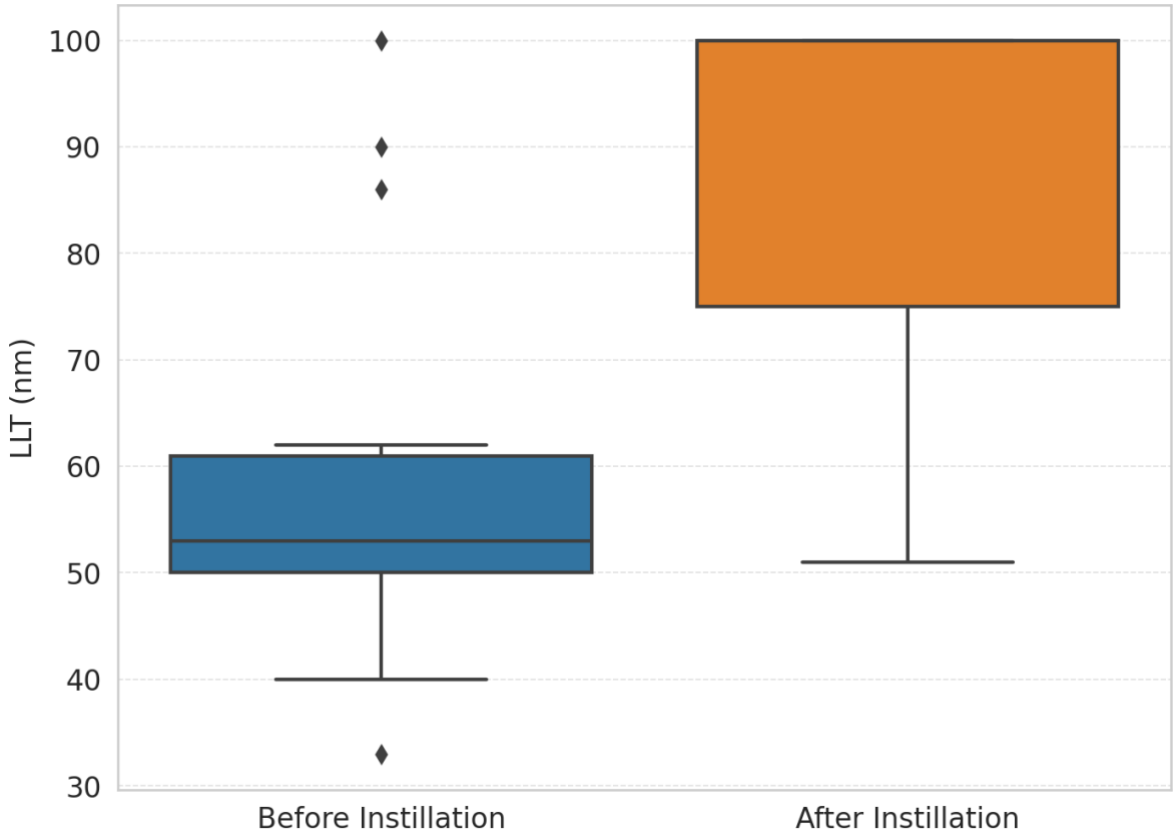


Figure 4-10: Boxplot representation of LLT before and after lipid drop instillation (n=23). A statistically significant increase in LLT was observed following instillation (Wilcoxon Signed-Rank test, $p < 0.001$). LLT values are presented as median and interquartile range due to non-normal distribution. The median line for the After Instillation condition overlaps with the top edge of the box due to a ceiling effect at 100 nm, the maximum measurable limit of the LipiView II device.

4.3.3.4.2 NITBUT

Paired-sample t-tests were conducted for both the first measurement and the average measurement of NITBUT, before and after lipid eye drop instillation.

The First NITBUT Measurement significantly decreased following the lipid drop (mean before: 16.6 ± 6.09 s, after drop: 13.9 ± 6.4 s; t (24) = 2.92, p = 0.008). This result is illustrated in Figure 4-11, which showed the change in NITBUT First Measurement before and after lipid drop instillation.

The Average NITBUT Measurement slightly decreased after instillation, although this reduction was not statistically significant (18.3 ± 5.2 s before vs. 17.2 ± 5.0 s after; t (24) = 2.38, p = 0.226).

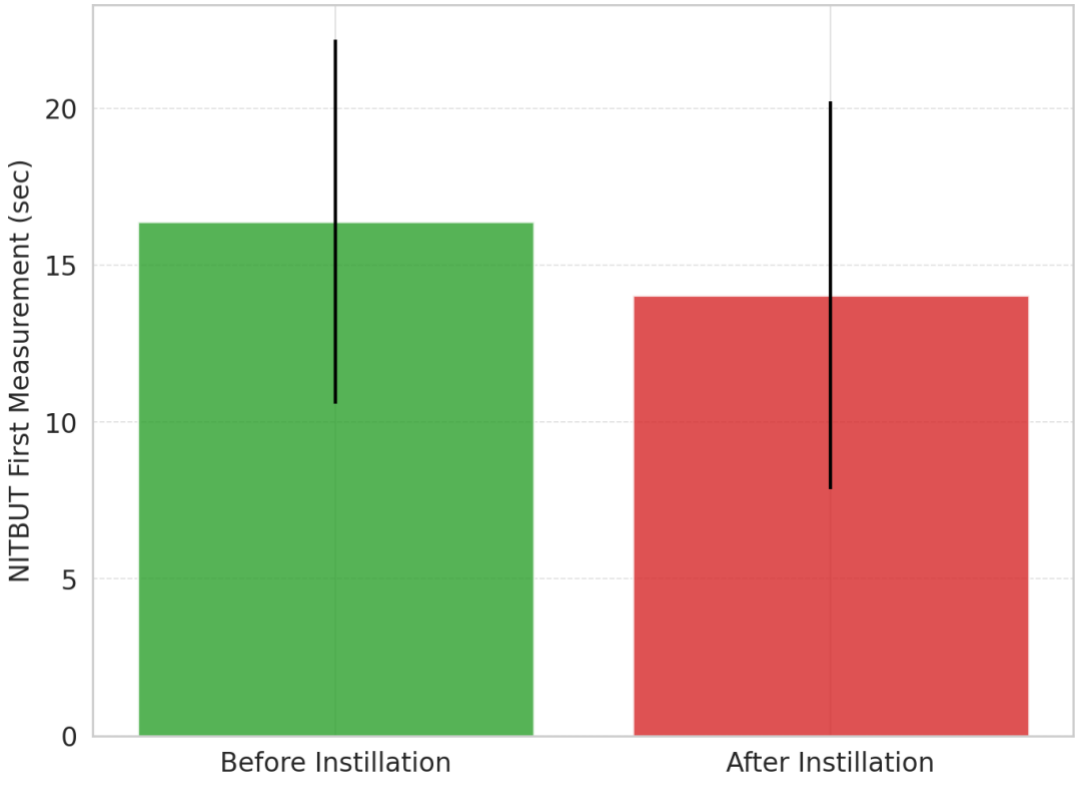


Figure 4-11: Bar graph illustrating the change in mean ± SD NITBUT First Measurement before and after lipid drop instillation (n=23). A statistically significant decrease in NITBUT First was observed after drop instillation (paired t-test, p = 0.008).

4.3.3.4.3 TER

Paired-sample t-tests revealed a statistically significant increase in TER following lipid eye drop instillation (0.08 ± 0.06 g/m²/hr before versus 0.11 ± 0.06 g/m²/hr after; t (24) = -2.53, p = 0.019), indicating that lipid supplementation affected tear evaporation dynamics significantly. This finding is illustrated in Figure 4-12, which depicts the change in TER before and after lipid drop instillation.

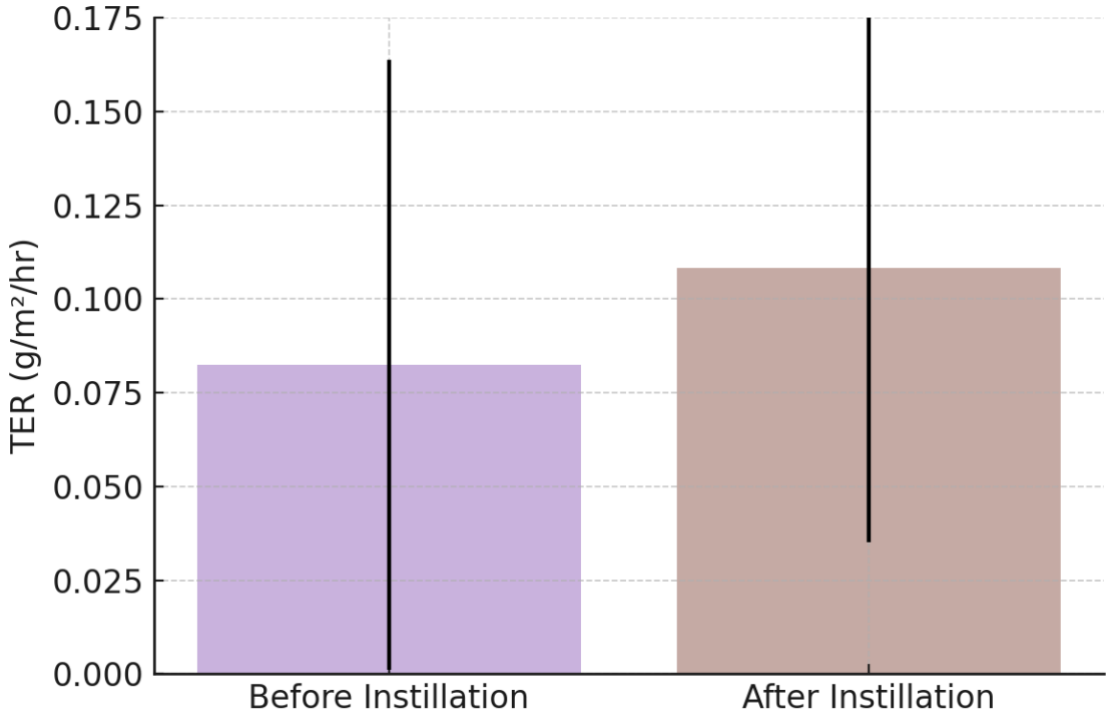


Figure 4-12: Bar graph illustrating the change in mean ± SD TER before and after lipid drop instillation (n=23). A statistically significant increase in TER was observed post-instillation (paired t-test, p = 0.019).

4.3.3.5 Correlation Analysis of Tear Film Parameter Changes

To explore potential relationships between LLT**,** NITBUT, and TER**,** a Pearson correlation analysis was conducted on the observed changes in these parameters following lipid drop instillation. The results are summarized in Table 4-14**.**

Table 4-14: Correlation analysis of changes in LLT, NITBUT, and TER

Variables Compared	**Correlation Coefficient (*r*)**	**p-value**
LLT Change ↔ NITBUT First Change	0	1
LLT Change ↔ NITBUT Average Change	0.04	0.857
LLT Change ↔ TER Change	0.18	0.382
NITBUT First Change ↔ NITBUT Average Change	0.94	**<0.001**
NITBUT First Change ↔ TER Change	0.28	0.173
NITBUT Average Change ↔ TER Change	0.3	0.145

The correlation analysis revealed several key findings:

- No significant correlation was found between LLT and NITBUT or TER.
- A strong correlation was observed between NITBUT First and Average Measurements ($r = 0.940$, $p < 0.001$).
- Weak to moderate correlations were found between NITBUT and TER changes but were not statistically significant.
- Changes in NITBUT First and TER ($r = 0.28$, $p = 0.173$) and NITBUT Average and TER ($r = 0.30$, $p = 0.145$) suggest a potential relationship between tear film stability and tear evaporation, but the lack of statistical significance indicates variability among participants.

To illustrate these findings, the Figure 4-13 presents a pairwise scatter plot with trend lines, visually representing the correlation relationships between LLT, NITBUT, and TER.

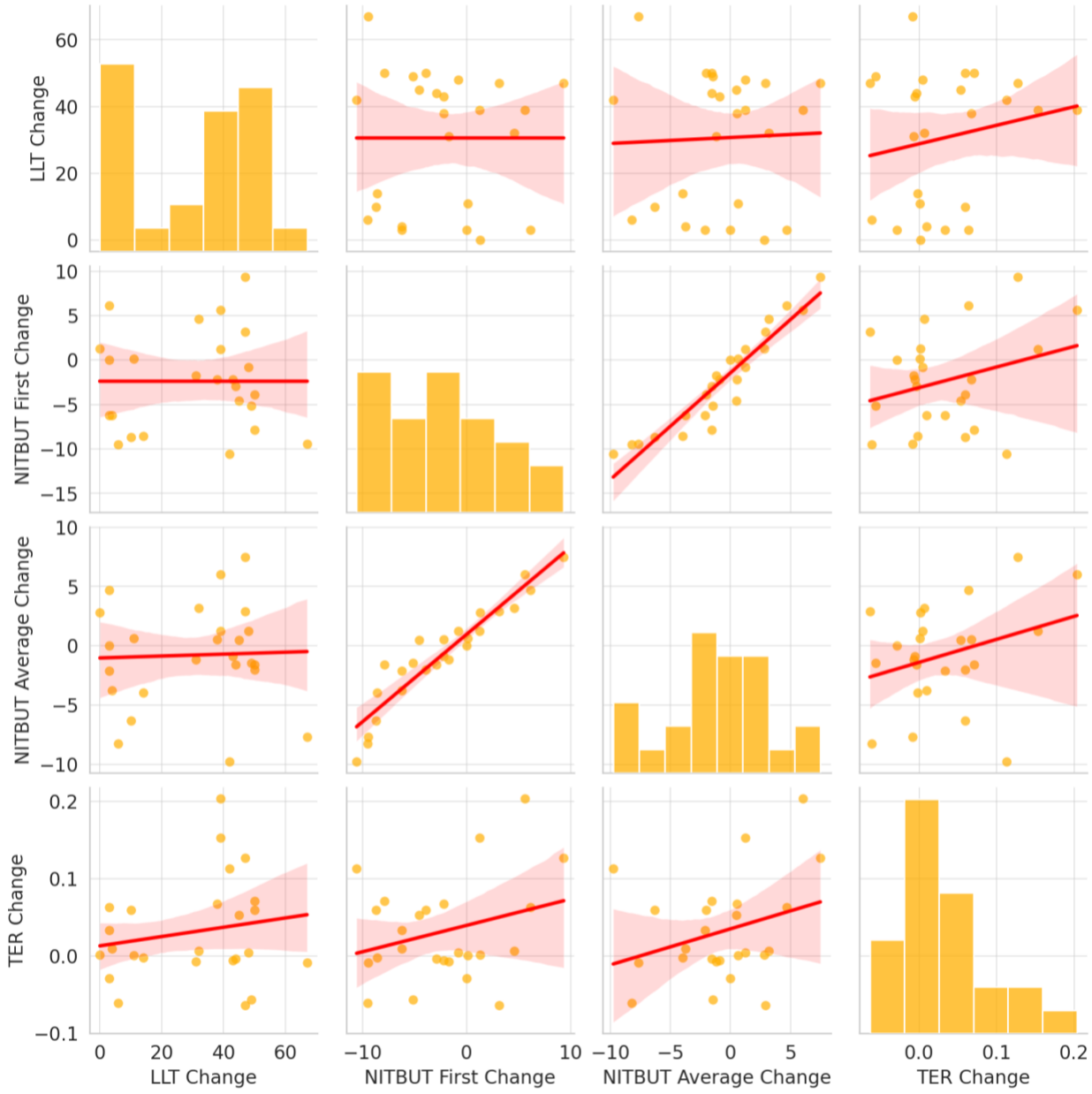


Figure 4-13: Pairwise scatter plots with regression lines showing relationships among changes in LLT, first and average NITBUT, and TER following lipid eye drop instillation (n = 23). Pearson correlation coefficients revealed no statistically significant relationships among LLT, NITBUT, and TER changes. Only the relationship between NITBUT first and average changes was significant ($r = 0.94$, $p < 0.001$). Shaded areas represent 95% confidence intervals.

4.3.3.6 Analysis of the Effect of PAS and VIG on TER

Previous research has reported that TER is influenced by various anatomical and environmental factors. Two potential anatomical contributors are:

PAS: The exposed ocular surface area affects how much of the tear film is exposed to evaporation. A larger PAS may result in higher ERs, while a smaller PAS could provide more protection against moisture loss.

VIG: The internal volume of the evaporimeter goggle chamber influences airflow and RH conditions inside the chamber, which could theoretically impact TER measurements.

To assess the potential influence of PAS and VIG on TER dynamics following lipid drop instillation, Pearson correlation analyses were conducted between PAS, VIG, and TER change, where TER change was defined as the difference between post-instillation and pre-instillation TER values. The results are presented in Table 4-15.

Table 4-15: Correlation analysis between PAS, VIG, and TER change. (TER change = post-instillation TER – pre-instillation TER).

Variable	Correlation with TER Change (r)	P Value
PAS	0.150	0.474
VIG	-0.021	0.921

Findings from the correlation analysis revealed that PAS showed a very weak positive correlation with TER change ($r = 0.150$), suggesting that a larger exposed ocular surface area may only slightly increase TER. In contrast, VIG demonstrated a near-zero correlation with TER change ($r = -0.021$), indicating that the goggle volume inside the evaporimeter had no significant effect on evaporation measurements. (TER change refers to the difference between post- and pre-instillation values). Overall, these results suggest that PAS may play a minor role in influencing TER, whereas VIG

does not appear to impact tear evaporation. To further illustrate the relationships between PAS, VIG, and TER, Figure 4-14 presents scatter plots with regression lines.

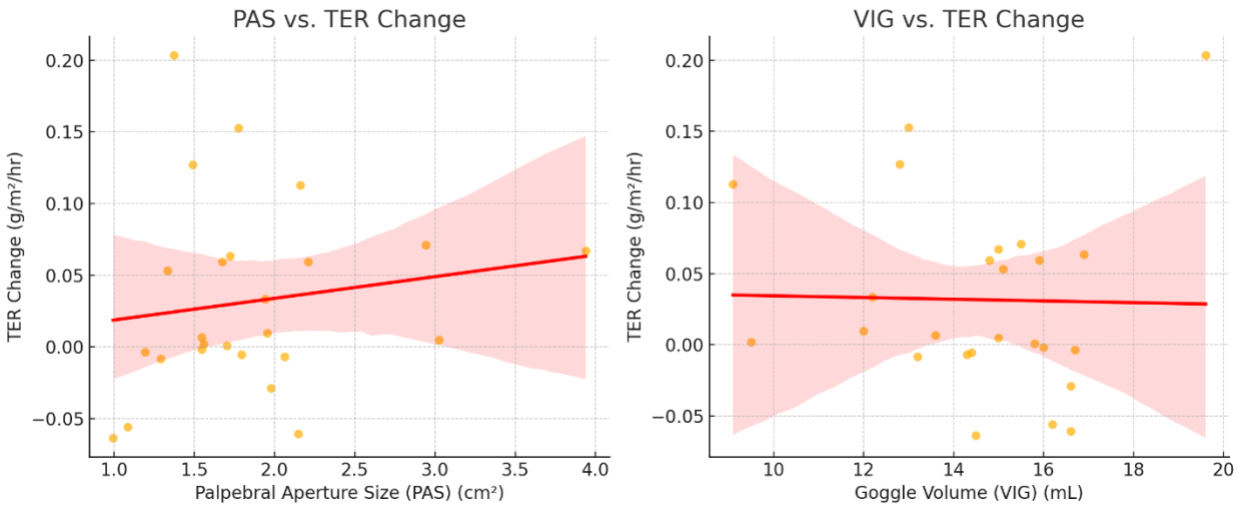


Figure 4-14: Scatter plots with regression lines illustrating the relationship between TER change and PAS and VIG (n = 23). Pearson correlation analysis showed a weak positive correlation between PAS and TER change (r = 0.150), and no meaningful correlation between VIG and TER change (r = -0.021). Shaded regions represent 95% confidence intervals; neither relationship was statistically significant. (TER change = post-instillation TER – pre-instillation TER).

4.3.3.7 Intraclass Correlation Coefficient (ICC) for TER Validity

To evaluate the reliability of the evaporimeter in measuring TER, an ICC analysis was conducted. ICC is used to assess the consistency of repeated measurements and determine how much of the variation in the data is due to true differences between subjects versus measurement error. In this study, TER values obtained before and after lipid drop instillation were treated as repeated measures. Although the physiological state differed slightly between the two time points, the same device, conditions, and measurement protocol were used, making ICC a suitable method for assessing the tool's stability.

The strength of ICC lies in its ability to show whether the device consistently captures differences between individuals across sessions. It provides more than just a comparison of means; it indicates whether the instrument ranks or measures participants in a reliable and repeatable way. A two-way random effects model with absolute agreement (ICC (2,1)) was used, following the guidance of Koo and Li[241] The resulting ICC value of 0.84 reflects excellent reliability, supporting the conclusion that the evaporimeter can consistently measure TER across conditions and is a dependable tool for studying tear film evaporation. Although the ICC suggests good consistency, it should not be interpreted as a strict repeatability analysis, as the post-instillation state introduced significant physiological changes. The result therefore reflects reliability under similar, but not identical, conditions.

4.3.3.8 Analysis of Baseline LLT Influence on Tear Film Parameters

The lipid layer of the tear film plays a crucial role in reducing tear evaporation and maintaining tear film stability. Individuals with thinner baseline lipid layers may experience higher TER, potentially leading to more significant changes in tear film parameters following lipid drop instillation. Conversely, individuals with thicker baseline lipid layers may have more stable tear films that are less affected by lipid supplementation.

To assess the potential impact of baseline LLT on tear film responses, participants were categorized into two groups:

- **Low LLT Group:** Participants whose baseline LLT was below the median LLT value.
- **High LLT Group:** Participants whose baseline LLT was equal to or above the median LLT value.

This classification allowed the investigation of whether participants with different baseline LLT levels responded differently to lipid drop instillation, particularly in LLT, NITBUT, and TER

change. The median LLT value before lipid drop instillation was calculated as 53.0 nm, and this threshold was used to categorize participants into two groups. Those with baseline LLT values below 53.0 nm were assigned to the Low LLT Group (n = 11), while those with values equal to or greater than 53.0 nm were assigned to the High LLT Group (n = 14). The difference in group sizes occurred because several participants had baseline LLT values exactly equal to the median (53.0 nm), resulting in their inclusion in the High LLT group and thus slightly unequal group sizes. Table 4-16 summarizes the classification of participants into Low and High LLT groups based on their baseline LLT.

Table 4-16: LLT Group distribution based on baseline LLT measurements.

LLT Group	LLT Threshold (nm)	Number of Participants (n)	LLT Range (nm)
Low LLT	< 53.0 nm	11	33.0 - 51.0
High LLT	≥ 53.0 nm	14	54.0 - 100.0

The descriptive statistics (Median ± IQR for LLT changes; Mean ± SD for NITBUT and TER changes) for the Low LLT and High LLT groups are summarized in Table 4-17. These statistics provide a comparison of how tear film parameters changed before and after lipid drop instillation in each LLT group. The median and IQR are reported for LLT due to its non-normal distribution, while mean and SD values are reported for NITBUT and TER, as these variables showed normal distribution.

Table 4-17: Descriptive statistics of tear film parameter changes in low LLT and high LLT groups.

LLT Group	**LLT Change (nm)**	**NITBUT First Change (sec) (Mean ± SD)**	**NITBUT Average Change (sec) (Mean ± SD)**	**TER Change ($g/m^2/hr$) (Mean ± SD)**
Low LLT	Median:47.0 (IQR: 35.0 –49.5)	-1.26 ± 5.70	0.44 ± 3.94	0.03 ± 0.05
High LLT	Median:22.5 (IQR: 7.0 –41.25)	-3.23 ± 5.14	-1.73 ± 4.42	0.03 ± 0.08

To determine whether LLT, NITBUT, and TER significantly changed after lipid drop instillation, a Wilcoxon signed-rank test was conducted for LLT due to non-normal distribution, and paired t-tests were used for NITBUT and TER. These analyses were performed separately for the Low LLT and High LLT groups, as shown in Table 4-18.

Table 4-18: Wilcoxon signed-rank (LLT) and paired t-test (NITBUT, TER) comparisons of tear film parameters before and after lipid drop instillation in Low LLT and High LLT groups.

Parameter		**Statistical Test**	**Test Statistic**	**p-value**
LLT (nm)	Low LLT	Wilcoxon Signed-Rank	Z = 0.00	**0.001**
	High LLT	Wilcoxon Signed-Rank	Z = 0.00	**0.001**
NITBUT (sec)				
First Measurement	Low LLT	Paired-sample t-test	t (10) = -0.71	0.496
	High LLT	Paired-sample t-test	t (13) = -2.35	**0.035**
Average Measurement	Low LLT	Paired-sample t-test	t (10) = 0.37	0.718
	High LLT	Paired-sample t-test	t (13) = -1.46	0.167
TER (g/m²/hr)	Low LLT	Paired-sample t-test	t (10) = 0.65	0.530
	High LLT	Paired-sample t-test	t (13) = 1.50	0.157

As shown in the graph above, Wilcoxon signed-rank test results revealed that LLT significantly increased after lipid drop instillation in both the Low LLT group ($p = 0.001$) and the High LLT group ($p = 0.001$). A significant decrease in NITBUT First measurement was observed only in the High LLT group (paired t-test, $p = 0.035$), but no significant change was found in the Low LLT group. No significant changes were observed for NITBUT Average or TER in either group following lipid drop instillation.

To explore potential relationships between LLT, NITBUT, and TER changes within each LLT group, correlation analyses were performed separately for the Low LLT and High LLT groups. These correlations are presented in Figure 4-15.

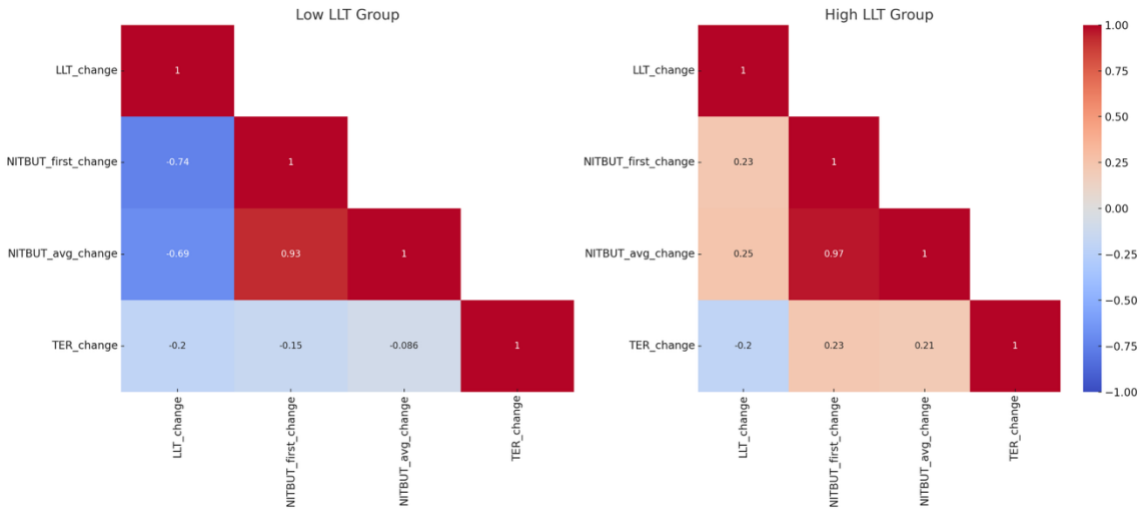


Figure 4-15: Correlation heatmaps for Low LLT (left, n = 11) and High LLT (right, n = 14) groups, illustrating relationships among changes (post–pre) in LLT, NITBUT First, NITBUT Average, and TER following lipid eye drop instillation. Strong correlations (r > 0.92) were observed only between NITBUT First and NITBUT Average in both groups. Correlations involving LLT and TER were weak and not statistically significant.

The correlation analysis revealed distinct patterns between the Low and High LLT groups. In the Low LLT group, LLT changes showed strong and significant negative correlations with NITBUT First Change (Spearman r = -0.74, p = 0.009) and NITBUT Average Change (Spearman r = -0.69, p = 0.018), suggesting that increased LLT was associated with reduced tear film stability in participants with initially thinner lipid layers. In contrast, the High LLT group exhibited weak and non-significant correlations between LLT changes and both NITBUT First (Spearman r = 0.23, p = 0.422) and NITBUT Average Change (Spearman r = 0.25, p = 0.396), indicating little to no association between LLT increases and tear stability in individuals with thicker baseline lipid layers.

TER changes showed weak correlations with LLT, NITBUT First, and NITBUT Average in both groups, none reaching statistical significance. However, strong and significant correlations were consistently observed between NITBUT First and NITBUT Average changes within both the Low

LLT group (Pearson r = 0.93, $p < 0.001$) and the High LLT group (Pearson r = 0.97, $p < 0.001$), reinforcing the reliability of these two measures in assessing tear film stability.

4.3.3.9 Analysis of RH Influence on Tear Film Parameters

Environmental factors, particularly RH, play a crucial role in influencing TER and overall tear film stability. Previous research has demonstrated that lower RH levels contribute to increased TER, exacerbating symptoms of EDE. Conversely, higher RH levels may reduce TER and enhance tear film stability.

To assess the potential impact of RH on LLT, NITBUT, and TER, participants were categorized into two groups based on their ambient RH levels during testing:

- **Low RH Group:** Participants whose ambient RH was below the median RH value.
- **High RH Group:** Participants whose ambient RH was equal to or above the median RH value.

This classification allowed the investigation of whether baseline RH influenced the response to lipid drop instillation, and whether tear film parameters responded differently under different environmental RH conditions.

The median RH before lipid drop instillation was calculated as 53.42%, and this value was used as the threshold for categorizing participants into two groups. Participants with RH(Ave) values below 53.42% were assigned to the Low RH Group (n = 12), while those with RH(Ave) values equal to or above this threshold were assigned to the High RH Group (n = 13).

Table 4-19 summarizes the classification of participants into Low and High RH groups based on the median ambient RH measured prior to lipid drop instillation as well as during the experiment.

Table 4-19: RH group distribution based on baseline ambient relative humidity measurements.

RH Group	RH Threshold (%)	Number of Participants (n)	RH Range (%)
Low RH	< 53.42%	12	21.17 - 52.92
High RH	≥ 53.42%	13	53.42 - 63.33

The descriptive statistics (Median ± IQR for LLT changes; Mean ± SD for NITBUT and TER changes) for the Low RH and High RH groups are summarized in Table 4-20. These statistics provide a comparison of how tear film parameters changed before and after lipid drop instillation under different baseline RH conditions. Median and IQR are reported for LLT due to its non-normal distribution, while mean ± SD values are reported for NITBUT and TER, as these variables showed normal distribution.

Table 4-20: Descriptive statistics of tear film parameter changes in low RH and high RH groups.

RH Group	LLT Change (nm)	NITBUT First Change (sec) (Mean ± SD)	NITBUT Average Change (sec) (Mean ± SD)	TER Change ($g/m^2/hr$) (Mean ± SD)
Low RH	Median:30.0 (IQR: 15.25 –46.50)	-2.96 ± 6.29	-2.06 ± 5.20	0.02 ± 0.06
High RH	Median:24.0 (IQR: 18.0 –44.0)	-1.81 ± 4.75	0.41 ± 2.93	0.04 ± 0.07

To determine whether LLT, NITBUT, and TER significantly changed after lipid drop instillation, a Wilcoxon signed-rank test was conducted for LLT (due to its non-normal distribution), while paired t-tests were used for NITBUT and TER. These analyses were performed separately within the Low RH and High RH groups, as shown in Table 4-21.

Table 4-21: Wilcoxon signed-rank (LLT) and paired t-test (NITBUT, TER) comparisons of tear film parameters before and after lipid drop instillation in Low RH and High RH groups.

Parameter		Statistical Test	Test Statistic	p-value
LLT (nm)	Low RH	Wilcoxon Signed-Rank	Z = 0.00	**0.0005**
	High RH	Wilcoxon Signed-Rank	Z = 0.00	**0.0022**
NITBUT (sec)				
First Measurement	Low RH	Paired-sample t-test	t (11) = -1.63	0.131
	High RH	Paired-sample t-test	t (12) = -1.37	0.196
Average Measurement	Low RH	Paired-sample t-test	t (11) = -1.37	0.197
	High RH	Paired-sample t-test	t (12) = 0.51	0.620
TER (g/m²/hr)	Low RH	Paired-sample t-test	t (11) = 0.31	0.765
	High RH	Paired-sample t-test	t (12) = 1.86	0.088

Wilcoxon signed-rank tests indicated that LLT significantly increased after lipid drop instillation in both the Low RH group ($p = 0.0005$) and the High RH group ($p = 0.0022$). However, paired t-tests revealed no significant changes in NITBUT First, NITBUT Average, or TER parameters in either RH group. These results suggest that lipid supplementation consistently enhanced LLT regardless of ambient RH but did not significantly affect tear film stability or evaporation rate within the short-term observation window.

To explore relationships among LLT, NITBUT, and TER changes within each RH group, correlation analyses were conducted separately for Low RH and High RH groups, with results presented in Figure 4-16.

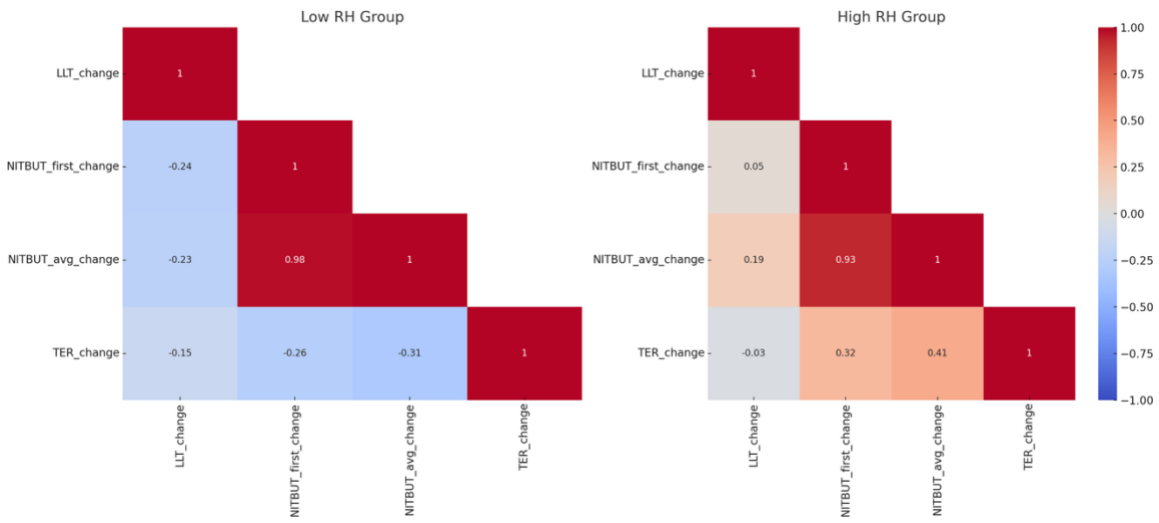


Figure 4-16: Correlation heatmaps for Low RH (left, n = 12) and High RH (right, n = 13) groups, illustrating relationships among LLT change, NITBUT (first and average) change, and TER change following lipid drop instillation. LLT correlations (Spearman's rank) with other parameters were weak and non-significant in both groups. Strong positive Pearson correlations were observed only between NITBUT First and Average changes ($r \geq 0.93$, $p < 0.001$) in both RH groups.

The correlation analysis revealed weak and non-significant correlations between LLT changes and both NITBUT First and Average changes in both Low RH ($r = -0.24$ and $r = -0.23$, respectively) and High RH groups ($r = 0.05$ and $r = 0.19$, respectively). Similarly, LLT change showed weak and non-significant correlations with TER change in both groups (Low RH: $r = -0.15$, High RH: $r = -0.03$). These results suggest limited association between LLT improvements and changes in tear film stability or evaporation rate, regardless of RH conditions.

Strong and significant positive correlations were clearly observed between NITBUT First and NITBUT Average changes in both the Low RH ($r = 0.98$) and High RH groups ($r = 0.93$), highlighting the consistency between these two measures of tear film stability. However, correlations involving TER with NITBUT First or Average remained weak and not statistically significant in both RH groups.

4.3.4 Discussion

This study evaluated the impact of lipid-based eye drop instillation (Systane Complete®) on tear film dynamics, specifically focusing on LLT, NITBUT, and TER, under physiological conditions. The findings demonstrated that lipid eye drop instillation significantly increased LLT, clearly indicating an enhancement of the lipid layer. While increased LLT is typically expected to improve tear film stability, this study did not find statistically significant improvements in tear film stability (as measured by NITBUT) or reductions in evaporation rate (TER). This aligns partially with previous research suggesting lipid supplementation reinforces the lipid barrier, though the current findings indicate that improved LLT alone may not translate immediately into measurable improvements in stability or reduced evaporation within the short measurement period used in this study.

Interestingly, despite the significant improvement in LLT post-instillation, the first measurement of NITBUT significantly decreased, while the average NITBUT did not significantly change. This contradictory outcome could be attributed to immediate disturbances in tear film equilibrium following drop instillation, as transient destabilization or redistribution of tear film components might occur before lipid integration stabilizes the surface.[175,179] This emphasizes the complexity of the tear film response immediately following supplementation.

Notably, the study identified a significant increase in TER post-drop, contrary to expectations. Typically, increased LLT should reduce TER by forming a more effective barrier against evaporation.[30,200] However, sub-group analysis revealed that participants with a lower baseline LLT exhibited a more pronounced increase in LLT following lipid supplementation, while those with higher baseline LLT showed a less substantial gain. Notably, because the LipiView II device measures LLT only up to a maximum of 100 nm, some participants, especially those already close

to this upper limit, couldn't accurately show further increases after lipid drop instillation. Using the Wilcoxon signed-rank test and reporting medians instead of means helped reduce the impact of this measurement ceiling. This statistical approach makes our results less influenced by extreme values or the device's limitations, providing a more accurate comparison of LLT changes between groups. Despite these differences, both groups exhibited comparable increases in TER, suggesting that lipid layer enhancement alone may not be sufficient to reduce tear evaporation in the short term (5 minutes), potentially due to transient instability or changes in lipid layer spreading dynamics.[207,242]

Beyond LLT, NITBUT, and TER, an emerging factor in evaluating tear film dynamics is OST. OST reflects the balance between tear film cooling due to evaporation and heat retention from ocular perfusion.[35,37] While OST was not directly measured in this study, future research will incorporate IRT to assess the interplay between lipid supplementation and OST fluctuations. Given that OST has been shown to correlate with TER and stability, its inclusion could provide a more comprehensive understanding of tear film dynamics and improve the precision of EDE assessment.[190,242]

4.3.5 Limitations and Future Directions

This study's primary limitation was the immediate post-instillation measurement window (5 minutes after drop instillation), which might not capture the prolonged effects of lipid supplementation adequately and be affected by short destabilisation of the tear film due to the drop instillation. Future research should incorporate longer follow-up intervals to evaluate sustained changes in tear film dynamics.

Another limitation involved environmental and anatomical factors, such as ambient RH and ocular surface area (PAS), which might have influenced TER measurements. Although this study

controlled and assessed these variables, future research could employ a wider range of environmental conditions to better represent real-world variability. Additionally, PAS was measured outside the goggle, and while the goggle was designed not to compress the eyelids, subtle changes in palpebral aperture size once the goggle was applied cannot be fully ruled out.

An additional limitation pertains to the LipiView II® device, which can only measure LLT up to 100 nm. This ceiling effect may have contributed to the observed greater LLT increase in participants who initially had lower LLT values, as those with higher baseline LLT may have reached the device's measurement limit. Future studies should consider alternative or supplementary methods for LLT measurement to ensure accurate tracking of lipid layer changes beyond this threshold.

The final sample size (n = 25) was also smaller than initially planned. A power calculation suggested a target of 54 participants, but recruitment was paused after 25 when interim analysis showed that a 5-minute observation period might not be sufficient. This led to a protocol revision, including the integration of OST measurement using the ThermOcular camera. This method was developed after the Phase I study and applied in the revised Phase II design. However, the smaller sample size remains a limitation and may have reduced the statistical power to detect subtler differences.

The sex distribution of the study sample was also imbalanced (17 males, 8 females), which does not reflect the typical sex distribution seen in DED, where prevalence is generally higher in females.[120–122] This imbalance may have influenced the results, as sex-related differences in tear film physiology and response to lipid supplementation have been reported. Future studies should aim for a more representative distribution to improve generalizability.

Further investigation with diverse lipid formulations could elucidate whether specific lipid compositions or concentration differentially influence tear evaporation dynamics, potentially identifying optimal treatments for different sub-types of DEDs.

Additionally, integrating OST measurement into future studies will allow for a more detailed characterization of the thermal stability of the tear film and its response to lipid supplementation.

4.3.6 Conclusion

This study demonstrates for the first time that lipid-based eye drop instillation significantly enhances LLT yet paradoxically causes an immediate increase in TER, contrary to traditional expectations. A unique contribution of this work was the subgroup analysis, revealing that participants with thinner baseline lipid layers experienced greater LLT improvements, yet still showed increased evaporation rates. Another novel aspect was assessing how environmental factors such as RH influenced immediate tear film responses, showing distinct patterns in tear dynamics under different ambient conditions. These findings reveal previously underappreciated complexities in the immediate tear film response to lipid supplementation. Future research incorporating OST measurements with infrared thermography will build upon these novel insights, providing a more comprehensive and innovative framework for evaluating tear film stability and evaporative dynamics in dry eye management.

4.4 Optimizing Measurement Parameters for OST Assessment Using ResearchIR Software

4.4.1 Overview

The measurement of OST has been an essential tool in ocular diagnostics, offering valuable insights into tear film stability, ocular surface health, and disease pathophysiology.[186,198,210] Advances in IRT facilitated non-contact, high-resolution assessment of OST, allowing for precise spatial and temporal analysis of temperature variations across different ocular surface ROIs.[33,186,243] However, a lack of standardized protocols introduced variability across studies, limiting the reproducibility and clinical applicability of OST measurement.[30,176,185]

IRT enables real-time, non-invasive measurement of OST fluctuations, which are influenced by factors, such as tear film stability, blink rate, and environmental conditions.[33,186,244] The interblink interval (IBI), defined as the duration between consecutive blinks, plays a key role in OST dynamics because it is directly linked to evaporation-driven cooling of the ocular surface.[30,245] Faster tear evaporation produces a steeper temperature decline, and this drop in OST can stimulate the cold-sensitive corneal nerves that trigger the blink reflex.[30,198] In this way, higher cooling rates are associated with shorter IBIs. Conversely, when the IBI is longer, the OST profile reflects both the rapid early cooling phase and the slower plateau phase, so the average cooling rate across the interval appears lower. This concept is illustrated in Figure 4-17, which compares temperature profiles for short and long IBIs under idealized conditions. Additionally, temperature variations exist across different ocular regions, with the sclera generally exhibiting higher temperatures than the cornea due to differences in vascularization and tear film distribution.[31,188,194,246,247]

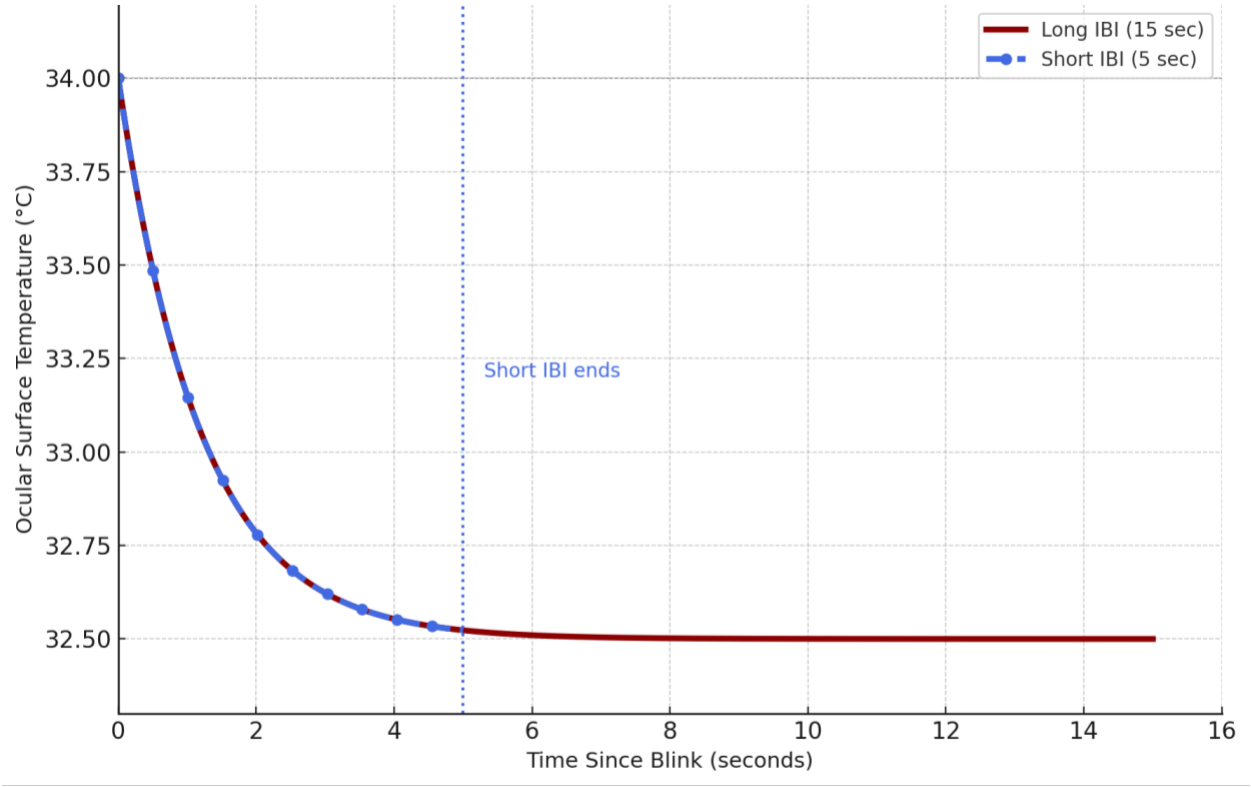


Figure 4-17: Simulated OST cooling profiles following a blink during short (5 sec) and long (15 sec) IBIs.

Despite prior efforts to establish robust OST measurement techniques, inconsistencies remain regarding optimal IBIs, ideal measurement locations, and the number of required measurements for reliable data.[176,185,248] In this context, the term "optimal" specifically refers to identifying measurement conditions, such as IBIs, anatomical locations, and measurement repetitions, that provide the greatest repeatability and lowest variability for detecting clinically meaningful changes in ocular surface temperature. High-resolution IR cameras, such as the Teledyne FLIR IR A655sc (FLIR Systems, Wilsonville, OR, USA), provide enhanced thermal mapping capabilities, improving precision and repeatability.[243,249] The ResearchIR software (FLIR Systems, Wilsonville, OR, USA, v.4.40) provides enhanced data acquisition through automated ROI selection and real-

time temperature analysis.[248] However, determining the most effective parameters for OST measurement remains a challenge.[185]

This study aimed to optimize OST measurement protocols by systematically evaluating key variables, including:

- **Temperature metric selection:** Comparing the rate of temperature change (RTC) versus absolute temperature change (ΔT) to determine the most proper OST measurement approach.[210,248]
- **Interblink interval:** Identifying the optimal IBI for detecting meaningful OST changes while maintaining subject comfort.[30,185,198]
- **Measurement locations:** Assessing temperature variations across multiple ocular surface regions to determine the most stable and representative sites.[31,188,194,246,247]
- **Average vs. single measurements:** Investigating whether multiple measurements significantly enhance the reliability of OST data compared to single-point assessments.[200]

By addressing these methodological concerns, this study aimed to refine OST measurement protocols and improve standardization for both clinical and research applications.[185,248] The findings will enhance the reproducibility of OST assessment, facilitating its integration into routine ophthalmic evaluations and advancing its utility in diagnosing and monitoring ocular surface disorders.[185,198,248]

4.4.2 Materials and Methods

4.4.2.1 Subjects and Ethical Approval

This study received ethics clearance through a University of Waterloo Research Ethics Board (REB #46626). The study adhered to the tenets of the Declaration of Helsinki.

Seven healthy adult participants (4 males, 3 females, mean age: 32.9 ± 11.7 years) were recruited following a structured eligibility assessment. Inclusion criteria required participants to be 18 years or older, have no known active ocular disease or infections, be able to keep their eyes open for at least 10 seconds, and be willing to comply with the study protocol, including refraining from wearing contact lenses on the day of the visit. Participants were excluded if they had any ocular pathology, recent ocular infections, or were unable to follow the study procedures. Prior to participation, all subjects provided written informed consent, confirming their understanding of the study's purpose, procedures, potential risks, and data confidentiality. Given the methodological focus of the study, a small sample size was deemed appropriate for protocol refinement, as supported by guidelines for pilot and feasibility studies.[250,251]

4.4.2.2 Instrumentation

OST measurements were conducted using the ThermOcular dual-camera system, which included an IR camera for thermal imaging and a FLIR BFS 51S5C-C visible (VIS) camera for alignment and tracking (Section 3-2 on Methodology chapter). The camera system was mounted on a modified slit-lamp biomicroscope to ensure precise positioning and measurement consistency. The FLIR ResearchIR software was used for image acquisition and analysis.

The detailed specifications of all equipment used in this experiment, including camera resolution, sensitivity, and software settings, is reported in the Methodology Chapter.

4.4.2.3 Experimental Procedure

To minimize external variability, ambient conditions were carefully monitored throughout data collection. The average ambient temperature was 22.73 ± 0.65°C, and RH was 55.4 ± 3.4%. Measurements were performed under dim room lighting to reduce corneal reflection artifacts in OST measurements.

Subjects were positioned with their forehead and chin stabilized in a headrest, and a fixation target was used to maintain gaze stability during the experiment.

Subjects followed a structured blinking task, where they were instructed to blink six times at predetermined IBIs. The IBIs tested were 2, 4, 6, 8, and 10 seconds. A 2-minute rest period was given between each set to allow the tear film to reset. A metronome-generated auditory cue was used to standardize the blinking intervals across subjects. The blinking protocol is detailed in Table 4-22.

Table 4-22: Blinking protocol with predefined IBIs and rest periods for OST measurement.

Step	Task	Total Duration
1	Blink 6 times every 2 seconds	12 sec
2	Rest (blink normally)	2 min
3	Blink 6 times every 4 seconds	24 sec
4	Rest (blink normally)	2 min
5	Blink 6 times every 6 seconds	36 sec
6	Rest (blink normally)	2 min
7	Blink 6 times every 8 seconds	48 sec
8	Rest (blink normally)	2 min
9	Blink 6 times every 10 seconds	60 sec

4.4.2.4 OST Measurement and Data Acquisition

4.4.2.4.1 Measurement Locations

OST was recorded from a single pixel at eight distinct ocular surface locations, including the superior, temporal, inferior, nasal, and central regions of the cornea, as well as a circular central region with a 2 cm diameter representing the average OST over a defined area. Measurements were also taken from single pixel locations on the temporal and nasal sclera. Figure 4-18 illustrates the eight ocular surface locations where OST measurements were recorded. Regions 1 through 5 correspond to the superior, temporal, inferior, nasal, and central corneal locations, respectively. Region 6 represents a circular central area used for averaging OST across the cornea, while regions 7 and 8 indicate the nasal and temporal scleral locations. These specific locations were consistently tracked throughout the measurement periods (12, 24, 36, 48, and 60 seconds), clearly capturing temperature changes at each site over time.

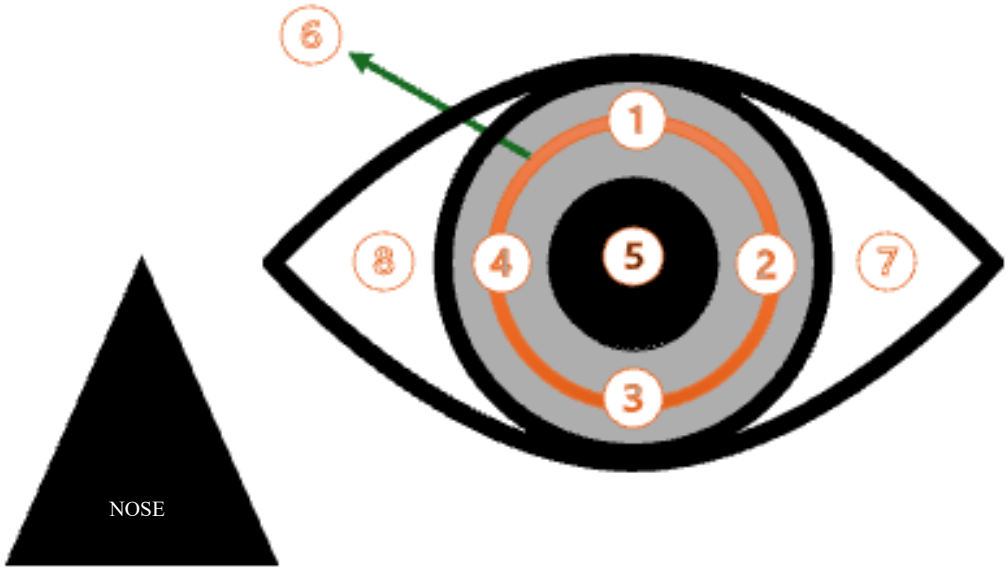


Figure 4-18: OST measurement locations: Superior Cornea (1), Temporal Cornea (2), Inferior Cornea (3), Nasal Cornea (4), and Central Cornea (5); Circular Central Region (average OST over a defined area of a circle with a 2 cm diameter) (6); Temporal Sclera (7), and Nasal Sclera (8) (Image created by the author).

4.4.2.4.2 Standardization of Measurement Locations

To ensure consistent and standardized ROI placement across all participants, a clear overlay template was used to align the corneal center at a uniform location by referencing the canthus of the eye. This method ensures that measurements across different individuals remain comparable by maintaining consistent distance measurements between the corneal center and peripheral ROIs, reducing variability and improving reproducibility in data collection. The overlay was manually adjusted using visible anatomical landmarks to ensure precision in temperature mapping (Figure 4-19).

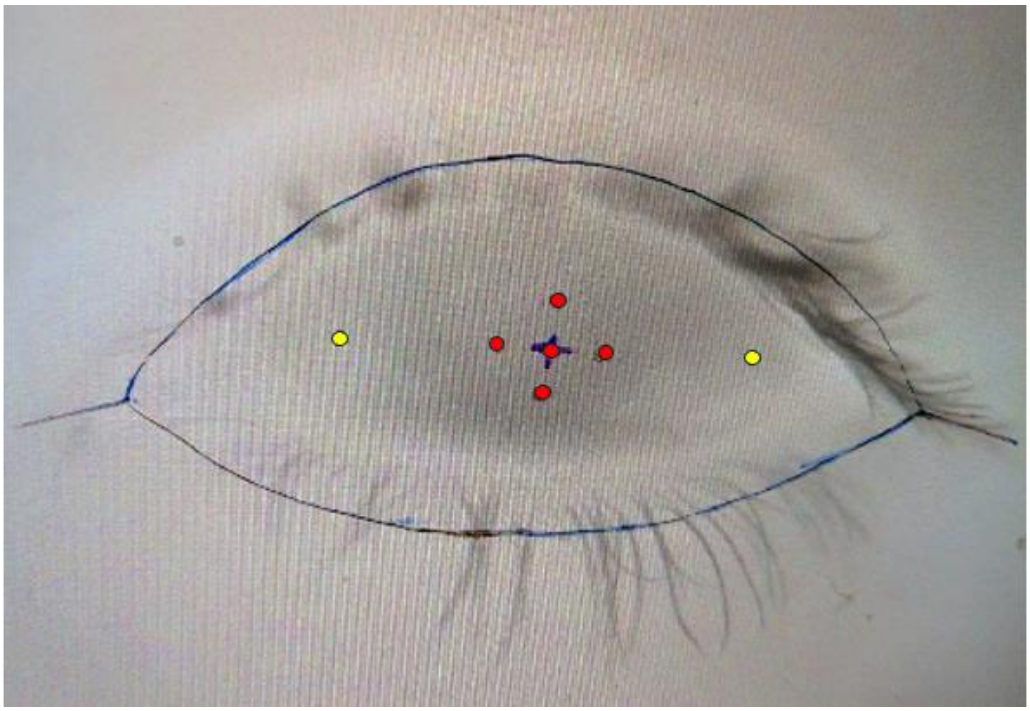


Figure 4-19: Standardized ROI selection using a clear overlay template to ensure consistent placement across participants. The corneal ROIs (red markers) were aligned at a uniform location by referencing the canthus of the eye, while the scleral ROIs (yellow markers) were positioned at fixed distances from the corneal center (Image created by the author).

4.4.2.5 Statistical Analysis

All statistical analyses were conducted using SPSS (IBM Corp., Armonk, NY, USA).

To compare temperature metrics, both RTC and absolute temperature change (ΔT) were initially analyzed across IBI conditions using one-way repeated measures ANOVA. Normality was assessed using the Shapiro-Wilk test.

Analyses were conducted to evaluate the effects of IBI, ocular surface location, and measurement strategies on OST, with RTC used as the primary outcome variable. Post-hoc comparisons between IBIs were conducted using the HSD test, which is appropriate for parametric datasets meeting normality assumptions.

To investigate the effect of ocular surface location, a repeated measures ANOVA was used to compare RTC values across corneal cursor locations. For comparisons involving scleral locations, where normality assumptions were violated, the Wilcoxon signed-rank test was used as a non-parametric alternative.

Pearson correlation analysis was conducted to assess RTC consistency across cursor locations, with heatmaps used for visual representation of intra-corneal and corneal-scleral relationships across different IBIs.

Measurement reliability was evaluated using ICC, which were calculated for both single cursor locations and averaged cursor combinations. Additional ICC analyses were performed to assess the effect of averaging across multiple interblink sequences.

Non-parametric tests, including the Friedman and Kruskal-Wallis tests, were used in cases where normality or sphericity assumptions were violated. All statistical tests were two-tailed, and significance was determined at an alpha level of 0.05.

4.4.3 Results

4.4.3.1 Effect of IBI on OST Measurement

To investigate the impact of IBI on OST, temperature data from Location 5 (central cornea) only were used as a representative site. The following temperature metrics were analyzed:

- ΔT (absolute temperature change) – calculated as the difference between the OST measured immediately after eye opening (start point) and the last measurement immediately before eyelid closure (end point), representing the total decrease in OST during each IBI.

- RTC (rate of temperature change) – calculated by exporting temperature data to Excel and determining the slope of the temperature decrease from the first measurement immediately after

eye opening to the last measurement immediately before eyelid closure, representing the cooling rate during each IBI.

Table 4-23 presents the Mean ± SD of RTC and ΔT at different IBIs for Cursor 5.

Table 4-23: Mean RTC and ΔT (± SD) at the center of the cornea for different IBIs.

	2 sec	**4 sec**	**6 sec**	**8 sec**	**10 sec**
Mean RTC ± SD (°C/S)	-0.15 ± 0.07	-0.04 ± 0.04	-0.05 ± 0.04	-0.03 ± 0.01	-0.02 ± 0.01
Mean ΔT ± SD (°C)	-0.32 ± 0.16	-0.22 ± 0.17	-0.31 ± 0.19	-0.33 ± 0.17	-0.21 ± 0.19

Considering the Table above, RTC and ΔT showed systematic changes across IBIs, suggesting potential effects of IBI on temperature dynamics. Also, the standard deviations indicated substantial variability, particularly at shorter IBIs.

The Shapiro-Wilk normality test was conducted to assess whether RTC and ΔT follow a normal distribution. Table 4-24 presents the test results.

Table 4-24: Normality test results (Shapiro-Wilk test) for RTC and ΔT.

IBI	**Shapiro W RTC**	**P value RTC**	**Shapiro W ΔT**	**P value ΔT**
2 sec	0.97	0.905	0.76	**0.017**
4 sec	0.84	0.097	0.96	0.854
6 sec	0.87	0.201	0.70	0.307
8 sec	0.94	0.655	0.93	0.557
10 sec	0.94	0.593	0.96	0.824

Mean RTC was normally distributed for all IBIs. Mean ΔT, on the other hand, was not normally distributed for IBI = 2 sec, but was normally distributed for the rest. A Repeated Measures ANOVA test was performed to assess the effect of IBI on RTC and ΔT. The results are summarized in Table 4-25.

Table 4-25: Repeated measures ANOVA results for RTC and ΔT.

Metric	Repeated Measures ANOVA F (4,24)	p-value
RTC	12.88	**< 0.001**
ΔT	1.10	0.378

Since $p < 0.05$, the effect of IBI on RTC is statistically significant. However, this pattern should be interpreted with caution: the apparent differences in RTC at shorter versus longer IBIs arise from the cooling profile itself. Most of the temperature drop occurs in the first few seconds after a blink, followed by a plateau phase. At short IBIs, the average RTC captures mainly this steep early decline, while at longer IBIs, the average includes both the early steep drop and the later plateau, which lowers the mean rate. In contrast, ΔT remained relatively stable across IBIs, indicating that absolute temperature change does not reflect these profile-related differences. Thus, the IBI does not mechanistically dictate RTC; rather, the observed variation reflects the kinetics of ocular surface cooling. For this reason, RTC was still chosen as the primary outcome measure, as it provides a more dynamic representation of the cooling process than ΔT.

To assess whether RTC values significantly differed between different IBIs, a post-hoc analysis was used to determine which IBIs significantly differed from each other. Among various post-hoc tests, HSD test was selected. This test was chosen because it effectively controls Type I error while allowing multiple pairwise comparisons without being overly conservative. Also, since the

Shapiro-Wilk test confirmed that RTC was mostly normally distributed, Tukey's HSD was appropriate for this parametric dataset. The results are presented in Table 4-26.

Table 4-26: Tukey's HSD results for RTC

IBI 1 (sec)	IBI 2 (sec)	Mean diff	p-adj	lower	upper
2	4	0.11	**0.0004**	0.04	0.17
2	6	0.10	**0.0015**	0.03	0.16
2	8	0.12	**0.0001**	0.05	0.18
2	10	0.13	**< 0.001**	0.07	0.20
4	6	-0.01	0.9861	-0.08	0.05
4	8	0.01	0.9856	-0.05	0.08
4	10	0.02	0.8343	-0.04	0.09
6	8	0.02	0.8451	-0.04	0.09
6	10	0.04	0.541	-0.03	0.10
8	10	0.01	0.9836	-0.05	0.08

The findings indicate that RTC increased significantly as IBI lengthens, particularly when comparing short IBIs (2 sec) with longer IBIs (4 sec, 6 sec, 8 sec, and 10 sec). This suggests that the rate of change in OST stabilizes as the eye remains open longer before blinking.

Figure 4-20 illustrates the different RTCs across IBIs with Mean ± SD.

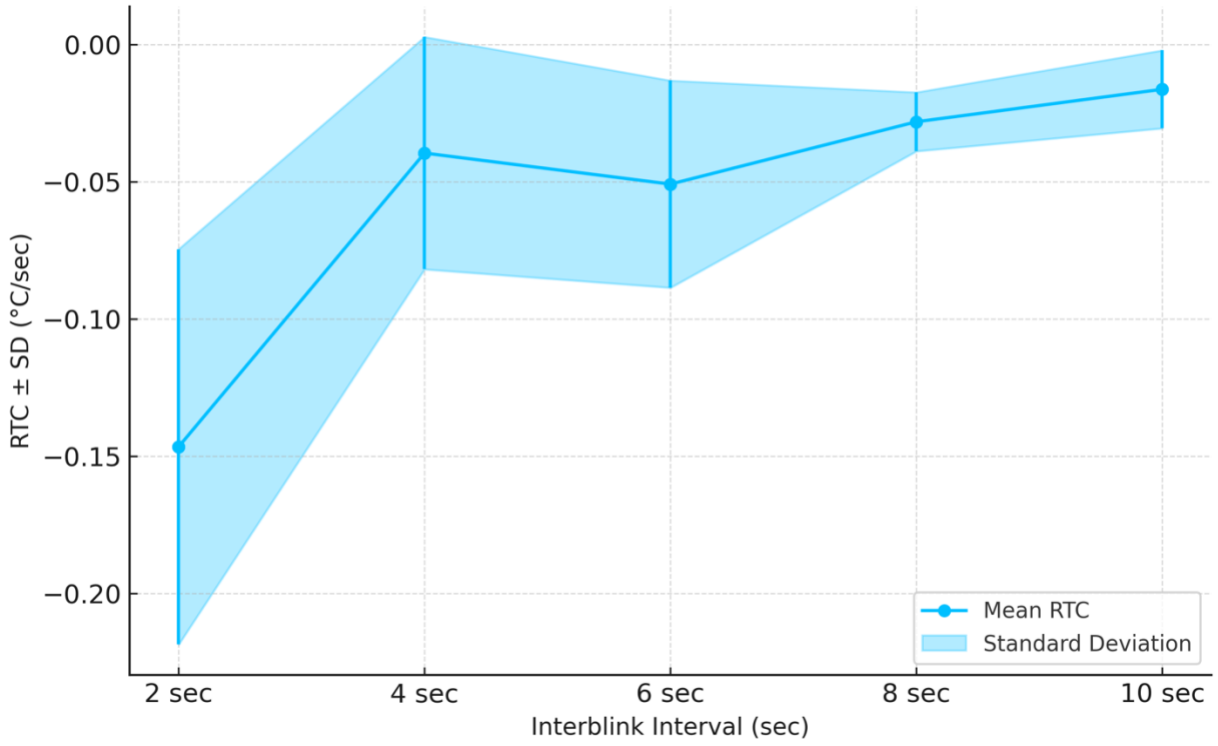


Figure 4-20: RTC across interblink intervals (n = 7), shown as mean ± SD for Location 5 (Central Cornea). Significant differences were found across intervals ($p < 0.001$, repeated-measures ANOVA), with 2 sec showing the steepest decline. Error shading represents SD; 2 sec differed significantly from all longer intervals.

The correlation analysis shows a strong negative relationship between IBI and RTC ($r = -0.64$, $p < 0.001$), indicating that as IBI increases, RTC decreases. This means that with longer IBIs, the temperature change on the ocular surface becomes smaller, suggesting that the cooling rate stabilizes over time. This relationship is visualized in Figure 4-21, which presents the correlation between IBI and RTC at the central corneal location (Cursor 5).

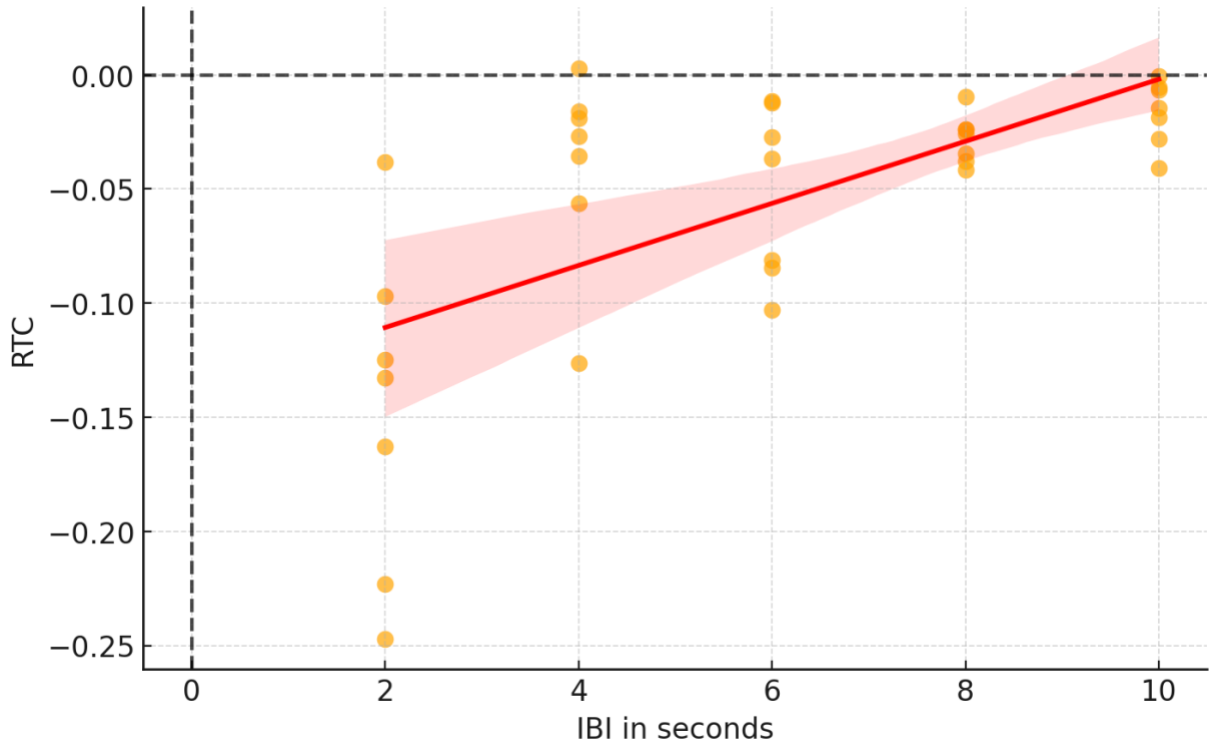


Figure 4-21: Scatter plot of RTC vs. IBI (n = 7) for Location 5 (Central Cornea). A significant negative correlation was observed ($r = –0.64$, $p < 0.001$), indicating that longer IBIs are associated with slower cooling. Shaded area shows 95% CI.

To further illustrate how IBI influences OST over time, Figure 4-22 illustrates the real-time OST changes for different IBIs (2, 4, 6, 8, and 10 seconds) at the center of the cornea (Cursor 5) for one individual. Each line represents actual temperature data from a single representative measurement, showing how OST changes dynamically over each interblink interval. The variations and oscillations within these traces may result from single-pixel measurement noise, subtle eye movements, or changes in tear film distribution occurring over the interblink period.

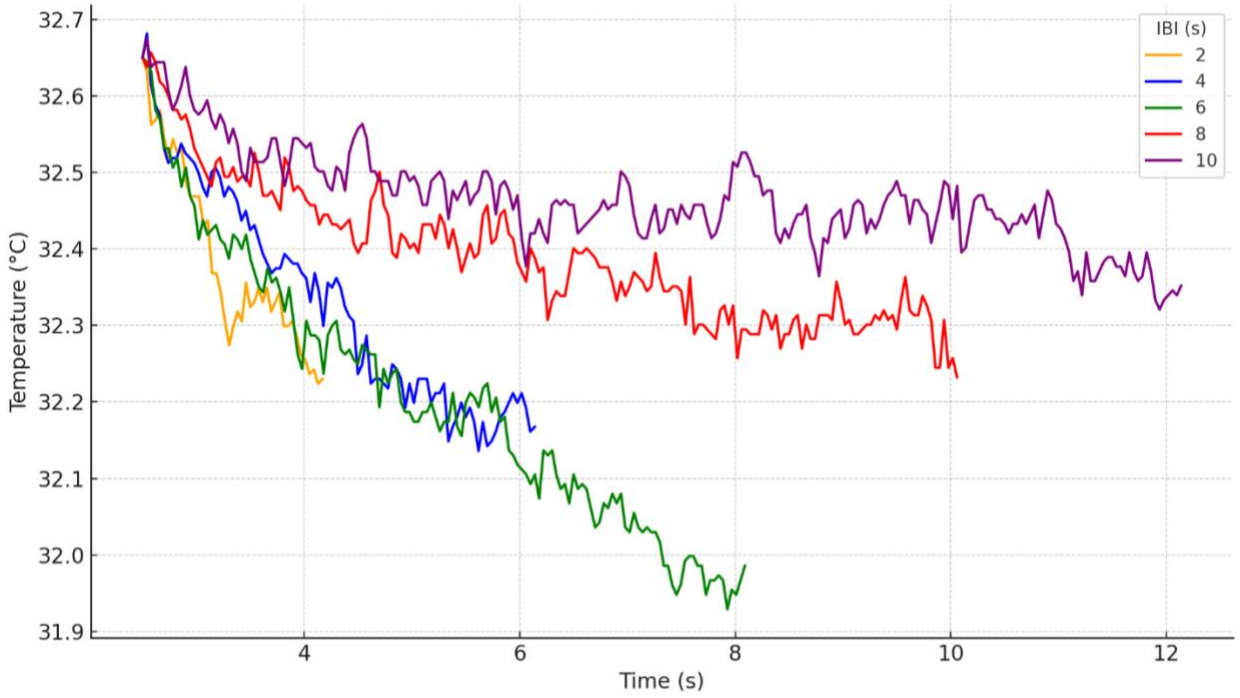


Figure 4-22: Examples of OST temperature traces at the center of the cornea for different IBIs.

4.4.3.2 Effect of Ocular Surface Location on OST Measurement

To determine whether OST changes varied across different ocular surface locations, RTC values were compared across all eight measurement sites. The Mean RTC ± SD values for all subjects at each IBI and ocular surface location are shown in the Table 4-27.

Table 4-27: Mean ± SD of RTC across different IBIs at various corneal and scleral locations

	Corneal Locations						Scleral Locations	
IBI	**1**	**2**	**3**	**4**	**5**	**6**	**7**	**8**
2	-0.18 ± 0.12	-0.20 ± 0.12	-0.18 ± 0.10	-0.16 ± 0.10	-0.15 ± 0.07	-0.17 ± 0.09	-0.09 ± 0.08	-0.05 ± 0.06
4	-0.04 ± 0.03	-0.06 ± 0.03	-0.10 ± 0.09	-0.04 ± 0.04	-0.04 ± 0.04	-0.05 ± 0.03	-0.05 ± 0.06	-0.03 ± 0.04
6	-0.03 ± 0.03	-0.06 ± 0.05	-0.04 ± 0.04	-0.04 ± 0.04	-0.05 ± 0.04	-0.05 ± 0.03	-0.02 ± 0.02	-0.02 ± 0.03
8	-0.02 ± 0.01	-0.03 ± 0.01	-0.02 ± 0.01	-0.03 ± 0.01	-0.03 ± 0.01	-0.03 ± 0.01	-0.02 ± 0.01	-0.02 ± 0.02
10	-0.01 ± 0.01	-0.01 ± 0.01	-0.01 ± 0.01	-0.01 ± 0.01	-0.02 ± 0.01	-0.01 ± 0.01	-0.02 ± 0.03	-0.01 ± 0.01

To assess whether the distribution of RTC values was appropriate for parametric testing, a Shapiro-Wilk test was conducted at each corneal cursor location (Cursors 1–6), with RTC values averaged across all IBIs for each participant. As shown in Table 4-28, none of the cursor locations exhibited significant deviations from normality ($p > 0.05$), indicating that the assumption of normality was met.

Table 4-28: Shapiro-Wilk normality test results for RTC values at each corneal location

Cursor	W-statistic	p-value
Cursor 1	0.90	0.3585
Cursor 2	0.85	0.1130
Cursor 3	0.84	0.1087
Cursor 4	0.93	0.5083
Cursor 5	0.94	0.6619
Cursor 6	0.86	0.1391

Given that the normality assumption was satisfied, a repeated measures ANOVA was performed to evaluate whether RTC significantly differed across the six corneal cursor locations. The analysis revealed no statistically significant effect of cursor location on RTC ($F = 1.44$, $p = 0.239$), suggesting that temperature change across the ocular surface was generally consistent regardless of measurement site. However, it is also possible that this non-significant result reflects the relatively large variability observed across locations, which may have limited the ability to detect subtle regional differences in RTC.

While no significant RTC differences were observed among corneal locations, a significant difference was detected between the scleral sites (Locations 7 and 8) and the corneal locations. To assess this difference, a Shapiro-Wilk test confirmed that RTC values were not normally distributed in either region ($p < 0.001$). Given this violation of normality, the Wilcoxon signed-rank test was used as a non-parametric alternative to compare RTC between the two groups. The

results (W = 0.000, p = 0.016) indicated a significant difference, suggesting that RTC fluctuations are greater in corneal locations than in scleral regions. This difference is illustrated in Figure 4-23, which compares the mean RTC between corneal and scleral locations, highlighting the greater temperature change observed across the corneal surface.

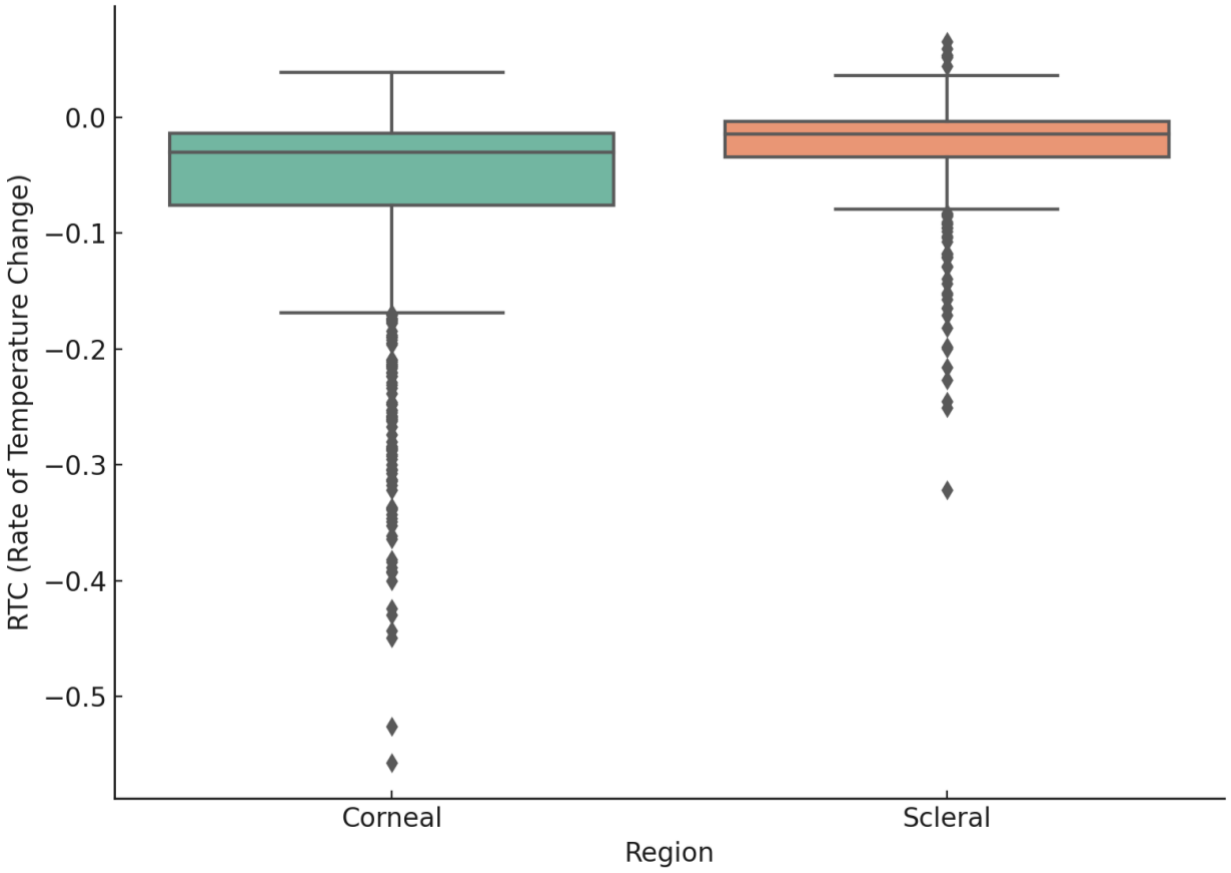


Figure 4-23: RTC distribution for corneal vs. scleral regions across all IBIs (n = 7). RTC was significantly greater in corneal locations compared to scleral (Wilcoxon signed-rank test W = 0.000, p = 0.016). Boxes show median and IQR.

The relationship between corneal locations in terms of RTC was assessed by calculating the mean correlation among Cursor 1–5 at different IBIs. As shown in the Figure 4-24, the correlation between different corneal sites was not constant, but varied across IBIs, with the highest correlation

observed at IBI 6 seconds. The observed peak RTC synchronization at IBI 6 second likely reflects a transient physiological state, during which the tear film attains a relatively uniform thickness and evaporation rate across the corneal surface. At shorter intervals (such as 2 or 4 seconds), rapid evaporation immediately after blinking may cause uneven tear film thinning, resulting in localized variability. Conversely, at longer intervals (8 or 10 seconds), the tear film may begin to break up, creating regional dry spots or uneven temperature changes. Thus, the 6 second interval could represent an optimal physiological balance point, where uniform tear film stability leads to synchronized temperature dynamics across corneal regions.

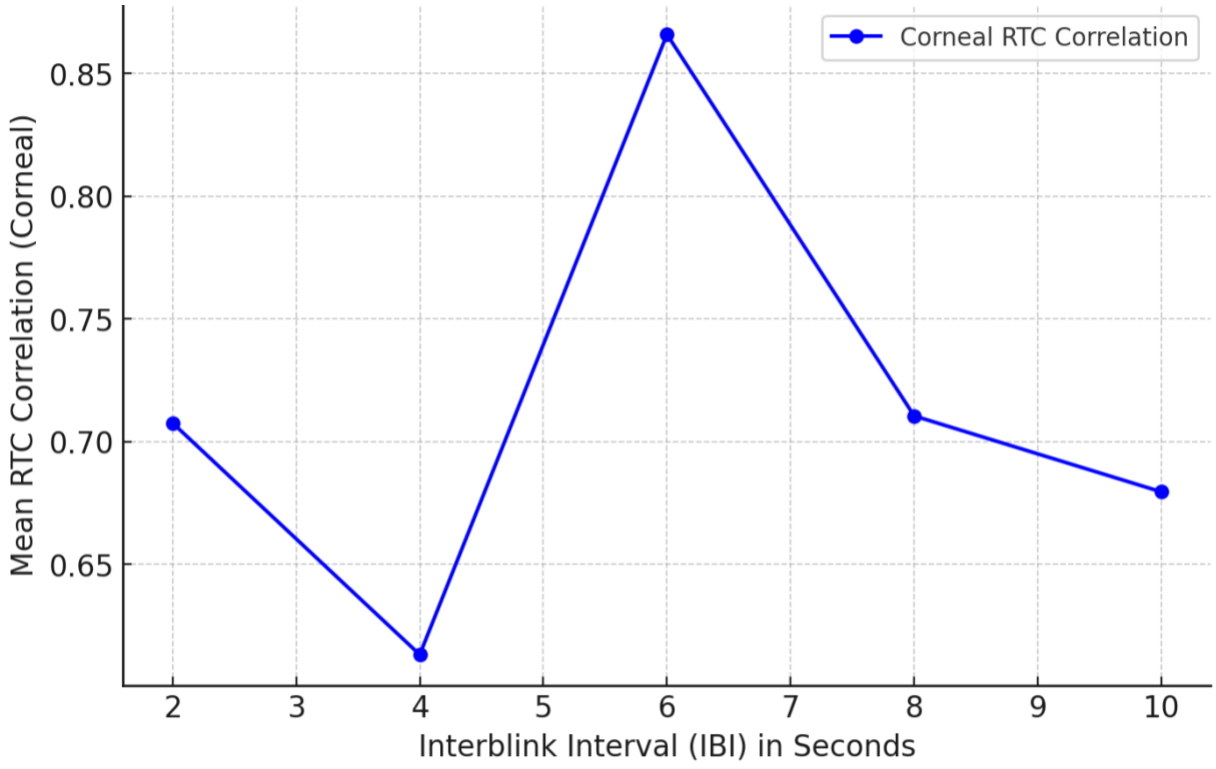


Figure 4-24: Mean RTC correlation among corneal locations across IBIs (n = 7). The highest correlation at 6 sec IBI suggested synchronized temperature changes, while decreasing correlation at longer IBIs indicates increasing thermal variability.

Now that the pattern of RTC synchrony among corneal locations has been established in Figure 4-24, this relationship can be visualized even more clearly through the correlation heatmaps presented in Figure 4-25. Figure below displays the correlation heatmaps of RTC across cursor locations for each IBI. At IBI 2 sec and 4 sec, corneal locations exhibit strong correlations, though slight variations are present. At IBI 6 sec, correlations among corneal locations reach their peak, indicating the most uniform RTC pattern. At IBI 8 sec and 10 sec, correlations weaken, showing increased variability in RTC among corneal locations. Additionally, across all IBIs, correlations between corneal locations (Cursor 1–5: superior, temporal, inferior, nasal, and central cornea) and scleral locations (Cursor 7: temporal sclera; Cursor 8: nasal sclera) remain lower than intra-corneal correlations.

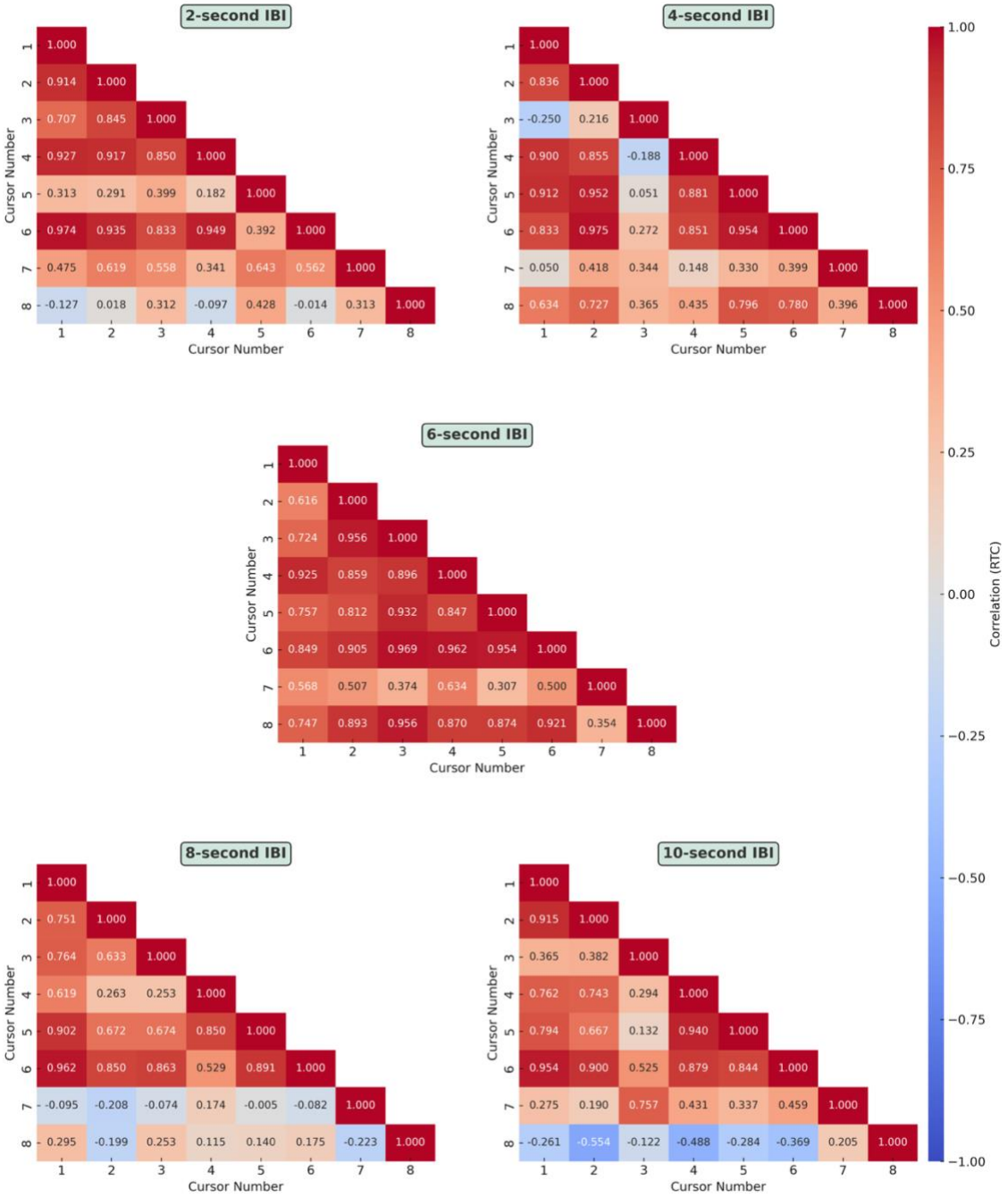


Figure 4-25: Heatmaps of RTC correlation across cursor locations at different IBIs (n = 7). Strong correlations (red) indicate synchronized temperature changes, while weaker correlations (blue) reflect increasing thermal variability.

4.4.3.3 Effect of Averaging vs. Single Measurements

The reliability of RTC measurements was assessed by calculating ICC for individual cursor locations and various averaging combinations**.** Table 4-29 summarizes the ICC values obtained, demonstrating that averaging across multiple cursor locations consistently improved measurement reliability compared to single cursor measurements.

Table 4-29: ICC values for averaged and single cursor measurements

Averaging Combination	**ICC Value**	**Reliability**	**Notable Findings**
(1, 4)	0.99	Excellent	Near-perfect reliability
(1, 3, 4)	0.98	Excellent	High stability trio
(1, 6)	0.98	Excellent	Near-perfect reliability
(5, 6)	0.96	Very High	Reliable pair
(4, 6)	0.95	Very High	Reliable pair
(2, 6)	0.94	Very High	Reliable pair
(3, 4)	0.92	Very High	Consistently reliable pair
(2, 3)	0.92	Very High	Reliable pair
(1, 2)	0.91	Very High	Optimal pair
Cursor 5	0.74	High	Most reliable single location
Cursor 4	0.73	High	Single location
Cursor 6	0.72	High	Single location
Cursor 3	0.71	High	Single location
Cursor 1	0.67	Moderate	Single location
Cursor 2	0.65	Moderate	Single location

While cursor combinations consistently demonstrated very high to near-perfect reliability, it is noteworthy that several single cursor locations also provided high reliability, with ICC values above 0.70. Among these, Cursor 5 yielded the highest reliability as an individual site. Figure 4-26 visually compares ICC values for both single and combined cursor measurements, emphasizing the enhanced stability achieved through averaging, while also showing that single-point measurements can still offer dependable results. The dashed red line (ICC = 0.9) represents the threshold for high reliability, clearly distinguishing the performance gap between individual and combined cursor strategies.

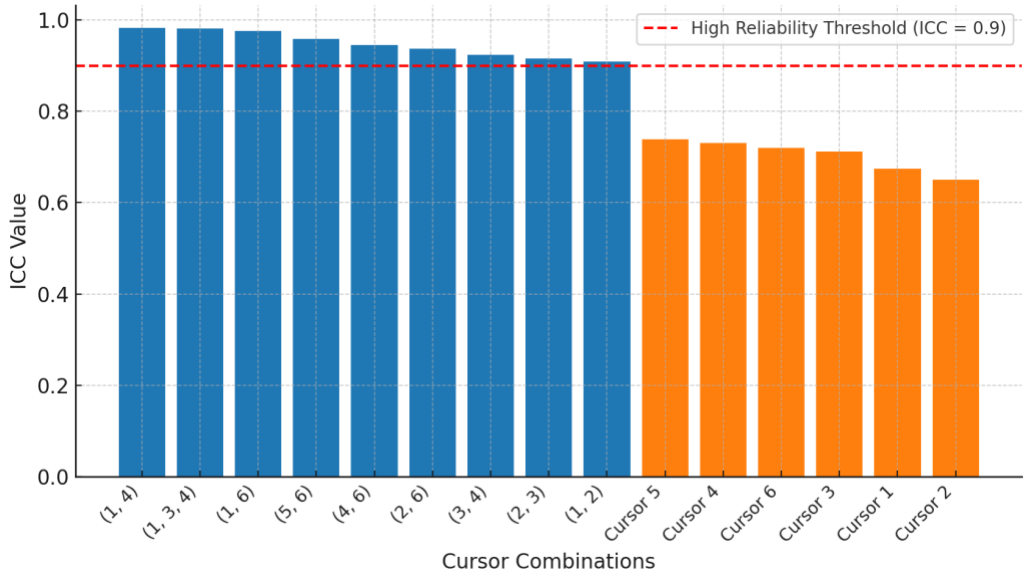


Figure 4-26: ICC values for RTC across individual cursors (orange) and cursor combinations (blue). All combinations exceeded the high-reliability threshold (ICC ≥ 0.9), while single cursors ranged from moderate to high reliability. Cursor 5 was the most reliable individual location.

4.4.3.4 Necessity of Averaging Multiple Measurements

The reliability of RTC measurements across IBI sequences was evaluated using ICC analysis. Table 4-30 summarizes the ICC values obtained for single measurements and averaged measurements across multiple IBI sequences.

Table 4-30: ICC for RTC measurements

Number of Sequences Averaged	ICC
1	0.88
2	0.90
3	0.91
4	0.91
5	0.89

The results show that averaging RTC measurements improves reliability, with ICC values increasing as more sequences are averaged. The ICC value for a single measurement was lower compared to averaged measurements, with reliability improving significantly when combining two or three sequences. However, beyond three averaged measurements, no substantial improvement in ICC was observed, indicating that averaging more than three sequences does not provide additional reliability gains. These findings suggest that averaging at least three IBI sequences is sufficient to achieve stable and reliable RTC measurements, without requiring additional sequences. The dashed red line (ICC = 0.9) in the Figure 4-27 represents the high reliability threshold, showing that averaging three sequences is optimal for achieving consistent measurements.

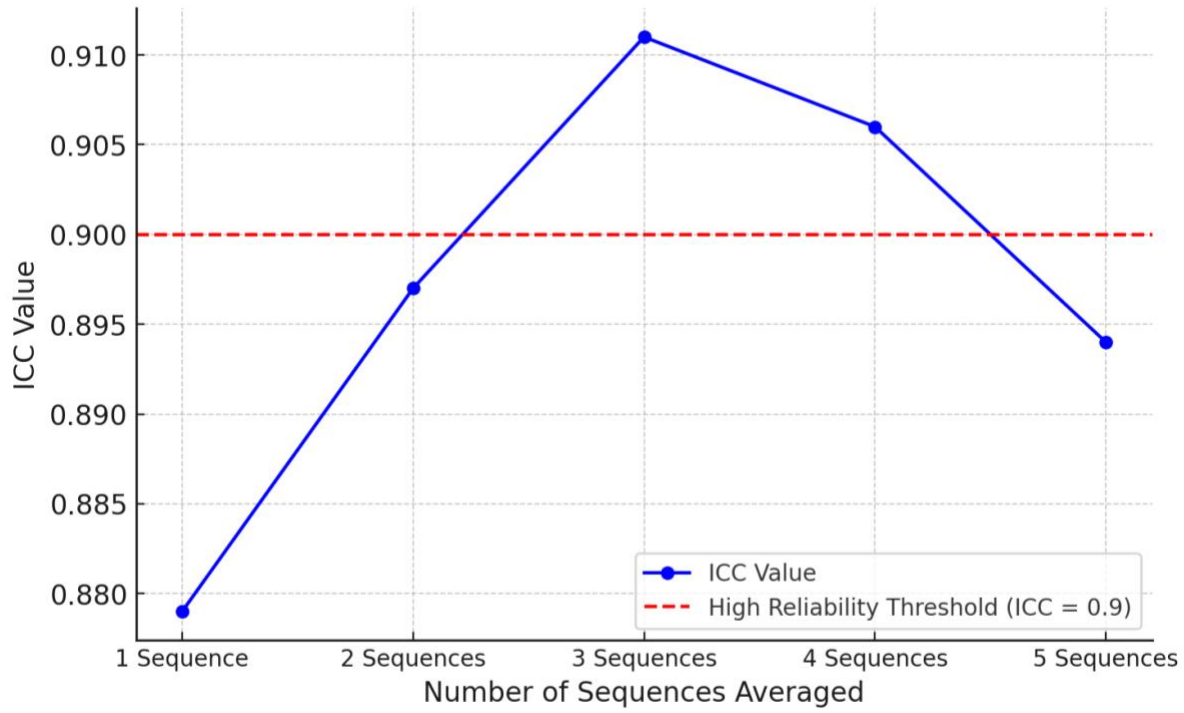


Figure 4-27: ICC values for RTC based on the number of sequences averaged. Averaging 3 sequences yielded the highest reliability (ICC = 0.91), surpassing the high-reliability threshold (dashed line).

4.4.4 Discussion

This study aimed to optimize OST measurement using IRT by examining key factors such as temperature metrics, IBI, measurement location, and the reliability of single versus averaged measurements. The findings align with and extend existing research, offering practical insights for improving OST measurement protocols and standardization.

4.4.4.1 RTC as a Superior OST Metric

The results demonstrated that the RTC, which reflects the rate of temperature change, is a more reliable and consistent metric than absolute temperature change (ΔT). While some researchers found both methods valuable,[210] the findings from this study align with other studies, emphasizing the superiority of dynamic measurements for understanding thermal regulation of the ocular

surface. The cooling rate of the ocular surface – particularly the temperature fluctuations that occur between blinks – has been shown to offer greater insight than static temperature values when assessing tear film stability, diagnosing ocular surface diseases, and distinguishing between different forms of DED.[30] It has further been demonstrated that single-point measurements of OST, when analyzed dynamically, correlated effectively with indicators of tear film stability, such as NITBUT, in contact lens wearers.[248] Collectively, these findings underscore the significance of evaluating dynamic OST changes rather than relying solely on static values.

4.4.4.2 Influence of IBI on OST Measurements

The analysis revealed that longer IBI's lead to more consistent OST measurements, with the lowest variability observed at the 8- and 10-second intervals. However, practical limitations, such as a participant's ability to maintain their gaze without blinking, often make longer IBIs challenging, particularly in an individual with DED. Previous studies have noted the difficulty in sustaining longer IBIs without affecting measurement reliability.[252] Although longer IBIs inherently lead to lower temperature variability due to the gradual convergence toward baseline OST (~32°C), this reduced variability alone does not necessarily imply greater diagnostic value. Instead, prolonged IBIs may diminish the sensitivity required to detect subtle but clinically meaningful differences in tear film stability. The current study identified the 6-second IBI as an optimal balance, offering a compromise between measurement consistency and participant comfort, while preserving diagnostic sensitivity by capturing more immediate and relevant variations in tear film dynamics before temperatures fully stabilize. This finding aligns with recommendations suggesting that while longer IBIs improve measurement stability, they may not be practical for all participants.[200] A 6-second IBI has also been used for similar reasons, with an emphasis on the fact that shorter

IBIs minimize reflex tearing, which might otherwise affect the accuracy of IR imaging measurements.[198]

4.4.4.3 Ocular Surface Location and OST Variability

The study also explored temperature variations across different ocular surface locations, revealing high correlations among central corneal locations, suggesting redundancy in multiple measurements from these sites. This result corroborates findings indicating that central corneal measurements are highly consistent due to the relatively uniform temperature distribution across these locations.[210] In contrast, peripheral regions, such as the nasal and temporal sclera, showed distinct temperature profiles, reflecting differences in vascularization and exposure to environmental factors. It has been demonstrated that peripheral temperature measurements provide valuable diagnostic information for conditions affecting these regions, such as conjunctival inflammation or localized dry eye.[31,188,194,246,247]

The importance of peripheral temperature measurements is further supported by evidence exploring the relationship between OST and peripheral vasoconstriction. This suggests that peripheral blood flow significantly influences OST, highlighting the broader implications of these measurements in ocular and systemic health assessments.[253]

4.4.4.4 Measurement Reliability. Single vs. Averaged Data

This study assessed the reliability of OST measurements by calculating ICC for both individual cursors and various cursor combinations. The results showed that averaging measurements across multiple cursor locations significantly enhanced reliability compared to single cursor measurements. Combining measurements from multiple cursor locations, such as (1, 4) or (1, 3, 4), resulted in ICC values approaching near-perfect reliability (0.98 and 0.98, respectively), suggesting that strategic averaging across selected cursor locations improves measurement

consistency. While single cursors still provided reasonable reliability, Cursor 5 was the most reliable single location (ICC = 0.74), though slightly lower than combined measurements, emphasizing the benefit of averaging.

This supports the finding that averaging of measurements reduces variability and enhances the consistency of OST readings, making it a preferable approach for obtaining reliable data.[225] The high reproducibility of OST measurements using thermographic devices has also been demonstrated, reinforcing the importance of combining multiple measurement points to achieve consistent and accurate readings.[200] While single-location measurements remain useful due to time or resource constraints, selecting optimal cursor combinations greatly enhances consistency, making it the preferred approach in clinical practice.

4.4.4.5 Necessity of Averaging Multiple RTC Measurements

The analysis showed that while averaging multiple RTC measurements slightly improves reliability (with ICC values increasing from 0.87–0.88 for single measurements to 0.972–0.973 for averaged ones), the difference is small and that single measurements still demonstrate good reliability. Support for the use of single measurements has also been shown, demonstrating their effective correlation with systemic cardiovascular risk factors, which is valuable in large-scale screenings or routine clinical use.[254] Thus, while averaging enhances consistency, single measurements are often adequate, especially when time or resources are limited.

4.4.4.6 Implications for OST Standardization and Clinical Utility

The findings of this study provide critical insights into optimizing OST measurement protocols, particularly in refining standardized procedures for IRT-based tear film assessment. Several key recommendations emerge:

- RTC should be prioritized over ΔT for assessing ocular surface cooling dynamics.

- Longer IBIs (6–10 sec) provide more stable temperature readings, reducing RTC variability and enhancing reliability.
- Averaging RTC across multiple cursor locations and IBIs significantly improves measurement reliability.

By addressing these methodological aspects, this study enhances the standardization of OST measurements, ultimately contributing to the development of more reliable diagnostic tools for assessing tear film function and ocular surface health. Future research should aim to validate these findings in larger and more diverse populations, including individuals with specific ocular conditions, such as DED and glaucoma. Additionally, further investigation into the impact of environmental factors, such as RH and lighting conditions, on OST readings could refine protocols. Integrating machine learning algorithms for automated IRT analysis holds promise for improving OST measurement precision and accessibility in clinical settings.

4.4.5 Limitations and Future Directions

Despite the significant contributions of this study in optimizing OST measurement protocols, several limitations must be acknowledged.

First, the sample size was relatively small (n=7), consisting of healthy participants without diagnosed ocular surface disease. While the findings provide valuable insights into OST measurement standardization, a larger and more diverse sample, including patients with DED, glaucoma, and other ocular surface disorders, is necessary to enhance generalizability. It is important to note that this study was designed as a protocol optimization investigation, with the primary aim of refining OST measurement procedures specifically, identifying appropriate blink intervals and anatomical regions for temperature acquisition using infrared thermography. As the study did not involve hypothesis testing or effect size estimation, a formal sample size calculation

was not undertaken. Previous literature supports the use of small samples in pilot and feasibility studies when the objective is to assess procedural feasibility and optimize methodology. For example, Billingham et al.[250] and Teresi et al.[251] both emphasize that small sample sizes can be acceptable in this context, particularly when multiple within-subject measurements are obtained under controlled conditions. However, it is important to acknowledge that the sample size of seven participants falls below the threshold recommended for pilot studies that are also intended to inform future trial planning. Whitehead et al.[255] suggest that 10 to 15 participants per group may be more appropriate when aiming to estimate parameters for sample size calculation or assess intervention effects. This limitation should be considered when interpreting the broader applicability of any findings.

Second, while this study identified the 6-second IBI as an optimal balance between stability and feasibility**,** some participants may struggle to maintain prolonged IBIs. In individuals with severe DED or blink abnormalities**,** alternative measurement strategies, such as adaptive blinking protocols, should be investigated to enhance feasibility without compromising data accuracy**.**

Third, while this study emphasized averaging across cursor locations and IBI sequences to enhance measurement reliability**,** it remains unclear whether automated approaches, such as machine learning-based region selection, could further improve standardization and efficiency. Future work should explore AI-driven methods for automating OST analysis, potentially reducing variability associated with manual region selection.

Finally, while RTC was identified as the most reliable metric for OST assessment, other dynamic temperature parameters**,** such as thermal recovery time (i.e., the time it takes for the ocular surface temperature to return to baseline after a blink) or regional temperature gradients**,** may also offer

additional diagnostic value. Future investigations should explore these alternative thermographic parameters in different ocular conditions to expand the clinical utility of OST measurements.

4.4.6 Conclusion

This study provides a framework for optimizing OST measurement, emphasizing the importance of standardized methods to improve reliability, reproducibility, and clinical utility**.** The findings contribute to better ocular health monitoring through advanced IRT techniques, offering a pathway toward improved diagnosis and management of ocular surface disorders. By identifying optimal IBIs, reliable measurement locations, and the benefits of averaging**,** this research lays the groundwork for standardized OST assessment, improving its integration into routine ophthalmic evaluations. Future efforts should focus on clinical validation, automation, and environmental adaptability to further enhance the precision and accessibility of OST as a diagnostic tool.

4.5 Investigating Tear Film Dynamics Following Lipid Eye Drop Instillation (PHASE II)

4.5.1 Overview

The tear film is critical for maintaining ocular surface health by providing lubrication, minimizing friction, and protecting the cornea from environmental stressors. The primary cause of instability of the tear film is often a compromised lipid layer, resulting in rapid tear film break-up and increased ocular surface cooling.[7]

Artificial tears containing lipids aim to enhance lipid layer integrity and consequently reduce tear evaporation, but their exact effect on OST and tear film stability remains unclear and requires further investigation.[99,215]

IRT has emerged as a valuable, non-invasive method for assessing OST variations related to tear film dynamics. Prior research showed OST decreases progressively during sustained eye opening, reflecting tear evaporation, with regional differences in cooling rates.[178,185] Despite this clinical potential, standardized OST measurement methodologies are lacking, and there is an ongoing need to identify optimal techniques and ocular surface regions for reliable IRT assessments.[33,185,186]

In Phase I of this investigation (Section 4-3) into tear film dynamics following lipid eye drop instillation, the immediate effects of lipid-based drops were explored, but this did not include OST measurements. The primary focus in the Phase I study was on evaluating tear film stability and subjective effects and, while the study provided important insights, it became evident that a longer observation period than 5 mins post-instillation was required to capture sustained effects of lipid supplementation on tear film stability. Building on these findings, a follow-up study was designed with an extended evaluation timeframe to determine whether lipid-based eye drops provide

prolonged protection against tear evaporation or induce transient destabilization before stabilization occurs.

In the ResearchIR study (Section 4-4), a refined methodology for OST measurement was established. That study allowed procedural elements to be established, including monitoring of environmental conditions, standardized IBIs, and optimized image processing techniques. Importantly, the ResearchIR study revealed that RTC was more informative and provided superior insight into tear film dynamics than ΔT alone, further supporting the significance of cooling rate in thermographic assessments. With a framework for OST analysis, the current study aims to integrate the ThermOcular IR camera with the ResearchIR software to systematically measure OST and evaluate its correlation with tear film stability following lipid eye drop instillation.

A significant aspect of this investigation is the comparison of different measurement methods and locations to determine the most accurate and reproducible approach. Instead of relying on a single-point OST measurement, temperature variations were analyzed across multiple ocular surface regions, and with different numbers of pixels within the sample location. This comparative approach helped optimize the use of the ThermOcular camera for OST measurements.

4.5.2 Materials and Methods

4.5.2.1 Subjects and Ethical Approval

Since this study was a continuation of Phase I with some refinements, an amendment was submitted and approved by University of Waterloo Research Ethics Board (REB #44425). The study adhered to the tenets of the Declaration of Helsinki.

Twenty-seven healthy adult participants (mean age 24.6 ± 2.3 years; 21 females, 6 males) were enrolled in the study. Participants were eligible for inclusion if they were 18 years or older, had no known active ocular disease or infection, and were able to comply with the study protocol, which

included refraining from contact lens wear, eye makeup, and ocular lubricants on the day of the study visit. Participants were also required to be awake for at least two hours prior to their scheduled visit. Exclusion criteria included the presence of active ocular disease or infection, a history of ocular surgery within the past six months, or the use of systemic or ocular medications that could potentially influence tear film properties. Individuals with known sensitivities to Systane Complete eye drops or petroleum jelly, as well as those with a history of refractive surgery or aphakia, were also excluded. All participants provided written informed consent prior to participation in the study.

4.5.2.2 Instrumentation

The following instruments were used for this study, with their detailed specifications previously described in the methodology chapter and thus not repeated here:

- Waterloo Evaporimeter: TER.
- Keratograph 5M (Oculus, Germany): NITBUT.
- LipiView II (Johnson & Johnson Vision, USA): LLT.
- ThermOcular Camera: OST.
- Systane Complete Eye Drop (Alcon, Canada): TFLL enhancement.

4.5.2.3 Experimental Procedure

The experimental tasks were conducted in the following chronological order:

4.5.2.3.1 Baseline Measurements

At the beginning of the study visit, demographic, ocular, and medical history information was collected for each participant. This included age, sex, contact lens use, recent eye drop use, past or current ocular surgeries, history of ocular infections or conditions, use of ocular or systemic

medications or supplements, and any history of epilepsy or known sensitivities to eye drops or petroleum jelly.

Visual acuity was assessed using a Bailey-Lovie LogMAR chart to confirm that participants had normal or corrected-to-normal vision prior to testing. LLT was then measured using the LipiView II interferometer, followed by three consecutive NITBUT measurements performed with the Keratograph 5M.

OST was measured using the ThermOcular camera system. Participants were instructed to begin by closing their eyes for 10 seconds and then initiate a blinking cycle in which they blinked every 6 seconds. This cycle was repeated four times, with the timing guided by a metronome providing an auditory cue. Temperature measurements were recorded at five pre-defined corneal cursor locations, including the central, superior, inferior, nasal, and temporal regions, to capture regional differences in OST.

Prior to evaporimetry measurements, petroleum jelly was carefully applied around the eyes to reduce skin evaporation within the goggle and ensure a proper seal between the skin and the evaporimeter goggles. TER was measured with the eyes open while participants blinked every 3 seconds for a total of 20 seconds, guided by a metronome. After ventilating the goggles to restore baseline humidity, TER was measured a second time with the eyes closed for another 20 seconds.

Note on Device Malfunction: During Phase II of data collection, the right-side sensor in the Waterloo Evaporimeter stopped transmitting data due to a malfunction in the custom “Goggle” software. Despite troubleshooting efforts, the right goggle could not be restored in time to resume randomized bilateral measurements. As a result, all TER recordings in the later part of the study were obtained from the left eye only. While not ideal, this deviation allowed continued data acquisition.

4.5.2.3.2 Lipid Drop Instillation

One drop of Systane Complete® was instilled into one eye (randomly assigned). Post-instillation measurements were conducted at two time points: the first after a five-minute wait period and the second at an interval of twenty-minutes after drop instillation.

4.5.2.3.3 Post-Drop Measurements (5 Minutes)

LLT was measured using the LipiView II interferometer. This was followed by three consecutive NITBUT measurements obtained using the Keratograph 5M.

OST was then assessed using the ThermOcular camera. For this measurement, participants were instructed to close their eyes for 10 seconds, then begin blinking every 6 seconds while looking directly into the camera. This blinking cycle was repeated four times, guided by auditory cues from a metronome to ensure consistency. Temperature measurements were recorded at five pre-defined corneal cursor locations, including the central, superior, inferior, nasal, and temporal regions, to capture regional differences in OST.

TER was measured using the Waterloo Evaporimeter. The first measurement was taken with the eyes open while participants blinked every 3 seconds for 20 seconds, again guided by a metronome. Following a brief ventilation period to restore baseline humidity inside the goggles, a second TER measurement was performed with the eyes closed for another 20 seconds.

4.5.2.3.4 Post-Drop Measurements (20 Minutes)

All measurements were repeated 20 minutes after the instillation of the lipid eye drop. LLT was measured using the LipiView II interferometer, followed by three consecutive NITBUT measurements performed with the Keratograph 5M.

OST was then assessed using the ThermOcular camera. For this procedure, participants were instructed to close their eyes for 10 seconds and then begin blinking every 6 seconds while looking

toward the camera. This blinking cycle was repeated four times, with auditory cues provided by a metronome to ensure timing consistency. Temperature measurements were recorded at five pre-defined corneal cursor locations, including the central, superior, inferior, nasal, and temporal regions, to capture regional differences in OST.

TER was measured using the Waterloo Evaporimeter. The first measurement was taken with the eyes open while participants blinked every 3 seconds for 20 seconds, guided by a metronome. After ventilating the goggles to restore baseline humidity, a second TER measurement was taken with the eyes closed for another 20 seconds.

4.5.2.3.5 Completion Procedures

Exit visual acuity was reassessed using the Bailey-Lovie LogMAR chart to confirm that no adverse effects had occurred during testing. Participants then completed a study completion form and received remuneration for their participation.

The following table (Table 4-31) summarises the structured sequence of experimental procedures conducted throughout the study.

Table 4-31: Summary of the experimental procedure of the study.

Baseline Measurements	Collection of demographic data, ocular, and medical history
	Entrance VA with Bailey-Lovie LogMAR chart
	LLT with LipiView II
	NITBUT with Keratograph 5M
	OST with ThermOcular Camera
	TER with Waterloo Evaporimeter
Lipid Drop Instillation	Instillation of one drop of Systane Complete into one eye
	Wait period of 5 minutes and 20 minutes
Post Drop Measurements (@ 5 Minutes)	LLT with LipiView II.
	NITBUT with Keratograph 5M
	OST with ThermOcular Camera
	TER with Waterloo Evaporimeter
Post Drop Measurements (@ 20 Minutes)	LLT with LipiView II
	NITBUT with Keratograph 5M
	OST with ThermOcular Camera
	TER with Waterloo Evaporimeter
Completion Procedure	Exit VA with Bailey-Lovie LogMAR chart

4.5.2.4 Statistical Analysis

All statistical analyses were conducted using SPSS (IBM Corp., Armonk, NY, USA). Analyses were designed to evaluate the effects of lipid-based eye drop instillation on tear film characteristics and ocular surface thermodynamics across multiple time points and spatial locations.

To assess the distribution of data, the Shapiro-Wilk test was used for each parameter at all measurement time points. Based on the outcomes of normality testing, appropriate statistical methods were selected for subsequent analysis.

For variables that followed a normal distribution, such as NITBUT repeated-measures ANOVA was employed to evaluate within-subject changes across time (baseline, 5 minutes, and 20 minutes post-instillation). Where significant effects were identified, post-hoc comparisons with Bonferroni Correction were performed using paired-sample t-tests to identify specific time point differences.

For non-normally distributed variables, including LLT, RTC and TER, the Friedman test was used as a non-parametric alternative for repeated-measures comparisons. In cases of significance, Wilcoxon signed-rank tests with Bonferroni Correction were used for post-hoc pairwise comparisons.

Pearson correlation analyses with Bonferroni Correction were conducted to examine the relationships among changes in LLT, NITBUT, RTC, and TER at 5- and 20-minutes post-instillation. Correlations were interpreted based on both the strength and direction of the relationship and supported by scatter plots with regression lines.

All statistical tests were two-tailed, with a significance level set at $p \leq 0.05$.

4.5.3 Results

4.5.3.1 Participant Demographics and Environmental Conditions

Initially, 31 participants were enrolled in the study. After applying the inclusion and exclusion criteria, data from 27 participants were included in the final analysis. Table 4-32 presents the demographic characteristics of the study participants and the environmental conditions under which data collection was performed. These values provide context for interpreting the physiological measurements collected during the study.

Table 4-32: Participant demographics and environmental conditions

Characteristics	**Mean ± SD or n**
Age (years)	24.7 ± 2.34
Sex	7 Male, 20 Female
Eye Measured (OD/OS)	6 OD, 21 OS
Room Temperature (°C)	22.5 ± 0.81
Ambient RH (%)	35.8 ± 8.1

4.5.3.2 Tear Film Characteristics Before and After Lipid Drop Instillation

The primary tear film characteristics evaluated in this study were LLT, NITBUT, RTC and TER. These parameters were measured at baseline (before lipid eye drop instillation) and repeated following administration of Systane Complete eye drops after 5 minutes and 20 minutes. Table 4-33 summarizes the descriptive statistics for LLT, NITBUT, RTC (First Measurement, Single Pixel at the center of the cornea) and TER measurements, illustrating the tear film dynamics associated with lipid supplementation.

Table 4-33: Tear film characteristics before and after lipid drop instillation

Parameter	Before Drop (Mean ± SD)	5 mins After Drop (Mean ± SD)	20 Mins After Drop (Mean ± SD)
LLT (nm)	64.41 ± 16.73	83.48 ± 15.53	80.48 ± 18.69
NITBUT (sec)			
First Measurement	13.55 ± 6.15	12.02 ± 5.57	10.43 ± 4.99
Average Measurement	16.20 ± 5.06	15.04 ± 4.89	13.75 ± 4.89
RTC (°C/sec)	-0.04 ± 0.04	-0.04 ± 0.03	-0.04 ± 0.03
TER (g/m²/hr)	0.08 ± 0.07	0.11 ± 0.06	0.11 ± 0.05

4.5.3.3 Normality Analysis of Tear Film Characteristics

The normality of distributions for LLT, NITBUT, RTC and TER measurements, both before and after lipid eye drop instillation, was assessed using the Shapiro-Wilk test. The results are summarized in the Table 4-34.

Table 4-34: Normality analysis of tear film characteristics (Shapiro-Wilk test)

Parameter	Condition	Shapiro-Wilk W	p-value
LLT (nm)	Before Drop	0.86	**0.002**
	5 Mins After Drop	0.90	**0.013**
	20 Mins After Drop	0.82	**<0.001**
NITBUT (sec)			
First Measurement	Before Drop	0.94	0.139
	5 Mins After Drop	0.95	0.183
	20 Mins After Drop	0.94	0.134
Average Measurement	Before Drop	0.93	0.058
	5 Mins After Drop	0.96	0.319
	20 Mins After Drop	0.94	0.136
RTC (°C/sec)	Before Drop	0.89	**0.01**
	5 Mins After Drop	0.87	**0.003**
	20 Mins After Drop	0.88	**0.004**
TER (g/m²/hr)	Before Drop	0.88	**0.004**
	5 Mins After Drop	0.96	0.347
	20 Mins After Drop	0.99	0.973

4.5.3.4 Comparative Analysis of Tear Film Characteristics Before and After Lipid Drop Instillation

Following normality analysis using the Shapiro-Wilk test, appropriate statistical methods were selected. Due to non-normal distributions for LLT, RTC, and TER (before drop), the non-parametric Friedman test was used for these variables. For NITBUT (both first and average measurements), which showed normal distributions across all time points, Repeated-Measures ANOVA was performed. Pairwise comparisons following significant overall results were corrected for multiple comparisons using Bonferroni adjustment.

The summary of these statistical analyses, including test statistics and p-values, is presented in Table 4-35.

Table 4-35: Summary table of inferential statistical analysis

Parameter	Statistical Test	Test Statistic	p-value	Post-hoc Comparisons (Bonferroni-adjusted)
LLT (nm)	Friedman	13.0	**0.002**	Significant differences: "Before vs. 5 mins" (p = 0.003), "Before vs. 20 mins" (p = 0.012). No difference "5 mins vs. 20 mins" (p = 0.975).
NITBUT (sec)				
First Measurement	Repeated-Measures ANOVA	4.16	**0.021**	No significant pairwise differences after Bonferroni correction (all p > 0.05).
Average Measurement	Repeated-Measures ANOVA	3.39	**0.041**	No significant pairwise differences after Bonferroni correction (all p > 0.05).
RTC (°C/sec)	Friedman	0.0	1.0	No significant differences (all p > 0.05).
TER (g/m²/hr)	Friedman	18.67	**<0.001**	Significant differences: "Before vs. 5 mins" (p < 0.001), "Before vs. 20 mins" (p = 0.007). No difference "5 mins vs. 20 mins" (p = 0.939).

Each tear film parameter that demonstrated a statistically significant difference across time points is examined in detail in the sections below. These analyses include post-hoc comparisons with Bonferroni correction to identify specific time intervals where meaningful changes occurred following lipid drop instillation.

4.5.3.4.1 LLT

After establishing a significant difference in LLT across the three time points (Before Drop, 5 minutes after drop, and 20 minutes after drop) using the Friedman test ($p = 0.002$), a post-hoc analysis was conducted using the Wilcoxon signed-rank test with a Bonferroni correction to identify specific pairwise differences between these measurements. Table 4-36 presents the results of the post-hoc Wilcoxon signed-rank tests conducted to compare LLT measurements across the three time points. These comparisons were used to identify where significant changes in LLT occurred following drop instillation.

Table 4-36: Results of the post-hoc analysis comparing LLT measurements across three different time points

Comparison	**Wilcoxon Statistic**	**p-value**	**Bonferroni-adjusted significance (α=0.0167)**
LLT (before) vs LLT (after 5 mins)	15	**<0.001**	**Significant**
LLT (before) vs LLT (after 20 mins)	45.5	**0.002**	**Significant**
LLT (after 5 mins) vs LLT (after 20 mins)	116.5	0.513	Not significant

The LLT measurements showed a significant increase immediately after the drop ($p < 0.001$), and this increase remained significant even after 20 minutes ($p = 0.002$). However, no significant difference was observed between 5- and 20-minutes post-drop, indicating that LLT stabilized after

the initial increase. It should be noted that the LipiView II interferometer has an upper measurement ceiling of 100 nm, beyond which LLT values cannot be quantified, potentially leading to an underestimation of post-instillation increases in LLT. Figure 4-28 visually illustrates the distribution of LLT measurements at baseline, 5 minutes, and 20 minutes post-instillation. The boxplot highlights median values and interquartile ranges, allowing for a clear comparison of LLT changes over time.

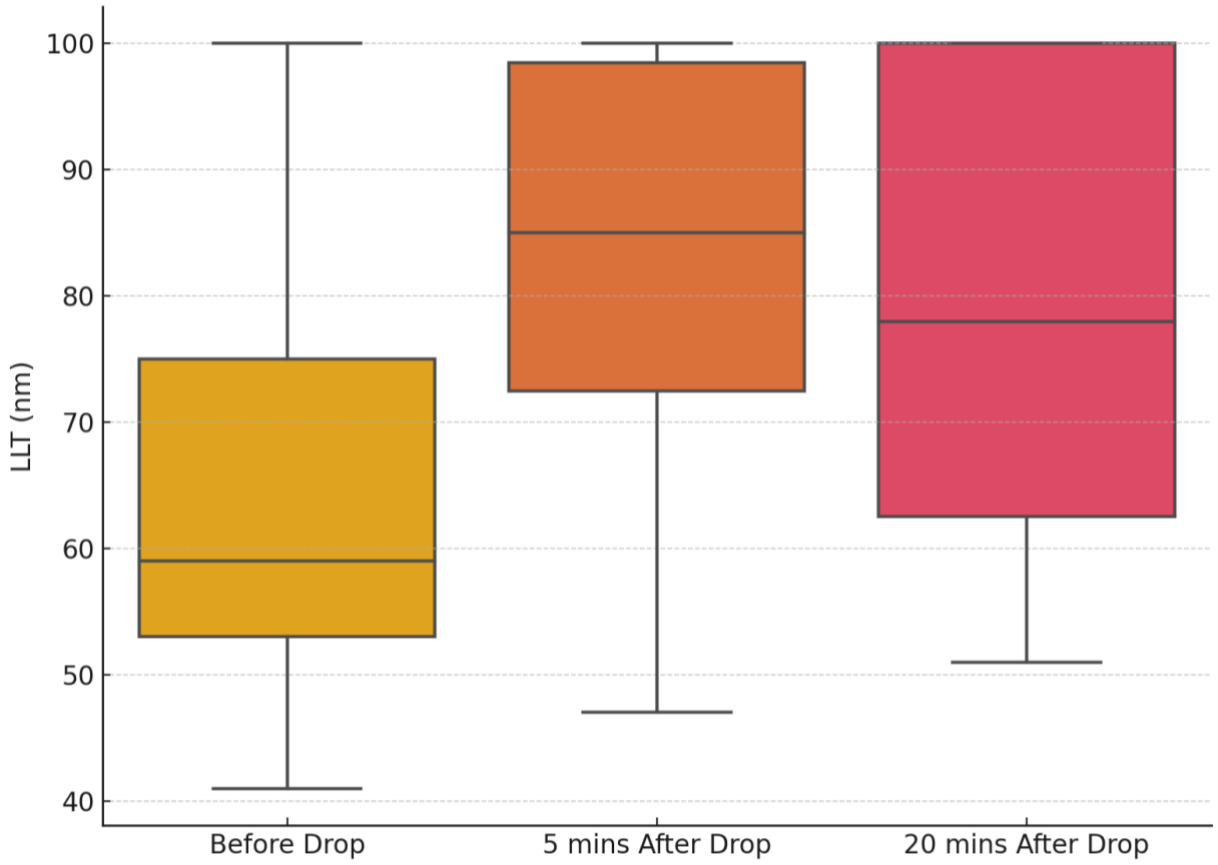


Figure 4-28: LLT before, 5 min after, and 20 min after drop (n = 27), shown as median and IQR. LLT increased significantly from baseline to 5 min ($p < 0.001$) and remained significantly elevated at 20 min ($p = 0.002$). No significant difference was found between 5 and 20 min ($p = 0.513$).

4.5.3.4.2 NITBUT

After establishing a significant difference in NITBUT measurements (First and Average) across the three time points (Before Drop, 5 minutes after drop, and 20 minutes after drop) using the repeated-measures ANOVA (NITBUT First: $p = 0.021$; NITBUT Average: $p = 0.041$), post-hoc analyses were conducted using paired t-tests with a Bonferroni correction to identify specific pairwise differences between these measurements. Table 4-37 presents the results of post-hoc paired t-tests conducted to compare NITBUT First and Average measurements across the three time points. These comparisons were used to identify specific intervals where significant changes in tear film stability occurred following lipid drop instillation.

Table 4-37: Results of the post-hoc analysis comparing NITBUT measurements across three different time points

Measurement Type	**Comparison**	**t-Statistic**	**p-value**	**Bonferroni-adjusted significance (α=0.0167)**
NITBUT First	Before vs After 5min	1.28	0.214	Not significant
	Before vs After 20min	3.04	**0.005**	**Significant**
	After 5min vs After 20min	1.58	0.127	Not significant
NITBUT Average	Before vs After 5min	1.08	0.29	Not significant
	Before vs After 20min	2.96	**0.007**	**Significant**
	After 5min vs After 20min	1.43	0.166	Not significant

The NITBUT First Measurement showed a significant decrease only at 20 minutes post-drop compared to before the drop ($p = 0.005$), indicating a delayed yet significant effect of the drop. No significant differences were observed between before and 5 minutes after the drop ($p = 0.214$), or

between 5 and 20 minutes after the drop (p = 0.127). Figure 4-29 and Figure 4-30 illustrate the changes in NITBUT First and Average measurements, respectively, across baseline, 5 minutes, and 20 minutes post-drop. The bar plots display mean values and standard deviations, providing a visual summary of the observed temporal trends in tear film break-up time.

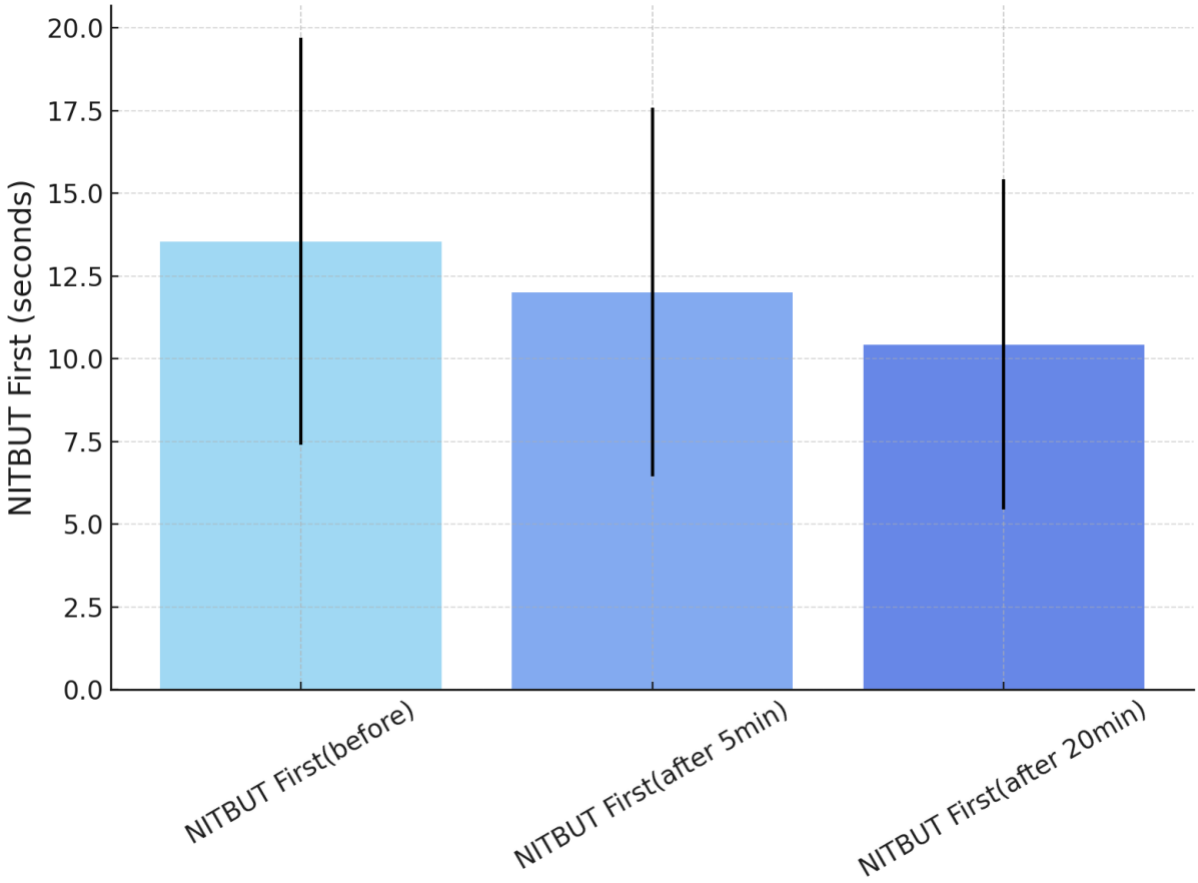


Figure 4-29: NITBUT (first) before, 5 min after, and 20 min after drop (n = 27), shown as mean ± SD. A statistically significant reduction was observed from baseline to 20 min (p = 0.005). Changes between baseline and 5 min (p = 0.214) and between 5 and 20 min (p = 0.127) were not significant.

Similarly, for NITBUT Average Measurement, a significant increase was observed only between before and 20 minutes after the drop (p = 0.007). Comparisons between before and 5 minutes (p = 0.290) and between 5 and 20 minutes (p = 0.166) after the drop were not significant. These results

consistently indicate a significant delayed improvement in NITBUT measurements occurring by 20 minutes post-drop.

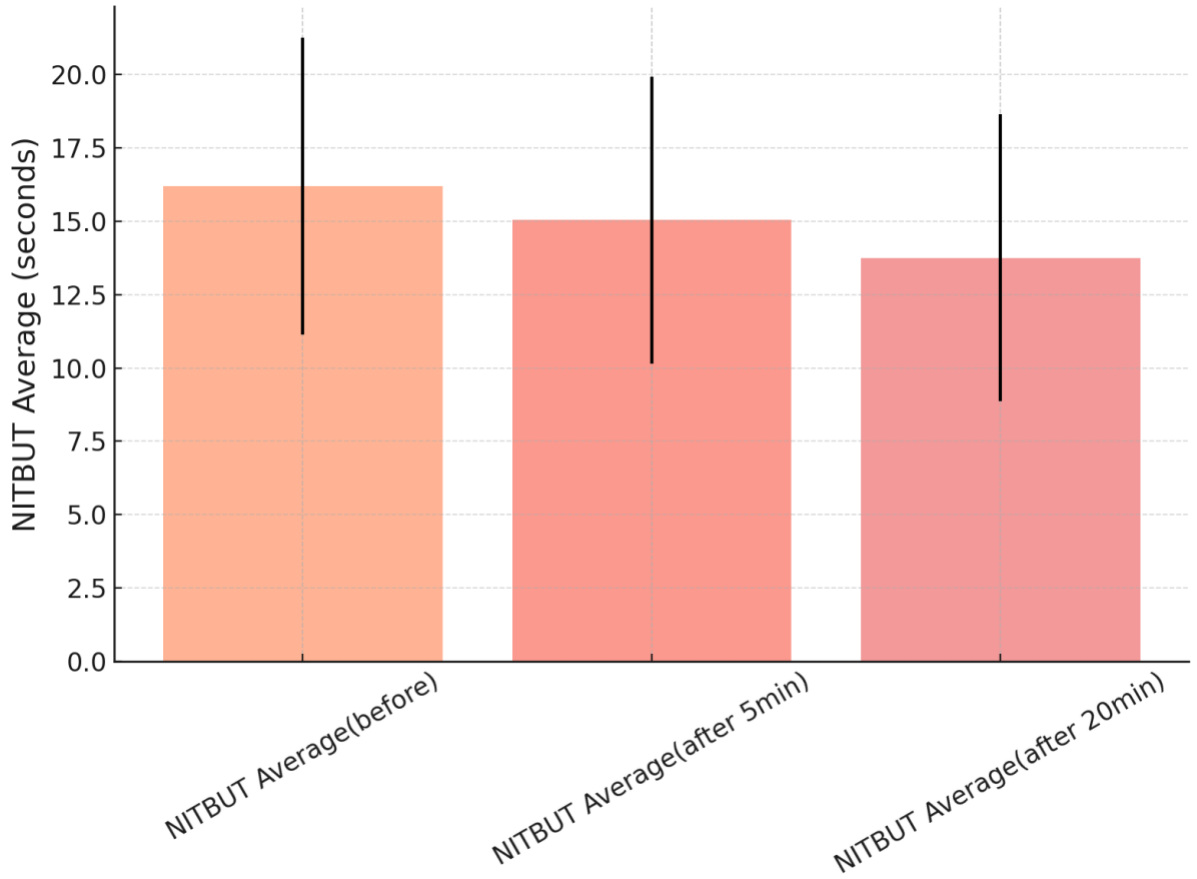


Figure 4-30: NITBUT (average) before, 5 min after, and 20 min after drop (n = 27), shown as mean ± SD. A statistically significant reduction occurred from baseline to 20 min (p = 0.007). No significant difference was found between baseline and 5 min (p = 0.290) or between 5 and 20 min (p = 0.166).

4.5.3.4.3 TER

After establishing a significant difference in TER across the three time points (Before Drop, 5 minutes after drop, and 20 minutes after drop) using a non-parametric Friedman test, a post-hoc analysis was conducted using Wilcoxon signed-rank test with Bonferroni correction to identify specific pairwise differences between these measurements. Table 4-38 summarizes the results of

the post-hoc Wilcoxon signed-rank test with Bonferroni correction used to compare TER measurements across the three time points. These comparisons were conducted to determine when significant changes in TER occurred following lipid drop instillation.

Table 4-38: Results of the post-hoc analysis comparing TER measurements across three different time points.

Comparison	**Wilcoxon Statistic**	**p-value**	**Bonferroni-adjusted significance (α = 0.0167)**
TER (before) vs TER (after 5 mins)	27.0	**<0.001**	**Significant**
TER (before) vs TER (after 20 mins)	65.5	**0.007**	**Significant**
TER (after 5 mins) vs TER (after 20 mins)	180.0	0.939	Not significant

The TER measurements showed a significant increase immediately after the drop ($p = <0.001$), and this increase remained significant even after 20 minutes ($p = 0.007$). However, no significant difference was observed between 5- and 20-minutes post-drop ($p = 0.939$), indicating that TER stabilized after the initial increase. Figure 4-31 provides a visual representation of TER measurements at baseline, 5 minutes, and 20 minutes post-drop. The bar plot displays the mean and standard deviation at each time point, illustrating the pattern and stability of TER changes over time.

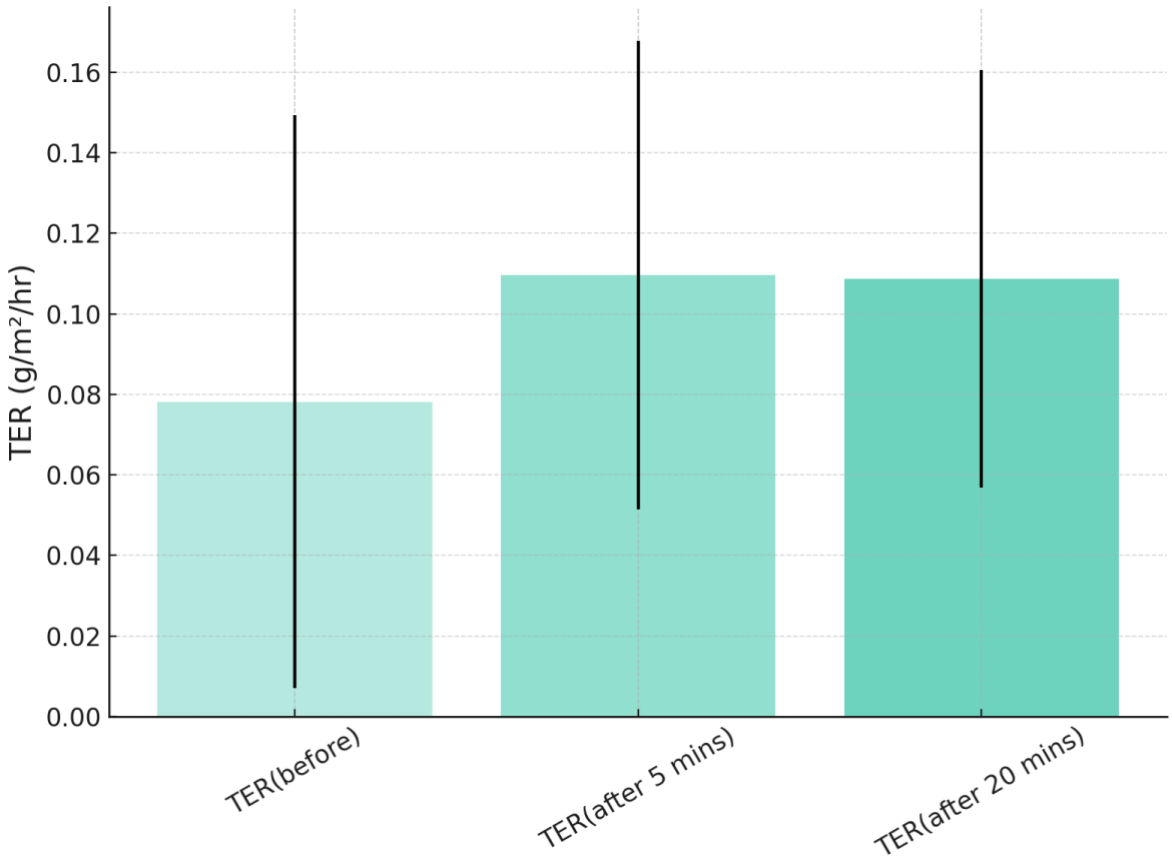


Figure 4-31: TER before, 5 min after, and 20 min after drop (n = 27), shown as mean ± SD. TER increased significantly from baseline to 5 min ($p < 0.001$) and from baseline to 20 min ($p = 0.007$). No significant difference was found between 5 and 20 min ($p = 0.939$).

4.5.3.5 Correlation Analysis of Tear Film Parameter Changes

To examine the evolving relationships between LLT, NITBUT, and TER, Pearson correlation analyses were performed at two time points following lipid eye drop instillation: 5 minutes and 20 minutes. The goal was to explore how these tear film parameters interact over time post-instillation. Due to multiple comparisons, a Bonferroni correction was applied, adjusting the significance threshold to $\alpha = 0.0083$ (0.05/6).

The results are summarized in Tables 4-39 and 4-40.

Table 4-39: Correlation analysis of changes (5 minutes post-instillation)

Variables Compared	Correlation Coefficient (*r*)	p-value	Significance (Bonferroni-adjusted α = 0.0083)
LLT Change ↔ NITBUT First Change	0.17	0.391	Not Significant
LLT Change ↔ NITBUT Average Change	0.15	0.466	Not Significant
LLT Change ↔ TER Change	0.03	0.875	Not Significant
NITBUT First Change ↔ NITBUT Average Change	0.94	**<0.001**	**Significant**
NITBUT First Change ↔ TER Change	-0.50	**0.0082**	**Significant**
NITBUT Average Change ↔ TER Change	-0.36	**0.062**	Not Significant

Table 4-40: Correlation analysis of changes (20 minutes post-instillation)

Variables Compared	Correlation Coefficient (*r*)	p-value	Significance (Bonferroni-adjusted α = 0.0083)
LLT Change ↔ NITBUT First Change	0.37	0.061	Not Significant
LLT Change ↔ NITBUT Average Change	0.33	0.097	Not Significant
LLT Change ↔ TER Change	-0.03	0.87	Not Significant
NITBUT First Change ↔ NITBUT Average Change	0.86	**<0.001**	**Significant**
NITBUT First Change ↔ TER Change	-0.17	0.397	Not Significant
NITBUT Average Change ↔ TER Change	-0.12	0.557	Not Significant

The correlation analysis revealed several key findings:

At 5 minutes post-instillation:

- No significant correlation was found between LLT and NITBUT or TER changes.
- A strong positive correlation was observed between NITBUT First and Average Measurements ($r = 0.94$, $p < 0.001$), indicating high internal consistency in tear film stability measures.
- A moderate negative correlation was found between NITBUT First and TER ($r = -0.50$, $p = 0.0082$), suggesting that increased tear stability may be associated with reduced tear evaporation shortly after lipid drop instillation.

At 20 minutes post-instillation:

- No significant correlation was found between LLT and NITBUT or TER.
- A strong correlation remained between NITBUT First and Average Measurements ($r = 0.86$, $p < 0.001$), further reinforcing the reliability of NITBUT as a stability metric.
- Weak correlations were observed between NITBUT and TER changes, but these were not statistically significant (e.g., NITBUT First ↔ TER: $r = -0.17$, $p = 0.397$), indicating that the relationship between tear stability and evaporation may diminish over time or be influenced by other factors.

To illustrate these findings, the Figures below (Figure 4-32 and 4-33) present pairwise scatter plots with trend lines, visually representing the relationships between LLT, NITBUT, and TER changes at both 5 minutes and 20 minutes following lipid drop instillation.

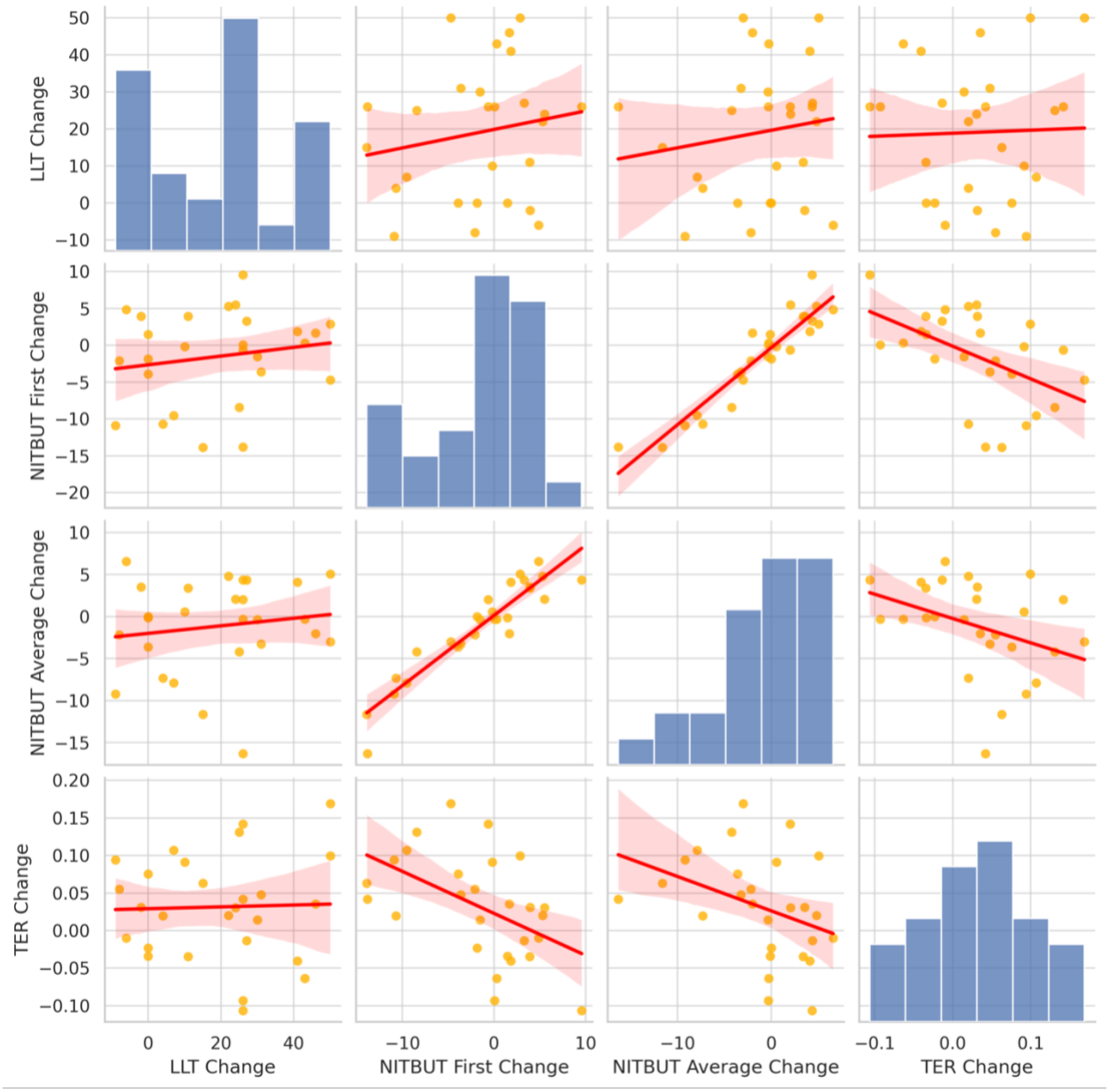


Figure 4-32: Pairwise scatter plots with regression lines showing relationships among changes in LLT, NITBUT (first and average), and TER at 5 min after drop instillation (n = 27). Shaded areas represent 95% confidence intervals. A strong correlation was found between NITBUT first and average change ($r = 0.94$, $p < 0.001$). NITBUT first changes was significantly and negatively correlated with TER change ($r = –0.50$, $p = 0.0082$).

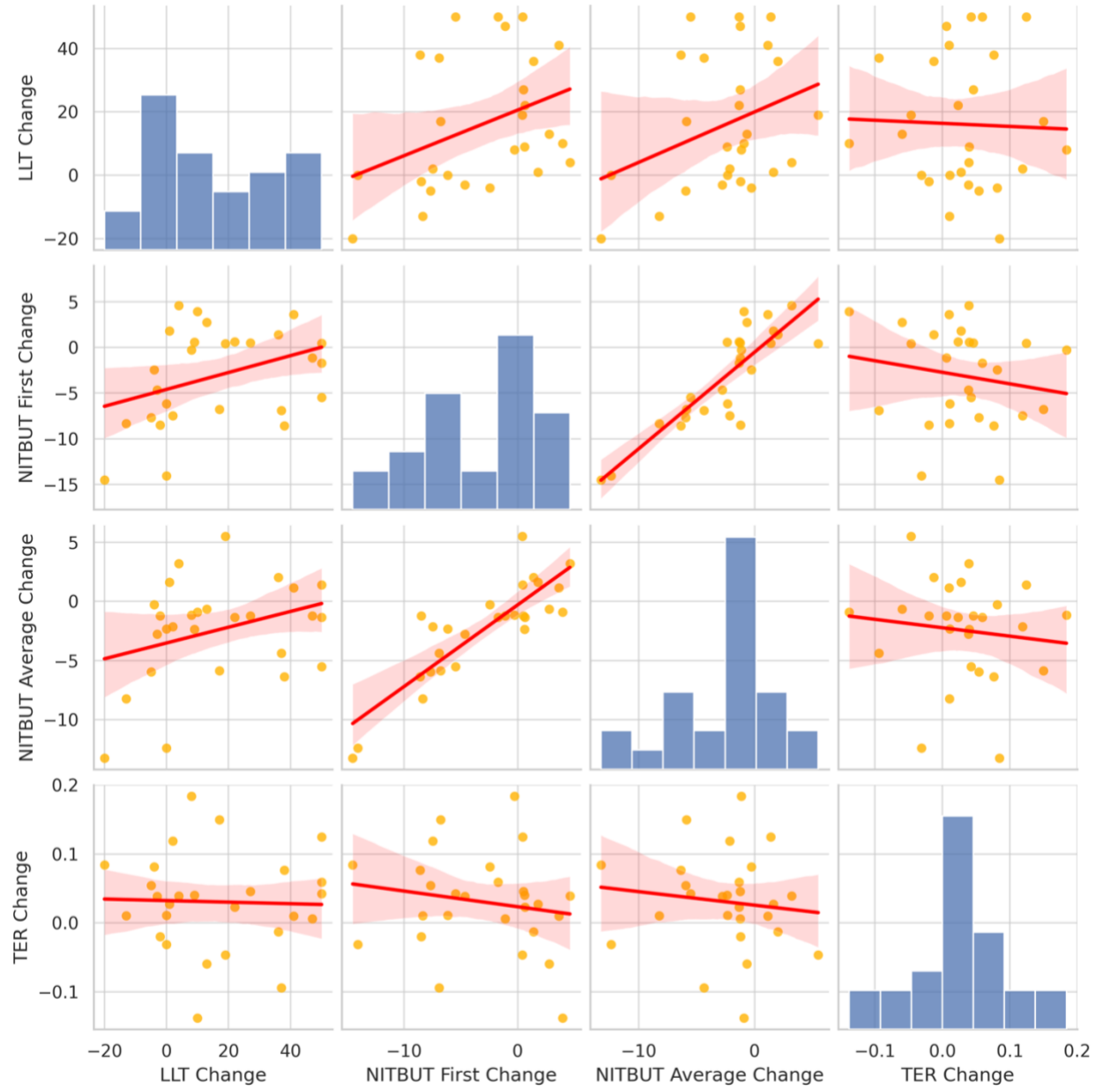


Figure 4-33: Pairwise scatter plots with regression lines and 95% confidence intervals showing relationships among changes in LLT, NITBUT (first and average), and TER at 20 min after drop instillation (n = 27). A strong correlation was observed between NITBUT first and average change ($r = 0.86$, $p < 0.001$). Other relationships, including those between LLT and NITBUT or TER, and between NITBUT and TER, were not statistically significant.

4.5.4 Spatial Variation in OST and Impact of ROI Size

To gain further insight into ocular surface thermodynamics, additional analyses were performed on the OST data. These extended investigations aimed to assess spatial variations in OST across different corneal regions and to evaluate how the size of the measurement ROI influenced OST readings. Although regional differences (superior vs. inferior) had been previously established, the primary objective here was to closely examine how OST changes over time in these regions by dividing the interblink interval into smaller segments. Additionally, the influence of different ROI sizes was evaluated to determine their impact on measurement stability and sensitivity. Specifically, larger ROIs could potentially provide more stable and reliable OST measurements by averaging out random temperature fluctuations, whereas smaller ROIs might capture subtle local variations more sensitively but with increased variability. This analysis aimed to identify the optimal ROI size that balances spatial sensitivity with measurement reliability, thus enhancing future OST-based assessments of tear film stability.

4.5.4.1 OST Variability Across Different ROI Sizes

To examine the effect of ROI size on OST dynamics, RTC was computed across six concentric ROIs (1, 9, 52, 104, 208, and 516 pixels) for each participant. A visual representation of ROI distribution is shown in Figure 4-34. These ROIs reflect progressively larger areas used to average temperature data and were chosen to evaluate whether RTC is sensitive to the spatial scale of measurement.

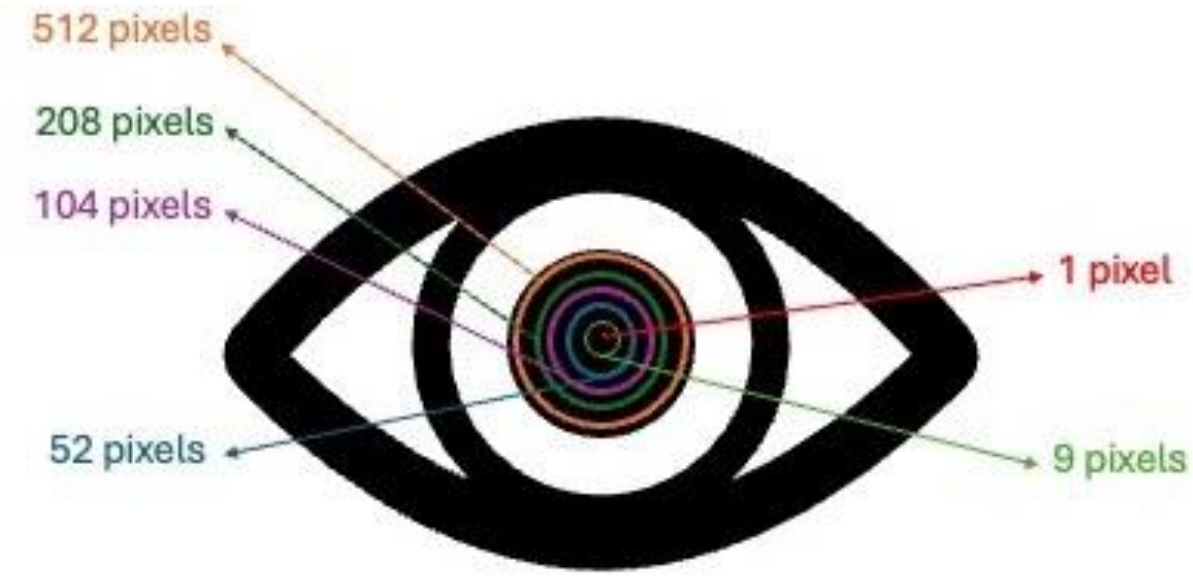


Figure 4-34: Concentric ROIs used for measuring RTC. Each ring represents a different ROI size, ranging from 1 pixel to 516 pixels.

Descriptive statistics for each ROI size are presented in Table 4-41. The mean RTC values were relatively consistent across all ROIs, ranging from –0.036 °C/sec (1 pixel) to –0.038 °C/sec (516 pixels). Median values showed a similar pattern, and standard deviations remained stable across ROI sizes. This suggested minimal influence of ROI size on average RTC outcomes.

Table 4-41: RTC descriptive statistics across ROI sizes.

ROI Size	Mean	SD	Min	25%	Median	75%	Max
1_pix	-0.036	0.029	-0.137	-0.040	-0.030	-0.021	-0.002
9_pixs	-0.037	0.027	-0.136	-0.039	-0.029	-0.021	-0.005
52_pixs	-0.037	0.028	-0.135	-0.040	-0.028	-0.021	-0.004
104_pixs	-0.037	0.028	-0.134	-0.040	-0.028	-0.022	-0.003
208_pixs	-0.038	0.028	-0.130	-0.041	-0.029	-0.023	-0.003
516_pixs	-0.038	0.027	-0.123	-0.045	-0.031	-0.022	-0.002

The RTC distribution across ROI sizes is further illustrated in Figure 4-35. The boxplot showed consistent medians and interquartile ranges across all six ROI conditions, with slightly more variability in the smaller ROIs. However, no clear trend or substantial shift in RTC values was observed with increasing ROI size.

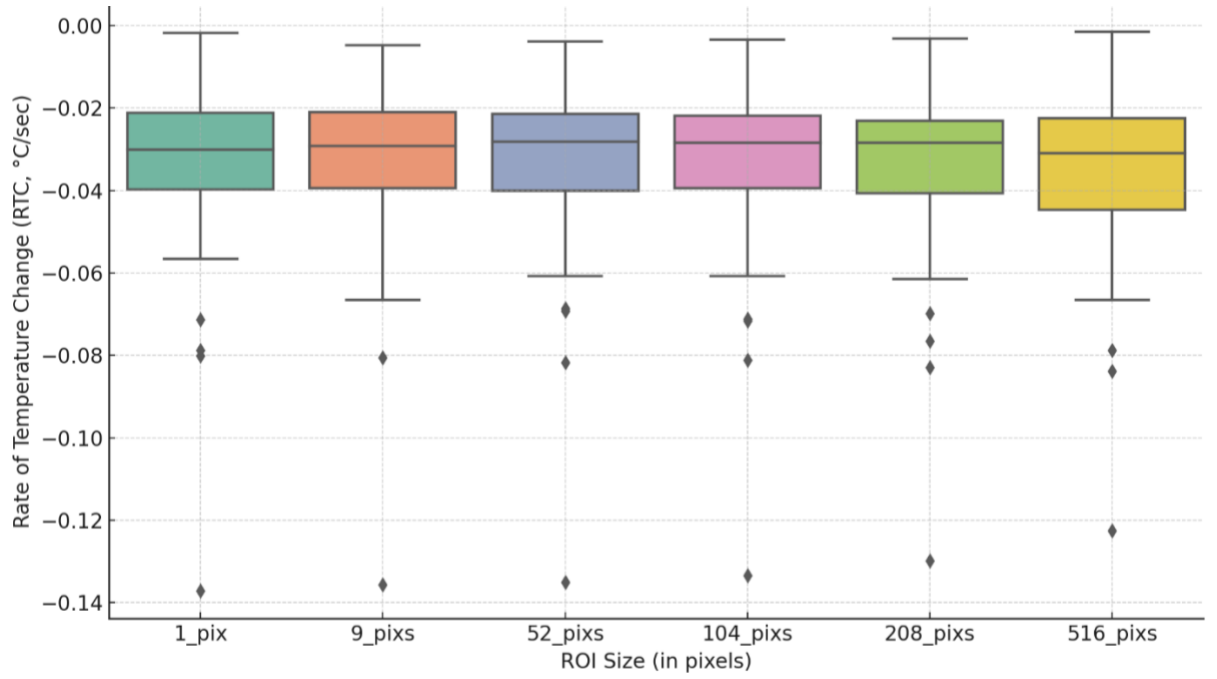


Figure 4-35: Boxplot illustrating RTC across six concentric ROI sizes (1, 9, 52, 104, 208, and 516 pixels), derived from OST measurements (n = 27). Median RTC values and interquartile ranges remained consistent across ROI sizes.

To statistically assess whether ROI size had a measurable effect on RTC, a Friedman test was conducted due to the non-normal distribution of RTC values (Shapiro-Wilk test $p < 0.01$ for all ROIs). The test revealed no significant differences across ROI sizes, χ^2 (5) = 4.53, p = 0.476, reinforcing the conclusion that ROI size does not meaningfully influence RTC under the conditions tested.

A linear mixed-effects model (LMM) was also explored to account for participant-level variability. The LMM results were consistent with the non-parametric findings, indicating no significant fixed effect of ROI size (β = –0.000, p = 0.145). The LMM is reported for completeness but is not emphasized due to added complexity and non-normal residual structure in some conditions.

4.5.4.2 OST Variation Across Different Corneal Locations

Having established in the previous section that ROI size did not significantly influence RTC outcomes, a standardized of 25 pixels square ROI (5×5 pixels) was selected for further spatial analysis. This size was selected as it offers a practical compromise: it is small enough to capture region-specific variations in OST without overlapping anatomical zones, yet large enough to minimize noise and improve the temporal stability of RTC measurements. Using this fixed ROI, RTC was assessed across five distinct corneal regions to evaluate spatial variations in tear film cooling.

As illustrated in Figure 4-36, the five measurement locations included the central cornea (Center), two superior regions (S1 and S2), and two inferior regions (I1 and I2). All ROIs were vertically aligned along the central corneal axis, forming a straight line from superior to inferior positions. Each location was separated by two 5 × 5-pixel blocks using a standardized grid template, ensuring uniform spacing and consistent placement across participants.

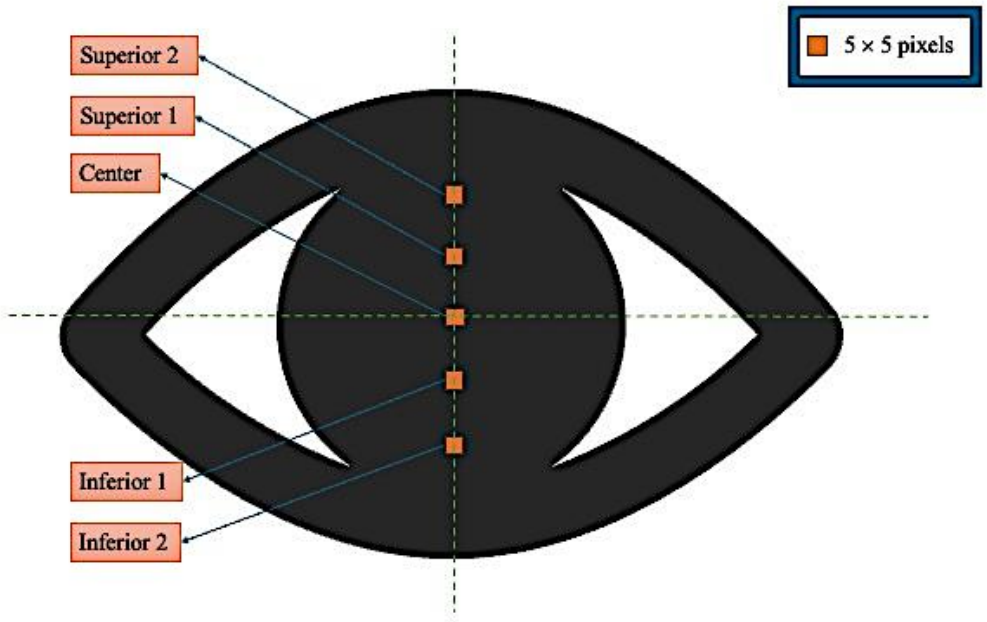


Figure 4-36: Schematic of vertically aligned 5×5-pixel ROIs used to measure RTC.

Descriptive statistics for each vertical ROI location are presented in Table 4-42. While mean RTC values were generally consistent across the five ROIs, a slight trend was observed, with the inferior region I1 showing the most pronounced cooling (–0.039 °C/sec) and I2 showing the least (–0.027 °C/sec). The center and superior regions (S1 and S2) fell between these two extremes, ranging from –0.030 to –0.034 °C/sec. Median values followed a similar pattern, and standard deviations remained comparable across all positions (0.028 to 0.044). Overall, this indicates a minor increase in cooling at the lower corneal positions, though the variation was not statistically significant under controlled blink conditions.

Table 4-42: Descriptive statistics for the RTC across five vertically aligned ocular surface ROIs.

Location	Mean	SD	Min	Q1	Median	Q3	Max
S2	-0.034	0.044	-0.172	-0.058	-0.033	-0.002	0.049
S1	-0.034	0.044	-0.161	-0.055	-0.024	-0.007	0.027
Center	-0.03	0.028	-0.084	-0.041	-0.027	-0.016	0.032
I1	-0.039	0.038	-0.168	-0.042	-0.03	-0.021	0.013
I2	-0.027	0.04	-0.113	-0.041	-0.02	-0.008	0.069

The distribution of RTC values across the five vertical ROIs is illustrated in Figure 4-37. The boxplot highlights the consistency in median RTC and interquartile ranges across all regions, with slightly wider spread observed in the superior and inferior areas. Notably, although I2 demonstrated the lowest mean RTC, the overall variability remained similar between regions, reinforcing the observation that vertical position exerts only a subtle effect on ocular surface cooling.

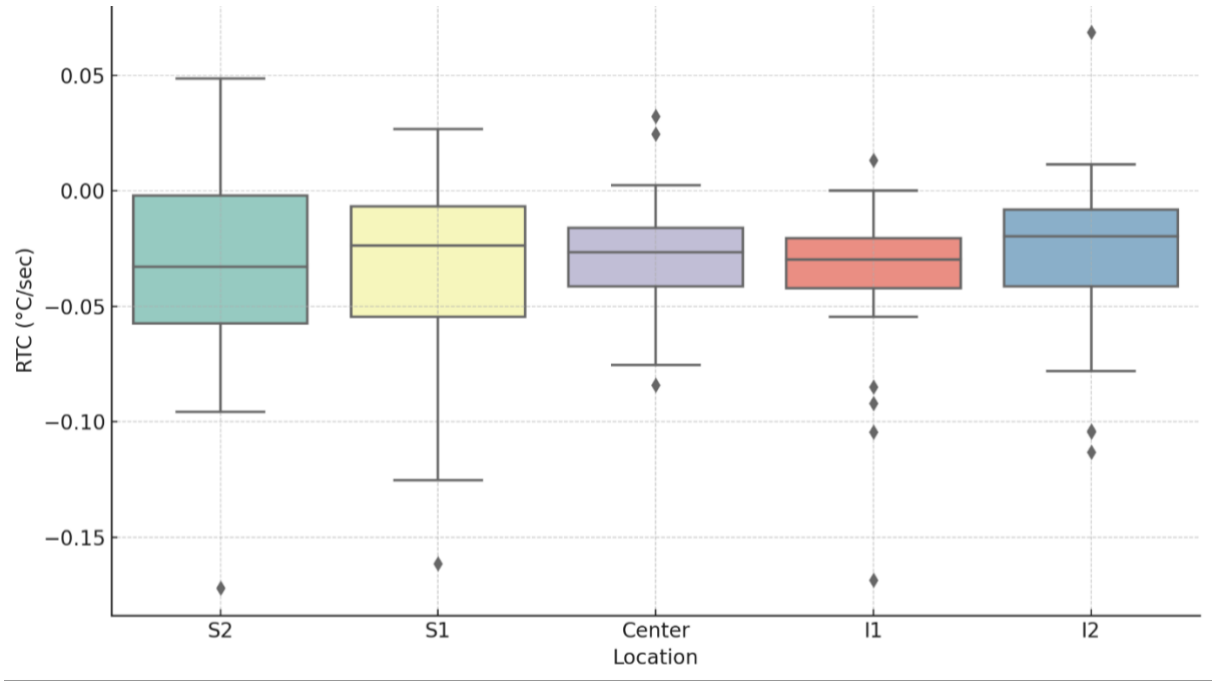


Figure 4-37: Boxplot illustrating RTC distribution across vertical corneal locations (S2, S1, Center, I1, and I2), derived from OST measurements (n = 27). Median RTC values and interquartile ranges remained consistent across vertical corneal locations, with slightly greater variability observed in superior regions.

To determine whether RTC varied significantly across vertical ocular surface ROIs, normality of the data distribution was first assessed using the Shapiro-Wilk test. Results indicated that RTC values for several ROIs (S1, I1, and I2) significantly deviated from a normal distribution ($p < 0.05$), thereby violating the assumptions required for parametric tests such as ANOVA. Consequently, a Friedman test (non-parametric alternative suitable for repeated measures) was performed to compare RTC across the five vertically aligned ROIs (S2, S1, Center, I1, I2). The test revealed no statistically significant differences between locations, χ^2 (4) = 2.75, p = 0.600, suggesting that the rate of ocular surface cooling remained consistent across superior, central, and inferior regions during the 6-second IBI. Although the overall Friedman test was not significant, pairwise Wilcoxon signed-rank tests were conducted to explore potential localized differences and

support interpretation of visual trends across the five vertically aligned ROIs. These post-hoc comparisons revealed that none of the pairwise differences reached statistical significance after correcting for multiple comparisons, with most p-values > 0.05. An exception was observed between S1 and I1 ($p = 0.046$), suggesting a borderline difference in RTC between these two ROIs; however, this result should be interpreted cautiously in the context of the non-significant global test and multiple comparisons. Collectively, these post-hoc results reinforce the conclusion that vertical ROI placement exerts minimal influence on RTC under the standardized measurement conditions used in this study. This interpretation is further supported by the correlation heatmap (Figure 4-38), which shows that, while adjacent regions tend to exhibit moderate to strong co-variation in RTC, distant ROIs demonstrate weaker relationships, underscoring localized, but non-directional thermal behavior. Detailed pairwise comparisons are presented in Table 4-43.

A LMM was also explored to account for inter-individual variability in RTC measurements across regions. Consistent with the non-parametric results, the LMM revealed no significant fixed effect of ROI location ($\beta = –0.0004$, $p = 0.172$). While reported here for completeness, the LMM is not emphasized due to the presence of residual non-normality in several conditions and the increased model complexity relative to the observed outcome patterns.

Table 4-43: Pairwise Wilcoxon signed-rank tests comparing RTC across five vertically aligned ROIs.

ROI Pair	W-statistic	p-value
S2 vs S1	174	0.98
S2 vs Center	170	0.901
S2 vs I1	150	0.532
S2 vs I2	160	0.708
S1 vs Center	138	0.51
S1 vs I1	97	**0.046**
S1 vs I2	170	0.901
Center vs I1	100	0.056
Center vs I2	175	1
I1 vs I2	125.5	0.208

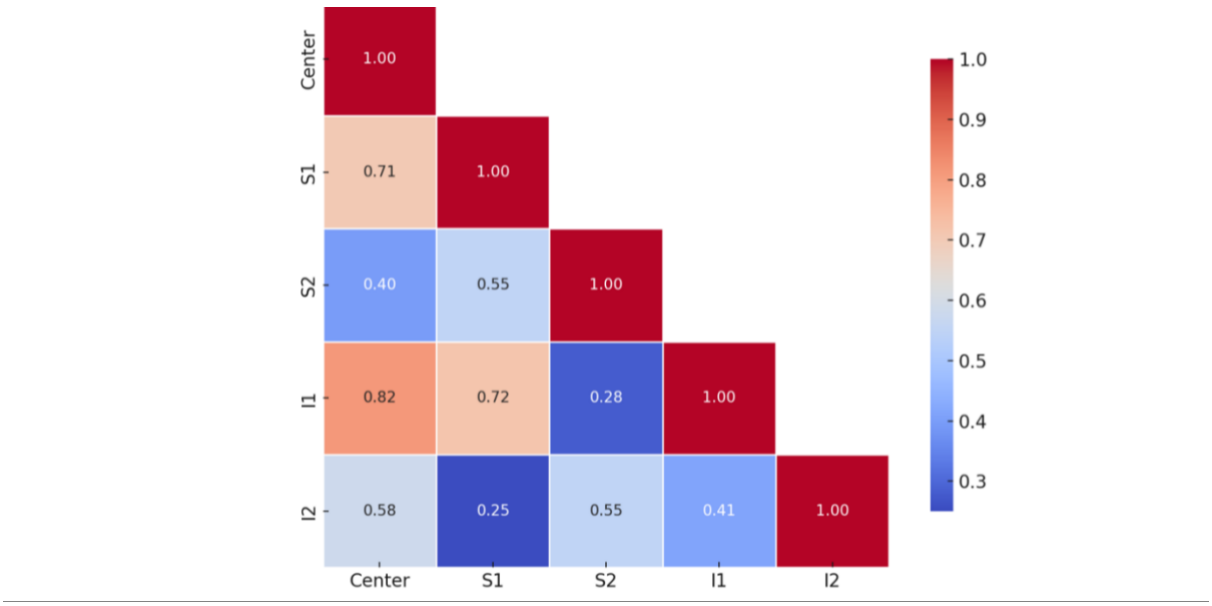


Figure 4-38: Correlation heatmap of RTC across five vertically aligned ocular surface ROIs (n = 27). Stronger correlations (shown in red) indicate more synchronized temperature changes between regions, while weaker correlations (blue) reflect greater regional thermal variability.

To further investigate the potential gradient of RTC values across vertical corneal locations (from superior to inferior), a linear regression analysis was performed (Figure 4-39). The analysis tested the slope of RTC against zero across the five vertically aligned corneal regions. The regression revealed no statistically significant linear gradient (slope = 0.001, r = 0.36, p = 0.556). Thus, although a subtle visual trend suggesting slightly increased cooling towards inferior corneal regions was observed, the statistical analysis confirmed that this was not significant. This additional analysis supports the conclusion of minimal spatial variation in RTC under these measurement conditions.

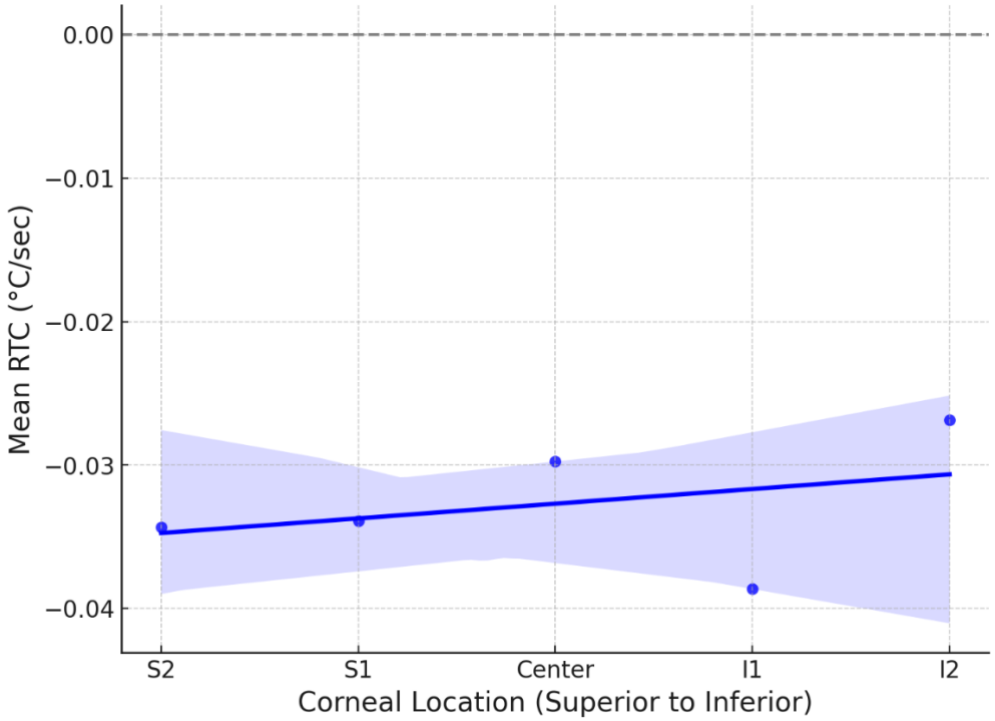


Figure 4-39: Linear regression analysis of mean RTC values across five vertically aligned corneal locations (from superior to inferior: S2, S1, Center, I1, I2). The regression revealed no statistically significant linear gradient (slope = 0.001, r = 0.36, p = 0.556), indicating minimal spatial variation in RTC under the current measurement conditions. Shaded areas represent the 95% confidence interval of the regression line.

4.5.4.3 Temporal RTC Dynamics Across Vertical Corneal Locations

To further explore the dynamics of ocular surface cooling, the 6-second IBI was divided into six one-second intervals to examine how RTC evolved across time and location. This approach allowed for the detection of transient versus stabilized thermal responses that may otherwise be masked in cumulative 6-second RTC averages. A fixed ROI size of 25 pixels was used, and RTC was measured for each second across five vertically aligned ocular surface regions (S2, S1, Center, I1, I2). These vertically stacked ROIs were selected to capture subtle anatomical influences on OST behavior. The primary goal of this temporal decomposition was to determine whether differences between regions were evident at specific moments, such as immediately following a blink, and to evaluate whether RTC stabilization occurs uniformly across the ocular surface.

Figure 4-40 illustrates the RTC trend across all locations during the six-seconds post-blink. A consistent cooling pattern was observed across all ROIs, with the most substantial OST drop occurring in the first second. Subsequent IBIs showed a progressive stabilization in RTC, particularly in the superior and central corneal regions. The inferior corneal region (I2), however, demonstrated a prolonged thermal response with less rapid stabilization.

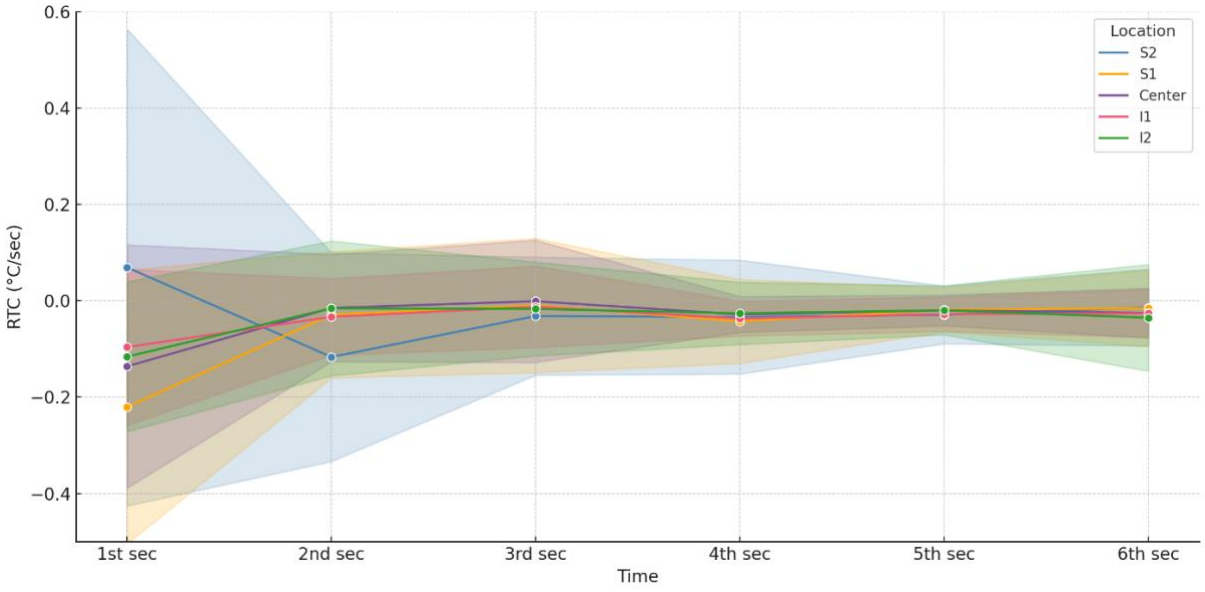


Figure 4-40: Interaction effect of time and location on RTC. Line plot of mean RTC across 6 seconds at each vertical ROI (n = 27). Error bars shown with shadings represent standard deviation.

To assess statistical differences across time within each ROI, normality of the RTC distributions was first evaluated using the Shapiro-Wilk test. Several timepoints across all five ROIs significantly deviated from a normal distribution (e.g., $p < 0.05$ for S2 at 1st and 3rd seconds, and for S1 at 4th and 6th seconds), indicating that parametric tests were not appropriate. Consequently, a non-parametric Friedman test was employed to evaluate changes in RTC across the six one-second intervals for each region. The test revealed a statistically significant variation in RTC across time for S1 ($\chi^2 = 11.55$, $p = 0.041$) and a borderline effect for I2 ($\chi^2 = 10.74$, $p = 0.057$). No significant temporal variation was observed in S2, Center, or I1 (all $p > 0.1$), indicating greater stability across these regions. A summary of the Friedman test results is presented in Table 4-44.

Table 4-44: Friedman test results comparing RTC across 6-time intervals for each vertical ROI (25-pixel).

Location	χ^2	p-value
S2	4.55	0.474
S1	11.55	**0.041**
Center	8.81	0.117
I1	7.79	0.168
I2	10.74	0.057

Pairwise Wilcoxon signed-rank tests with Bonferroni correction were conducted to further explore the S1 findings. For S1, significant differences were observed between the 1st second and both the 3rd ($p = 0.002$) and 5th seconds ($p < 0.001$). These results indicate that the superior S1 region exhibited notable cooling dynamics immediately following eye opening, stabilizing significantly by the 3rd and 5th seconds post-blink. No other pairwise comparisons in the S1 region reached statistical significance after correction. These corrected pairwise comparison results for the S1 region are summarized in Table 4-45.

Table 4-45: Statistically significant pairwise Wilcoxon signed-rank test with Bonferroni correction comparisons of RTC across six one-second intervals at the S1 corneal region. Only comparisons with p-values less than 0.05 are shown.

Region	Time Point Comparison	Wilcoxon Statistic	p-value	Significant (Bonferroni $\alpha = 0.0033$)
S1	1 sec vs 2 sec	81.0	**0.008**	**No**
	1 sec vs 3 sec	66.0	**0.002**	Yes
	1 sec vs 4 sec	88.0	**0.014**	**No**
	1 sec vs 5 sec	51.0	**0.001**	Yes
	1 sec vs 6 sec	80.0	**0.008**	Yes

This analysis confirmed that ocular surface cooling was most pronounced immediately after eye opening, with superior and central regions reaching thermal stabilization more quickly. Pairwise analyses specifically identified significant cooling differences within the superior S1 region, particularly between the first second and both the third- and fifth-seconds post-blink ($p \leq 0.002$ after Bonferroni correction). These results highlight the rapid stabilization of cooling in this superior corneal region within the first few seconds. Although the inferior cornea demonstrated a visually evident prolonged cooling trend, statistical analyses did not confirm significant temporal differences in RTC for inferior regions after correcting for multiplicity.

To complement the non-parametric results, a linear mixed-effects model (LMM) was also applied, examining the effects of location and time on RTC while accounting for participant-level variability. The LMM revealed a significant main effect of time, confirming that RTC values differed significantly between the 1st second and all subsequent seconds (2nd to 6th, all $p < 0.01$),

thus reinforcing the rapid initial cooling pattern observed post-blink. However, no location-specific differences reached statistical significance in the LMM (all $p > 0.05$).

Collectively, these findings underscore the importance of temporal factors in evaluating OST-based tear film dynamics, with a rapid initial cooling phase followed by relative stabilization across corneal regions.

4.5.4.4 Temporal RTC Dynamics Within the First Three Seconds

Given that the most pronounced RTC changes occurred during the first three seconds of the IBI, this segment was analyzed in greater temporal detail by dividing it into six consecutive 0.5-second intervals. RTC values were extracted at each interval for five vertically aligned 25-pixel ROIs (S2, S1, Center, I1, and I2) to evaluate short-term thermal dynamics across the ocular surface. This finer temporal resolution allowed for a more nuanced examination of the onset and stabilization of tear film-related temperature changes.

Figure 4-41 illustrates the RTC trends for each region across these 0.5-second windows. As expected, the first second exhibited steep drops in RTC for all ROIs, followed by partial recovery or fluctuation over the next 2 seconds. Superior regions (S2, S1) demonstrated a relatively quick stabilization in RTC, while inferior ROIs (I1, I2) exhibited more extended or erratic patterns of thermal change.

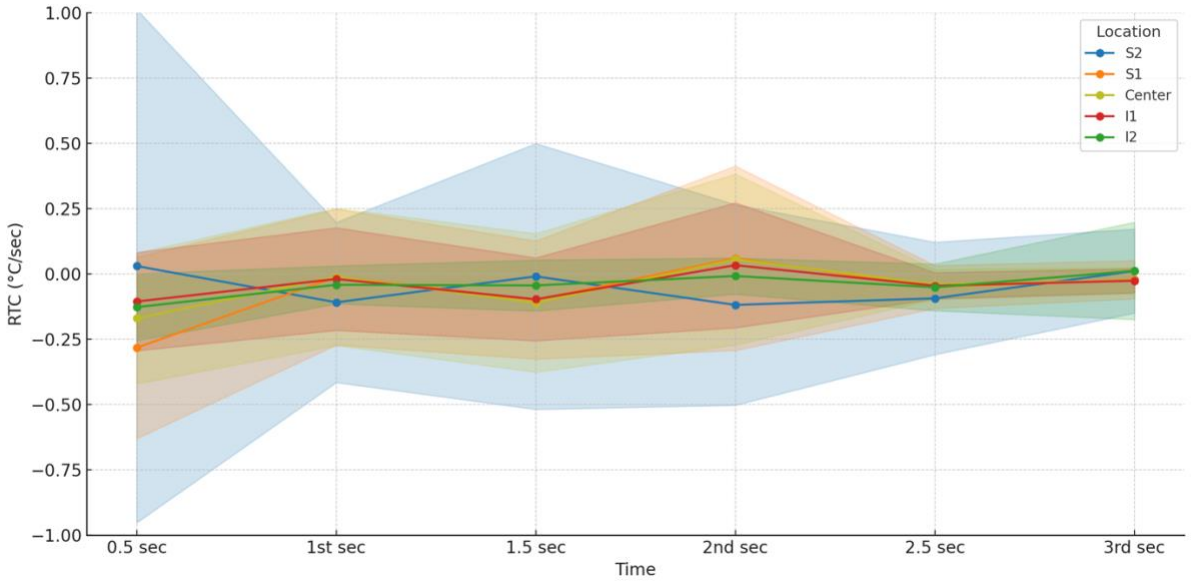


Figure 4-41: RTC across five corneal regions measured at six 0.5-second intervals. Values represent mean RTC (n = 27) from 0 to 3 seconds. Error bars shown with shadings represent standard deviation.

Shapiro-Wilk tests indicated significant non-normality at several intervals within all five ROIs, particularly in the early phase (e.g., $p < 0.01$ for Center intervals 1–4). Consequently, Friedman tests were used to evaluate temporal differences in RTC for each location. Results revealed significant variation across time for I2 ($\chi^2 = 26.64$, $p < 0.001$) and I1 ($\chi^2 = 15.29$, $p = 0.009$), with borderline trends in Center ($\chi^2 = 10.37$, $p = 0.065$) and S1 ($\chi^2 = 9.39$, $p = 0.095$). No significant temporal differences were observed in S2 ($\chi^2 = 4.50$, $p = 0.480$). These results are summarized in Table 4-46.

Table 4-46: Friedman test results comparing RTC across 0.5-second intervals at each ROI.

Location	χ^2	p-value
S2	4.50	0.48
S1	9.39	0.095
Center	10.37	0.065
I1	15.29	**0.009**
I2	26.64	**<0.001**

Pairwise Wilcoxon signed-rank tests were conducted to further explore the significant effects for I2 and I1. For I2, RTC at the first interval was significantly different from intervals 2, 3, 4, 5, and 6 (all $p < 0.02$), suggesting prolonged cooling dynamics in this region. Significant differences were also detected for I1 across several early intervals. All statistically significant pairwise comparisons are listed in Table 4-47.

Table 4-47: Statistically significant Wilcoxon signed-rank test comparisons across 0.5-second intervals at I1 and I2 ROI.

Region	Time Point Comparison	p-value
I1	0.5 sec vs 2.0 sec	**0.006**
	1.0 sec vs 2.0 sec	**0.018**
	1.5 sec vs 2.0 sec	**0.001**
	1.5 sec vs 3.0 sec	**0.010**
I2	0.5 sec vs 1.0 sec	**0.001**
	0.5 sec vs 1.5 sec	**0.007**
	0.5 sec vs 2.0 sec	**0.000**
	0.5 sec vs 2.5 sec	**0.018**
	0.5 sec vs 3.0 sec	**<0.001**

To complement the non-parametric results, a LMM was also employed. The model included Location and Interval as fixed effects and Patient ID as a random intercept to account for individual variability. The LMM revealed a significant main effect of Interval, with multiple timepoints showing significantly different RTC values compared to the reference interval (first 0.5 sec, all $p < 0.01$). No significant fixed effect was observed for Location, consistent with the non-parametric findings, although subtle variations in cooling trajectory were visually apparent across regions. These results further emphasize that RTC dynamics during the early post-blink phase are primarily driven by time.

Collectively, these findings reinforce the importance of high temporal resolution in evaluating tear film behavior and ocular surface thermodynamics. The inferior regions of the cornea appear to undergo more sustained thermal fluctuations, highlighting their relevance in early evaporative processes. These results suggest that the first few second post-blink provide critical insight into tear film cooling behavior, particularly in the inferior cornea.

To further contextualize the early-phase RTC patterns, the full 6-second IBI was plotted using combined data from both the 0.5-second and 1-second interval analyses. This extended visualization (Figure 4-42) highlights the transition from the initial rapid cooling phase (0.5–3 seconds) to a more gradual cooling trend (3–6 seconds). As shown in the plot, RTC values shift from strongly negative to near-zero or slightly positive in the early phase, particularly in superior regions, suggesting thermal stabilization or slight rebound. In the latter phase, RTC values return to a more consistently negative pattern, especially in inferior regions, reflecting the onset of evaporative cooling. This biphasic pattern reinforces the dynamic nature of OST immediately following eye opening and supports the value of high temporal resolution for capturing both short-term thermal stabilization and longer-term cooling processes across the ocular surface.

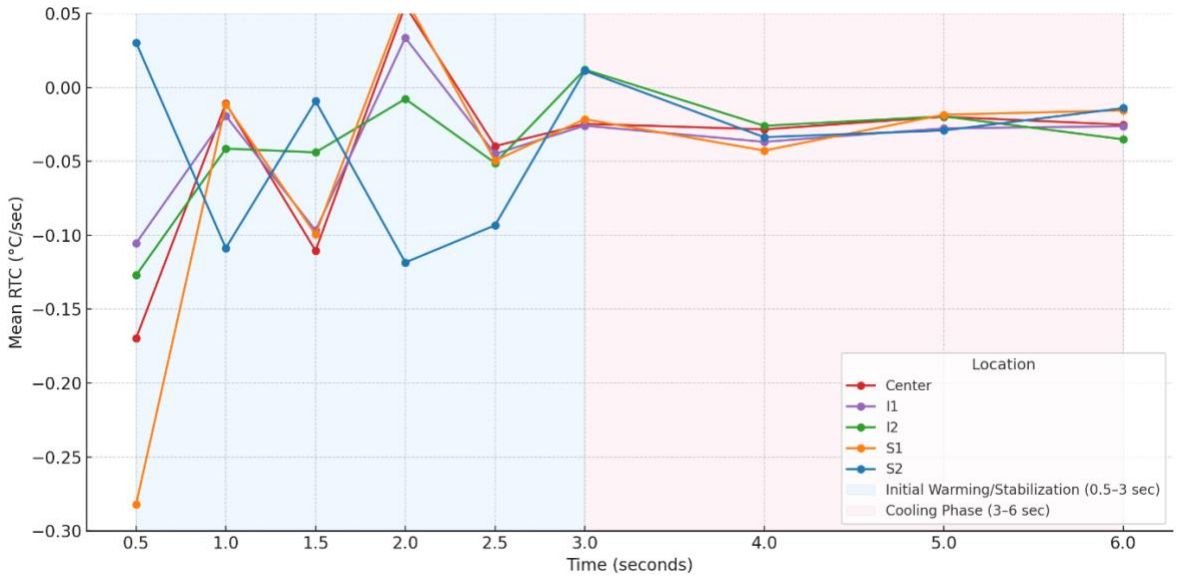


Figure 4-42: Mean RTC across five vertical corneal regions over a 6-second IBI, combining 0.5-sec and 1-sec interval data (n = 27). Shaded regions represent initial slope deceleration (blue) and evaporative cooling phase (pink).

4.5.5 Discussion

The Phase II study examined the impact of lipid-based eye drop instillation on multiple aspects of tear film behavior, including LLT, NITBUT, TER, and OST dynamics, measured via RTC. Together, these parameters offered a comprehensive view of tear film response over a 20-minute period following drop instillation.

The findings revealed that LLT significantly increased after lipid drop instillation and remained elevated at both 5 and 20 minutes, indicating a sustained enhancement of the tear film's lipid component. This aligns with previous reports demonstrating the ability of lipid-based artificial tears to thicken the lipid layer and improve barrier function.[236,256] However, despite this improvement, TER also increased significantly at both timepoints post-instillation. This unexpected finding may reflect an initial re-distribution effect or transient instability in the tear

film following lipid delivery. While LLT thickened, the functional barrier to evaporation may have required more time to equilibrate across the ocular surface.

NITBUT measurements exhibited a delayed response. Neither the First nor Average measurements showed significant improvement at 5 minutes. This pattern suggested that tear film stabilization, particularly in terms of its structural integrity and retention time, required a longer adaptation phase following drop administration. Notably, correlation analyses revealed strong internal consistency between NITBUT First and Average measurements, while moderate negative correlations between NITBUT and TER changes at 5 minutes suggested a possible short-term interplay between improved stability and reduced evaporation.[215]

Following this tear film assessment, the analysis was deepened using dynamic IR imaging of the ocular surface. The RTC measurements confirmed that the thermal behavior of the ocular surface was highly time-sensitive, with the most substantial changes occurring within the first second post-blink. Sub-dividing the early 3-second interval into 0.5-second segments provided a detailed view of cooling deceleration, with inferior corneal regions (particularly I1 and I2) showing more sustained thermal shifts compared to superior ROIs. This suggested a greater vulnerability of the inferior cornea to evaporative stress, consistent with its anatomical positioning.[227]

As the IBI extended to 6 seconds, RTC values across most regions trended downward again, reflecting a return to steady-state cooling driven by evaporation. Superior corneal sites demonstrated greater thermal stability throughout this period, while central and inferior locations continued to exhibit dynamic fluctuations.

Linear mixed-effects models and non-parametric tests consistently indicated that time was the dominant factor influencing RTC. Spatial differences, while physiologically meaningful, were

more variable and only occasionally reached statistical significance. Localized differences, such as early timepoint comparisons in I2 and I1, demonstrated statistical and clinical relevance.

Taken together, these results emphasize the complex and layered response of the tear film to lipid supplementation. LLT increased rapidly and consistently, while NITBUT and TER responded more variably and over a longer time scale. RTC analysis complemented these findings by illustrating the immediate and region-specific thermal effects of tear film modification. These data highlight the value of combining structural, evaporative, and thermal markers to fully characterize tear film behavior, and support the integration of RTC into the clinical tool-kit for DED assessment and treatment monitoring.

4.5.6 Limitations and Future Directions

This study incorporated a comprehensive approach to characterizing tear film behavior by examining structural (LLT), functional (NITBUT and TER), and thermodynamic (RTC) parameters. While this multifactorial approach provides a more complete view of tear film dynamics, several limitations should be acknowledged.

First, the sample size in this phase was limited, as it represented a continuation of Phase I with protocol refinements. A formal sample size calculation was not performed for this phase, and the number of participants was determined pragmatically based on the updated design and available resources. While each participant contributed a large volume of repeated measures across timepoints and regions, the smaller sample may have reduced the statistical power for detecting subtler effects. This should be considered when interpreting the generalizability of the findings. Also, the sex distribution of the study sample was also imbalanced (7 males, 20 females), which does not reflect the typical sex distribution seen in DED, where prevalence is generally higher in females.[120–122] This imbalance may have influenced the results, as sex-related differences in tear

film physiology and response to lipid supplementation have been reported. Future studies should aim for a more representative distribution to improve generalizability.

Second, although LLT, NITBUT, and TER were measured before and after lipid drop instillation, all measurements were performed within a 20-minute observation window. While this timeframe was adequate to detect early responses, it may not have captured the full trajectory of lipid re-distribution, tear film stabilization, or delayed physiological effects. Future studies should consider extending the monitoring period to 60 minutes or longer to assess prolonged tear film changes.

Third, although LLT was measured using LipiView II, the device has an upper measurement limit of 100 nm, which may have led to ceiling effects in individuals with thicker lipid layers post-drop. More advanced or complementary imaging methods may be needed to more accurately quantify LLT in these cases.

Fourth, while TER was measured under controlled IBIs, the evaporimeter set-up does not replicate real-world blinking behavior or the dynamic mechanical redistribution of lipid following blinking. Incorporating more physiologically valid blink patterns or real-time lipid layer imaging would enhance the physiological relevance of the findings.

Fifth, although RTC offers a unique and sensitive measure of thermodynamic behavior, it remains an indirect index of tear film thinning. RTC reflects the net thermal balance between evaporative loss and heat supply but cannot directly distinguish between lipid instability and aqueous deficiency. Integration with direct imaging of tear film layers or concurrent evaporimetry could improve its interpretability.

Lastly, while mixed-effects models were used to account for individual variability, potential influences, such as PAS, ambient RH, and baseline LLT grouping, were only secondarily analyzed.

Future studies should include these covariates more formally within the statistical model to better account for environmental and anatomical variability.

Future directions include the inclusion of DED patient populations, comparisons between different lipid formulations, and integration of OST measurements into multimodal DED diagnostics. Longer follow-ups will also help clarify whether early changes in LLT, TER, and RTC predict long-term clinical outcomes.

4.5.7 Conclusion

This phase of the study demonstrated that lipid-based eye drop instillation significantly enhances LLT. TER unexpectedly increased immediately following drop instillation, suggesting that structural improvements in the lipid layer may not instantly translate to functional evaporation control. These findings underscore the complex and time-dependent response of the tear film to lipid supplementation.

Using RTC as a non-invasive thermographic marker, a biphasic pattern in OST behavior was identified, incorporating an initial deceleration of cooling followed by more gradual evaporation-driven temperature loss. RTC patterns varied across corneal regions, with inferior locations exhibiting greater and more prolonged changes, highlighting their anatomical vulnerability to evaporative stress.

Together, these findings illustrate that combining LLT, NITBUT, TER, and RTC enables a more nuanced understanding of tear film dynamics. This multimodal approach strengthens the rationale for including dynamic thermal imaging in dry eye diagnostics and underscores the importance of evaluating tear film responses both spatially and temporally.

Chapter 5 Discussion

5.1 Overview and Integration of Findings

This thesis aimed to address fundamental gaps in the understanding and measurement of tear evaporation dynamics and ocular surface stability. This thesis examined how LLT, artificial tears, and OST influence TER using *in vitro* and *in vivo* models. Alongside that, it evaluated the Waterloo Evaporimeter and optimized the method of investigation for IRT using the ThermOcular cameras in both clinical and experimental settings. Across the experimental series, several consistent patterns emerged.

First, the lipid layer was confirmed as a critical determinant of tear film evaporation, with *in vitro* findings showing that thicker lipid layers significantly reduced TER. In contrast, TheraTears®, an aqueous-based artificial tear, did not show a statistically significant difference in evaporation rate compared to distilled water under *in vitro* conditions. This finding highlights the limited effectiveness of non-lipid formulations in responding to evaporative stress, thereby underscoring the inadequacy of purely aqueous solutions for managing EDE.

- Second, ocular surface area was found to be another key contributor to TER, as larger exposed areas consistently exhibited higher rates of evaporation. These findings emphasize the importance of anatomical and behavioral factors, such as palpebral aperture size and blink rate, in tear film stability.

- Third, the Waterloo Evaporimeter demonstrated high sensitivity in detecting real-time changes in RH within a controlled chamber environment. Its compatibility with both *in vitro* models and human participants (*in vivo*) made it a versatile and clinically promising tool for TER assessment. Similarly, IRT, supported by ResearchIR software, enabled non-invasive, high-resolution mapping

of OST and post-blink thermal dynamics. The convergence of TER and OST patterns suggests that these metrics can be used in a complementary fashion to assess tear film stability.

Taken together, the findings of this thesis reinforce the multifactorial nature of tear film evaporation and highlight the interdependence of biophysical, environmental, anatomical, and technological variables in shaping ocular surface health. The integrated methodology developed here not only supports future clinical diagnostics but also lays the groundwork for improved tear film modeling.

5.2 Tear Film Lipid Layer. Functional Role in Evaporation Dynamics

The *in vitro* experiments demonstrated that increasing lipid content via CALMO® Eye Spray resulted in a progressive and statistically significant reduction in TER, particularly in the larger (2.5 cm^2) model eye. These results are consistent with extensive prior evidence showing that the lipid layer plays a primary role in suppressing tear evaporation, particularly when it is thick, stable, and evenly distributed.[35,37,76] Studies have shown that a deficient lipid layer can increase evaporation rates by up to 17 times, emphasizing its significance in ocular surface protection.[35,37] However, this consistent trend was not observed under *in vivo* conditions. Paradoxically, the instillation of a clinically validated lipid-based eye drop (Systane Complete®) led to an increase in TER, despite a measurable post-instillation increase in LLT, as measured by LipiView II interferometry. This divergence from the *in vitro* trend has been previously noted in other studies and is often attributed to the complex dynamics that unfold immediately after instillation.[81,170] Short-term interactions between the eye drop and the native tear film can result in uneven spreading of the lipid emulsion or transient thermal artifacts that contribute to evaporation rather than suppressing it.

Another major contributor to tear evaporation was ocular surface exposure. In the *in vitro* experiments, TER was significantly higher in the larger model eye across all LLT conditions. This supports a large body of literature indicating that palpebral aperture size, lagophthalmos, and incomplete blinking are strongly associated with increased evaporation.[257,258]

One explanation for this paradox may lie in the interplay between drop volume, blink mechanics, and tear film restructuring. The immediate post-instillation phase is characterized by thermal disturbance and dilution of the tear film architecture, which may increase surface volatility, even in the presence of a thicker lipid signal. However, these changes may be short-lived: findings from Phase II of the experiment suggest that LLT and TER may stabilize over time, with a delayed onset of the lipid barrier's protective function.

Taken together, these findings reinforce the lipid layer's role as a modifiable and often protective factor in evaporation control, but one whose efficacy depends heavily on context. While LLT is crucial, it should not be viewed in isolation. Its real-world performance is influenced by blinking frequency, ocular surface area, lipid spreading behavior, and the physicochemical properties of the formulation itself. This thesis therefore challenged the assumption that simply increasing LLT guarantees evaporation reduction *in vivo*, and instead supported a more nuanced, dynamic interpretation of lipid-based interventions.

5.3 Utility and Validation of Measurement Technologies

A central aim of this thesis was not only to investigate the biophysical behavior of the tear film, but also to evaluate and refine the tools used to measure it. Accurate and repeatable assessment of TER and OST is essential for both diagnostic and research purposes. Investigations using the Waterloo Evaporimeter and the ThermOcular IRT camera, addressed several limitations noted in earlier literature regarding evaporimetry and thermography platforms.[8,170]

The Waterloo Evaporimeter demonstrated high sensitivity in detecting changes in RH within the eye goggle under both *in vitro* and *in vivo* conditions. Its dual-eye capability and closed-chamber design allowed for bilateral, real-time TER recordings while minimizing external confounding factors, such as airflow and inconsistent blink behavior. Notably, the device achieved excellent reliability, with an intraclass correlation coefficient (ICC) of 0.84 during Phase I of *in vivo* testing. These findings validate its potential as a research-grade and possibly clinical tool for measuring TER under controlled conditions.

While other devices such as the Delfin Eye-Vapometer have been used to assess TER, they often rely on closed-chamber configurations or single-eye measurements, which are more vulnerable to external environmental variation.[10,138] The Waterloo Evaporimeter's incorporation of petroleum jelly barriers and metronome-guided blinking helped standardize conditions and limit variability, particularly important when comparing pre- and post-intervention TER changes.

In parallel, the ThermOcular IRT camera enabled non-invasive, high-resolution mapping of OST. When integrated with ResearchIR software and synchronized with a visible-light camera, this dual-camera system allowed for dynamic, spatially resolved thermal imaging of the ocular surface. Standardized ROI templates and machine learning-assisted segmentation ensured consistent data extraction across participants and conditions. These features align with recent advances in ocular IRT and offer improvements in reproducibility and regional temperature assessment.[33,54,60]

Although OST and TER represent different aspects of tear film behavior, thermal versus evaporative, they are inherently linked. TER reflects aqueous loss, whereas OST indicates the thermal consequences of that loss. The simultaneous use of these technologies allowed for multimodal insight: TER quantified evaporative potential, while OST visualized the spatial and temporal effects of tear film disruption. Previous literature has emphasized that such combined

approaches may enhance diagnostic specificity for EDE, particularly when single-parameter tools fail to capture multifactorial tear film dysfunction.[73,82,170]

In summary, this thesis validated two novel measurement platforms that, when used together, provide a complete and more dynamic picture of tear film behavior. The Waterloo Evaporimeter offers precise, chamber-based assessment of evaporation, while the ThermOcular IRT camera in combination with the ResearchIR software delivers sensitive thermal imaging of ocular surface changes.

5.4 Artificial Tear Formulations and Evaporation Control

Artificial tears are widely regarded as the first-line treatment for DED, particularly for symptoms associated with tear film instability and evaporation. However, their efficacy varies significantly based on formulation, especially with respect to their ability to reduce tear evaporation. Most commercial products aim to supplement tear volume and restore surface lubrication, but not all are designed to counteract evaporative loss. Notably, formulations that lack lipid components tend to offer limited protection against TER, even when they contain viscosity-enhancing or mucoadhesive agents, such as carboxymethylcellulose.[14,16]

This trend was directly confirmed in the *in vitro* study that compared TheraTears®, a non-lipid artificial tear, with distilled water. Despite containing carboxymethylcellulose and other electrolytes intended to prolong retention, TheraTears® did not significantly reduce evaporation relative to water under controlled conditions. These findings are consistent with prior research indicating that aqueous-based formulations, even when enriched with polymers, are insufficient to form a stable barrier against evaporation.[15,74,215] The absence of a lipid layer in these solutions likely allows rapid aqueous loss once the drop is exposed to ambient air.

By contrast, formulations containing lipid-based emulsions have demonstrated more favorable effects on TER in several studies.[14,170] These drops are designed to reinforce or mimic the natural tear film lipid layer, reducing evaporation and enhancing surface coverage. In this thesis, application of CALMO® Eye Spray *in vitro* resulted in a dose-dependent reduction in TER as lipid thickness increased. This aligns with previous reports showing that lipid sprays or oil-in-water emulsions with phospholipid components can improve lipid layer stability and reduce evaporative loss.[14,15] However, the performance of lipid-containing tears *in vivo* remains more variable. As discussed, a paradoxical TER increase was observed in the *in vivo* results.

This complexity suggests that the mere presence of lipid is not sufficient for optimal evaporation control. The formulation characteristics, such as droplet size, lipid type, emulsification method, and spreading behavior, play a decisive role. Furthermore, individual patient factors, such as baseline LLT, blink rate, and surface exposure, may modulate the *in vivo* efficacy of lipid drops.

Taken together, these findings highlight that the effect of artificial tear formulations on evaporation is strongly dependent on their composition and physical behavior. Lipid-based formulations show promise for enhancing tear film stability, but their performance appears to be both formulation-specific and temporally variable. Because the current work was conducted in model eyes and healthy participants, the results should be interpreted cautiously and cannot be directly generalized to patients with DED. Nevertheless, the data provide a useful framework for understanding how formulation properties such as lipid content, droplet size, and spreading dynamics may influence evaporative control. Future studies involving DED populations are needed to determine how these mechanisms translate clinically and to guide the rational design of artificial tears that achieve rapid, uniform lipid integration without transient destabilization.

5.5 Inter-relationships between LLT, NITBUT, TER, and OST

Understanding the dynamic inter-relationships among tear film parameters is essential for building a comprehensive model of ocular surface stability. This thesis evaluated four key markers LLT, NITBUT, TER, and OST across a series of *in vitro* and *in vivo* conditions to explore how they interact and to assess their combined utility in diagnosing EDE.

From a theoretical standpoint, LLT has been widely regarded as a critical determinant of both TER and NITBUT. A thicker and more uniform lipid layer is believed to retard evaporation and prolong tear film stability between blinks.[35,76,78] Accordingly, LLT has often been used as a surrogate indicator of tear film performance. Likewise, TER is conceptually linked to both LLT and NITBUT, as it quantifies the rate of aqueous loss, which directly affects the time to tear film break-up. OST, although less commonly used in routine diagnostics, is understood to reflect the thermal consequence of tear film behavior and has been shown to decrease more rapidly in patients with unstable or thinning tear films.[73,170,259]

However, the data presented in this thesis revealed that these parameters do not exhibit strong, linear correlations under physiological conditions. In the Phase I *in vivo* experiment, a significant increase in LLT was observed following lipid drop instillation, yet this was accompanied by a statistically significant decrease in first NITBUT and an increase in TER, both typically interpreted as indicators of tear film instability. These seemingly contradictory outcomes suggest that an increase in LLT alone does not guarantee functional tear film improvement, especially in the immediate post-instillation phase.

Further correlation analyses found no statistically significant relationship between changes in LLT and either NITBUT or TER, despite theoretical expectations. This is consistent with previous studies indicating that while LLT may enhance structural aspects of the tear film, its protective

effect depends on uniform distribution and integration into the pre-existing tear film.[81,170] Additional factors, such as blink behavior, drop spreading dynamics, and anatomical variations likely modulate these relationships.

OST, while not strongly correlated with the other parameters in this study, offers a complementary dimension to tear film analysis. OST complements structural measures and offers an indirect thermal readout of evaporative behavior.[33,258–260] Although OST alone may not fully characterize tear film dysfunction, its integration into multimodal assessment strategies may enhance the sensitivity of EDE diagnosis.

Overall, the absence of strong correlations among LLT, NITBUT, TER, and OST in this thesis supports a multifactorial view of tear film stability. Rather than relying on a single parameter as a diagnostic proxy, these findings reinforce the importance of using multiple, complementary measurements. This approach reflects the complex and adaptive nature of the tear film, where structural enhancements may not immediately translate to functional improvements and where anatomical and environmental variables significantly influence outcomes.

5.6 Limitations

While this thesis was designed to address major gaps in the assessment of tear film evaporation and ocular surface dynamics, several limitations must be acknowledged.

First, although the *in vitro* models allowed for tight control of environmental conditions and fluid composition, they lacked critical physiological features, most notably with blinking. In the human eye, blinking plays a fundamental role in distributing the lipid layer, restoring tear film integrity, and regulating TER. The absence of dynamic lipid redistribution in the static *in vitro* set-up may have led to over- or underestimation of lipid layer effects under real-world conditions. Future work

incorporating automated blinking mechanisms, such as the OcuBlink platform, could help bridge this gap and yield more physiologically representative data.

Second, while LLT was modulated in a controlled fashion using CALMO® Eye Spray, the application method-defined by number of spray puffs-was approximate rather than volumetrically precise. This may have introduced subtle inconsistencies in lipid coverage, especially in smaller model eyes where even minor volumetric differences could disproportionately affect surface behavior.

Third, although the *in vivo* studies were conducted under environmentally stable conditions, small fluctuations in room temperature and RH during longer testing sessions may have contributed to variability in TER. These environmental effects are difficult to eliminate entirely in real-world clinical settings but should be minimized in future work through tighter real-time environmental logging or use of enclosed climate-controlled chambers.

Fourth, the timeline of post-instillation measurements was relatively short. All post-drop measurements were conducted within minutes of artificial tear instillation, capturing only early-phase tear film responses. As demonstrated in the Phase I study, this timing may have coincided with transient destabilization of the tear film, masking the longer-term benefits of lipid supplementation. Follow-up studies with extended time-point measurements would help resolve these early dynamic effects.

Fifth, although several tear film parameters were evaluated (TER, LLT, NITBUT, and OST), direct statistical associations among them were limited. Specifically, no significant correlations were observed between LLT and either NITBUT or TER, despite theoretical expectations. This may reflect inter-individual variability, limitations of measurement sensitivity, or the complexity of multifactorial tear film interactions.

Finally, although the study evaluated the influence of anatomical features, such as palpebral aperture size and goggle chamber volume, no significant associations with TER were found. While this supports the reliability of the measurement setup, it also highlights the possibility that other unmeasured anatomical variables, such as lid contour, blink completeness, or ocular protrusion, may still contribute to inter-subject variation in TER and should be explored in future studies.

5.7 Conclusion

This thesis investigated the mechanisms of tear film evaporation and ocular surface thermal behavior through a combination of *in vitro* and *in vivo* studies, with a particular emphasis on the role of the lipid layer and the performance of measurement technologies. The overarching aim was to deepen understanding of EDE and improve methods for its evaluation.

In one of the *in vitro* experiments, increasing the applied lipid layer was associated with lower TER, indicating a possible role of LLT in modulating evaporation under controlled conditions. However, because LLT was not directly measured (and was instead inferred from the applied lipid volume), this interpretation remains indirect and should be treated with caution. However, the *in vivo* findings were more complex, revealing that lipid-based drops may not produce immediate or predictable reductions in TER, especially in the short period following instillation. This highlights the dynamic and sometimes counterintuitive nature of tear film behavior under physiological conditions and the need to evaluate artificial tear performance over extended timelines.

The Waterloo Evaporimeter and ThermOcular imaging system both proved effective in capturing key parameters of tear film function. The evaporimeter provided reliable measurements of TER under both experimental and clinical conditions, while the ThermOcular system allowed non-invasive, high-resolution tracking of OST. While each instrument offers value independently, their

combined use has the potential to enhance diagnostic specificity by linking structural, evaporative, and thermal data.

Although this work confirmed many theoretical expectations, such as the protective role of the lipid layer and the impact of ocular surface exposure, it also revealed gaps in current assumptions. Not all enhancements in LLT led to improved NITBUT or reduced TER, and inter-individual variability remained high. These findings support a multimodal diagnostic approach that integrates several metrics rather than relying on any single parameter.

Ultimately, this thesis contributes to the field of ocular surface research by offering validated tools, detailed experimental evidence, and a more nuanced understanding of how lipid supplementation and measurement timing influence evaporation. It underscores the importance of considering anatomical, environmental, and temporal factors in both clinical practice and research, and it lays the groundwork for future innovations in EDE diagnosis and management.

5.8 Novelty of the Thesis

This thesis makes several original contributions to the study of tear film dynamics and dry eye disease mechanisms. A key innovation is the development and validation of the Waterloo Evaporimeter, a custom-built instrument designed to measure bilateral tear evaporation with high sensitivity under controlled experimental conditions. Complementing this, the work also applied infrared thermal imaging with a dual-camera system to optimize OST assessment, advancing non-invasive approaches for evaluating tear film physiology.

Another novel aspect lies in the integration of multiple tear film parameters including OST, TER, NITBUT, and LLT within both *in vitro* and *in vivo* experimental designs. By examining these measures together, the thesis provides new insights into their interrelationships and the complex, sometimes counterintuitive, behavior of the tear film under physiological conditions. The *in vitro*

studies demonstrated how lipid supplementation in the form of calibrated spray doses could reduce evaporation in a dose-dependent manner, while the *in vivo* studies revealed that short-term responses to lipid instillation may be destabilizing rather than protective. This dual approach bridges the gap between controlled laboratory modeling and human physiological variability.

Overall, the thesis introduces new methodological tools and experimental perspectives for studying tear film stability, while also highlighting the temporal, compositional, and environmental factors that govern artificial tear performance. These contributions expand current understanding of tear film dynamics and provide a foundation for refining both diagnostic strategies and therapeutic formulations for evaporative dry eye disease.

References

1. Stapleton F, Alves M, Bunya VY, et al. TFOS DEWS II Epidemiology Report. *Ocul Surf*. Published online 2017. doi:10.1016/j.jtos.2017.05.003

2. Mohamed Z, Alrasheed S, Abdu M, Allinjawi K. Dry Eye Disease Prevalence and Associated Risk Factors Among the Middle East Population: A Systematic Review and Meta-Analysis. *Cureus*. 16(9):e70522. doi:10.7759/cureus.70522

3. Britten-Jones AC, Wang MTM, Samuels I, Jennings C, Stapleton F, Craig JP. Epidemiology and Risk Factors of Dry Eye Disease: Considerations for Clinical Management. *Medicina (Mex)*. 2024;60(9):1458. doi:10.3390/medicina60091458

4. Yu J, Asche CV, Fairchild CJ. The economic burden of dry eye disease in the United States: a decision tree analysis. *Cornea*. 2011;30(4):379-387. doi:10.1097/ICO.0b013e3181f7f363

5. Chan C, Ziai S, Myageri V, Burns JG, Prokopich CL. Economic burden and loss of quality of life from dry eye disease in Canada. *BMJ Open Ophthalmol*. 2021;6(1). doi:10.1136/bmjophth-2021-000709

6. Lemp MA, Crews LA, Bron AJ, Foulks GN, Sullivan BD. Distribution of aqueous-deficient and evaporative dry eye in a clinic-based patient cohort: a retrospective study. *Cornea*. 2012;31(5):472-478. doi:10.1097/ICO.0b013e318225415a

7. Wolffsohn JS, Arita R, Chalmers R, et al. TFOS DEWS II Diagnostic Methodology report. *Ocul Surf*. 2017;15(3):539-574. doi:10.1016/j.jtos.2017.05.001

8. Rolando M, Refojo MF. Tear evaporimeter for measuring water evaporation rate from the tear film under controlled conditions in humans. *Exp Eye Res*. 1983;36(1):25-33. doi:10.1016/0014-4835(83)90086-6

9. Tsubota K, Yamada M. Tear evaporation from the ocular surface. *Invest Ophthalmol Vis Sci*. 1992;33(10):2942-2950.

10. Mathers WD, Binarao G, Petroll M. Ocular water evaporation and the dry eye. A new measuring device. *Cornea*. 1993;12(4):335-340. doi:10.1097/00003226-199307000-00010

11. Khanal S, Tomlinson A, McFadyen A, Diaper C, Ramaesh K. Dry eye diagnosis. *Invest Ophthalmol Vis Sci*. 2008;49(4):1407-1414. doi:10.1167/iovs.07-0635

12. Uchiyama E, Di Pascuale MA, Butovich IA, McCulley JP. Impact on Ocular Surface Evaporation of an Artificial Tear Solution Containing Hydroxypropyl (HP) Guar. *Eye Contact Lens*. 2008;34(6):331-334. doi:10.1097/ICL.0b013e31818c66b5

13. Wojtowicz JC, Arciniega JC, McCulley JP, Mootha VV. Effect of systane and optive on aqueous tear evaporation in patients with dry eye disease. *Eye Contact Lens*. 2010;36(6):358-360. doi:10.1097/ICL.0b013e3181f9b36e

14. Khanal S, Tomlinson A, Pearce EI, Simmons PA. Effect of an oil-in-water emulsion on the tear physiology of patients with mild to moderate dry eye. *Cornea*. 2007;26(2):175-181. doi:10.1097/ICO.0b013e31802b492d

15. Tomlinson A, Trees GR. Effect of preservatives in artificial tear solutions on tear film evaporation. *Ophthalmic Physiol Opt J Br Coll Ophthalmic Opt Optom*. 1991;11(1):48-52.

16. Wong S, Murphy PJ, Jones L. Tear evaporation rates: What does the literature tell us? *Contact Lens Anterior Eye J Br Contact Lens Assoc*. 2018;41(3):297-306. doi:10.1016/j.clae.2017.12.003

17. McCulley JP, Aronowicz JD, Uchiyama E, Shine WE, Butovich IA. Correlations in a change in aqueous tear evaporation with a change in relative humidity and the impact. *Am J Ophthalmol*. 2006;141(4):758-760. doi:10.1016/j.ajo.2005.10.057

18. Wojtowicz JC, McCulley JP. Assessment and Impact of the Time of day on Aqueous Tear Evaporation in normal subjects. *Eye Contact Lens*. 2009;35(3):117-119. doi:10.1097/ICL.0b013e31819c2963

19. Shimazaki J, Sakata M, Tsubota K. Ocular surface changes and discomfort in patients with meibomian gland dysfunction. *Arch Ophthalmol Chic Ill 1960*. 1995;113(10):1266-1270. doi:10.1001/archopht.1995.01100100054027

20. Willcox MDP, Argüeso P, Georgiev GA, et al. TFOS DEWS II Tear Film Report. *Ocul Surf*. 2017;15(3):366-403. doi:10.1016/j.jtos.2017.03.006

21. Mathers WD. Ocular evaporation in meibomian gland dysfunction and dry eye. *Ophthalmology*. 1993;100(3):347-351. doi:10.1016/s0161-6420(93)31643-x

22. Tomlinson A, Doane MG, McFadyen A. Inputs and outputs of the lacrimal system: review of production and evaporative loss. *Ocul Surf*. 2009;7(4):186-198. doi:10.1016/s1542-0124(12)70186-6

23. Craig JP, Singh I, Tomlinson A, Morgan PB, Efron N. The role of tear physiology in ocular surface temperature. *Eye Lond Engl*. 2000;14 (Pt 4):635-641. doi:10.1038/eye.2000.156

24. Gugleta K, Orgül S, Flammer J. Is corneal temperature correlated with blood-flow velocity in the ophthalmic artery? *Curr Eye Res*. 1999;19(6):496-501. doi:10.1076/ceyr.19.6.496.5286

25. Keeney AH, Guibor P. Thermography and ophthalmology. *Trans - Am Acad Ophthalmol Otolaryngol Am Acad Ophthalmol Otolaryngol*. 1970;74(5):1032-1043.

26. Leshno A, Stern O, Barkana Y, et al. Ocular surface temperature differences in glaucoma. *Eur J Ophthalmol*. 2022;32(3):1518-1524. doi:10.1177/11206721211023723

27. Li W, Graham AD, Selvin S, Lin MC. Ocular Surface Cooling Corresponds to Tear Film Thinning and Breakup. *Optom Vis Sci*. 2015;92(9):e248. doi:10.1097/OPX.0000000000000672

28. Coroneo MT, Kokkinakis J, Lee BWH, Chen H, Tat L. High-Resolution Ocular Surface Imaging: Real-Time Visualization of Tear Film Dysfunction. *Cornea*. 2024;43(9):1072. doi:10.1097/ICO.0000000000003579

29. Hodges RR, Dartt DA. Tear film mucins: front line defenders of the ocular surface; comparison with airway and gastrointestinal tract mucins. *Exp Eye Res*. 2013;117:62-78. doi:10.1016/j.exer.2013.07.027

30. Ding JE, Kim YH, Yi SM, Graham AD, Li W, Lin MC. Ocular surface cooling rate associated with tear film characteristics and the maximum interblink period. *Sci Rep*. 2021;11(1). doi:10.1038/s41598-021-94568-9

31. Su TY, Chang SW. Normalized ocular surface temperature models for tear film characteristics and dry eye disease evaluation. *Ocul Surf*. 2021;19:74-82. doi:10.1016/j.jtos.2020.04.002

32. Kim YH, Lee J, Yi SM, Lin MC, Radke CJ. Localized Evaporative Cooling Explains Observed Ocular Surface-Temperature Patterns. *Invest Ophthalmol Vis Sci*. 2024;65(10):15. doi:10.1167/iovs.65.10.15

33. Tan JH, Ng EYK, Rajendra Acharya U, Chee C. Infrared thermography on ocular surface temperature: A review. *Infrared Phys Technol*. 2009;52(4):97-108. doi:10.1016/j.infrared.2009.05.002

34. Narang P, Donthineni PR, D'Souza S, Basu S. Evaporative dry eye disease due to meibomian gland dysfunction: Preferred practice pattern guidelines for diagnosis and treatment. *Indian J Ophthalmol*. 2023;71(4):1348-1356. doi:10.4103/IJO.IJO_2841_22

35. Craig JP, Tomlinson A. Importance of the lipid layer in human tear film stability and evaporation. *Optom Vis Sci Off Publ Am Acad Optom*. 1997;74(1):8-13. doi:10.1097/00006324-199701000-00014

36. IWATA S, LEMP MA, HOLLY FJ, DOHLMAN CH. Evaporation rate of water from the precorneal tear film and cornea in the rabbit. *Invest Ophthalmol Vis Sci*. 1969;8(6):613-619.

37. Mishima S, Maurice DM. The oily layer of the tear film and evaporation from the corneal surface. *Exp Eye Res*. 1961;1:39-45. doi:10.1016/s0014-4835(61)80006-7

38. Wolff E. The mucocutaneous junction of the lidmargin and the distribution of the tear fluid. In: ; 1946. Accessed January 20, 2025. https://www.semanticscholar.org/paper/The-mucocutaneous-junction-of-the-lidmargin-and-the-Wolff/428a38d06318d3c733474dd01f41b6cc1eaa7160

39. Nicolaides N, Kaitaranta JK, Rawdah TN, Macy JI, Boswell FM, Smith RE. Meibomian gland studies: comparison of steer and human lipids. *Invest Ophthalmol Vis Sci*. 1981;20(4):522-536.

40. Nicolaides N. SKIN LIPIDS. II. Lipid class composition of samples from various species and anatomical sites. *J Am Oil Chem Soc*. 1965;42:691-702. doi:10.1007/BF02540042

41. Knop E, Knop N, Millar T, Obata H, Sullivan DA. The international workshop on meibomian gland dysfunction: report of the subcommittee on anatomy, physiology, and pathophysiology of the meibomian gland. *Invest Ophthalmol Vis Sci*. 2011;52(4):1938-1978. doi:10.1167/iovs.10-6997c

42. McCulley JP, Shine W. A compositional based model for the tear film lipid layer. *Trans Am Ophthalmol Soc*. 1997;95:79-88; discussion 88-93.

43. Wolff E. The mucocutaneous junction of the lidmargin and the distribution of the tear fluid. Published online 1946.

44. Craig JP, Willcox MDP, Argüeso P, et al. The TFOS International Workshop on Contact Lens Discomfort: report of the contact lens interactions with the tear film subcommittee. *Invest Ophthalmol Vis Sci*. 2013;54(11):TFOS123-156. doi:10.1167/iovs.13-13235

45. Downie LE, Bandlitz S, Bergmanson JPG, et al. CLEAR - Anatomy and physiology of the anterior eye. *Contact Lens Anterior Eye J Br Contact Lens Assoc*. 2021;44(2):132-156. doi:10.1016/j.clae.2021.02.009

46. Dilly PN. Structure and function of the tear film. *Adv Exp Med Biol*. 1994;350:239-247. doi:10.1007/978-1-4615-2417-5_41

47. Downie LE, Craig JP. Tear film evaluation and management in soft contact lens wear: a systematic approach. *Clin Exp Optom*. 2017;100(5):438-458. doi:10.1111/cxo.12597

48. Wang J, Fonn D, Simpson TL, Jones L. Precorneal and Pre- and Postlens Tear Film Thickness Measured Indirectly with Optical Coherence Tomography. *Invest Ophthalmol Vis Sci*. 2003;44(6):2524-2528. doi:10.1167/iovs.02-0731

49. Prydal JI, Artal P, Woon H, Campbell FW. Study of human precorneal tear film thickness and structure using laser interferometry. *Invest Ophthalmol Vis Sci*. 1992;33(6):2006-2011.

50. King-Smith PE, Fink BA, Fogt N, Nichols KK, Hill RM, Wilson GS. The thickness of the human precorneal tear film: evidence from reflection spectra. *Invest Ophthalmol Vis Sci*. 2000;41(11):3348-3359.

51. King-Smith PE, Fink BA, Hill RM, Koelling KW, Tiffany JM. The thickness of the tear film. *Curr Eye Res*. 2004;29(4-5):357-368. doi:10.1080/02713680490516099

52. Lin MC, Graham AD, Polse KA, Mandell RB, McNamara NA. Measurement of Post–Lens Tear Thickness. *Invest Ophthalmol Vis Sci*. 1999;40(12):2833-2839.

53. Fogt N, King-Smith PE, Tuell G. Interferometric measurement of tear film thickness by use of spectral oscillations. *J Opt Soc Am A Opt Image Sci Vis*. 1998;15(1):268-275. doi:10.1364/josaa.15.000268

54. Schmoll T, Unterhuber A, Kolbitsch C, Le T, Stingl A, Leitgeb R. Precise thickness measurements of Bowman's layer, epithelium, and tear film. *Optom Vis Sci Off Publ Am Acad Optom*. 2012;89(5):E795-802. doi:10.1097/OPX.0b013e3182504346

55. Guillon JP. *Tear film structure of the contact lens wearer a thesis submitted for the degree of Doctor of Philosophy the city university*. 1987.

56. Bron AJ, de Paiva CS, Chauhan SK, et al. TFOS DEWS II pathophysiology report. *Ocul Surf*. 2017;15(3):438-510. doi:10.1016/j.jtos.2017.05.011

57. Bai Y, Ngo W, Nichols JJ. Characterization of the Thickness of the Tear Film Lipid Layer using High Resolution Microscopy. *Ocul Surf*. 2019;17(2):356-359. doi:10.1016/j.jtos.2018.12.003

58. Segev F, Geffen N, Galor A, et al. Dynamic assessment of the tear film muco-aqueous and lipid layers using a novel tear film imager (TFI). *Br J Ophthalmol*. 2020;104(1):136-141. doi:10.1136/bjophthalmol-2018-313379

59. Reflectometry of the precorneal film - Olsen - 1985 - Acta Ophthalmologica - Wiley Online Library. Accessed January 20, 2025. https://onlinelibrary.wiley.com/doi/abs/10.1111/j.1755-3768.1985.tb01559.x

60. Huang J, Hindman HB, Rolland JP. In vivo thickness dynamics measurement of tear film lipid and aqueous layers with optical coherence tomography and maximum-likelihood estimation. *Opt Lett*. 2016;41(9):1981-1984. doi:10.1364/OL.41.001981

61. Bai Y, Nichols JJ. Advances in thickness measurements and dynamic visualization of the tear film using non-invasive optical approaches. *Prog Retin Eye Res*. 2017;58:28-44. doi:10.1016/j.preteyeres.2017.02.002

62. Craig JP, Willcox MDP, Argüeso P, et al. The TFOS International Workshop on Contact Lens Discomfort: report of the contact lens interactions with the tear film subcommittee. *Invest Ophthalmol Vis Sci*. Published online 2013. doi:10.1167/iovs.13-13235

63. Craig JP, Tomlinson A. Importance of the Lipid Layer in Human Tear Film Stability and Evaporation. *Optom Vis Sci*. 1997;74(1):8.

64. Abusharha AA, Pearce EI. The Effect of Low Humidity on the Human Tear Film. *Cornea*. 2013;32(4):429. doi:10.1097/ICO.0b013e31826671ab

65. Bron AJ, Tiffany JM, Gouveia SM, Yokoi N, Voon LW. Functional aspects of the tear film lipid layer. *Exp Eye Res*. 2004;78(3):347-360. doi:10.1016/j.exer.2003.09.019

66. Bron AJ, de Paiva CS, Chauhan SK, et al. TFOS DEWS II pathophysiology report. *Ocul Surf*. 2017;15(3):438-510. doi:10.1016/j.jtos.2017.05.011

67. Rubin BK. Physiology of airway mucus clearance. *Respir Care*. 2002;47(7):761-768.

68. Mantelli F, Argüeso P. Functions of ocular surface mucins in health and disease. *Curr Opin Allergy Clin Immunol*. 2008;8(5):477. doi:10.1097/ACI.0b013e32830e6b04

69. McDermott AM. Antimicrobial compounds in tears. *Exp Eye Res*. 2013;117:53-61. doi:10.1016/j.exer.2013.07.014

70. Efron N, Brennan NA. The clinical relevance ofhydrogel lens water content. *J Br Contact Lens Assoc*. 1987;10:9-14. doi:10.1016/S0141-7037(87)80040-X

71. Rohit A, Willcox M, Stapleton F. Tear lipid layer and contact lens comfort: a review. *Eye Contact Lens*. 2013;39(3):247-253. doi:10.1097/ICL.0b013e31828af164

72. Watanabe H. Significance of mucin on the ocular surface. *Cornea*. 2002;21(2 Suppl 1):S17-22. doi:10.1097/00003226-200203001-00005

73. Monfared N, Murphy PJ. Features and influences on the normal tear evaporation rate. *Contact Lens Anterior Eye*. 2023;46(2):101809. doi:10.1016/j.clae.2022.101809

74. McCulley JP, Uchiyama E, Aronowicz JD, Butovich IA. IMPACT OF EVAPORATION ON AQUEOUS TEAR LOSS. *Trans Am Ophthalmol Soc*. 2006;104:121-128.

75. Kessing SV. A new division of the conjunctiva on the basis of x-ray examination. *Acta Ophthalmol (Copenh)*. 1967;45(5):680-683. doi:10.1111/j.1755-3768.1967.tb06537.x

76. Bron AJ, Tiffany JM, Gouveia SM, Yokoi N, Voon LW. Functional aspects of the tear film lipid layer. *Exp Eye Res*. 2004;78(3):347-360. doi:10.1016/j.exer.2003.09.019

77. King-Smith PE, Begley CG, Braun RJ. Mechanisms, imaging and structure of tear film breakup. *Ocul Surf*. 2018;16(1):4-30. doi:10.1016/j.jtos.2017.09.007

78. King-Smith PE, Fink BA, Fogt N. Three interferometric methods for measuring the thickness of layers of the tear film. *Optom Vis Sci Off Publ Am Acad Optom*. 1999;76(1):19-32. doi:10.1097/00006324-199901000-00025

79. Hwang HS, Kim EC, Kim MS. Novel tear interferometer made of paper for lipid layer evaluation. *Cornea*. 2014;33(8):826-831. doi:10.1097/ICO.0000000000000161

80. Doane MG. Abnormalities of the structure of the superficial lipid layer on the in vivo dry-eye tear film. *Adv Exp Med Biol*. 1994;350:489-493. doi:10.1007/978-1-4615-2417-5_82

81. King-Smith PE, Nichols JJ, Nichols KK, Fink BA, Braun RJ. Contributions of evaporation and other mechanisms to tear film thinning and break-up. *Optom Vis Sci*. 2008;85:623-630.

82. Wang MT, Murphy PJ, Blades KJ, Craig JP. Comparison of non-invasive tear film stability measurement techniques. *Clin Exp Optom*. 2018;101(1):13-17. doi:10.1111/cxo.12546

83. Nichols JJ, Nichols KK, Puent B, Saracino M, Mitchell GL. Evaluation of tear film interference patterns and measures of tear break-up time. *Optom Vis Sci Off Publ Am Acad Optom*. 2002;79(6):363-369. doi:10.1097/00006324-200206000-00009

84. Paugh JR, Tse J, Nguyen T, et al. Efficacy of the Fluorescein Tear Breakup Time (TBUT) Test in Dry Eye. *Cornea*. 2020;39(1):92-98. doi:10.1097/ICO.0000000000002148

85. Norn MS. Desiccation of the Precorneal Film. *Acta Ophthalmol (Copenh)*. 1969;47(4):865-880. doi:10.1111/j.1755-3768.1969.tb03711.x

86. Braun RJ, King-Smith PE, Begley CG, Li L, Gewecke NR. Dynamics and function of the tear film in relation to the blink cycle. *Prog Retin Eye Res*. 2015;45:132-164. doi:10.1016/j.preteyeres.2014.11.001

87. Carney LG, Hill RM. The nature of normal blinking patterns. *Acta Ophthalmol (Copenh)*. 1982;60(3):427-433. doi:10.1111/j.1755-3768.1982.tb03034.x

88. Bentivoglio AR, Bressman SB, Cassetta E, Carretta D, Tonali P, Albanese A. Analysis of blink rate patterns in normal subjects. *Mov Disord*. 1997;12(6):1028-1034. doi:10.1002/mds.870120629

89. Al-Abdulmunem M. Relation between tear breakup time and spontaneous blink rate. *Int Contact Lens Clin*. 1999;26(5):117-120. doi:10.1016/S0892-8967(00)00033-X

90. Himebaugh NL, Begley CG, Bradley A, Wilkinson JA. Blinking and tear break-up during four visual tasks. *Optom Vis Sci Off Publ Am Acad Optom*. 2009;86(2):E106-114. doi:10.1097/OPX.0b013e318194e962

91. Wolkoff P, Nojgaard J, Troiano P, Piccoli B. Eye complaints in the office environment: precorneal tear film integrity influenced by eye blinking efficiency. *Occup Environ Med*. 2005;62(1):4-12. doi:10.1136/oem.2004.016030

92. Yap M. Tear break-up time is related to blink frequency. *Acta Ophthalmol (Copenh)*. 1991;69(1):92-94. doi:10.1111/j.1755-3768.1991.tb01999.x

93. Prause JU, Norn M. Relation between blink frequency and break-up time? *Acta Ophthalmol (Copenh)*. 1987;65(1):19-22. doi:10.1111/j.1755-3768.1987.tb08484.x

94. (PDF) Factors Affecting Evaporation Rates of Tear Film Components Measured In Vitro. *ResearchGate*. Published online October 22, 2024. doi:10.1097/ICL.0b013e318193f4fc

95. Davidson HJ, Kuonen VJ. The tear film and ocular mucins. *Vet Ophthalmol*. 2004;7(2):71-77. doi:10.1111/j.1463-5224.2004.00325.x

96. Hisatake K, Tanaka S, Aizawa Y. Evaporation rate of water in a vessel. *J Appl Phys*. 1993;73(11):7395-7401. doi:10.1063/1.354031

97. Isreb MA, Greiner JV, Korb DR, et al. Correlation of lipid layer thickness measurements with fluorescein tear film break-up time and Schirmer's test. *Eye*. 2003;17(1):79-83. doi:10.1038/sj.eye.6700224

98. Di Zazzo A, Barabino S, Fasciani R, et al. One Soul and Several Faces of Evaporative Dry Eye Disease. *J Clin Med*. 2024;13(5):1220. doi:10.3390/jcm13051220

99. Blackie CA, Solomon JD, Scaffidi RC, Greiner JV, Lemp MA, Korb DR. The relationship between dry eye symptoms and lipid layer thickness. *Cornea*. 2009;28(7):789-794. doi:10.1097/ICO.0b013e318191b870

100. Tsubota K, Yamada M. Tear evaporation from the ocular surface. *Invest Ophthalmol Vis Sci*. 1992;33(10):2942-2950.

101. Pansell T, Porsblad M, Abdi S. The effect of vertical gaze position on ocular tear film stability. *Clin Exp Optom*. 2007;90(3):176-181. doi:10.1111/j.1444-0938.2007.00136.x

102. Kessel L, Johnson L, Arvidsson H, Larsen M. The Relationship between Body and Ambient Temperature and Corneal Temperature. *Invest Ophthalmol Vis Sci*. 2010;51(12):6593-6597. doi:10.1167/iovs.10-5659

103. SCHWARTZ B. Environmental Temperature and the Ocular Temperature Gradient. *Arch Ophthalmol*. 1965;74(2):237-243. doi:10.1001/archopht.1965.00970040239022

104. Fujishima H, Toda I, Yamada M, Sato N, Tsubota K. Corneal temperature in patients with dry eye evaluated by infrared radiation thermometry. *Br J Ophthalmol*. 1996;80(1):29-32. doi:10.1136/bjo.80.1.29

105. Mori A, Oguchi Y, Okusawa Y, Ono M, Fujishima H, Tsubota K. Use of high-speed, high-resolution thermography to evaluate the tear film layer. *Am J Ophthalmol*. 1997;124(6):729-735. doi:10.1016/s0002-9394(14)71689-7

106. Craig JP, Tomlinson A. Importance of the lipid layer in human tear film stability and evaporation. *Optom Vis Sci Off Publ Am Acad Optom*. 1997;74(1):8-13. doi:10.1097/00006324-199701000-00014

107. Korb DR, Baron DF, Herman JP, et al. Tear film lipid layer thickness as a function of blinking. *Cornea*. 1994;13(4):354-359. doi:10.1097/00003226-199407000-00012

108. Tsubota K, Nakamori K. Effects of ocular surface area and blink rate on tear dynamics. *Arch Ophthalmol Chic Ill 1960*. 1995;113(2):155-158. doi:10.1001/archopht.1995.01100020037025

109. Evaluation of tear evaporation from ocular surface by functional infrared thermography - Tan - 2010 - Medical Physics - Wiley Online Library. Accessed January 24, 2025. https://aapm.onlinelibrary.wiley.com/doi/full/10.1118/1.3495540

110. Kaneko K, Sakamoto K. Spontaneous blinks as a criterion of visual fatigue during prolonged work on visual display terminals. *Percept Mot Skills*. 2001;92(1):234-250. doi:10.2466/pms.2001.92.1.234

111. Abusharha AA, Pearce EI. The effect of low humidity on the human tear film. *Cornea*. 2013;32(4):429-434. doi:10.1097/ICO.0b013e31826671ab

112. FREEMAN RD, FATT I. Environmental Influences on Ocular Temperature. *Invest Ophthalmol Vis Sci*. 1973;12(8):596-602.

113. Murakami S. Analysis and design of micro-climate around the human body with respiration by CFD. *Indoor Air*. 2004;14 Suppl 7:144-156. doi:10.1111/j.1600-0668.2004.00283.x

114. Tomlinson A, H. Cedarstaff T. Diurnal variation in human tear evaporation. *J Br Contact Lens Assoc*. 1992;15(2):77-79. doi:10.1016/0141-7037(92)80043-Y

115. Sun WS, Baker RS, Chuke JC, et al. Age-related changes in human blinks. Passive and active changes in eyelid kinematics. *Invest Ophthalmol Vis Sci*. 1997;38(1):92-99.

116. Chew CK, Hykin PG, Jansweijer C, Dikstein S, Tiffany JM, Bron AJ. The casual level of meibomian lipids in humans. *Curr Eye Res*. 1993;12(3):255-259. doi:10.3109/02713689308999471

117. McMonnies CW, Ho A. Patient history in screening for dry eye conditions. *J Am Optom Assoc*. 1987;58(4):296-301.

118. Aliò J, Padron M. Influence of age on the temperature of the anterior segment of the eye. Measurements by infrared thermometry. *Ophthalmic Res*. 1982;14(3):153-159. doi:10.1159/000265187

119. Age and Gender Effects on the Normal Tear Film | SpringerLink. Accessed January 24, 2025. https://link.springer.com/chapter/10.1007/978-1-4615-5359-5_57

120. Guillon M, Maïssa C. Tear film evaporation--effect of age and gender. *Contact Lens Anterior Eye J Br Contact Lens Assoc*. 2010;33(4):171-175. doi:10.1016/j.clae.2010.03.002

121. Mathers WD, Lane JA, Zimmerman MB. Tear film changes associated with normal aging. *Cornea*. 1996;15(3):229-234. doi:10.1097/00003226-199605000-00001

122. Wolkoff P, Skov P, Franck C, Petersen LN. Eye irritation and environmental factors in the office environment--hypotheses, causes and a physiological model. *Scand J Work Environ Health*. 2003;29(6):411-430. doi:10.5271/sjweh.748

123. Girardin F, Orgül S, Erb C, Flammer J. Relationship between corneal temperature and finger temperature. *Arch Ophthalmol Chic Ill 1960*. 1999;117(2):166-169. doi:10.1001/archopht.117.2.166

124. Truong S, Cole N, Stapleton F, Golebiowski B. Sex hormones and the dry eye. *Clin Exp Optom*. 2014;97(4):324-336. doi:10.1111/cxo.12147

125. Sullivan DA, Sullivan BD, Ullman MD, et al. Androgen influence on the meibomian gland. *Invest Ophthalmol Vis Sci*. 2000;41(12):3732-3742.

126. Sullivan DA, Yamagami H, Liu M, et al. Sex steroids, the meibomian gland and evaporative dry eye. *Adv Exp Med Biol*. 2002;506(Pt A):389-399. doi:10.1007/978-1-4615-0717-8_56

127. Sullivan BD, Evans JE, Dana MR, Sullivan DA. Impact of androgen deficiency on the lipid profiles in human meibomian gland secretions. *Adv Exp Med Biol*. 2002;506(Pt A):449-458. doi:10.1007/978-1-4615-0717-8_63

128. Okun MS, McDonald WM, DeLong MR. Refractory nonmotor symptoms in male patients with Parkinson disease due to testosterone deficiency: a common unrecognized comorbidity. *Arch Neurol*. 2002;59(5):807-811. doi:10.1001/archneur.59.5.807

129. Sullivan BD, Evans JE, Dana MR, Sullivan DA. Influence of aging on the polar and neutral lipid profiles in human meibomian gland secretions. *Arch Ophthalmol Chic Ill 1960*. 2006;124(9):1286-1292. doi:10.1001/archopht.124.9.1286

130. Suzuki T, Schirra F, Richards SM, Jensen RV, Sullivan DA. Estrogen and progesterone control of gene expression in the mouse meibomian gland. *Invest Ophthalmol Vis Sci*. 2008;49(5):1797-1808. doi:10.1167/iovs.07-1458

131. Azzi L, El-Alfy M, Labrie F. Gender differences and effects of sex steroids and dehydroepiandrosterone on androgen and oestrogen alpha receptors in mouse sebaceous glands. *Br J Dermatol*. 2006;154(1):21-27. doi:10.1111/j.1365-2133.2005.06847.x

132. Wickham LA, Gao J, Toda I, Rocha EM, Ono M, Sullivan DA. Identification of androgen, estrogen and progesterone receptor mRNAs in the eye. *Acta Ophthalmol Scand*. 2000;78(2):146-153. doi:10.1034/j.1600-0420.2000.078002146.x

133. Esmaeli B, Harvey JT, Hewlett B. Immunohistochemical evidence for estrogen receptors in meibomian glands. *Ophthalmology*. 2000;107(1):180-184. doi:10.1016/s0161-6420(99)00040-8

134. Sullivan DA, Jensen RV, Suzuki T, Richards SM. Do sex steroids exert sex-specific and/or opposite effects on gene expression in lacrimal and meibomian glands? *Mol Vis*. 2009;15:1553-1572.

135. Richards SM, Jensen RV, Liu M, et al. Influence of sex on gene expression in the mouse lacrimal gland. *Exp Eye Res*. 2006;82(1):13-23. doi:10.1016/j.exer.2005.04.014

136. Tomlinson A, Pearce EI, Simmons PA, Blades K. Effect of oral contraceptives on tear physiology. *Ophthalmic Physiol Opt J Br Coll Ophthalmic Opt Optom*. 2001;21(1):9-16.

137. Chen SP, Massaro-Giordano G, Pistilli M, Schreiber CA, Bunya VY. Tear osmolarity and dry eye symptoms in women using oral contraception and contact lenses. *Cornea*. 2013;32(4):423-428. doi:10.1097/ICO.0b013e3182662390

138. Imhof RE, De Jesus MEP, Xiao P, Ciortea LI, Berg EP. Closed-chamber transepidermal water loss measurement: microclimate, calibration and performance. *Int J Cosmet Sci*. 2009;31(2):97-118. doi:10.1111/j.1468-2494.2008.00476.x

139. Abusharha AA, Al Yami A, Alsreea K, et al. Repeatability and Reproducibility of Tear Film Evaporation Rate Measurement using a new Closed-Chamber Evaporimeter. doi:10.2174/1874364102115010117

140. Rogiers V, EEMCO Group. EEMCO guidance for the assessment of transepidermal water loss in cosmetic sciences. *Skin Pharmacol Appl Skin Physiol*. 2001;14(2):117-128. doi:10.1159/000056341

141. Creasey NH, Battensby J, Fletcher JA. Factors affecting the permeability of skin. The relation between in vivo and in vitro observations. *Curr Probl Dermatol*. 1978;7:95-106.

142. Langmuir I. The Condensation and Evaporation of Gas Molecules. *Proc Natl Acad Sci U S A*. 1917;3(3):141-147. doi:10.1073/pnas.3.3.141

143. Hardy JD. Physiology of temperature regulation. *Physiol Rev*. 1961;41:521-606. doi:10.1152/physrev.1961.41.3.521

144. (PDF) In vivo transepidermal water loss: Validation of a new multi-sensor open chamber water evaporation system Tewameter TM Hex. *ResearchGate*. Published online March 1, 2025. doi:10.1111/srt.13307

145. Mohd Ariffin NH, Hasham R. Assessment of non-invasive techniques and herbal-based products on dermatological physiology and intercellular lipid properties. *Heliyon*. 2020;6(5):e03955. doi:10.1016/j.heliyon.2020.e03955

146. Cohen JC, Hartman DG, Garofalo MJ, et al. Comparison of closed chamber and open chamber evaporimetry. *Skin Res Technol Off J Int Soc Bioeng Skin ISBS Int Soc Digit Imaging Skin ISDIS Int Soc Skin Imaging ISSI*. 2009;15(1):51-54. doi:10.1111/j.1600-0846.2008.00334.x

147. Jeon HS, Youn SW, Jeon HE, Kim JH, Hyon JY. Assessment of Transepidermal Water Loss From the Ocular Area in Dry Eye Disease. *Invest Ophthalmol Vis Sci*. 2016;57(11):4831-4836. doi:10.1167/iovs.16-20109

148. Fluhr JW, Darlenski R. Transepidermal Water Loss (TEWL). In: Berardesca E, Maibach HI, Wilhelm KP, eds. *Non Invasive Diagnostic Techniques in Clinical Dermatology*. Springer; 2014:353-356. doi:10.1007/978-3-642-32109-2_32

149. Gaudenzi D, Mori T, Crugliano S, et al. AS-OCT and Ocular Hygrometer as Innovative Tools in Dry Eye Disease Diagnosis. *Appl Sci*. 2022;12(3):1647. doi:10.3390/app12031647

150. Trees GR, Tomlinson A. Effect of artificial tear solutions and saline on tear film evaporation. *Optom Vis Sci Off Publ Am Acad Optom*. 1990;67(12):886-890. doi:10.1097/00006324-199012000-00002

151. Nuutinen J, Alanen E, Autio P, Lahtinen MR, Harvima I, Lahtinen T. A closed unventilated chamber for the measurement of transepidermal water loss. *Skin Res Technol Off J Int Soc Bioeng Skin ISBS Int Soc Digit Imaging Skin ISDIS Int Soc Skin Imaging ISSI*. 2003;9(2):85-89. doi:10.1034/j.1600-0846.2003.00025.x

152. Goto E, Endo K, Suzuki A, Fujikura Y, Matsumoto Y, Tsubota K. Tear Evaporation Dynamics in Normal Subjects and Subjects with Obstructive Meibomian Gland Dysfunction. *Invest Ophthalmol Vis Sci*. 2003;44(2):533-539. doi:10.1167/iovs.02-0170

153. Rohit A, Ehrmann K, Naduvilath T, Willcox M, Stapleton F. Validating a new device for measuring tear evaporation rates. *Ophthalmic Physiol Opt J Br Coll Ophthalmic Opt Optom*. 2014;34(1):53-62. doi:10.1111/opo.12096

154. McCann LC, Tomlinson A, Pearce EI, Diaper C. Tear and meibomian gland function in blepharitis and normals. *Eye Contact Lens*. 2009;35(4):203-208. doi:10.1097/ICL.0b013e3181a9d79d

155. Peng CC, Cerretani C, Li Y, et al. Flow Evaporimeter To Assess Evaporative Resistance of Human Tear-Film Lipid Layer. *Ind Eng Chem Res*. 2014;53(47):18130-18139. doi:10.1021/ie5030497

156. Abusharha AA, Pearce EI, Fagehi R. Effect of Ambient Temperature on the Human Tear Film. *Eye Contact Lens*. 2016;42(5):308-312. doi:10.1097/ICL.0000000000000210

157. Arciniega JC, Wojtowicz JC, Mohamed EM, McCulley JP. Changes in the evaporation rate of tear film after digital expression of meibomian glands in patients with and without dry eye. *Cornea*. 2011;30(8):843-847. doi:10.1097/ICO.0b013e31820cd291

158. Bilkhu P, Wolffsohn J, Purslow C. Provocation of the ocular surface to investigate the evaporative pathophysiology of dry eye disease. *Contact Lens Anterior Eye J Br Contact Lens Assoc*. 2021;44(1):24-29. doi:10.1016/j.clae.2020.03.014

159. Alanazi SA, Abusharha A, Fagehi R, et al. Assessment of the Tear Evaporation Rate in Chronic Smokers Using Delfin VapoMeter. *Int J Ophthalmol Vis Sci*. 2019;4(2):37-41. doi:10.11648/j.ijovs.20190402.12

160. Siddireddy JS, Tan J, Vijay AK, Willcox MDP. The Effect of Microblepharon Exfoliation on Clinical Correlates of Contact Lens Discomfort. *Optom Vis Sci Off Publ Am Acad Optom*. 2019;96(3):187-199. doi:10.1097/OPX.0000000000001354

161. Alghamdi WM, Markoulli M, Holden BA, Papas EB. Impact of duration of contact lens wear on the structure and function of the meibomian glands. *Ophthalmic Physiol Opt J Br Coll Ophthalmic Opt Optom*. 2016;36(2):120-131. doi:10.1111/opo.12278

162. Abusharaha A, Alturki AA, Alanazi SA, et al. Assessment of tear-evaporation rate in thyroid-gland patients. *Clin Ophthalmol Auckl NZ*. 2019;13:131-135. doi:10.2147/OPTH.S188614

163. Cedarstaff TH, Tomlinson A. A comparative study of tear evaporation rates and water content of soft contact lenses. *Am J Optom Physiol Opt*. 1983;60(3):167-174. doi:10.1097/00006324-198303000-00004

164. Liu DTS, Di Pascuale MA, Sawai J, Gao YY, Tseng SCG. Tear film dynamics in floppy eyelid syndrome. *Invest Ophthalmol Vis Sci*. 2005;46(4):1188-1194. doi:10.1167/iovs.04-0913

165. Craig JP, Chen YH, Turnbull PRK. Prospective trial of intense pulsed light for the treatment of meibomian gland dysfunction. *Invest Ophthalmol Vis Sci*. 2015;56(3):1965-1970. doi:10.1167/iovs.14-15764

166. Wang MTM, Cho ISH, Jung SH, Craig JP. Effect of lipid-based dry eye supplements on the tear film in wearers of eye cosmetics. *Contact Lens Anterior Eye J Br Contact Lens Assoc*. 2017;40(4):236-241. doi:10.1016/j.clae.2017.03.001

167. McCulley JP, Shine WE, Aronowicz J, Oral D, Vargas J. Presumed hyposecretory/hyperevaporative KCS: tear characteristics. *Trans Am Ophthalmol Soc*. 2003;101:141-152; discussion 152-154.

168. Tomlinson A, Cedarstaff TH. Tear evaporation from the human eye: the effects of contact lens wear. *J Br Contact Lens Assoc*. 1982;5(4):141-144,146-147. doi:10.1016/S0141-7037(82)80012-8

169. Rolando M, Refojo MF, Kenyon KR. Increased tear evaporation in eyes with keratoconjunctivitis sicca. *Arch Ophthalmol Chic Ill 1960*. 1983;101(4):557-558. doi:10.1001/archopht.1983.01040010557003

170. Craig JP, Singh I, Tomlinson A, Morgan PB, Efron N. The role of tear physiology in ocular surface temperature. *Eye*. 2000;14(4):635-641. doi:10.1038/eye.2000.156

171. Kawali AA. Thermography in ocular inflammation. *Indian J Radiol Imaging*. 2013;23(03):281-283. doi:10.1055/s-0041-1734381

172. Purslow C, Wolffsohn J. The relation between physical properties of the anterior eye and ocular surface temperature. *Optom Vis Sci*. 2007;84(3). doi:10.1097/OPX.0b013e3180339f6e

173. Itokawa T, Okajima Y, Suzuki T, et al. Association among Blink Rate, Changes in Ocular Surface Temperature, Tear Film Stability, and Functional Visual Acuity in Patients after Cataract Surgery. *J Ophthalmol*. 2019;2019(1):8189097. doi:10.1155/2019/8189097

174. Zeev MSB, Miller DD, Latkany R. Diagnosis of dry eye disease and emerging technologies. *Clin Ophthalmol*. 2014;8:581-590. doi:10.2147/OPTH.S45444

175. Su TY, Ho WT, Lu CY, Chang SW, Chiang HK. Correlations among ocular surface temperature difference value, the tear meniscus height, Schirmer's test and fluorescein tear

film break up time. *Br J Ophthalmol*. 2015;99(4):482-487. doi:10.1136/bjophthalmol-2014-305183

176. Mapstone R. Measurement of corneal temperature. *Exp Eye Res*. 1968;7(2). doi:10.1016/S0014-4835(68)80073-9

177. Ring EF. Progress in the measurement of human body temperature. *IEEE Eng Med Biol Mag Q Mag Eng Med Biol Soc*. 1998;17(4):19-24. doi:10.1109/51.687959

178. Purslow C, Wolffsohn JS. Ocular surface temperature: a review. *Eye Contact Lens*. 2005;31(3):117-123. doi:10.1097/01.icl.0000141921.80061.17

179. Tan L, Cai ZQ, Lai NS. Accuracy and sensitivity of the dynamic ocular thermography and inter-subjects ocular surface temperature (OST) in Chinese young adults. *Contact Lens Anterior Eye J Br Contact Lens Assoc*. 2009;32(2):78-83. doi:10.1016/j.clae.2008.09.003

180. Mapstone R. Ocular thermography. *Br J Ophthalmol*. 1970;54(11):751-754. doi:10.1136/bjo.54.11.751

181. Chan TCY, Wan KH, Shih KC, Jhanji V. Advances in dry eye imaging: the present and beyond. *Br J Ophthalmol*. 2018;102(3):295-301. doi:10.1136/bjophthalmol-2017-310759

182. Mapstone R. Determinants of corneal temperature. *Br J Ophthalmol*. 1968;52(10):729-741. doi:10.1136/bjo.52.10.729

183. Mapstone R. Normal thermal patterns in cornea and periorbital skin. *Br J Ophthalmol*. 1968;52(11):818-827. doi:10.1136/bjo.52.11.818

184. The transmission of infra-red rays by the media of the eye and the transmission of radiant energy by crookes and other glasses. *Proc R Soc Lond Ser B Contain Pap Biol Character*. 1915;89(610):58-76. doi:10.1098/rspb.1915.0026

185. Tan LL, Sanjay S, Morgan PB. Static and dynamic measurement of ocular surface temperature in dry eyes. *J Ophthalmol*. 2016;2016(1). doi:10.1155/2016/7285132

186. Kamao T, Yamaguchi M, Kawasaki S, Mizoue S, Shiraishi A, Ohashi Y. Screening for dry eye with newly developed ocular surface thermographer. *Am J Ophthalmol*. 2011;151(5):782-791. doi:10.1016/j.ajo.2010.10.033

187. Matteoli S, Favuzza E, Mazzantini L. Ocular surface temperature in patients with evaporative and aqueous-deficient dry eyes: a thermographic approach. *Physiol Meas*. 2017;38(8). doi:10.1088/1361-6579/aa78bd

188. Efron N, Young G, Brennan N. Ocular surface temperature. *Curr Eye Res*. 1989;8(9):901-906.

189. Morgan PB, Tullo AB, Efron N. Infrared thermography of the tear film in dry eye. *Eye*. 1995;9(5):615-618. doi:10.1038/eye.1995.149

190. Galassi F, Giambene B, Corvi A, Falaschi G. Evaluation of ocular surface temperature and retrobulbar haemodynamics by infrared thermography and colour Doppler imaging in patients with glaucoma. *Br J Ophthalmol*. 2007;91(7):878-881. doi:10.1136/bjo.2007.114397

191. Sodi A, Giambene B, Falaschi G, et al. Ocular surface temperature in central retinal vein occlusion: preliminary data. *Eur J Ophthalmol*. 2007;17(5):755-759. doi:10.1177/112067210701700511

192. Development of infrared thermal imager for dry eye diagnosis - Astrophysics Data System. Accessed March 4, 2025. https://ui.adsabs.harvard.edu/abs/2006SPIE.6294E..06C/abstract

193. Ng: Variations of ocular surface temperature with... - Google Scholar. Accessed March 4, 2025. https://scholar.google.com/scholar_lookup?title=Variations%20of%20ocular%20surface%20temperature%20with%20different%20age%20groups&publication_year=2008&author=E.Y.K.%20Ng&author=J.H.%20Tan&author=E.H.%20Ooi&author=C.%20Chee&author=U.R.%20Acharya

194. Morgan PB, Soh MP, Efron N, Tullo AB. Potential applications of ocular thermography. *Optom Vis Sci*. 1993;70(7). doi:doi:10.1097/00006324-199307000-00008

195. Zelichowska B, Rózycki R, Tłustochowicz M, Kujawa A, Kalicki B, Murawski P. [The usefulness of thermography in the diagnostics of dry eye syndrome]. *Klin Oczna*. 2005;107(7-9):483-487.

196. Singh G, Bhinder HS. Comparison of noncontact infrared and remote sensor thermometry in normal and dry eye patients. *Eur J Ophthalmol*. 2005;15(6):668-673.

197. Chiang HK, Chen CY, Cheng HY, Chen KH, Chang DO. Development of infrared thermal imager for dry eye diagnosis. 2006;6294:629406. doi:10.1117/12.678421

198. Su TY, Chiang HK, Hwa CK. Noncontact detection of dry eye using a custom designed infrared thermal image system. *J Biomed Opt*. 2011;16(4). doi:10.1117/1.3562964

199. Kottaiyan R, Yoon G, Wang Q, Yadav R, Zavislan JM, Aquavella JV. Integrated multimodal metrology for objective and noninvasive tear evaluation. *Ocul Surf*. 2012;10(1):43-50. doi:10.1016/j.jtos.2011.12.001

200. Klamann MKJ, Maier AKB, Gonnermann J, Klein JP, Pleyer U. Measurement of dynamic ocular surface temperature in healthy subjects using a new thermography device. *Curr Eye Res*. 2012;37(8):678-683. doi:10.3109/02713683.2012.674610

201. Su TY, Chang SW, Yang CJ, Chiang HK. Direct observation and validation of fluorescein tear film break-up patterns by using a dual thermal-fluorescent imaging system. *Biomed Opt Express*. 2014;5(8):2614-2619. doi:10.1364/BOE.5.002614

202. Gonnermann J, Maier AKB, Klein JP, Bertelmann E, Pleyer U, Klamann MKJ. Evaluation of ocular surface temperature in patients with pterygium. *Curr Eye Res*. 2014;39(4):359-364. doi:10.3109/02713683.2013.844262

203. Azharuddin M, Bera SKr, Datta H, Dasgupta AKr. Thermal fluctuation based study of aqueous deficient dry eyes by non-invasive thermal imaging. *Exp Eye Res*. 2014;120:97-102. doi:10.1016/j.exer.2014.01.007

204. Acharya UR, Tan JH, Vidya S, et al. Diagnosis of response and non-response to dry eye treatment using infrared thermography images. *Infrared Phys Technol*. 2014;67:497-503. doi:10.1016/j.infrared.2014.09.011

205. Zhang A, Maki KL, Salahura G, et al. Thermal analysis of dry eye subjects and the thermal impulse perturbation model of ocular surface. *Exp Eye Res*. 2015;132:231-239. doi:10.1016/j.exer.2015.01.021

206. Versura P, Giannaccare G, Fresina M, Campos EC. Subjective Discomfort Symptoms Are Related to Low Corneal Temperature in Patients With Evaporative Dry Eye. *Cornea*. 2015;34(9):1079. doi:10.1097/ICO.0000000000000512

207. Matteoli S, Finocchio L, Biagini I, et al. A thermographic study on eyes affected by Age-related Macular Degeneration: Comparison among various forms of the pathology and analysis of risk factors. *Infrared Phys Technol*. 2016;76:402-407. doi:10.1016/j.infrared.2016.03.016

208. Sudarshan VK, Koh JEW, Acharya UR, et al. Evaluation of Evaporative Dry Eye Disease Using Thermal Images of Ocular Surface Regions with DWT and Gabor Transform. In: Ng EY, Etehadtavakol M, eds. *Application of Infrared to Biomedical Sciences*. Springer; 2017:359-375. doi:10.1007/978-981-10-3147-2_20

209. Matteoli S, Coppini D, Corvi A. A novel image processing procedure for thermographic image analysis. *Med Biol Eng Comput*. 2018;56(10):1747-1756. doi:10.1007/s11517-018-1800-9

210. Matteoli S, Vannetti F, Sodi A, Corvi A. Infrared thermographic investigation on the ocular surface temperature of normal subjects. *Physiol Meas*. 2020;41(4). doi:10.1088/1361-6579/ab6b48

211. Acharya UR, Ng EYK, Yee GC, Hua TJ, Kagathi M. Analysis of normal human eye with different age groups using infrared images. *J Med Syst*. 2009;33(3):207-213. doi:10.1007/s10916-008-9181-5

212. A Novel Method for Eye Contour Extraction from Blurred Infrared Images | Request PDF. In: *ResearchGate*. doi:10.1109/IHMSC.2016.84

213. Kricancic H, McNeill H, Titze M, Alonso-Caneiro D, Collins MJ. Instrument for simultaneous assessment of fluorescein and thermal dynamics of the tear film. conference

presented at: 2017 ARVO ASIA Meeting (including Translational Vision Summit); February 2017; Brisbane, Australia. Accessed March 4, 2025. https://eprints.qut.edu.au/105600/

214. Bidaki EZ, Wong A, Murphy PJ. A novel system for ocular surface temperature measurement and tracking. *IEEE Access*. 2023;11:140893-140899. doi:10.1109/ACCESS.2023.3341354

215. Craig JP, Nichols KK, Akpek EK, et al. TFOS DEWS II Definition and Classification Report. *Ocul Surf*. 2017;15(3):276-283. doi:10.1016/j.jtos.2017.05.008

216. Jones L, Downie LE, Korb D, et al. TFOS DEWS II Management and Therapy Report. *Ocul Surf*. 2017;15(3):575-628. doi:10.1016/j.jtos.2017.05.006

217. Wong S. Examination of Contact Lenses and Dry Eye Using Evaporimetry. Published online January 14, 2022. Accessed April 28, 2025. http://hdl.handle.net/10012/17879

218. Tiffany JM. The viscosity of human tears. *Int Ophthalmol*. 1991;15(6):371-376. doi:10.1007/BF00137947

219. Mishima S, Gasset A, Klyce SD Jr, Baum JL. Determination of Tear Volume and Tear Flow. *Invest Ophthalmol Vis Sci*. 1966;5(3):264-276.

220. Semp DA, Beeson D, Sheppard AL, Dutta D, Wolffsohn JS. Artificial Tears: A Systematic Review. *Clin Optom*. 2023;15:9-27. doi:10.2147/OPTO.S350185

221. Labetoulle M, Benitez-del-Castillo JM, Barabino S, et al. Artificial Tears: Biological Role of Their Ingredients in the Management of Dry Eye Disease. *Int J Mol Sci*. 2022;23(5):2434. doi:10.3390/ijms23052434

222. Abusharha A, Shbear AA, Fagehi R, et al. Assessment of the Efficiency of HP-Guar and hyaluronic Acid Tear Supplements to Control Tear Film Evaporation Rate in Dry Eye Subjects. doi:10.2174/1874364102115010299

223. Lemp MA, Foulks GN. The definition and classification of dry eye disease. *Ocul Surf*. 2007;5:75-92.

224. Kwok LS. Calculation and application of the anterior surface area of a model human cornea. *J Theor Biol*. 1984;108(2):295-313. doi:10.1016/s0022-5193(84)80072-7

225. Shah AM, Galor A. Impact of ocular surface temperature on tear characteristics: current insights. *Clin Optom*. 2021;13:51-62. doi:10.2147/OPTO.S281601

226. Aragona P, Benítez-Del-Castillo JM, Coroneo MT, et al. Safety and Efficacy of a Preservative-Free Artificial Tear Containing Carboxymethylcellulose and Hyaluronic Acid for Dry Eye Disease: A Randomized, Controlled, Multicenter 3-Month Study. *Clin Ophthalmol Auckl NZ*. 2020;14:2951-2963. doi:10.2147/OPTH.S256480

227. Song JK, Lee K, Park HY, et al. Efficacy of Carboxymethylcellulose and Hyaluronate in Dry Eye Disease: A Systematic Review and Meta-Analysis. *Korean J Fam Med*. 2017;38(1):2-7. doi:10.4082/kjfm.2017.38.1.2

228. Lee JH, Ahn HS, Kim EK, Kim T im. Efficacy of Sodium Hyaluronate and Carboxymethylcellulose in Treating Mild to Moderate Dry Eye Disease. *Cornea*. 2011;30(2):175. doi:10.1097/ICO.0b013e3181e9adcc

229. Schuerer N, Stein E, Inic-Kanada A, et al. Implications for Ophthalmic Formulations: Ocular Buffers Show Varied Cytotoxic Impact on Human Corneal-Limbal and Human Conjunctival Epithelial Cells. *Cornea*. 2017;36(6):712-718. doi:10.1097/ICO.0000000000001199

230. Paugh JR, Nguyen AL, Huang P, Hwang JS. Retention and retention of effect of topical formulations in dry eye subjects. *Optom Vis Sci Off Publ Am Acad Optom*. 2008;85(9):873-879. doi:10.1097/OPX.0b013e318185279d

231. Garrigue JS, Amrane M, Faure MO, Holopainen JM, Tong L. Relevance of Lipid-Based Products in the Management of Dry Eye Disease. *J Ocul Pharmacol Ther*. 2017;33(9):647-661. doi:10.1089/jop.2017.0052

232. Bai Y, Ngo W, Khanal S, Nichols JJ. Characterization of the Thickness of the Tear Film Lipid Layer in Meibomian Gland Dysfunction using High Resolution Optical Microscopy. *Ocul Surf*. 2022;24:34-39. doi:10.1016/j.jtos.2021.12.011

233. Foulks GN. The Correlation Between the Tear Film Lipid Layer and Dry Eye Disease. *Surv Ophthalmol*. 2007;52(4):369-374. doi:10.1016/j.survophthal.2007.04.009

234. CALMO® Eye Spray. CANDORVISION. Accessed March 14, 2025. https://www.candorvision.com/calmo-eye-spray

235. Xu X, Li G, Zuo YY. Effect of Model Tear Film Lipid Layer on Water Evaporation. *Invest Ophthalmol Vis Sci*. 2023;64(1):13. doi:10.1167/iovs.64.1.13

236. Pult H, Khatum FS, Trave-Huarte S, Wolffsohn JS. Effect of Eye Spray Phospholipid Concentration on the Tear Film and Ocular Comfort. *Eye Contact Lens*. 2021;47(8):445-448. doi:10.1097/ICL.0000000000000788

237. Walther H, Chan VW, Phan CM, Jones LW. Modelling non-invasive tear break-up times of soft lenses using a sophisticated in vitroblink platform. *Invest Ophthalmol Vis Sci*. 2019;60(9):6328.

238. King-Smith PE, Nichols JJ, Braun RJ, Nichols KK. High resolution microscopy of the lipid layer of the tear film. *Ocul Surf*. 2011;9(4):197-211.

239. Tomlinson A, Khanal S, Ramaesh K, Diaper C, McFadyen A. Tear film osmolarity: determination of a referent for dry eye diagnosis. *Invest Ophthalmol Vis Sci*. 2006;47(10):4309-4315. doi:10.1167/iovs.05-1504

240. Tomlinson A, Bron AJ, Korb DR, et al. The international workshop on meibomian gland dysfunction: report of the diagnosis subcommittee. *Invest Ophthalmol Vis Sci*. 2011;52(4):2006-2049. doi:10.1167/iovs.10-6997f

241. Koo TK, Li MY. A Guideline of Selecting and Reporting Intraclass Correlation Coefficients for Reliability Research. *J Chiropr Med*. 2016;15(2):155-163. doi:10.1016/j.jcm.2016.02.012

242. García-Porta N, Gantes-Nuñez FJ, Tabernero J, Pardhan S. Characterization of the ocular surface temperature dynamics in glaucoma subjects using long-wave infrared thermal imaging. *J Opt Soc Am A Opt Image Sci Vis*. 2019;36(6):1015-1021. doi:10.1364/JOSAA.36.001015

243. Tan LL, Sanjay S, Morgan PB. Repeatability of infrared ocular thermography in assessing healthy and dry eyes. *Contact Lens Anterior Eye*. 2016;39(4):284-292. doi:10.1016/j.clae.2016.01.010

244. Su TY, Ho WT, Chiang SC, Lu CY, Chiang HK, Chang SW. Infrared thermography in the evaluation of meibomian gland dysfunction. *J Formos Med Assoc*. 2017;116(7):554-559. doi:10.1016/j.jfma.2016.09.012

245. Portello JK, Rosenfield M, Chu CA. Blink rate, incomplete blinks and computer vision syndrome. *Optom Vis Sci*. 2013;90(5). doi:10.1097/OPX.0b013e31828f09a7

246. Alio J, Padron M. *Norm Var Thermogr Pattern Orbito-Ocul Reg*. 1982;51(2):93-98.

247. Fielder AR, Winder AF, Sheraidah GA, Cooke ED. Problems with corneal arcus. *Trans Ophthalmol Soc U K*. 1981;101(1):22-26.

248. Itokawa T, Okajima Y, Suzuki T. Association between ocular surface temperature and tear film stability in soft contact lens wearers. *Invest Ophthalmol Vis Sci*. 2018;59(2):771-775. doi:10.1167/iovs.17-23173

249. Purslow C, Wolffsohn JS, Santodomingo-Rubido J. The effect of contact lens wear on dynamic ocular surface temperature. *Contact Lens Anterior Eye*. 2005;28(1):29-36. doi:10.1016/j.clae.2004.10.001

250. Billingham SA, Whitehead AL, Julious SA. An audit of sample sizes for pilot and feasibility trials being undertaken in the United Kingdom registered in the United Kingdom Clinical Research Network database. *BMC Med Res Methodol*. 2013;13(1):104. doi:10.1186/1471-2288-13-104

251. Teresi JA, Yu X, Stewart AL, Hays RD. Guidelines for Designing and Evaluating Feasibility Pilot Studies. *Med Care*. 2022;60(1):95-103. doi:10.1097/MLR.0000000000001664

252. Tan JH, Ng EYK, Acharya UR. Evaluation of topographical variation in ocular surface temperature by functional infrared thermography. *Infrared Phys Technol*. 2011;54(6):469-477. doi:10.1016/j.infrared.2011.07.010

253. Vannetti F, Matteoli S, Finocchio L. Relationship between ocular surface temperature and peripheral vasoconstriction in healthy subjects: A thermographic study. *Proc Inst Mech Eng H*. 2014;228(3):297-302. doi:10.1177/0954411914523755

254. Cohen GY, Ben-David G, Singer R. Ocular surface temperature: characterization in a large cohort of healthy human eyes and correlations to systemic cardiovascular risk factors. *Diagnostics*. 2021;11(10). doi:10.3390/diagnostics11101877

255. Whitehead AL, Julious SA, Cooper CL, Campbell MJ. Estimating the sample size for a pilot randomised trial to minimise the overall trial sample size for the external pilot and main trial for a continuous outcome variable. *Stat Methods Med Res*. 2016;25(3):1057-1073. doi:10.1177/0962280215588241

256. Tiffany JM. The Lipid Secretion of the Meibomian Glands. In: Paoletti R, Kritchevsky D, eds. *Advances in Lipid Research*. Vol 22. Elsevier; 1987:1-62. doi:10.1016/B978-0-12-024922-0.50005-9

257. Pansell T, Porsblad M, Abdi S. The effect of vertical gaze position on ocular tear film stability. *Clin Exp Optom*. 2007;90:176-181.

258. Tsubota K, Nakamori K. Effects of Ocular Surface Area and Blink Rate on Tear Dynamics. *Arch Ophthalmol*. 1995;113(2):155-158. doi:10.1001/archopht.1995.01100020037025

259. Purslow C, Wolffsohn J. The relation between physical properties of the anterior eye and ocular surface temperature. *Optom Vis Sci*. Published online 2007. doi:10.1097/OPX.0b013e3180339f6e

260. Craig JP, Singh I, Tomlinson A, Morgan PB, Efron N. The role of tear physiology in ocular surface temperature. *Eye*. Published online 2000. doi:10.1038/eye.2000.156

Appendices

Appendix A

UNIVERSITY OF WATERLOO

Notification of Ethics Clearance to Conduct Research with Human Participants

---

Principal Investigator: Paul J Murphy (School of Optometry and Vision Science)

Student investigator: Naeimeh Monfared (School of Optometry and Vision Science)

File #: 44425

Title: Human tear evaporation rate assessment using evaporimetry and thermography

---

The Clinical Research Ethics Board is pleased to inform you this study has been reviewed and given ethics clearance.

Initial Approval Date: 11/16/22 (m/d/y)

University of Waterloo Research Ethics Boards are composed in accordance with, and carry out their functions and operate in a manner consistent with, the institution's guidelines for research with human participants, the Tri-Council Policy Statement for the Ethical Conduct for Research Involving Humans (TCPS, 2nd edition), International Conference on Harmonization: Good Clinical Practice (ICH-GCP), the Ontario Personal Health Information Protection Act (PHIPA), the applicable laws and regulations of the province of Ontario. Both Boards are registered with the U.S. Department of Health and Human Services under the Federal Wide Assurance, FWA00021410, and IRB registration number IRB00002419 (HREB) and IRB00007409 (CREB).

This study is to be conducted in accordance with the submitted application and the most recently approved versions of all supporting materials.

Expiry Date: 11/17/23 (m/d/y)

Multi-year research must be renewed at least once every 12 months unless a more frequent review has otherwise been specified. Studies will only be renewed if the renewal report is received and approved before the expiry date. Failure to submit renewal reports will result in the investigators being notified ethics clearance has been suspended and Research Finance being notified the ethics clearance is no longer valid.

Level of review: Delegated Review

Signed on behalf of the Clinical Research Ethics Board



Heather Root, Senior Manager, Ethics, heather.root@uwaterloo.ca, 519-888-4567, ext. 41469

This above named study is to be conducted in accordance with the submitted application and the most recently approved versions of all supporting materials.

Documents reviewed and received ethics clearance for use in the study and/or received for information:

file: Vaseline Safety Data Sheet_Version1_07072022.PDF

file: Study completion & Renumeration form_Version1_13102022.pdf

file: Soothe Restore package insert_Version1_27062022.pdf

file: CALMO Package Insert_Version 1_ 20220622.pdf

file: Consent Letter_Version3_11162022.pdf

file: letter of appreciation_Version 3_11162022.pdf

file: Recruitment Advertisement_Version 2_19102022.pdf

file: Poster_Version2_11162022.pdf

file: List of variables_ version1_20220530.pdf

file: List of variables_ version1_20220530.pdf

file: Demographic and Medical History_Version1_14102022.pdf

file: Eligibility Checklist_Version2_11162022.pdf

file: OCULUS Keratograph 5M User Manual_Version1_20220622.pdf

file: LipiView II User Manual_Version 1_ 20220622.pdf

file: Murphy - Evaporimeter eye glasses - July 5, 2022.pdf

file: BULLDOG Evaporimetry SOP 01aug2019 signed - Copy.pdf

file: BULLDOG Safety Office Email Approval 01aug2019.pdf

file: BULLDOG Goggle Volume SOP 01aug2019 signed.pdf

file: Thermocular Camera Saftey form_version1_ 20072022.pdf

file: Standard Operatin Procedure for thermal camera_Version 1_ 20220808.pdf

Approved Protocol Version 3 in Research Ethics System

This is an official document. Retain for your files.

You are responsible for obtaining any additional institutional approvals that might be required to complete this study.

Appendix B

UNIVERSITY OF WATERLOO

Notification of Ethics Clearance to Conduct Research with Human Participants

---

Principal Investigator: Paul J Murphy

Student investigator: Mana Monfared

File #: 46626

Title: Optimizing Blinking Patterns for Accurate Ocular Surface Temperature Measurement Using Research IR Application.

The Clinical Research Ethics Board is pleased to inform you this study has been reviewed and given ethics clearance.

Initial Approval Date: 07/08/24 (m/d/y)

University of Waterloo Research Ethics Boards are composed in accordance with, and carry out their functions and operate in a manner consistent with, the institution's guidelines for research with human participants, the Tri-Council Policy Statement for the Ethical Conduct for Research Involving Humans (TCPS2 2022), the Ontario Personal Health Information Protection Act (PHIPA), and all laws and regulations of the province of Ontario (as applicable). Additionally, CREB operates in a manner consistent with the International Conference for Harmonization of Technical Requirements for Pharmaceuticals for Human Use (ICH) Guidance E6(R2): Good Clinical Practice , the International Organization for Standardization of Good Clinical Practices (GCP) as set out by ISO 14155 - Clinical investigation of medical devices for human subjects, Part C, Division 5 of the Food and Drug Regulations, Part 4 of the Natural Health Products Regulations, Part 3 of the Medical Devices Regulations. Both Boards are registered with the U.S. Department of Health and Human Services under the Federal Wide Assurance, FWA00021410, and IRB registration number IRB00002419 (HREB) and IRB00007409 (CREB).

Expiry Date: 07/09/25 (m/d/y)

Multi-year research must be renewed at least once every 12 months unless a more frequent review has otherwise been specified. Studies will only be renewed if the renewal report is received and approved before the expiry date. Failure to submit renewal reports will result in the investigators being notified ethics clearance has been suspended and Research Finance being notified the ethics clearance is no longer valid.

Level of review: Delegated Review

Signed on behalf of the Clinical Research Ethics Board



Heather Root, Senior Manager, Ethics, heather.root@uwaterloo.ca, 519-888-4567, ext. 41469

This above-named study is to be conducted in accordance with the submitted application and the most recently approved versions of all supporting materials.

Documents reviewed and received ethics clearance for use in the study and/or received for information:

file: ThermOcular SOP Version 1 20220808.pdf

file: ThermOcular System Safety form 20072022.pdf

file: Poster_Version2_02072024.pdf

file: Eligibility checklist_Version2_08072024.pdf

file: Task Order_Version1_02072024.pdf

file: Information and Consent letter_Version2_02072024.pdf

file: Letter of apperciation_Version2_02072024.pdf

Approved Protocol Version 3 in Research Ethics System

This is an official document. Retain for your files.

You are responsible for obtaining any additional institutional approvals that might be required to complete this study.

Appendix C

Contact Lens and Anterior Eye 46 (2023) 101809

Contents lists available at ScienceDirect

Contact Lens and Anterior Eye

journal homepage: www.elsevier.com/locate/clae

Review article

Features and influences on the normal tear evaporation rate

Naeimeh Monfared *, Paul J. Murphy

School of Optometry and Vision Science, University of Waterloo, Waterloo, Canada

ARTICLE INFO

Keywords:
Tear evaporation rate
Tear film
Lipid layer
Dry eye
Tear stability

ABSTRACT

Tear evaporation is a normal physiological phenomenon that has an important role in regulating blink activity and tear production. An altered tear evaporation rate (TER) is a defining characteristic of evaporative dry eye disease (DED), and the measurement of tear evaporation is a useful clinical test for diagnosis. Reported values for a normal TER cover a broad range, which may be due to the influence of ocular, environmental, and systemic factors. For improved disease diagnosis, a fuller understanding of the normal TER range is essential. This paper reports on a literature review of the current knowledge of these normal influences on TER.

1. Introduction

It is estimated that between 5 and 35 % of the global population is affected by Dry Eye Disease (DED). This high prevalence imposes a substantial economic burden on society. For example, Yu et al estimated that DED in the USA costs approximately US$55 billion per year in societal costs (i.e., reduced productivity and indirect costs) [1]. The Tear Film and Ocular Surface Dry Eye Disease Workshop (TFOS DEWS II) has classified DED into three main types: evaporative, aqueous deficient, and mixed. The predominant type (over 86 %) is evaporative, caused by Meibomian Gland Dysfunction (MGD) [2]. The assessment of evaporation from the eye surface has been proposed as a key diagnostic criterion for DED [3].

The instruments available to measure evaporation can be divided into two groups: closed chamber and open chamber designs. Both designs rely on a humidity sensor(s) that measure the change in humidity within the chamber. Closed chamber designs can be unventilated or ventilated within a controlled environment, while open chamber designs are exposed to the ambient environment. Currently, the only commercially available evaporimeter is the Eye-VapoMeter (Delfin Technologies, Finland) [3]. The published literature has shown a wide range of normal tear evaporation rates (TER), partly due to inconsistencies in instrument methodology, and partly due to inconsistent study parameters and conditions. This was compounded by inconsistency in the units used to describe the TER. As a first step in clarifying the literature, Wong et al. recently produced updated tables of TER for normal and dry eyes that transforms all of the various measurements to a standard unit of $g/cm^2/sec$ [4]. With this analysis, the literature suggests that a healthy human adult TER varies between 4.07 and $15.6 \times 10^{-7} g/cm^2/sec$, when the ambient relative humidity is between 30 % and 40 %. While this result helps to make study results comparable, the wide range of values reported suggests that other factors are influencing the measurements.

As far as the authors are aware, no previous authors have completed a review of the literature on tear evaporation to identify the systemic, ocular, and environmental factors that influence normal TER, and which may be the source of some of the variation in normal TER reported by Wong et al. This review aims to provide a detailed examination of the factors that can influence TER.

2. Background

Evaporation is the process by which molecules from a liquid escape to the surrounding atmosphere by transitioning into a gas or vapour [5–7]. In this process, the molecule must have sufficient energy to break the inter-molecular bonds with its' neighbouring molecules at the liquid/gas interface and be released into the atmosphere [8]. Evaporation is a constant feature of all liquids, but the extent of evaporation is affected by the volatility of the liquid (the ease with which inter-molecular bonds are broken), the temperature of the liquid, the exposed surface area of the liquid, the presence of other substances in the liquid (which will alter the inter-molecular bond ratios), and the characteristics of the atmosphere directly above the liquid surface: presence/absence of gas, gas type, temperature, humidity, pressure, and presence of air movement [9–15]. The evaporation of a molecule from a liquid results in a reduction in the surface temperature of the liquid. In

* Corresponding author at: School of Optometry and Vision Science, University of Waterloo, 200 University Avenue West, Waterloo N2L 3G1, Canada.
E-mail address: nmonfared@uwaterloo.ca (N. Monfared).

https://doi.org/10.1016/j.clae.2022.101809
Received 13 May 2022; Received in revised form 23 December 2022; Accepted 28 December 2022
Available online 6 January 2023
1367-0484/© 2022 British Contact Lens Association. Published by Elsevier Ltd. All rights reserved.

response, heat is drawn into this cooler area by conduction from neighbouring molecules within the liquid. If the liquid is closely associated with a solid, then heat energy will also be drawn from the solid.

Evaporation from the tear film is a normal feature of the ocular surface/tear film physiological system, and it acts as a stimulus for tear aqueous production and basal eyelid blinking [16,17]. Evaporation produces localised cooling across the ocular surface, which then produces cooling in the underlying tissue (cornea and conjunctiva) [6,18]. This tissue cooling is detected by the sensory nerves across the ocular surface [19,20]. The localised cooling is part of the feedback loops for tear aqueous production and for normal, basal (unprovoked) blinking [16,21]. Alternatively, the evaporation may produce a localised increase in the osmolarity of the tear film. This relative hyperosmolarity may then be detected by ocular surface sensory nerves and act as the trigger for aqueous production and blinking [21,22].

3. Methods

A literature search was conducted for articles published on or before January 30, 2021. Only full text articles written in English were considered. Since the purpose of the search was to provide an overview of the process of evaporation in general, in the human body, and in the eye, the search terms included: "evaporation" plus "general", or "evaporation" plus "human body", or "evaporation" plus "eye", "tear evaporation rate" plus "tear break up time", or "tear evaporation rate" plus "tear film stability", "tear evaporation rate" plus "lipid layer", or "tear evaporation rate" plus "ocular surface size" or "tear evaporation rate" plus "ocular surface temperature" or "tear evaporation rate" plus "blink rate", or "tear evaporation rate" plus "ambient relative humidity", or "tear evaporation rate" plus "ambient temperature", or "tear evaporation rate" plus "airflow", or "tear evaporation rate" plus "age", or "tear evaporation rate" plus "gender", or "tear evaporation rate" plus "sex hormones". When several research papers reporting on similar findings appeared during the literature search, the most updated article (s) was typically used for review. Furthermore, the reference lists of recovered papers were used to identify articles missed during the primary search.

4. Factors affecting TER

TER measurement has been identified as an important clinical tool for the diagnosis and monitoring of treatment in subjects with DED symptoms [23,24]. The TFOS DEWS II Report on Dry Eye specifically mentions that reliable methods for measuring tear evaporation are needed [25]. It is therefore essential that both a firm understanding of what constitutes normal tear evaporation and those factors that can affect it are known, in order to understand when tear evaporation is abnormal.

4.1. Ocular factors

4.1.1. Tear film stability and quality

TER is strongly influenced by the tear film's stability and thickness, which is greatly determined by the intactness, confluency, and thickness of the lipid layer [26,27]. Since evaporation from the aqueous layer is restricted by the lipid layer, any thinning or removal of the lipid layer will permit increasing volume of water molecules to escape from the underlying aqueous layer, leading to thinning of the tear film and, eventually, tear break-up. Lipid layer thickness (LLT) is not consistent over the eye, and its appearance under a cold cathode light source (to produce specular reflection from the tear film) reveals these variations [25,28,29]. Lower tear film stability and higher TERs have been reported when no lipid layer is apparent or for thin LLT, whereas higher tear stability and lower TERs have been reported for thicker LLT [26,28,30].

4.1.2. Size of the exposed ocular surface area and eye gaze position

Generally, with a larger ocular surface area exposed to the atmosphere, there is a greater opportunity for more water molecules to escape to the air, and unless the ocular surface area is also considered, a higher overall TER will be recorded [29]. To correct for this effect, the surface area size is included in the TER calculation, as specified in the standard unit of measurement ($g/cm^2/sec$). Besides inherent eye size and palpebral aperture variations in the population, eye gaze position also has an effect. In eye up-gaze, as well as in a straight-ahead position, a larger portion of the eye surface is exposed to air, resulting in a x3.4 and x2.5 higher level of evaporation, respectively, than for an eye in down-gaze [31,32]. This benefit from down-gaze was confirmed by Nielsen et al., who found that lowering the eye-gaze angle by 25° produced a decrease in blink rate [33], an effect likely due to the reduction in exposed ocular surface area [34].

4.1.3. Ocular surface temperature (OST)

It has been suggested that an increase in ocular surface temperature (OST), which might be due to an increase in local or systemic body temperature [35,36], will lead to an increase in TER. Homeostatic OST is primarily determined by body temperature via the ocular blood supply [37,38]. Kessel et al. found that OST increased linearly with increasing body temperature up to 37 °C [35], and Purslow et al. reported that a 1 °C increase in body temperature results in 0.98 °C increase in OST [18]. It can be hypothesised that a warmer eye will provide additional heat energy to the water molecules in the tear film, permitting more to escape and so produce a higher TER. However, other researchers argue that a higher OST will enhance lipid layer mobility and enable a smoother flow of lipid over the aqueous layer, leading to a more stable tear film and less tear evaporation [39]. Dursch et al. argue that OST can provide a quantitative analysis for *in vivo* measurement of TER that is in good agreement with the literature [40], and Li et al. have argued that OST cooling between blinks assessment is an indirect method of tear evaporation measurement [41].

The rate of OST cooling is also linked to tear stability, another surrogate of tear evaporation. Efron et al. found that subjects with a slower OST cooling rate were more likely to have a longer inter-blink interval, a more stable tear film or a thicker tear film and a lower TER [42].

4.1.4. Blink rate

Basal blinking is a reflexive response to ocular surface cooling due to tear evaporation [43,44]. It is essential for maintaining a stable tear film [45], and can indirectly affect TER [46,47]. Blinking acts to spread the tear film over the eye surface and to reform a stable tear film. The new lipid layer thus formed impedes, but does not prevent, tear evaporation, and the localised cooling produced by the evaporation becomes the trigger for the next blink. If the blink-rate is insufficient to maintain a stable tear film for the full inter-blink period [48–50], there will be a cascading effect between the loss of tear stability and the increase in TER [51]. This situation may happen due to altered tear film stability caused by decreased lipid quantity or quality, or by an interruption in the normal blink rate [26]. A delay in blinking beyond the period of full tear stability across the ocular surface will prolong the period of water evaporation, and dry spots will develop if break-up occurs before the next blink. Blinking is also a stimulus for the release of meibum lipid from the meibomian glands with the upper and lower eyelids, which replenishes the supply of lipid to the superficial lipid layer [52]. A reduced blink rate will thus have a compounding effect on LLT resulting in a chronically-thinner lipid layer, and a likely increase in LLT variation across the ocular surface that promotes increased tear evaporation and tear film thinning [53,54].

A faster blink rate than normal can also increase TER, although its effect is greater at higher TERs [31,55]. This may be 'cause and effect' – a higher TER promotes a higher blink rate [56,57], but a higher blink rate may cause a greater release of aqueous from the lacrimal glands that increases the tear volume. In turn, this larger tear volume will be

gathered along the eyelid tear menisci, providing an additional source of water vapour during tear evaporation measurement [55].

Incomplete blinking may also increase TER by producing an uneven distribution of the tear film across the eye surface, and, in particular, not replenish the tear film over the inferior portion of the cornea [58]. This type of blinking is prevalent in patients with psychological fatigue or patients with prolonged work on VDUs [59,60]. To compensate for the effect of a reduced blink-rate, compulsory blinking could induce a thicker LLT by stimulation of lipid secretion from meibomian glands, as well as by spreading the lipid layer over the ocular surface. These have the effect of reducing TER [52,61]. Benedetto et al. found that forceful blinking results in a thicker central cornea tear film, while weak blinking reduces tear film thickness due to decreased lipid production and increased tear film evaporation [61].

4.2. Environmental factors

4.2.1. Ambient relative humidity (RH)

Relative humidity (RH) refers to the amount of water vapour present in the air at any specific temperature. This amount is expressed as a percentage of the maximum amount of water vapour the air is capable of containing at the same temperature. Therefore, evaporation is affected by the capacity of the air to absorb water. Air with high RH has a larger amount of water molecules and a limited capacity to absorb more. Air with low RH has a smaller amount of water and a higher capacity to absorb more. Consequently, in a low RH environment, evaporation will occur more easily and produce a higher evaporation rate, while the converse is true for a high RH environment. For tear evaporation, changes in RH will impact the TER [62,63]. McCulley et al. found that a 10 % decrease in RH resulted in an average increase of 28.33 % to 59.42 % in TER [64], and reducing the RH in an aircraft cabin from 40 to 45 % to 20–25 % increased the TER by 100 %, on average [65,66]. On the other hand, Madden et al. found that increasing RH to 70 % can reduce TER to almost zero [67].

Besides a direct effect on TER, RH may have an effect on lipid layer formation. Peng et al reported that an increase in RH up to 75 % could lead to a significant increase in tear BUT [68]. Korb et al. fitted dry eye patients with modified swimming goggles in which the right eye had a higher RH than the left eye. They found a significantly thicker lipid layer in the right eyes and a lower TER [69]. Conversely in low RH environments, such as airplane cabins, deserts, or cold/dry seasons, tear evaporation may increase more than expected and enhance any dry eye symptoms in subjects [65,70–72]. Peng et al. found that a decrease in RH from 30 % to 15 %, which is a representation of an airplane cabin environment, produced a reduction in tear BUT (from 33 to 28 s), indicating a higher TER. The aircraft cabin environment also has a reduced atmospheric pressure in the cabin (corresponding to 1.2–2 km above sea level), which will enable higher rates of evaporation from ocular surface, since there is a greater capacity within the air to absorb water vapour [65,73,74]. This combination of factors leads to an increased level of complaints of dry eye symptoms and the use of artificial tears among cabin crews when flying [73,75].

4.2.2. Ambient temperature

As mentioned above, ambient temperature plays a significant role in moderating RH. A higher ambient temperature will permit a higher volume of water vapour to be absorbed by the same volume of air, to produce a higher relative humidity. Abusharha et al. showed that for a constant RH of 40 %, created in a controlled environment chamber at different environmental temperatures (5, 10, 15, 20, and 25 °C), when ambient temperature was increased to 25 °C, or decreased to 5 °C, tear film stability was adversely affected, leading to an increase in TER [76].

In both temperature increase and temperature decrease, the lipid layer may also be affected. An increase in ambient temperature can promote greater lipid flow leading to an altered spread of lipid over the tear film. Alternatively, a colder ambient temperature may reduce lipid flow since the lipids found in the eye have a typical melting range of 19 °C to 40 °C [77,78], leading to a reduced lipid spread. It is also hypothesised that a more mobile lipid layer may promote lipid migration to, and interaction with, the tear film mucin layer, leading to a decrease in tear film stability and an increase in TER. Thus, chronic exposure to both very high and very low ambient temperatures may result in increased tear evaporation and dry eye symptoms [76,79–81]. For example, in a large study of patients with evaporative DED, van Setten et al. found that hot and cold weather aggravated symptoms in 42 % and 34 % of patients, respectively [82].

Abusharha et al. [76] also found that while decreasing the ambient temperature resulted in a thinner LLT, the TER decreased. They argued that the reduced ambient temperature produced a decrease in OST that inhibited the inner polar section of the lipid layer from migrating to the mucin layer, and thus the tear film became more stable [83]. In this situation, decreasing the ambient temperature will also reduce the capacity of the atmosphere to hold water, leading to less TER despite the existence of a thin lipid layer [84].

4.2.3. Airflow

Airflow over an evaporating surface will enhance the evaporation rate due to the effect that the air movement has on the local RH above the surface. Without airflow, the RH of the air close to the surface will be higher than the ambient humidity as the water evaporates, and since a higher RH decreases evaporation, the rate of evaporation will decrease. Diffusion of water molecules within the air will dissipate the increased humidity, but an airflow will more efficiently disperse the air with the higher RH and introduce air with a lower RH, so permitting a more rapid rate of evaporation. Borchman et al. showed a 10-fold increase in evaporation rate produced by a gentle stream of dry air at 25 °C [85]. Murakami found that a warm, dry wind that moves horizontally or downward across the ocular surface, will increase the evaporation rate significantly, leading to a decreased tear stability [86]. In healthy eyes, Wyon and Wyon found that exposure to high air velocity (1.0 m/s) for 30 min decreased tear film stability, while exposure to a lower air velocity of 0.5 m/s for 30 min did not result in significant differences [87].

4.3. Systemic factors

4.3.1. Time of day

Time of day may be another factor in TER measurement. LLT is greater in the morning than in the afternoon, due to overnight accumulation of oil on the lid margin and to increased meibum release from the eyelid glands just after wakening in the morning. This suggests there will be reduced evaporation from the tear film in the morning, or potentially more variability [88]. Wojtowicz and McCulley recommended measuring TER during the afternoon due to less fluctuation in their measurements in the afternoon compared to the morning [89]. This hypothesis is based on the assumption that meibum lipid is delivered to the lid margins when the terminal ducts within the eyelid glands are squeezed above a critical pressure. At night, while the lids are closed and there is no blinking, the ductal reservoirs expand due to the force of secretion. The oil accumulation in the ducts and acini of the eyelid glands is released upon waking with the resumption of blinking and the lipid level on the lid margins is temporarily raised above normal levels.

4.3.2. Age and sex

With increasing age, structural (anatomical) and functional (physiological) changes occur in both men and women. In particular, the blink rate, tear stability, and LLT all decrease. The decrease in blink rate may lead to an increase in TER, particularly if tear stability is also reduced [90]. Atrophy of meibomian gland acinar cells and hyper-keratinising of the ductal epithelium, alters meibum secretion in terms of their chemical composition, as well as lipid profile [91–93]. Sullivan et al. reported that aging in both sexes is accompanied by a significant increase in telangiectasia, meibomian gland orifice metaplasia, scurf, eyelid erythema,

Table 1
Factors affecting tear evaporation rate (TER) and their relationship with TER. (OST: Ocular Surface Temperature; NITBUT: Non-Invasive Tear Break-Up Time; RH: Relative Humidity; LLT: Lipid Layer Thickness; PBS: Phosphate Buffered Saline; MGD: Meibomian Gland Dysfunction; NIBUT: Non-Invasive Break-Up Time; CAIS: Complete Androgen Insensitivity Syndrome; OCP: Oral Contraceptive Pill; SANDE: Symptom Assessment iN Dry Eye; OSDI: Ocular Surface Disease Index).

Factor		Study	Year	Sample demographics	Results
Ocular	Tear film stability and quality	Tsubota and Yamada [29]	1992	60 (normal = 24, 29.4 ± 10.6 years; dry eye = 36, 52.1 ± 11.5 years)	Positive correlation between TER and lipid layer.
		Craig and Tomlinson [26]	1997	161 (13–85 years)	Negative correlation between lipid layer thickness and its stability and TER.
		Blackie et al. [27]	2009	137, 18–60 years (41.7 ± 15.5 years)	Negative correlation between lipid layer thickness and dry eye symptoms.
	Size of exposed ocular surface area	Tsubota and Yamada [29]	1992	60 (normal = 24, 29.4 ± 10.6 years; dry eye = 36, 52.1 ± 11.5 years)	Less blinking and eyes half open significantly decreased TER.
	Eye gaze position	Tsubota and Nakamori [31]	1995	15 (28.0 ± 3.9 years)	Higher TER in up-gaze, than in straight-ahead gaze and down-gaze.
		Pansell et al. [32]	2007	23 (21–36 years)	Lower TBUT in up-gaze due to an enlarged palpebral fissure height in this gaze.
		Nielsen et al. [33]	2008	10, 25–46 years (34.9 ± 7.2 years)	Lowering gaze angle by 25° decreased ocular surface area by 7 %.
	Ocular Surface Temperature (OST)	Purslow and Wolffsohn [18]	2007	25 (27.1 ± 3.8 years)	Changes in OST were correlated with changes in NITBUT, indicating higher TER in higher OST.
		Butovich et al. [39]	2010	2 (29 and 50 years of age)	Low temperature leads to stiffening of the tear film, which loses its ability to form continuous layers at the air–water interface, indicating higher TER in lower OST.
	Cooling rate of ocular surface	Craig et al. [5]	2000	21 (normal = 13, 19–32 years; dry eye = 8, 22–85 years)	Rapid cooling of the tear film in dry eyes related to reduced tear stability and increased TER.
		Li et al. [41]	2015	25 (18–27 years)	Areas of tear break-up and regions of ocular surface cooling were co-localised and positively correlated (r = 0.74).
	Blink rate	Tsubota and Nakamori [31]	1995	15 (28.0 ± 3.9 years)	When blink rate changed from 10 to 60 blinks/minute, TER did not change in individuals with TERs $> 7.8 \times 10^{-7}$ g/s/cm^2, but increased in those with a lower TER.
		Tan et al. [55]	2010	60 (age < 35 year = 30, 18.9 ± 0.8 years; age > 35 years = 30, 47 ± 8.4 years)	Higher corneal TER observed in > 35 years group with statistically significant lower blink rates.
	Blink style	Portello et al. [60]	2013	21 (21–29 years)	Positive correlation between total dry eye symptom score and percentage of incomplete blinks (p = 0.002).
		Wang et al. [58]	2018	154 (39 ± 14 years), (normal = 77, incomplete blinking = 77)	Participants exhibiting incomplete blinking had higher dry eye symptomology and poorer tear film parameters.
Environmental	RH	Abusharha and Pearce [62]	2013	12 (29.8 ± 3.3 years)	Higher TER in desiccating environment compared to normal environmental condition.
		McCulley et al. [63]	2006	29 (normal = 11, 42 ± 12 years; dry eye = 18, including 8 KCS, 60 ± 13 years, and 10 KCS + MGD, 63 ± 18 years)	TER Increased when RH decreased from 40 to 45 % to 20–25 % (p < 0.001). Similar change in all groups.
		McCulley et al. [64]	2006	47 (47.6 ± 20.4 years), (normal = 15, dry eye = 32)	When RH was reduced by 10 % from 35 % − 45 % to 25 % −35 %, TER increased by 28.33 % to 59.42 % on average.
		Uchiyama et al. [65]	2007	29 (normal = 11, 42 ± 12 years; dry eye = 18, including 9 KCS, 60 ± 13 years and 9 KCS + MGD, 63 ± 18 years)	A chance in RH from 20 to 25 % to 40–45 % produced a mean increase in TER for all study subjects of 99.72 % (P ≤ 0.001).
		Madden et al. [67]	2013	20 (normal = 10, 42.90 ± 14.11 years; dry eye = 10, 35 ± 18.67 years)	TER higher in dry eye group compared with normal subjects at 5 % or 40 % RH. TER inversely correlated with environmental RH between 5 and 70 %, with TER reduced to zero at 70 % RH in both groups.
		Korb et al. [69]	1996	13 dry eye (19–47 years)	LLT increased significantly within 5 mins of exposure to high RH (p < 0.0001). An increase in lipid layer thickness may lead to lower TER.
	Ambient temperature	Abusharha et al. [76]	2016	12 (29.4 ± 2.4 years)	Threefold increase in TER observed as ambient temperature increased from 5 to 25 °C (p = 0.00).
		Borchman et al. [85]	2009	1 (52-year-old white male)	Threefold increase in TER observed as ambient temperature increased from 5 to 25 °C in still air.
		van Setten et al. [82]	2016	738 patients with dry eye and/or Sjögren's syndrome (55.52 ± 9.33 years)	42 % reported heat as most important negative factor on dry eye symptoms. Cold weather aggravated dry eye sensation for 34 % of patients.
	Airflow	Borchman et al. [85]	2009	1 (52-year-old white male)	A stream of dry air over PBS raised evaporation rate c.10-fold to 31 ± 3 μm/min.
		Wyon and Wyon [87]	1987	41 (age range not reported)	Exposure of tear film to airflow of 1.0 m/s for 30 min caused a significant decrease in tear stability in healthy eyes. Exposure to airflow of 0.5 m/s for 30 min showed no significant change.
systemic	Time of Day	Tomlinson and Cedarstaff [88]	1992	9 (21–37 years)	TER is lowest on waking and rises within 2 h to a constant value for the rest of the day.
			2009	19 (40 ± 12 years)	

(continued on next page)

Table 1 (*continued*)

Factor	Study	Year	Sample demographics	Results
	Wojtowicz and McCulley [89]			Change in RH from 25 to 35 % to 35–45 % produced a higher TER for the lower RH in the morning ($p = 0.042$), but no change in the afternoon.
	Rohit et al. [3]	2014	15 (25.9 ± 4.4 years)	No change in TER with diurnal variation ($p = 0.85$) or for different days ($p = 0.65$).
Age	Sun et al. [90]	1997	40 (40–89 years)	Mean amplitude and peak velocity of blinks decreased with age for spontaneous blinks and, to a lesser extent, for voluntary blinks.
	Hykin and Bron [91]	1992	80 (5–87 years)	Higher incidence of MGD with ageing, which may contribute to higher TER.
	Pochi et al. [92]	1979	181 (40–79 years)	Decrease in sebaceous gland secretion with age in both males and females, which may contribute to higher TER.
	Sullivan et al. [94]	2006	Younger (37.3 ± 1.7 years) and older (70.1 ± 1.1 years) males (9–12 males per group) and younger (36.4 ± 2.4 years) and older (70.6 ± 3.1 years) females (7 females per group)	Aging in males and females accompanied by a significant decrease in neutral lipid profile and an increase in eyelid erythema, telangiectasia, sleeve and scurf, keratinisation, irregular posterior margins, meibomian gland orifice metaplasia, and meibomian gland secretion opacity, which may contribute to higher TER.
	Den et al. [96]	2006	177 (21–93 years)	Eyes with abnormal lid margin anatomy, hyposecretion of meibum, and meibomian gland dropout were seen in 26 (7.3 %), 46 (12.4 %), and 68 eyes (18.6 %), respectively, with a significant association between each finding and aging ($p < 0.0001$, $=0.0498$, and < 0.0001, respectively), which may contribute to higher TER.
	Tan et al. [55]	2010	60 (17–70 years)	TER in elder subjects was statistically higher than for younger subjects.
	Guillon and Maïssa [97]	2010	217 (18–83 years)	TER was higher in the older age group at 30 % and 40 % RH.
Sex	Guillon and Maïssa [97]	2010	217 (18–83 years)	TER was higher overall for females.
	Craig and Tomlinson [98]	1998	145 (35.8 ± 17.5 years, range: 13 to 75 years); 66 females and 79 males	No significant gender or age effects were found for TER, lipid layer characteristics, or tear production.
	Girardin et al. [99]	1999	266 (16–87 years)	Mean corneal temperature was 0.16 °C higher in males ($p = 0.002$).
Sex hormones	Tomlinson et al. [113]	2001	9 females using oral contraceptives (21–33 years old), 9 female controls	No effect on tear physiology was found for serum hormone changes induced by oral contraceptive use or by normal cyclic variations in healthy young females.
	Boga et al. [111]	2022	40 females (36.2 ± 4.0 years)	A greater oestradiol to testosterone (E2:T) ratio was associated with shorter NIBUT ($p = 0.04$), and lower progesterone (P4) was associated with greater ocular pain ($p = 0.01$).
	Sullivan et al. [107]	2002	Females with CAIS (n = 9, 40.4 ± 2.3 years), age-matched female (n = 9, 40.2 ± 3.0 years) and male controls (n = 10, 37.1 ± 1.5 years)	Androgen receptor dysfunction is associated with significant alterations in the appearance of numerous molecular species in the neutral and polar lipid fractions of meibomian gland secretions.
	Chen et al. [112]	2013	52 females using OCPs and 45 females not using any form of hormonal contraception (26.0 ± 3.7 years)	Although SANDE scores were significantly higher in subjects with OCP and recent contact lens use ($p < 0.01$), there were no significant differences in OSDI and tear osmolarity between the same subject groups. Tear osmolarity was not affected by OCP or contact lens use in young fmales. However, the combination of OCP use and contact lens wear may increase the severity of dry eye symptoms.
	Tomlinson et al. [113]	2001	18 females taking OCPs or age-matched controls (no medication) (21–33 years)	No significant differences for any tear parameters between Day 2 and Day 19 for either OCP users or controls, or in comparison of OCP users with controls. No effect on tear physiology found for serum hormone changes induced by OCP use or from normal cyclic variations in healthy young females.

irregular posterior margins, and meibomian gland secretion opacity [94]. Any accompanying age-related, eyelid disorder, such as a chronic blepharitis, could exacerbate this situation [91,94–96]. All of these effects can promote evaporation by disrupting lipid layer structure and composition. Indeed, Tan et al. evaluated TER using infrared thermography and found higher evaporation rates in older subjects than younger subjects [55].

In terms of sex, Guillon and Maissa reported a higher TER in women than men over 45 years of age [97], whereas Craig and Tomlinson found no relationship between TER and age or sex, and suggested that any potential increase in TER in older subjects is a result of pathological complications [98]. Another study reported OST as being higher (+0.16 °C) in male participants, which could be a trigger for higher TER in this sex [99]. As a result, the effect of sex on TER is still unclear.

4.3.3. Sex hormones

The gonads (ovaries or testes) and the adrenal glands produce and secrete steroid hormones called androgens, oestrogens, and progesterones into the bloodstream [100]. These sex hormones are known to affect meibomian gland function and alter lipid layer structure. These

changes are linked to an increase in evaporative dry eye, and thus are likely to produce an increase in the TER, although the mechanism has not been demonstrated yet [101]. Androgens can stimulate lipid secretion by the meibomian glands, and any deficiency in their production, due to aging, anti-androgen therapy, Complete Androgen Insensitivity Syndrome (CAIS), or some other disorder (e.g. Parkinson's disease), will adversely affect TER [94,102–107]. Females under 30 years old produce approximately-two-thirds as much androgen as males do [108,109]. Following menopause, the production of precursor steroids significantly decreases in both sexes, and women of menopausal age possess only 30 % of peak levels [108,109]. Differences in serum androgen levels between men and women may explain differences in meibomian gland secretions and lipid profiles [94].

The antagonist role of oestrogen against meibum secretion, and thus of developing a high TER, was investigated by Sullivan et al. [110]. This is compatible with the observation that the prevalence of evaporative dry eye signs and symptoms is higher than normal in post-menopausal women using oestrogen replacement therapy or during IVF (in vitro fertilisation) treatment [111]. However, there are some studies that argue the alteration in oestrogen and progesterone level will not change subjective symptoms and objective measurements, such as tear turnover rate, tear osmolarity, and tear stability, and thus TER [112,113].

5. Conclusion

As a natural physical phenomenon of any liquid, evaporation from the tear film is unavoidable. Evaporative fluid loss from the ocular surface have been incorporated as a key aspect of homeostasis, performing important roles in tear production and blinking. Research studies have shown that tear evaporation is altered in eye disease, and particularly for evaporative DED [155]. TER measurement has been proposed as a key clinical diagnostic tool for dry eye disease by the TFOS DEWS II report [3]. Cut-off diagnostic criteria for evaporative DED rely on the knowledge of what constitutes a normal TER, which, in turn, relies on precise TER measurement. The review by Wong et al. revealed the wide 'normal' range reported in the literature, which they attributed to the variety of methods used and the ocular and environmental conditions under which TER was measured [4]. If more precise measurements of TER are to be obtained, and thus a better diagnostic criterion established, a more consistent method of measurement is required involving better knowledge of instrument design and operation, and better understanding of the factors influencing TER measurement, and how to control for them.

This review has identified the main systemic, ocular, and environmental factors that can influence normal TER, and has reported on the current knowledge of their impact (Table 1). For some factors, such as RH and ambient temperature, the effect is well understood, while for others, such as time of day or blinking, the interaction is less clear. For these latter factors, a more careful investigation is required to assist in developing improved TER measurement. Suitable calibration curves should be developed to allow consistent comparison of TER in different ambient environments, while careful patient selection and data collection methods are also necessary.

6. Disclosure

The authors have no financial or proprietary interest in a product, method, or material described herein.

Funding

This research did not receive any specific grant from funding agencies in the public, commercial, or not-for-profit sectors.

Declaration of Competing Interest

The authors declare that they have no known competing financial interests or personal relationships that could have appeared to influence the work reported in this paper.

References

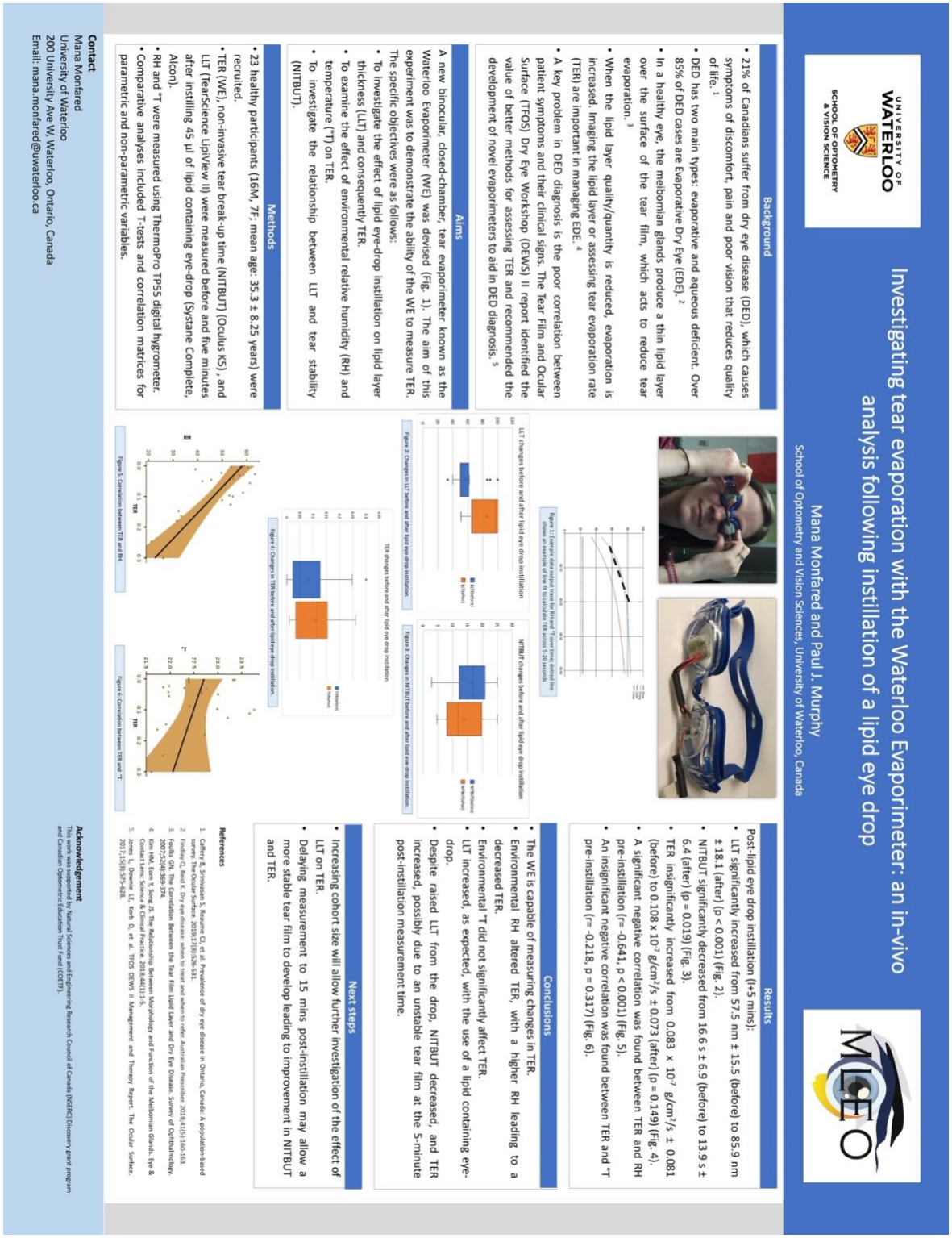
[1] Yu J, Asche CV, Fairchild CJ. The economic burden of dry eye disease in the United States: a decision tree analysis. Cornea 2011;30:379–87.
[2] Lemp MA, Crews LA, Bron AJ, Foulks GN, Sullivan BD. Distribution of aqueous-deficient and evaporative dry eye in a clinic-based patient cohort: a retrospective study. Cornea 2012;31:472–8.
[3] Rohit A, Ehrmann K, Naduvilath T, Willcox M, Stapleton F. Validating a new device for measuring tear evaporation rates. Ophthalmic Physiol Opt 2014;34(1):53–62.
[4] Wong S, Murphy PJ, Jones L. Tear evaporation rates: What does the literature tell us? Cont Lens Anterior Eye 2018;41(3):297–306.
[5] Craig JP, Singh I, Tomlinson A, Morgan PB, Efron N. The role of tear physiology in ocular surface temperature. Eye 2000;14(4):635–41.
[6] Tan J-H, Ng EYK, Rajendra Acharya U, Chee C. Infrared thermography on ocular surface temperature: a review. Infrared Phys Technol 2009;52(4):97–108.
[7] Girard F, Antoni M, Sefiane K. Infrared thermography investigation of an evaporating sessile water droplet on heated substrates. Langmuir 2010;26(7):4576–80.
[8] Nagata Y, Usui K, Bonn M. Molecular mechanism of water evaporation. Phys Rev Lett 2015;115:236102.
[9] Cunningham R, Brann Jr J, Fleming G. Factors affecting the evaporation of water from droplets in airblast spraying. J Econ Entomol 1962;55:192–9.
[10] Lurie M, Michailoff N. Evaporation from free water surface. Ind Eng Chem 1936;28(3):345–9.
[11] Davies JF, Haddrell AE, Reid JP. Time-resolved measurements of the evaporation of volatile components from single aerosol droplets. Aerosol Sci Tech 2012;46(6):666–77.
[12] Maatar A, Chikh S, Saada MA, Tadrist L. Transient effects on sessile droplet evaporation of volatile liquids. Int J Heat Mass Transf 2015;86:212–20.
[13] Galeev A, Salin A, Ponikarov S. Numerical simulation of evaporation of volatile liquids. J Loss Prev Process Indust 2015;38:39–49.
[14] Zhakhovskii VV, Anisimov SI. Molecular-dynamics simulation of evaporation of a liquid. JETP 1997;84(4):734–45.
[15] O'Hare KD, Spedding PL. Evaporation of a binary liquid mixture. Chem Engin J 1992;48(1):1–9.
[16] Ding J, Kim YH, Sarah MY, Graham AD, Li W, Lin MC. Ocular surface cooling rate associated with tear film characteristics and the maximum interblink period. Sci Rep 2021;11:15030.
[17] Tomlinson A, Trees GR, Occhipinti JR. Tear production and evaporation in the normal eye. Ophthalmic Physiol Opt 1991;11(1):44–7.
[18] Purslow C, Wolffsohn J. The relation between physical properties of the anterior eye and ocular surface temperature. Optom Vis Sci 2007;84:197–201.
[19] Gonzalez-Gonzalez O, Bech F, Gallar J, Merayo-Lloves J, Belmonte C. Functional properties of sensory nerve terminals of the mouse cornea. Invest Ophthalmol Vis Sci 2017;58:404–15.
[20] Gallar J, Pozo M, Tuckett R, Belmonte C. Response of sensory units with unmyelinated fibres to mechanical, thermal and chemical stimulation of the cat's cornea. J Physiol 1993;468:609–22.
[21] Hirata H, Meng ID. Cold-sensitive corneal afferents respond to a variety of ocular stimuli central to tear production: implications for dry eye disease. Invest Ophthalmol Vis Sci 2010;51:3969–76.
[22] Belmonte C, Aracil A, Acosta MC, Luna C, Gallar J. Nerves and sensations from the eye surface. Ocul Surf 2004;2(4):248–53.
[23] Foulks GN, Bron AJ. Meibomian gland dysfunction: a clinical scheme for description, diagnosis, classification, and grading. Ocul Surf 2003;1(3):107–26.
[24] Goto E, Endo K, Suzuki A, Fujikura Y, Matsumoto Y, Tsubota K. Tear evaporation dynamics in normal subjects and subjects with obstructive meibomian gland dysfunction. Invest Ophthalmol Vis Sci 2003;44:533–9.
[25] Wolffsohn JS, Arita R, Chalmers R, Djalilian A, Dogru M, Dumbleton K, et al. TFOS DEWS II diagnostic methodology report. Ocul Surf 2017;15(3):539–74.
[26] Craig JP, Tomlinson ALAN. Importance of the lipid layer in human tear film stability and evaporation. Optom Vis Sci 1997;74(1):8–13.
[27] Blackie CA, Solomon JD, Scaffidi RC, Greiner JV, Lemp MA, Korb DR. The relationship between dry eye symptoms and lipid layer thickness. Cornea 2009;28:789–94.
[28] Nichols KK, Foulks GN, Bron AJ, Glasgow BJ, Dogru M, Tsubota K, et al. The international workshop on meibomian gland dysfunction: executive summary. Invest Ophthalmol Vis Sci 2011;52(4):1922.
[29] Tsubota K, Yamada M. Tear evaporation from the ocular surface. Invest Ophthalmol Vis Sci 1992;33:2942–50.
[30] Lemp MA, Foulks GN. The definition and classification of dry eye disease. Ocul Surf 2007;5:75–92.
[31] Tsubota K, Nakamori K. Effects of ocular surface area and blink rate on tear dynamics. Arch Ophthalmol 1995;113:155–8.
[32] Pansell T, Porsblad M, Abdi S. The effect of vertical gaze position on ocular tear film stability. Clin Exp Optom 2007;90(3):176–81.

[33] Nielsen PK, Søgaard K, Skotte J, Wolkoff P. Ocular surface area and human eye blink frequency during VDU work: the effect of monitor position and task. Eur J Appl Physiol 2008;103(1):1–7.
[34] Nakamori K, Odawara M, Nakajima T, Mizutani T, Tsubota K. Blinking is controlled primarily by ocular surface conditions. Am J Ophthalmol 1997;124(1): 24–30.
[35] Kessel L, Johnson L, Arvidsson H, Larsen M. The relationship between body and ambient temperature and corneal temperature. Invest Ophthalmol Vis Sci 2010; 51:6593–7.
[36] Schwartz B. Environmental temperature and the ocular temperature gradient. Arch Ophthalmol 1965;74(2):237–43.
[37] Gugleta K, Orgül S, Flammer J. Is corneal temperature correlated with blood-flow velocity in the ophthalmic artery? Curr Eye Res 1999;19(6):496–501.
[38] Vogel B, Wagner H, Gmoser J, Wörner A, Löschberger A, Peters L, et al. Touch-free measurement of body temperature using close-up thermography of the ocular surface. MethodsX 2016;3:407–16.
[39] Butovich IA, Arciniega JC, Wojtowicz JC. Meibomian lipid films and the impact of temperature. Invest Ophthalmol Vis Sci 2010;51:5508–18.
[40] Dursch TJ, Li W, Taraz B, Lin MC, Radke CJ. Tear-film evaporation rate from simultaneous ocular-surface temperature and tear-breakup area. Optom Vis Sci 2018;95(1):5–12.
[41] Li W, Graham AD, Selvin S, Lin MC. Ocular surface cooling corresponds to tear film thinning and breakup. Optom Vis Sci 2015;92:e248–56.
[42] Efron N, Young G, Brennan NA. Ocular surface temperature. Curr Eye Res 1989;8: 901–6.
[43] Belmonte C, Nichols JJ, Cox SM, Brock JA, Begley CG, Bereiter DA, et al. TFOS DEWS II pain and sensation report. Ocul Surf 2017;15(3):404–37.
[44] Belmonte C, Gallar J. Cold thermoreceptors, unexpected players in tear production and ocular dryness sensations. Invest Ophthalmol Vis Sci 2011;52: 3888–92.
[45] Yap M. Tear break-up time is related to blink frequency. Acta Ophthalmol (Copenh) 1991;69:92–4.
[46] Fujishima H, Toda I, Yamada M, Sato N, Tsubota K. Corneal temperature in patients with dry eye evaluated by infrared radiation thermometry. Br J Ophthalmol 1996;80(1):29–32.
[47] **Mori A, Oguchi Y, Okusawa Y, Ono M, Fujishima H, Tsubota K. Use of high-speed, high-resolution thermography to evaluate the tear film layer. Am J Ophthalmol. 1997;124:729-35.**
[48] Golding TR, Bruce AS, Mainstone JC. Relationship between tear-meniscus parameters and tear-film breakup. Cornea 1997;16:649–61.
[49] Miller KL, Polse KA, Radke CJ. Black-line formation and the" perched" human tear film. Curr Eye Res 2002;25(3):155–62.
[50] Yee RW, Sperling HG, Kattek A, Paukert MT, Dawson K, Garcia M, et al. Isolation of the ocular surface to treat dysfunctional tear syndrome associated with computer use. Ocul Surf 2007;5(4):308–15.
[51] Blehm C, Vishnu S, Khattak A, Mitra S, Yee RW. Computer vision syndrome: a review. Surv Ophthalmol 2005;50(3):253–62.
[52] Korb DR, Baron DF, Herman JP, Finnemore VM, Exford JM, Hermosa JL, et al. Tear film lipid layer thickness as a function of blinking. Cornea 1994;13(4): 354–9.
[53] Wong H, Fatt I, Radke CJ. Deposition and thinning of the human tear film. J Colloid Interface Sci 1996;184(1):44–51.
[54] Aydemir E, Breward CJW, Witelski TP. The effect of polar lipids on tear film dynamics. Bull Math Biol 2011;73(6):1171–201.
[55] Tan J-H, Ng EYK, Acharya UR. Evaluation of tear evaporation from ocular surface by functional infrared thermography. Med Phys 2010;37(11):6022–34.
[56] Tsubota K, Hata S, Okusawa Y, Egami F, Ohtsuki T, Nakamori K. Quantitative videographic analysis of blinking in normal subjects and patients with dry eye. Arch Ophthalmol 1996;114:715–20.
[57] **Moore QL, De Paiva CS, Pflugfelder SC. Effects of dry eye therapies on environmentally induced ocular surface disease. Am J Ophthalmol. 2015;160: 135-42. e1.**
[58] Wang MTM, Tien L, Han A, Lee JM, Kim D, Markoulli M, et al. Impact of blinking on ocular surface and tear film parameters. Ocul Surf 2018;16(4):424–9.
[59] Kaneko K, Sakamoto K. Spontaneous blinks as a criterion of visual fatigue during prolonged work on visual display terminals. Percept Mot Skills 2001;92(1): 234–50.
[60] Portello JK, Rosenfield M, Chu CA. Blink rate, incomplete blinks and computer vision syndrome. Optom Vis Sci 2013;90:482–7.
[61] Benedetto DA, Clinch TE, Laibson PR. In vivo observation of tear dynamics using fluorophotometry. Arch Ophthalmol 1984;102(3):410–2.
[62] Abusharha AA, Pearce EI. The effect of low humidity on the human tear film. Cornea 2013;32:429–34.
[63] McCulley JP, Uchiyama E, Aronowicz JD, Butovich IA. Impact of evaporation on aqueous tear loss. Trans Am Ophthalmol Soc 2006;104:121.
[64] McCulley JP, Aronowicz JD, Uchiyama E, Shine WE, Butovich IA. Correlations in a change in aqueous tear evaporation with a change in relative humidity and the impact. Am J Ophthalmol 2006;141(4):758–60.
[65] Uchiyama E, Aronowicz JD, Butovich IA, McCulley JP. Increased evaporative rates in laboratory testing conditions simulating airplane cabin relative humidity: an important factor for dry eye syndrome. Eye Contact Lens 2007;33:174–6.
[66] Tsubota K. Tear dynamics and dry eye. Prog Retin Eye Res 1998;17(4):565–96.
[67] Madden LC, Tomlinson A, Simmons PA. Effect of humidity variations in a controlled environment chamber on tear evaporation after dry eye therapy. Eye Contact Lens 2013;39:169–74.
[68] Peng C-C, Cerretani C, Braun RJ, Radke C. Evaporation-driven instability of the precorneal tear film. Adv Colloid Interface Sci 2014;206:250–64.
[69] Korb DR, Greiner JV, Glonek T, Esbah R, Finnemore VM, Whalen AC. Effect of periocular humidity on the tear film lipid layer. Cornea 1996;15(2):129–34.
[70] Maruyama K, Yokoi N, Takamata A, Kinoshita S. Effect of environmental conditions on tear dynamics in soft contact lens wearers. Invest Ophthalmol Vis Sci 2004;45:2563–8.
[71] **González-García MJ, González-Sáiz A, De la Fuente B, de la Fuente B, Morilla-Grasa A, Mayo-Iscar A, et al. Exposure to a controlled adverse environment impairs the ocular surface of subjects with minimally symptomatic dry eye. Invest Ophthalmol Vis Sci. 2007;48:4026-32.**
[72] Hinninghofen H, Enck P. Passenger well-being in airplanes. Auton Neurosci 2006; 129(1-2):80–5.
[73] McCarty DJ, McCarty CA. Survey of dry eye symptoms in Australian pilots. Clin Exp Ophthalmol 2000;28(3):169–71.
[74] Rocher P, Fatt I. Hydrogel contact lenses. Optom Today 1995;35:18–22.
[75] Nagda NL, Koontz MD. Review of studies on flight attendant health and comfort in airliner cabins. Aviat Space Environ Med 2003;74:101–9.
[76] Abusharha AA, Pearce EI, Fagehi R. Effect of ambient temperature on the human tear film. Eye Contact Lens 2016;42:308–12.
[77] Bron AJ, Tiffany JM, Gouveia SM, Yokoi N, Voon LW. Functional aspects of the tear film lipid layer. Exp Eye Res 2004;78(3):347–60.
[78] Terada O, Chiba K, Senoo T, Obara Y. Ocular surface temperature of meibomia gland dysfunction patients and the melting point of meibomian gland secretions. Nippon Ganka Gakkai Zasshi 2004;108:690–3.
[79] Freeman R, Fatt I. Environmental influences on ocular temperature. Invest Ophthalmol Vis Sci 1973;12:596–602.
[80] Paschides C, Stefaniotou M, Papageorgiou J, Skourtis P, Psilas K. Ocular surface and environmental changes. Acta Ophthalmol Scand 1998;76:74–7.
[81] Zhong J-Y, Lee Y-C, Hsieh C-J, Tseng C-C, Yiin L-M. Association between dry eye disease, air pollution and weather changes in Taiwan. Int J Environ Res Public Health 2018;15:2269.
[82] van Setten G, Labetoulle M, Baudouin C, Rolando M. Evidence of seasonality and effects of psychrometry in dry eye disease. Acta Ophthalmol (Copenh) 2016;94 (5):499–506.
[83] Garai J. Physical model for vaporization. Fluid Phase Equilib 2009;283(1-2): 89–92.
[84] Gessert G. Measuring a medium's air space and water holding capacity. Ornamentals Northwest 1976;1:11–2.
[85] Borchman D, Foulks GN, Yappert MC, Mathews J, Leake K, Bell J. Factors affecting evaporation rates of tear film components measured in vitro. Eye Contact Lens 2009;35:32–7.
[86] Murakami S. Analysis and design of micro-climate around the human body with respiration by CFD. Indoor Air 2004;14(s7):144–56.
[87] Wyon N, Wyon D. Measurement of acute response to draught in the eye. Acta Ophthalmol (Copenh) 1987;65:385–92.
[88] Tomlinson A, H. Cedarstaff T. Diurnal variation in human tear evaporation. J Br Contact Lens Assoc 1992;15(2):77–9.
[89] Wojtowicz JC, McCulley JP. Assessment and impact of the time of day on aqueous tear evaporation in normal subjects. Eye Contact Lens 2009;35:117.
[90] Sun WS, Baker RS, Chuke JC, Rouholiman BR, Hasan SA, Gaza W, et al. Age-related changes in human blinks. Passive and active changes in eyelid kinematics. Invest Ophthalmol Vis Sci 1997;38:92–9.
[91] Hykin PG, Bron AJ. Age-related morphological changes in lid margin and meibomian gland anatomy. Cornea 1992;11(4):334–42.
[92] Pochi PE, Strauss JS, Downing DT. Age-related changes in sebaceous gland activity. J, Invest Dermatol 1979;73(1):108–11.
[93] Driver PJ, Lemp MA. Meibomian gland dysfunction. Surv Ophthalmol 1996;40 (5):343–67.
[94] Sullivan BD, Evans JE, Dana MR, Sullivan DA. Influence of aging on the polar and neutral lipid profiles in human meibomian gland secretions. Arch Ophthalmol 2006;124:1286–92.
[95] Mathers WD, Shields WJ, Sachdev MS, Petroll WM, Jester JV. Meibomian gland dysfunction in chronic blepharitis. Cornea 1991;10(4):277–85.
[96] Den S, Shimizu K, Ikeda T, Tsubota K, Shimmura S, Shimazaki J. Association between meibomian gland changes and aging, sex, or tear function. Cornea 2006; 25(6):651–5.
[97] Guillon M, Maissa C. Tear film evaporation—effect of age and gender. Cont Lens Anterior Eye 2010;33(4):171–5.
[98] Craig JP, Tomlinson A. Age and gender effects on the normal tear film. In: Lacrimal Gland, Tear Film, and Dry Eye Syndromes 2. Springer; 1998. p. 411–5.
[99] Girardin F, Orgül S, Erb C, Flammer J. Relationship between corneal temperature and finger temperature. Arch Ophthalmol 1999;117:166–9.
[100] Nussey SS, Whitehead SA. Endocrinology: an integrated approach. Oxford: BIOS Scientific Publishers; 2001.
[101] Truong S, Cole N, Stapleton F, Golebiowski B. Sex hormones and the dry eye. Clin Exp Optom 2014;97(4):324–36.
[102] Sullivan DA, Sullivan BD, Ullman MD, Rocha EM, Krenzer KL, Cermak JM, et al. Androgen influence on the meibomian gland. Invest Ophthalmol Vis Sci 2000;41: 3732–42.
[103] Knop E, Knop N, Millar T, Obata H, Sullivan DA. The international workshop on meibomian gland dysfunction: report of the subcommittee on anatomy, physiology, and pathophysiology of the meibomian gland. Invest Ophthalmol Vis Sci 2011;52:1938–78.

[104] Sullivan D, Yamagami H, Liu M, Steagall R, Schirra F, Suzuki T, et al. Sex steroids, the meibomian gland and evaporative dry eye. Lacrimal Gland, Tear Film, and Dry Eye Syndromes 3. Springer; 2002:389-99.
[105] Okun MS, McDonald WM, DeLong MR. Refractory nonmotor symptoms in male patients with Parkinson disease due to testosterone deficiency: a common unrecognized comorbidity. Arch Neurol 2002;59:807–11.
[106] Krenzer KL, Reza Dana M, Ullman MD, Cermak JM, Tolls DB, Evans JE, et al. Effect of androgen deficiency on the human meibomian gland and ocular surface. J Clin Endocr 2000;85:4874–82.
[107] Sullivan BD, Evans JE, Cermak JM, Krenzer KL, Dana MR, Sullivan DA. Complete androgen insensitivity syndrome: effect on human meibomian gland secretions. Arch Ophthalmol 2002;120:1689–99.
[108] Labrie F, Bélanger A, Cusan L, Gomez J-L, Candas B. Marked decline in serum concentrations of adrenal C19 sex steroid precursors and conjugated androgen metabolites during aging. J Clin Endocr 1997;82:2396–402.
[109] Labrie F. DHEA, important source of sex steroids in men and even more in women. Prog Brain Res 2010;182:97–148.
[110] Sullivan DA, Jensen RV, Suzuki T, Richards SM. Do sex steroids exert sex-specific and/or opposite effects on gene expression in lacrimal and meibomian glands? Mol Vis 2009;15:1553.
[111] Boga A, Stapleton F, Chapman M, Golebiowski B. Effects of elevated serum oestrogen on dry eye in women undergoing in vitro fertilisation. Invest Ophthalmol Vis Sci. 2022;63:1566–A0291-1566–A0291.
[112] Chen SP, Massaro-Giordano G, Pistilli M, Schreiber CA, Bunya VY. Tear osmolarity and dry eye symptoms in women using oral contraception and contact lenses. Cornea 2013;32:423.
[113] Tomlinson A, Pearce EI, Simmons PA, Blades K. Effect of oral contraceptives on tear physiology. Ophthalmic Physiol Opt 2001;21:9–16.

Appendix D

The poster presentation at ARVO 2024 (Seattle)



Optimizing Parameters for Ocular Surface Temperature Assessment Using ResearchIR® Software

Mana Monfared and Paul J. Murphy
School of Optometry and Vision Sciences, University of Waterloo, Canada

Abstract # 4232243

PURPOSE

Current methodologies for measuring ocular surface temperature (OST) using infrared (IR) thermography lack standardization, leading to poor reproducibility and inconsistent clinical utility.

This study aimed to optimize OST measurement by developing a **reliable, repeatable protocol** using **Teledyne FLIR IR A655sc** and **ResearchIR software**, focusing on:

1. Selection of the most robust temperature metric
2. Influence of **interblink interval (IBI)** on OST cooling dynamics
3. Impact of **measurement location** across the ocular surface
4. Value of **averaging versus single-point assessments** for reliability.

METHODS

Participants & Setup

- 7 healthy subjects (4 male, 3 female; mean age: 32.9 ± 11.7 years)
- IR thermography using Teledyne FLIR A655sc camera & ResearchIR v4.40 software
- 8 ocular surface sites (6 corneal, 2 scleral)

Blinking Protocol

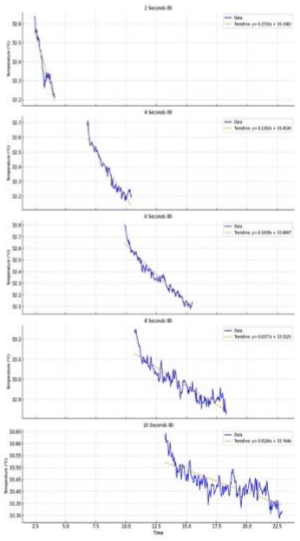
- 5 interblink intervals (IBIs): 2, 4, 6, 8, and 10 seconds
- 6 blinks per IBI
- 2-minute rest between each set

Analysis

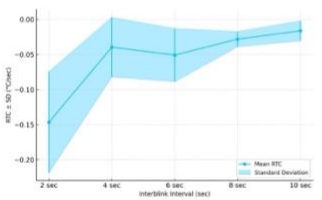
- Rate of Temperature Change (RTC) & Magnitude of Change (ΔT)
- One-way & two-way ANOVA to assess IBI & location effects
- Intraclass Correlation Coefficient (ICC) to evaluate reliability

	2 sec	4 sec	6 sec	8 sec	10 sec	F-Statistic (ANOVA)	p-Value (ANOVA)	Correlation
Mean RTC	-0.147 ± 0.072	-0.040 ± 0.042	-0.051 ± 0.038	-0.028 ± 0.011	-0.016 ± 0.014	10.89	< 0.001	0.168
Mean ΔT	-0.320 ± 0.159	-0.218 ± 0.174	-0.305 ± 0.191	-0.327 ± 0.167	-0.208 ± 0.191	0.75	0.566	- 0.184

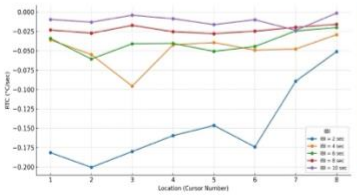
Mean RTC and ΔT (± SD) at the center of the cornea for different IBIs.



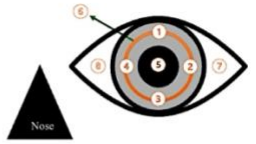
OST temperature traces at the center of the cornea for different IBIs.



Mean ± SD of RTC at the central cornea (Cursor 5) across interblink intervals.



Mean RTC for each IBI at each OST measurement location.



OST measurement locations: Superior Cornea (1), Temporal Cornea (2), Inferior Cornea (3), Nasal Cornea (4), and Central Cornea (5); Circular Central Region (average OST over a defined area) (6); Temporal Sclera (7), and Nasal Sclera (8).

RESULTS

- **RTC was more responsive than ΔT**, providing clearer temperature change trends across IBIs.
- **Cooling slowed as IBI increased**, with shorter intervals showing steeper RTC.
- **The 6-second IBI showed the most synchronized RTC across corneal sites,** supporting its suitability for standardization.
- **Corneal sites showed consistent RTC patterns**, while scleral regions- expectedly- displayed distinct thermal behavior.
- **Averaging improved reliability,** reducing variability across participants; ICC increased from 0.879 (1 measurement) to 0.911 (3 measurements).

CONCLUSIONS

- RTC is a more reliable OST metric than ΔT.
- A 6-second IBI balances comfort and consistency.
- Averaging enhances reliability, especially with select site combinations.
- **These findings support standardized OST protocols using IR thermography.**

References

1. Ding JE, Kim YH, Yi SM, Graham AD, Li W, Lin MC. Ocular surface cooling rate associated with tear film characteristics and the maximum interblink period. Sci Rep. 2021;11(1).
2. Tan LL, Sanjay S, Morgan PB. Repeatability of infrared ocular thermography in assessing healthy and dry eyes. Contact Lens Anterior Eye. 2016;39(4):284-292.
3. Mapstone R. Measurement of corneal temperature. Exp Eye Res. 1968;7(2).
4. Tan LL, Sanjay S, Morgan PB. Static and Dynamic Measurement of Ocular Surface Temperature in Dry Eyes. J Ophthalmol. 2016;2016(1).
5. Itokawa T, Okajima Y, Suzuki T. Association Between Ocular Surface Temperature and Tear Film Stability in Soft Contact Lens Wearers. Invest Ophthalmol Vis Sci. 2018;59(2):771-775.

Contact
Mana Monfared
University of Waterloo
200 University Ave W, Waterloo, Ontario, Canada
Email: mana.monfared@uwaterloo.ca

Acknowledgement
Research support was provided by the Natural Sciences and Engineering Research Council (NSERC) Discovery Horizons Grant (2024-00118).

Appendix F

School of Optometry and Vision Science
Faculty of Science

University of Waterloo
200 University Avenue West
Waterloo, Ontario, N2L 3G1
Canada

Tel 519-888-4567, ext. 33085
Fax 519-746-5977
optometry@uwaterloo.ca
www.optometry.uwaterloo.ca

Human tear evaporation rate assessment using evaporimetry and thermography

Information and Consent Letter

INFORMATION RELATED TO YOUR PARTICIPATION

Please note that your participation in this study does not replace the need for regular eye examinations

Attending regular eye examinations as recommended by your eye care professional (at least every two years) is essential to ensure that your eyes are healthy. Eye conditions such as glaucoma, diabetic retinopathy, cataracts, and macular disease can only be detected during a full eye examination. Only the front portion of the eye will be assessed during the initial screening visit of this study. This visit **should not** in any way replace any scheduled visits with your eye care practitioner. After completion of this study you should resume your regular eye care with your eyecare practitioner.

Title of Project
Human tear evaporation rate assessment using evaporimetry and thermography

Student Investigator
Mana Monfared, School of Optometry and Vision Science, T: (519)-888-4567 (ext. 37842),
nmonfared@uwaterloo.ca

Faculty Supervisor
Dr. Paul J. Murphy, PhD, School of Optometry and Vision Science, T: (519)-888-4567 (ext. 32020),
paul.murphy@uwaterloo.ca

Study Purpose
Approximately 40% of Canadians complain of dry eye symptoms. The most common type (86%) of dry eye is evaporative dry eye, which is caused by too much tear evaporation. When diagnosing dry eye, it is important to differentiate between the types of dry eye, to provide the best treatment. To help a clinician make that decision, it is important to be able to measure the tear evaporation. Tear evaporation can be measured in two ways using an evaporimeter or a thermal imaging camera.
In this study, the tear evaporation rate from each subject will be measured using the Waterloo Evaporimeter and the ThermOcular thermal imaging system. For each subject, the measurements from each instrument will be compared against each other, and with other measurements of the tear film on the eye. In addition, the thickness of the thin lipid layer on the eye, which has a natural role to reduce evaporation, will be altered by instilling very small quantities of lipid onto the surface of the eye. Increasing the lipid layer thickness should reduce the tear evaporation rate, and this will be a good test of the two instruments' ability to measure changes in tear evaporation.
By the end of the study, we will know more about how each instrument measures tear evaporation, how changes in lipid layer thickness affect tear evaporation, and how the results from these instruments compare with other methods for assessing the tear film. These new discoveries will help in diagnosing dry eye in the future.

Participation in this study
This study will involve up to 60 participants.
Participants will attend the School of Optometry and Vision Sciences (MLEO Lab) on one occasion.
To be eligible for this study, you must be at least 18 years. Your eye and general health eligibility will be determined at a screening visit.

You may be eligible for inclusion in this study if you:
a. Are at least 18 years of age and have full legal capacity to volunteer;
b. Have read and signed this information consent letter;
c. Are willing and able to follow instructions regarding the study procedures and visit, and maintain the appointment schedule;
d. Are willing to be awake for at least 2 hours before visit;
e. Are willing to not wear eye makeup on the day of visit;
f. Are willing to not use eye drops or artificial tears on the day of visit;
g. Meet the criteria for the study group classification.

You are not be eligible for the study if you;
a. Are presently participating in any ongoing clinical or research study;
b. Have any known active ocular disease and/or infection;
c. Have any general (systemic) condition that in the opinion of the investigator may affect the study measures;

d. Are using any medication (including medications applied directly to a part of the body, or eye drops) that,
in the opinion of the investigator, may affect the study measures;
f. Are aphakic;
g. Have had refractive error surgery;
h. Have undergone ocular surgery within the last 6 months;
i. Have a known sensitivity to Systane eye drops (including Systane Hydration, Systane Ultra, Systane Balance, Systane Original, Systane Complete, etc.) ;
k. Have a known sensitivity to petroleum jelly (Vaseline);
l. Have epilepsy and/or a sensitivity to flashing lights;
m. Have worn contact lenses on the day of the screening/data collection visit;
n. Have taken part in another clinical research study involving ocular drops or treatments within the last 14
days.

If you are determined to not be eligible for the study, you may be advised to see your healthcare professional, depending on the reason/s for ineligibility.

You have the following responsibilities as a research participant:
- Keep your study visit appointment and specific instructions provided to you by the study investigator.

If it is necessary to miss the appointment, please contact the study staff to reschedule as soon as you know you will miss the appointment.

- Tell the study investigator or study staff if you want to stop being in the study at any time.

Products used in this study
You will receive one drop of an artificial tear in one eye. The artificial tear drop used is Systane Complete (manufactured by Alcon) and is commercially available in Canada. This study does not involve contact lens wear.

Participation, Time Commitment, & Study Procedure:
Your participation in this study is purely voluntary and will involve 1 visit, scheduled according to your availability. The total time commitment for the study visit is estimated to be 1 hour. However, the total study time commitment can vary from participant to participant and may be a little longer if we need to retake measurements. Below is an outline of the procedure for this study.

Before Main Visit
Pre-screening will be conducted as part of subject recruitment. The information letter will be shared ahead of time, asking potential participants to carefully review the eligibility criteria and contact investigators if you have any questions. You will be screened to determine your eligibility at the start of the main visit with the general inclusion/exclusion criteria for the study: age range, tear supplement use, contact lens use, ocular health. Participants who meet these general criteria will be asked to attend for the Main Visit. You will be asked to prepare for the Main Visit by being awake for at least 2 hours and to not use any eye drops, or wear eye makeup, or wear contact lenses on the day of the Main Visit.

Main Visit
You will be asked to complete an informed consent form prior to any study measurements being conducted at the visit. Only after you have provided consent, will measurements be started. If you agree to participate in the study and you sign the consent letter, the study investigator will perform the procedures on the same

day. In appreciation for your assistance with our study, a prorated remuneration of $10 will be provided if you are ineligible, withdraw, or are discontinued. Please see the remuneration section for more details.

Main Study Measurements with and without Tear Supplement

Demographics: Participant demographics will be obtained from the participant, including age and sex (male, female) to describe the study population.
Health and medication questions: The participant will be asked about their current health, medical history, allergies, and medications. Information will be collected regarding any dry eye treatments the participant is currently using (i.e., name of eye drop, frequency of use, when it was last used, etc.).
You are asked to not wear any eye makeup or use any eye drops or artificial tears on the day of the visit or wear any contact lenses. A series of baseline measurements will be taken, followed by further measurements taken after the eye drop have been put in your eye.
At the end of the visit, the study completion forms will be signed, you will receive a cheque reimbursement and you will exit the study.

What is expected of you as a participant?
The following is a description of measurements that do not involve contact by the examiner, or by an instrument, or by the participant with your face. These measurements will be carried out on the day of visit:
Health and medication questions: You will be asked about your health, medical history, and the medications and supplements that you take.
Vision test: You will be asked to read a letter chart.
Tear film break-up time: You will be asked to hold your eyes open while looking into a device with an illuminated light. The light reflects off the tear film and the instrument measures when disturbances in the tear film first occur.
Tear film lipid layer thickness: The lipid layer is the outer layer of your tears. You will be asked to sit at an instrument that shines light onto the surface of your eye. You will be asked to look at a small spot of light while a series of blinking lights are reflected off the front surface of the eye. The instrument will then determine the thickness of the lipid layer by looking at the reflection of light from your eye. Please let the investigator know whether rapid blinking lights will cause discomfort or seizure.
Ocular Surface Temperature: You will be asked to look straight-ahead and blink normally, while the surface temperature of your eye will be recorded using a thermal camera.
Digital images of the eyes: Digital images will be taken of your eye. Any photographs will be labeled with an identification number and will not show any identifying features.

The following is a description of tests that require something to touch your face. These tests will be carried out at the day of visit.
Tear film evaporation rate: You will be asked to apply petroleum jelly onto the skin surrounding your eye prior to these measurements being taken. During the measurement, you will be asked to open your eyes and hold a pair of goggles over your eyes for approximately 20 seconds. You will look at a target and will be asked to blink when you hear a metronome. Sensors inside the goggle will record changes in the temperature and relative humidity. The measurements will be repeated for approximately 20 seconds while your eyes are closed.
Volume inside the goggle: You will be asked to wear a pair of swimming goggles and to keep your eyes closed. The swimming goggle will be filled with saline by the investigator, and the investigator will record the amount of saline added to the goggle to determine the amount of space inside the swimming goggle when against your face.

Risks associated with this study:

- A petroleum jelly (Vaseline) will be used in this study and applied to the skin surrounding the eye. Although rare, it is possible you may have an allergic reaction or experience temporary discomfort due

to the jelly, such as burning, stinging, or irritation. If you have a known allergy to petroleum jelly, please advise the investigator.

- It is possible that you may experience temporary discomfort associated with the study procedures (saline)/products (Systane eye drop/ devices including burning and stinging, blurred vision, sandiness or grittiness, light sensitivity, dryness, itching, crusty eyes, and foreign body sensation. Please advise the investigator if you are allergic to any eye drops.
- If the irritation persists for longer than a few hours, please contact the study investigator using the emergency contact number provided in this document. Additional visits will be arranged for you in the event of an adverse reason if you have a complaint or if the investigator believes it is in your best interest. Additional visits will occur until the adverse event is resolved.
- One instrument in this study uses rapidly blinking lights to image the tear film. Please inform the investigator if you have previously experienced discomfort and/or seizures due to rapidly blinking lights. Participants may experience temporary discomfort including blurred vision and light sensitivity.

Benefits associated with this study:

You may not benefit directly from the study.

This study may provide you with an opportunity to try marketed products that you may not have used previously.

This study may benefit optometric practitioners by expanding their knowledge of dry eye and the products available, allowing them to counsel their patients more effectively. This study may help MLEO to better understand the performance of the products being used in this study.

Remuneration:

In appreciation for your involvement in this study, you will receive $20 for your participation upon the completion of the study. The amount received is taxable, and it is your responsibility to report this amount for income tax purposes. In addition, we can provide you with a parking token to cover your parking expenses incurred on the day of your participation. Please Park in Lot OV next to the Optometry building. In appreciation for your assistance with our study, a prorated remuneration of $10 will be provided if you are ineligible, withdraw, or are discontinued.

Withdrawal from the Study:

You are free to decide whether you wish to participate in this study. It is important to note that your decision will in no way influence the eye care available to you at either the School of Optometry or with your own optometrist. You are also free to withdraw from the study at any time without penalty. To do so, please simply inform the student investigator, Mana Monfared, or the principal investigator, Dr. Paul J. Murphy that you no longer wish to proceed with the study. You may be removed from the study if you do not comply with the investigator's instructions, as given by the study protocol, or if the investigator has reason to believe that it is in your best interest. If you withdraw consent, you can also request the withdrawal of your data. Please note that it is not possible to withdraw your results once they have been published or otherwise disseminated.

Confidential and Security of Data:

All the information you provided as a participant, together with any data we collected because of your participation (including all the private health information, as well as our records of your participation in the study), will be remain confidential. In addition, disclosure will only occur when required by local, state, provincial, and federal laws, other regulations, or as explicitly outlined in the informed consent document. Moreover, as a participant, you were assigned an identification number to be used in place of your given name, and as such, this is the only identifying information on all study records. No identifying information will be released or published.

All records and data from this study will be retained for a minimum of 7 years. Paper copies of the study data will be stored safely in a storage cabinet located in a locked room (OPT 381) at the School of Optometry and Vision Science, University of Waterloo. They will only be made available to individuals involved in the data

collection or data analysis of this study. All electronic research data will be encrypted according to the guidelines outlined by the Information and Systems Technology. Any identifying information on the images obtained during the study will be removed and, together with the encrypted data, will be securely stored on a password-protected server in a locked office at the School of Optometry and Vision Science. Furthermore, these images may be shown to other researchers at the School of Optometry to explain data. They may also be shown publicly, as in the case of publications and presentations, but no identifying information will be disclosed. A list of the participants' names, their corresponding numbers, and any image data (which will be saved using a coding system whereby each code corresponds with a specific participant), will be stored in a separate file at the University of Waterloo. All the aforementioned study documents will only be accessible by individuals involved in the study. Records will be disposed in a confidential manner as given by the guidelines of the University. Interested parties can obtain more information about the policies on information security outlined by the University of Waterloo at the following website: https://uwaterloo.ca/secretariat-generalcounsel/policies-procedures-guidelines/policy-8. Any publications of your results will be de-identified and presented as group data.

Other important issues:

Should you have any questions regarding the study procedures please do not hesitate to contact the study investigator(s).

Your rights as a participant:

In the event that you are harmed as a direct result of your participation in this study, all the necessary medical and ocular treatment will be made available to you at no cost and will be covered by the School of Optometry and Vision Science.

Research-related injury:

If you sign this consent form, it does not release the investigators and/or institutions from their legal and professional responsibilities. Moreover, it does not mean that you have waived any legal rights you may have under law. As previously mentioned, if you are harmed as a direct result of taking part in this study, all the necessary medical treatment will be made available to you at no cost. If you have any urgent medical problems, injury, or illness, which are related to your participation in this study, or should you have any concerns or questions please call: Mrs. Monfared or Dr. Murphy by phone at (519)-888-4567 (ext. 37842), or (519)-888-4567 (ext. 32020), respectively. If neither of the researchers can be reached, please make an urgent appointment with an optometrist of your choice and if they are not available, please go to the emergency department at St. Mary's Hospital at 911 Queen's Boulevard, Kitchener, Ontario, Canada, N2M 1B2 (Telephone: (519)-744-3311).

Concerns or Questions about your participation:

If you have any questions about participation in this study, please do not hesitate to ask the researchers. Should you have additional questions later, please contact Mana Monfared via the email address listed at the beginning of this form. We would like to assure you that this study has been thoroughly reviewed by the University of Waterloo Research Ethics Committee and has received ethics clearance. The final decision to participate is purely yours. If you have any questions, comments, or concerns resulting from your participation in this study, please contact the Office of Research Ethics, at 1-519888-4567 ext. 36005 or reb@uwaterloo.ca. For all other queries contact Mrs. Monfared (nmonfared@uwaterloo.ca) or Dr. Paul Murphy (paul.murphy@uwaterloo.ca).

Declaration of Informed Consent

I have read the above description of the research study entitled "***Human tear evaporation rate assessment using evaporimetry and thermography***" prior to participating in it. I voluntarily agree to take part in this study, which is conducted by Mrs. Mana Monfared and Dr. Paul J. Murphy at the School of Optometry and Vision Sciences at the University of Waterloo. All the procedures, benefits, and risks were clearly explained to me in sufficient detail, and I have been given numerous opportunities to ask questions and gain further clarification about the study when needed.

I am aware that this study has been reviewed and received ethics clearance through a University Waterloo Research Ethics Board (REB [44425]). If I have questions for the Board, I should contact the Office of Research Ethics, at 1-519-888-4567 ext. 36005 or reb@uwaterloo.ca. For all other queries, I will contact Mrs. Monfared (nmonfared@uwaterloo.ca) or Dr. Paul Murphy (paul.murphy@uwaterloo.ca).

I understand that I may withdraw from this study at any point in time without penalty by simply advising the researchers. I understand that the investigator reserves the right to discontinue my participation from this study at any point in time if they have reason to believe that it is in my best interest, or if I fail to adhere to the protocol details of the study.

I understand that this study in no way replaces the need for regular eye examinations, and that regular eye examinations are essential to ensure that my eyes are healthy. I am aware of the importance of reporting to the investigators of any adverse events, or changes to my health or medication throughout the study.

I am aware that any data collected during the study will be kept secured in accordance with the University's policies. I understand that any images of my eye that are taken during this study are for educational purposes, and may be used in medical or scientific books, as well as journals or magazines.

With full knowledge of the study details, I agree, of my own free will to participate in this study. I give the investigators permission to collect, use, and disclose my personal health information, together with any study data obtained to individuals involved in the data collection or data analysis of this study. I acknowledge that I have received a copy of this information and consent form. By signing this consent form, I am not in any way waving my legal rights or releasing the investigators below from their legal and professional responsibilities.

_____ _____

Signature of participant Date

_____

Printed name of participant

_____ _____

Signature of person explaining consent Date

Appendix G

School of Optometry and Vision Science
Faculty of Science
University of Waterloo
200 University Avenue West
Waterloo, Ontario, N2L 3G1
Canada
Tel 519-888-4567, ext. 33085
Fax 519-746-5977
optometry@uwaterloo.ca
www.optometry.uwaterloo.ca

Optimizing Blinking Patterns for Accurate Ocular Surface Temperature Measurement Using Research IR Application.

Information and Consent Letter

INFORMATION RELATED TO YOUR PARTICIPATION

Please note that your participation in this study does not replace the need for regular eye examinations.

Attending regular eye examinations as recommended by your eye care professional (at least every two years) is essential to ensure that your eyes are healthy. Eye conditions such as glaucoma, diabetic retinopathy, cataracts, and macular disease can only be detected during a full eye examination. This visit **should not** in any way replace any scheduled visits with your eye care practitioner. After completion of this study, you should resume your regular eye care with your eyecare practitioner.

Title of Project

Optimizing Blinking Patterns for Accurate Ocular Surface Temperature Measurement Using Research IR Application.

Student Investigator

Mana Monfared, School of Optometry and Vision Science, T: (519)-888-4567 (ext. 37842), nmonfared@uwaterloo.ca

Faculty Supervisor

Dr. Paul J. Murphy, PhD, School of Optometry and Vision Science, T: (519)-888-4567 (ext. 32020), paul.murphy@uwaterloo.ca

Study Purpose

This study aims to investigate the effect of different interblink intervals on ocular surface temperature (OST) in healthy individuals. Blinking is crucial for maintaining tear film stability and ocular surface health. Variations in blinking patterns can impact OST, which is an important indicator of ocular health. By understanding these variations, we hope to enhance diagnostic accuracy and therapeutic strategies for ocular surface diseases.

Previous research indicates that abnormal blinking patterns are associated with conditions like dry eye disease, where increased tear evaporation leads to higher OST and discomfort. By systematically studying the relationship between interblink intervals and OST, we can identify optimal blinking patterns for maintaining a stable OST. This knowledge can improve diagnostic tools, inform clinical guidelines, and contribute to personalized treatment plans.

The findings from this study could lead to better management of ocular surface disorders, standardization of OST measurement practices, and advancements in ocular surface research. Ultimately, this research aims to improve eye care diagnostics and treatment, benefiting both patients and clinicians.

Participation in this study

To participate in this study, you must:

- Be at least 18 years old
- Have no known ocular diseases or conditions
- Be able to keep your eyes open for up to 10 seconds
- Be able not to use contact lenses during your visit.

Products used in this study

No product will be used in this study.

Participation, Time Commitment, & Study Procedure:

Your participation in this study is purely voluntary and will involve 1 visit, scheduled according to your availability. The total time commitment for the study visit is estimated to be **15 minutes**. However, the total study time commitment can vary from participant to participant and may be a little longer if we need to retake measurements.

Below is an outline of the procedure for this study.

- ***Consent:*** You will be asked to complete an informed consent form prior to any study measurements being conducted at the visit. Only after you have provided consent, will measurements be started. If you agree to participate in the study and you sign the consent letter, the study investigator will perform the procedures on the same day.
- ***Screening:*** We will first screen you to ensure you meet the eligibility criteria.

- ***Laboratory Visit:*** You will visit the Murphy Lab at the School of Optometry and Vision Science.
- ***Setup:*** You will be comfortably seated in front of a specialized infrared camera and asked to look through a lens.
- ***Blinking Protocol:*** You will blink in response to a 'bing' sound at intervals of 2, 4, 6, 8, and 10 seconds. You will keep your eyes open at all other times.
- ***OST Measurement:*** Your ocular surface temperature will be measured continuously during these intervals at seven specific points and one elliptical shape on your ocular surface:
  - Five points on the cornea
  - Two points on the sclera (temporal and nasal parts)
  - One elliptical shape encompassing the central corneal area

Risks associated with this study:

There are no significant risks associated with this study. However, you may experience mild discomfort from keeping your eyes open for extended periods.

Benefits associated with this study:

While there are no direct benefits to you as a participant, your involvement will contribute to important research that could enhance the understanding of ocular surface temperature regulation and tear film stability. This, in turn, may lead to improved clinical practices and treatments for ocular surface diseases.

Remuneration:

Please note that participation in this experiment is entirely voluntary, and no financial remuneration will be provided. However, your contribution to this research is invaluable, as it will significantly aid in advancing our understanding and exploration of this important topic.

Withdrawal from the Study:

You are free to decide whether you wish to participate in this study. It is important to note that your decision will in no way influence the eye care available to you at either the School of Optometry or with your own optometrist. You are also free to withdraw from the study at any time without penalty. To do so, please simply inform the student investigator, Mana Monfared, or the principal investigator, Dr. Paul J. Murphy that you no longer wish to proceed with the study. You may be removed from the study if you do not comply with the investigator's instructions, as given by the study protocol, or if the investigator has reason to believe that it is in your best interest. If you withdraw consent, you can also request the withdrawal of your data. Please note that it is not possible to withdraw your results once they have been published or otherwise disseminated.

Confidential and Security of Data:

All the information you provided as a participant, together with any data we collected because of your participation (including all the private health information, as well as our records of your participation in the study), will be remain confidential. As a participant, you were assigned an identification number to be used in place of your given name, and as such, this is the only identifying information on all study records. No identifying information will be released or published.

All records and data from this study will be retained for a minimum of 7 years. Paper copies of the study data will be stored safely in a storage cabinet located in a locked room (OPT 381) at the School of Optometry and Vision Science, University of Waterloo. They will only be made available to individuals involved in the data collection or data analysis of this study. All electronic research data will be encrypted according to the guidelines outlined by the Information and Systems Technology. Any identifying information on the images obtained during the study will be removed and, together with the encrypted data, will be securely stored on a password-protected server in a locked office at the School of Optometry and Vision Science. Furthermore, these images may be shown to other researchers at the School of Optometry to explain data. They may also be shown publicly, as in the case of publications and presentations, but no identifying information will be disclosed. A list of the participants' names, their corresponding numbers, and any image data (which will be

saved using a coding system whereby each code corresponds with a specific participant), will be stored in a separate file at the University of Waterloo. All the study documents will only be accessible by individuals involved in the study. Records will be disposed in a confidential manner as given by the guidelines of the University. Interested parties can obtain more information about the policies on information security outlined by the University of Waterloo at the following website: https://uwaterloo.ca/secretariat-generalhttps://uwaterloo.ca/secretariat-general-counsel/policies-procedures-guidelines/policy-8counsel/policies-procedures-guidelines/policy-8. Any publications of your results will be de-identified and presented as group data.

Other important issues:

Should you have any questions regarding the study procedures please do not hesitate to contact the study investigator(s).

Your rights as a participant:

In the event that you are harmed as a direct result of your participation in this study, all the necessary medical and ocular treatment will be made available to you at no cost and will be covered by the School of Optometry and Vision Science.

Concerns or Questions about your participation:

If you have any questions about participation in this study, please do not hesitate to ask the researchers. Should you have additional questions later, please contact Mana Monfared via the email address listed at the beginning of this form. We would like to assure you that this study has been thoroughly reviewed by the University of Waterloo Research Ethics Committee and has received ethics clearance. The final decision to participate is purely yours. If you have questions for the Board, contact the Office of Research Ethics, toll-free at 1-833-643-2379 (Canada and USA), 1-519-888-4440, or reb@uwaterloo.ca.

Declaration of Informed Consent

I have read the above description of the research study entitled "***Optimizing Blinking Patterns for Accurate Ocular Surface Temperature Measurement Using Research IR Application***" prior to participating in it. I voluntarily agree to take part in this study, which is conducted by Mrs. Mana Monfared and Dr. Paul J. Murphy at the School of Optometry and Vision Sciences at the University of Waterloo. All the procedures, benefits, and risks were clearly explained to me in sufficient detail, and I have been given numerous opportunities to ask questions and gain further clarification about the study when needed.

I am aware that this study has been reviewed and received ethics clearance through a University Waterloo Research Ethics Board (REB [46626]). If I have questions for the Board, I should contact the Office of Research Ethics, at 1-519-888-4567 ext. 36005 or reb@uwaterloo.ca. For all other queries, I will contact Mrs. Monfared (nmonfared@uwaterloo.ca) or Dr. Paul Murphy (paul.murphy@uwaterloo.ca).

I understand that I may withdraw from this study at any point in time without penalty by simply advising the researchers. I understand that the investigator reserves the right to discontinue my participation from this study at any point in time if they have reason to believe that it is in my best interest, or if I fail to adhere to the protocol details of the study.

I understand that this study in no way replaces the need for regular eye examinations, and that regular eye examinations are essential to ensure that my eyes are healthy. I am aware of the importance of reporting to the investigators of any adverse events, or changes to my health or medication throughout the study.

I am aware that any data collected during the study will be kept secured in accordance with the University's policies. I understand that any images of my eye that are taken during this study are for educational purposes, and may be used in medical or scientific books, as well as journals or magazines.

With full knowledge of the study details, I agree, of my own free will to participate in this study. I give the investigators permission to collect, use, and disclose my personal health information, together with any study data obtained to individuals involved in the data collection or data analysis of this study. I acknowledge that I have received a copy of this information and consent form. By signing this consent form, I am not in any way waving my legal rights or releasing the investigators below from their legal and professional responsibilities.

_____ _____

Signature of participant Date

_____

Printed name of participant

_____ _____

Signature of person explaining consent Date